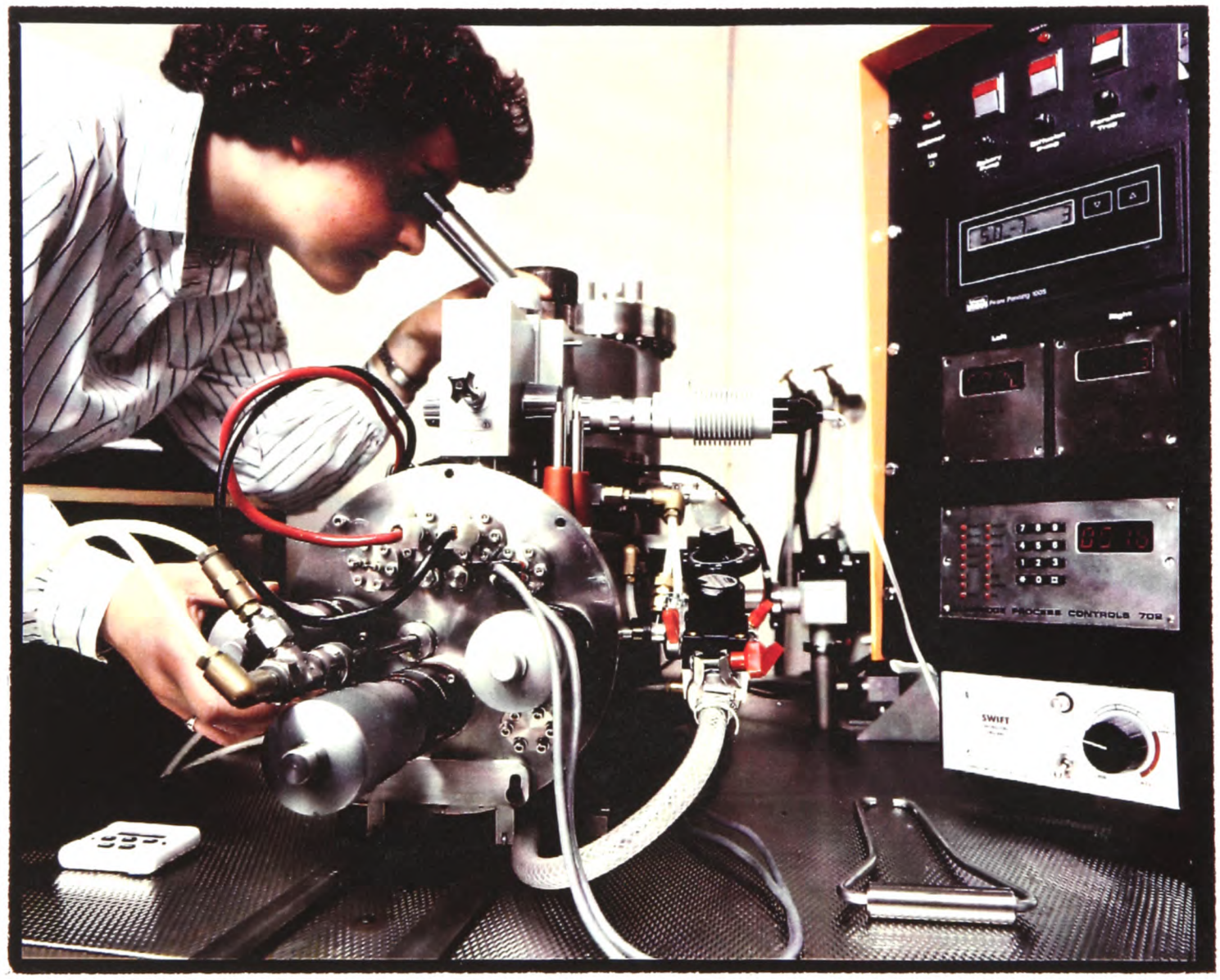


The Oxford University high temperature indentation tester.

INDENTATION CREEP AND ANISOTROPY

IN MAGNESIUM OXIDE AND GERMANIUM

by

Nicola Mary Everitt.

Submitted for the degree of D.Phil.,

Linacre College,

Oxford.

Michaelmas Term, 1990.

RADCLIFFE SCIENCE LIBRARY
OXFORD
DEPOSITED
THESIS
15.12.92

ABSTRACT

Nicola Mary Everitt
Linacre College, Oxford.

D.Phil. Thesis
Michaelmas Term, 1990

Indentation Creep and Anisotropy in Magnesium Oxide and Germanium.

Hardness tests have the potential to provide a simple means of investigating the mechanical properties of materials, both at room temperature, and at higher temperatures. However, the information gained can not be fully utilized unless the deformation processes and variables are properly understood. Careful consideration of such deformation on single crystals can help to clarify the situation and lead to better understanding.

This thesis describes indentation experiments on (001) MgO and Ge at temperatures up to 1175°C and 700°C respectively. Since anisotropy was one of the questions being addressed, the majority of the testing used Knoop indenters, although a few experiments used Vickers indenters. The work was carried out on a specially commissioned high temperature hardness tester (based on an original design by Wilberforce Scientific Developments). A main conclusion of the discussion on the design of high temperature hardness testers is the importance of independent heating of the indenter for accurate hardness results.

The indentation behaviour of MgO was shown to include creep, even at room temperature for the Knoop <110> orientation. However a region of no indentation creep was exhibited between 750°C and 1050°C for both Vickers and Knoop indentations. This has not been reported in previous studies. The anisotropy displayed at room temperature between <110> and <100> Knoop decreased with increasing temperature, due to the faster creep rate of the <110> orientation, and finally reversed.

on Ge
Knoop indentations in the <110> and <100> orientations also showed hardness anisotropy which changed with temperature. In this case there was no anisotropy at room temperature, but anisotropy developed as the temperature increased due to the faster creep rate of the <110> orientation.

The indentation hardness response of both MgO and Ge is explained in terms of the interaction of dislocation arrays which are formed in the first few moments of the indentation. Measurement of the two diagonals of the Knoop indentations showed that the ratio of the diagonal lengths, and also the morphology of the surrounding material, can be used to examine the extent and direction of material displacement. Surface etching, and etching of sections, were used to analyse the disposition of slip around the indentations.

LIST OF CONTENTS

Abstract
List of Contents
List of Figures
List of Tables
Preface and acknowledgements

Page

1. Introduction

1.1 The Concept of Hardness 1
1.2 The History of Hardness Testing and Various Indenters 2

2. Oxford Indentation Tester Development

2.1 Basic Description of the Oxford Machine 7
2.2 Load Calibration and Application 9
2.3 Furnace System 10
2.3.1 Effect of Indenter Heating 11
2.4 Loading Rate - LVDT and Dashpot 14

3. Hardness Measurement and Testing Variables

3.1 Optical Viewing Conditions 16
3.2 Pile up, Sink in and Elastic Recovery 19
3.3 Indentation Fracture 21
3.4 Environment and Surface Effects 22
3.5 Effects of Load scaling - ISE 23
3.6 Vibration and Other External Effects 24

4. Experimental Work

4.1 Magnesium Oxide Analysis and Sample Preparation 27
4.2 Germanium Analysis and Sample Preparation 27
4.3 Etching 28
4.3.1 The History of Etching 28
4.3.2 Formation of Etch Pits 29
4.3.3 The MgO Etch 29
4.3.4 The Germanium Etch 30
4.4 Sectioning 30
4.5 Treatment of Hardness Results 31

5. Previous Work on Magnesium Oxide

5.1 Slip Systems and General Features of Deformation 34
5.3 Flow Stresses and Impurity Effects 35
5.4 Creep and Work Hardening 36
5.5 Dislocation Mobility 36
5.6 Indentation Cracking 37

6. Magnesium Oxide Indentation Results

6.1 Indentation Creep and Anisotropy 39
6.2 Aspect Ratio of Knoop Indentations 40
6.3 Indentation Morphology 41
6.4 Cracking and Slip Steps 42
6.5 Effect of Pre- and Post-Annealing 42

7. Magnesium Oxide Dislocation Analysis and Conclusions

7.1 Slip Systems 44
7.2 <110> Knoop Indentations 45
7.3 Vickers Indentations 47
7.4 Indentation Creep 47
7.5 Region of Zero Indentation Creep 49
7.5.1 Impurity Effects 49
7.5.2 Mechanism for Zero Indentation Creep 50
7.6 Effects of Increased Temperature 51
7.7 Comparing Vickers and Knoop Anisotropy 51

8. Previous Work on Germanium

8.1 Crystal Structure 54
8.2 Dislocations in Germanium 54
8.2.1 Dislocation Generation and Multiplication 54
8.2.2 Dislocation Velocity and Disposition 55
8.2.3 Screw Dislocation Velocity Versus 60o Velocity 56
8.3 General Features of Deformation 57
8.3.1 Doping Effects 58
8.4 Deformation by Indentation 58
8.4.1 Effect of Temperature on Hardness 58
8.4.2 The Deformed Region 59
8.4.3 Anisotropy and Creep 59
8.4.4 Rosettes and Dislocation Arrangements 59
8.4.6 Transformed Phases Under Indentations in Ge 61

8.4.7 Dispute about Plastic Deformation at Room Temperature 61

9. Germanium Indentation Results

9.1 Variation of Hardness with Temperature 63
9.2 Anisotropy and Creep Rates 63
9.3 Effect of Doping 64
9.4 Aspect Ratio and Pile up 64
9.5 Effect of Post- and Pre-anneal 65

10. Germanium Dislocation Array Analysis and Conclusions

10.1 The <110> orientation dislocation arrays 67
10.1.1 Rosette Arms - <110> Indentations 67
10.1.2 <110> Indentations Subsurface Information 68
10.1.3 Progression of slip with time 69
10.2 Dislocation arrays around <100> Indentations 69
10.2.1 Rosette arms - <100> Indentations 69
10.2.2 <100> Orientation Subsurface Information 69
10.2.3 Progression with time - <100> Orientation 70
10.3 Variation of Dislocation Structure with Temperature 71
10.3.1 Rosettes 71
10.3.2 Three Dimensional Dislocation Structure at Higher Temperatures 72
10.4 The Micromechanisms of Creep 72
10.4.1 Slip planes 73
10.4.2 Loop configuration and dislocation locks 74
10.4.3 Difference in creep rate and the effect of temperature 74

11. Hardness Interpretation and models

11.1 Models of Hardness 76
11.1.1 Resolved Shear Stress Models 78
11.2 Relating Hardness to Physical Properties 80
11.3 The Variation of Hardness with Temperature 80
11.4 Time Dependent Hardness - Indentation Creep 82
11.5 Anisotropy 84
11.6 Interpretation of the Indentation Processes - The Fundamental Factors 84

12. Summary and Conclusions

12.1 Summary of the Magnesium Oxide Results 88
12.2 Summary of the Germanium Results 90

12.3 Hardness Testers 91
12.4 The Indentation Response 91

Appendix A - Calibration Strain-gauged Beam

List of References

LIST OF FIGURES

Frontispiece The Oxford University high temperature indentation tester.

Figure 1.1 Indenter geometries; (a) Brinell, (b) Vickers and (c) Knoop.

Figure 2.1 General view of the Oxford high temperature indentation tester.

Figure 2.2 Detailed views of the Oxford machine:
(a) Upper assembly - loading system and upper furnace,
(b) Lower assembly in pulled forward position.

Figure 2.3 (a) Specimen mounting block and furnace,
(b) Loading system and displacement monitor.

Figure 2.4 Furnaces and thermocouples: (a) Upper (indenter) assembly, (b) Lower (sample) assembly.

Figure 2.5 Plots of data with and without upper furnaces.

Figure 2.6 Schematic diagram of the LVDT and the indenter beam system.

Figure 2.7 A plot of the LVDT response.

Figure 3.1 Extrinsic effects on indentation size and measurement: (a) Topographic effects due to pile-up and sink-in. (b) Elastic recovery effects shown in the absence of topographic changes (after Sargent and Page 1985).

Figure 3.2 Idealized indentation crack morphologies (after Cook and Pharr 1990).

Figure 5.1. The two gliding planes in the rocksalt structure (Gilman 1961).

Figure 5.2. Structures of glide planes in rocksalt crytals for half glided positions (Gilman 1961).

Figure 5.3 Variation of CRSS for MgO on the {100} and {110} planes (Haasen et al 1985).

Figure 5.4 Schematic diagram of the cracks and slip lines typically found round an indentation on (001) MgO. The extent of the $\{110\}_{90}$ cracks OE,OF,OG and OH is limited by the outermost square-shaped slip trace EFGH (after Chaudhuri 1986.)

Figure 6.1 Variation of Knoop hardness with dwell time between room temperature and 1200°C, on (001) MgO; (a) Overview, (b) Higher temperature results.

Figure 6.2 Variation of Vickers hardness with dwell time at higher temperatures on (001) MgO; (a) 500g load, (b) 100g load.

Figure 6.3 Variation of the aspect ratio of Knoop indentations with the temperature of indentation on (001) MgO samples.

Figure 6.4 Interference fringes (and accompanying image without fringe contrast) for <110> Knoop indentations on (001) MgO: (a) 150°C, (b) 525°C, (c) 750°C, (d) 1050°C, (e) 1175°C and (f) 1175°C sample temperature but unheated indenter (927°C).

Figure 6.5 Schematic view of the surface morphology aound a <110> Knoop indentation on (001) MgO: (a) Sketch of fringe pattern indicating the position of various regions relative to the bulk sample surface, (b) Vertical section across the short diagonal of such an indentation.

Figure 6.6 Interference fringes (and accompanying image without fringe contrast) for <100> Knoop indentations on (001) MgO: (a) room temperature, (b) 150°C, (c) 525°C, (d) 750°C, (e) 1050°C and (f) 1175°C.

Figure 6.7 Interference fringes (and accompanying image without fringe contrast) for Vickers indentations on (001) MgO: (a) and (b) <100> orientation at 750°C, (c) and (d) <110> orientation at 750°C, (e) and (f) <110> orientation at 1050°C.

Figure 6.8 Interference fringes (and accompanying image without fringe contrast) for room temperature Vickers indentations on (001) MgO: (a) and (b) <100> orientation indentation made after the sample had been pre- annealed at 750°C for 3 hours, (c) and (d) <100> orientation indentation post-annealed at 750°C

for 4 hours, (e) and (f) <110> orientation indentation, post annealed at 750°C for 4 hours.

Figure 6.9 The effect of pre-anneal on Knoop hardness at 600°C on (001) MgO.

Figure 7.1 Primary slip system which might be activated by indentation on (001) MgO:(a) $\{110\}_{45}$ planes, (b) $\{110\}_{90}$ planes (after Keh 1960).

Figure 7 2 Dislocation patterns around <100> Knoop indentations on (001) MgO: (a) Room temperature, (b) 150°C, (c) - (f) 400°C indentations with dwell times of 60, 120, 240 and 600 seconds respectively.

Figure 7.3. Arrangement of the most active $\{110\}_{45}$ slip planes for (a)<100> orientaton, (b) <110> orientation.

Figure 7.4. Higher temperature dislocation patterns around <100> Knoop indentations on (001) MgO: (a) 600 second indentation at 525°C, (b) and (c) 60 and 600 second indentations at 600°C, (d) 600 second at 750°C, (e) 600 second indentation at 1050°C.

Figure 7.5 The dislocation pattern around <110> indentations on (001) MgO: (a) and (b) 60 and 600 second indentations at 300°C, (c) and (d) 60 and 600 second indentations at 450°C, (e) and (f) 60 and 600 second indentations at 600°C.

Figure.7.6. Serial sections of <110> 60 second indentation on (001) MgO:(a) Unetched, (b) surface etch, (c) ~4μm depth with orthophosphiric acid etch, (d) ~4μm depth with Stokes etch, (e) ~10μm depths with Stokes etch.

Figure 8 1. Variation of dislocation velocity with inverse temperature for various doping (Patel and Freeland unpublished work).

Figure 8.2. Possible arrangement of loops around a Vickers indentation on (001) Ge (after Roberts et al 1985).

Figure 9.1. Variation of Knoop hardness (50g) with temperature for n-doped Ge, 20 second and 300 second indentations (a) <110> orientation (b) <100> orientation.

Figure 9.2. Variation of <110> Vickers Hardness with temperature.

Figure 9.3. Variation of Knoop hardness with dwell time for the <110> and <100> orientations at various temperatures. (a) Lower temperature results, (b) Higher temperature results.
Note: the <100> indentations at 500°C were highly skewed (one half of the long diagonal 1.3x the whole length).

Figure 9.4. Variation of Knoop hardness with dwell time (up to 1800 sec) for <110> and <100> orientation on p-doped Ge at 700°C.
Note: 1800 sec values are means of 3 readings only.

Figure 9.5. Variation in Knoop Hardness with temperature for n- and p-doping (a) <110> and (b) <100> orientations.

Figure 9.6. Comparison of 700°C results for n- and p- doping.

Figure 9.7. Variation of aspect ratio with indentation temperature for <100> Knoop indentations on (001) Ge, 20 second and 300 second indentations

Figure 10.1 Dislocation surface arrays from <110>> indentations on (001) Ge at 350°C showing the effect of increasing dwell time

Figure 10.2. Plot of rosette length against long diagonal for <110> indentations (50g) at 350°C.

Figure 10.3. Series of etched arrays around a typical indent as the surface was stripped away, 20 second <110> orientation on (001) Ge at 400°C: (a) surface array, (b) 6μm depth, (c) 12μm, (d) 19μm, (e) 26μm, (f) 31 m, (g) 34 m, (h) 41 m, (i) 52 m, (j) 64μm: (k) 30 second <110> indentation also at 64μm depth.

Figure 10.4. <110> Knoop indentation, 120 seconds on (001) Ge at 400°C; (a) Surface array, (i) and (ii) Etched vertical sections across the chords indicated.

Figure 10.5. Series of etched arrays at the sample surface as it was striped away, 600 second <110> orientation on (001) Ge at 400°C: (a) surface array, (b) 6μm depth, (c) 12μm, (d) 19μm, (e) 26μm, (f) 31μm, (g) 41μm, (h) 52μm, (i) 64μm, (j) 75μm (k) 100 m.

Figure 10.6. Dislocation arrays from <100> indentations on (001) Ge at 350°C showing the effect of increasing dwell time, and a vertical section through a 60 second indentation

Figure 10.7. Average rosette length against dwell time of for a <100> indentation.

Figure 10.8. Series of etched arrays at the sample surface as it was stripped away, 20 second, <100> orientation on (001) Ge at 400°C: (a) Surface array, (b) 6μm depth, (c) 12μm, (d) 26μm, (e) 31μm, (f) 34μm, (g) 41μm, (h) 48μm, (i) 64μm, (j) 75μm, (k) 30 second indentation at 12μm depth.

Figure 10.9. Typical dislocation arrays for <100> indentations on (001) Ge at 350°C, (a) 20 second and (b) 60 second, sections (i), (ii) and (iii) as shown.

Figure 10.10. Slip geometry under Knoop Indentations on the (001) face of Ge; (a) <110> and (b) <100> orientation.

Figure.10.11. Series of etched arrays at the sample surface as it was stripped away, 600 second, <100> orientation on (001) Ge at 400°C; (a) Surface array, (b) 6μm depth, (c) 12μm, (d) 19μm, (e) 26μm, (f) 31μm, (g) 34μm (h) 48μm, (i) 64μm, (j) 75μm, (k) 93μm, (l) 100μm.

Figure 10.12. Surface dislocation arrays from 700°C <110> indentations: (a) 20 second, (b) 30 second, (c) 60 second, (d) 120 second, (e) 300 second, (f) 600 second.

Figure 10.13. Surface dislocation arrays from 700°C <100> indentations on (001) Ge: (a) 20 second, (b) 30 second, (c) 60 second, (d) 120 second, (e) 300 second, (f) 600 second.

Figure10.14. The etched dislocation patterns around two sets of same strain indentations made at differing temperatures and dwell times: (a) 600 sec <110> indent at 350°C, original diagonal 80.6μm, (b) 30 sec <110> indent at 400°C, original diagonal 80.4μm, (c) 600 sec <100> indent at 350°C, original diagonal 66.5μm, (d) 20 sec <100> indent at 400°C, original diagonal 67.7μm.

Figure 10.15. The various loop configurations which might be present under Knoop indentations on (001) Ge.(Roberts et al 1986.)

Figure 11.1 The expanding spherical cavity model elastic plastic indentation.

Figure 11.2 Arrhenius plot, log (Knoop hardness) against 1000/T for indentations on (001) Ge: (a) <110> orientation and (b) <100> orientation.

Figure 11.3. Arrhenius plot, log (Knoop hardness) against 1000/T for indentations on (001) MgO: (a) <110> orientation and (b) <100> orientation.

Figure 11.4. Variation of Knoop hardness with dwell time between room temperature and 700°C on (001) Ge:
(a) <110> orientation and (b) <100> orientation.

Figure 11.5. Variation of Knoop hardness with dwell time between room temperature and 1175°C on (001) MgO:
(a) <110> orientation and (b) <100> orientation.

Figure A.1 Strain gauged beam apparatus designed and built for calibration of the Oxford indentation tester:
(a) Top view, with upper loading piece in postion,
(b) Beam in position on the lower pin supports but with upper loading piece removed.

Figure A.2 Schematic view of the apparatus.

LIST OF TABLES

Table 2.1 Thermocouple read ings for the experiments without and upper furnace.

Table 3.1 Knoop hardness measurements by different observers; mean diagonal, standard and number of indentations accepted for each set of conditions.

Table 4.1 Results of Chemical analysis of the MgO crystal.

Table 5.1 Melting points of some rocksalt materials.

Table 5.2 Summary of the results of Gilman and Buerger (after Gilman 1961).

Table 5 3 List of the analyses of MgO crystals used in the references referred to in the text, as given by the authors.

Table 6.1 Various temperatures in ^{O}C, K and T_M for MgO.

Table 7.1 List of the analyses of MgO crystals used in the references referred to in the text, as given by the authors. (Reproduced from table 5.3 for easy reference).

Table 9.1 Various temperatures in ^{o}C, K and T_M for Ge.

Table 9.2 The sizes of straight and pre-annealed room temperature indentations before and after a 700°C, 8 hour post-anneal.

Table 11.1 Activation energies determined from the Arrhenius plots in figures 11.2 and 11.3, and values from literature.

PREFACE

The work presented in this thesis was carried out by the author in the Department of Materials, Oxford University, between October 1986 and December 1990 under the supervision of Dr. S.G. Roberts. The work was supported by the SERC and the National Physical Laboratory, Teddington, under the CASE award scheme.

No part of this thesis has previously been submitted for a degree at this University or elsewhere. The research described is original; where the work of others is cited in the text this is acknowledged and referenced.

Some of the work contained in this thesis was presented at the 19th Canadian Fracture Conference, Ottawa, Ontario, May 1989. This has been published as "Indentation creep in semi-brittle materials", by N.M. Everitt and S.G. Roberts, in *Constitutive Laws of Plastic Deformation and Fracture*, edited by A.S. Krausz, J.I. Dickson, J-P.A. Immarigeon an d W. Wallace, Kluwer Academic Publishers, Dordrecht, 1990, pp.147-153.

ACKNOWLEDGEMENTS

Working towards a thesis is an all consuming project. I would like to thank my family for their tremendous support and sympathy; and all my friends and colleagues at Oxford and Bristol who have given me such encouragement and help.

My supervisor, Dr. Steve Roberts has uncomplainingly guided and supported me to the completion of this project, and I offer him my thanks. I would also like to acknowledge Dr. M. Gee, the late Dr. E. Almond, and other staff at the National Physical Laboratory for their kind assistance to me as a CASE student.

Many people have provided technical and material help. I would like to thank Sir Peter Hirsch for the provision of laboratory facilities, and the technical staff at the department for their skilled assistance and patience. My thanks also to S. Holmes at the Imperial College of Science and Technology, London, and M. Bown at the Inorganic Chemistry Laboratory, Oxford for their analyses of my crystals.

1. INTRODUCTION

"Hardness measurements are at once among the most maligned and magnificent of physical measurements."

J.J. Gilman (1973)

Hardness is a property which our society has valued since man sought to harness the materials around him, the advent of a more technologically based lifestyle leading to a desire to explore and quantify the materials' behaviour. The hardness tests which have developed are widely used, and contain much material information, if we possess the expertise to unlock their potential. In the field of fundamental research, hardness tests on brittle and semi-brittle materials have already been used to examine slip systems, gain information on dislocation velocities and, using cracking, for fracture toughness measurements. In a sense this thesis attempts to reverse the process of study, and use results from indentation tests on magnesium oxide (MgO) and germanium (Ge) single crystals, to investigate the mechanisms leading to and controlling a "hardness result".

A series of experiments at various temperatures have been carried out looking at hardness anisotropy (the variation of hardness with the orientation of the principal axis of the indenter), and the change in such hardness values as the time of loading is increased (indentation creep). Evaluation of the results from such tests gives information on the dominant mechanisms under each set of conditions, and hence provides insight into the material processes that the hardness test investigates. Careful consideration of the deformation on single crystals should help to clarify the situation and lead to better understanding of more "complicated" materials. Since plastic flow and fracture are both heterogeneous processes, progress towards understanding their nature can not solely be achieved by measuring homogeneous mechanical parameters like stress, strain and strain rate. It is necessary to be able to study the heterogeneities themselves - dislocations and cracks - in order properly to link the homogeneous parameters to atomic phenomena (Gilman 1961).

The concept of indentation testing, and the methodology of some hardness tests, are covered in the remainder of this chapter. Chapter 2 describes the Oxford indentation tester, its development, and some important conclusions concerning the validity of high temperature hardness results with this and other systems. The simple elegance of the test is challenged by the sheer number of variables which may affect the data gained, and some of the factors affecting hardness measurement are discussed in chapter 3.

Chapter 4 details the methods and chemical analysis of the materials used in experimental work. Chapters 5 to 7 are concerned with MgO. They look at the conclusions drawn by previous workers on the behaviour of MgO, describe the indentation results obtained at Oxford, and discuss these results in the light of the dislocation arrays produced around the indentations. Chapters 8 to 10 carry out the same analysis for Ge.

Chpater 11 presents an explanation for the observed indentation creep and anisotropy of MgO and Ge. The main hardness models are then described, together with the temperature and time dependence of hardness, and compared with the results outlined in the previous chapters. The thesis concludes with a summary, and looks ahead to future work which might stem from it.

1.1 The Concept of Hardness

As mentioned in the previous chapter, hardness is a familiar concept but one which is difficult to quantify. Defining hardness in anything but relative terms (the Mohr scale for example) was the problem which concerned early workers in the field of hardness testing. In a contempory account of Brinell's new test (see next section), Wahlburg (1901) suggested that the most commonly accepted sense of the term hardness was "resistance offered by a solid substance to the entrance of another substance into it". Tabor (1986) defined hardness on a basic level as the resistance of a solid to local deformation. A wide variety of hardness test procedures have been used to quantify hardness in different contexts (see, Shaw's list, 1973, for example). The tests can be roughly grouped as to whether they principally measure a material's resistance under static loads (static indentation), to deformation under impact load (dynamic hardness), to scratching, or to wear by abrasion or erosion.

This thesis is concerned with the results and interpretation of "static" indentation tests in which a ball, cone or pyramid is forced into the surface of materrial by a known load for a controlled time. The hardness is then quantified as the load per unit area of impression. Perhaps the best known example of test is the Vickers hardness test using a square based pyramid. The hardness value (sometimes called DPN - diamond pyramid hardness number) is used to estimate bulk yield stresses, quality control etc., as well as giving hardness ranking. Diamond has the highest known hardness of ~10,000 kg/mm^2, soda-lime glass - ~560 kg/mm^2, cold rolled steel - 200 kg/mm^2, and 99.5% aluminium - 20 kg/mm^2 (Wyatt and Dew-Hughs 1974). The continued popularity of hardness tests bears testimony to the various advantages of the test. The test is simple to operate, and the testing temperature can easily be varied. Also, the amount of material required is small and

little shape fabrication is needed, a considerable bonus in the single crystal and ceramic fields. (Some surface preparation is sometimes necessary, of course).

Whilst Vickers testing conventionally uses loads between 1 and 100 kg to produce indentations of the order of mm across, testing with lower loads to produce smaller indentations is desirable for very small or thin samples, or to reduce cracking and chipping for brittle substances. Where the dividing line between ordinary and "microhardness" lies is ill defined, but work on microhardness machines designed to give accurate results at lower loads, typically 10-1000g, has been going on for some decades. The first reference to Vickers hardness testing with small loads appears to have occurred in the Annual Report for 1932 of the National Physical Laboratory, Teddington (Bückle 1959). Microhardness measurements offer a unique method to investigate plasticity and fracture of materials on the same scale as the mechanical interactions in such processes as friction, wear, abrasion, grinding, polishing and erosion (Sargent 1979). Recently indentation experiments using very small loads of the order of μN, have been carried out (Pethica, Hutchings and Oliver 1983, Doerner and Nix 1986). These have potential for investigating the mechancial properties of very small volumes of material.

The "hardness number", although a convenient quantity to quote, conveys only a small amount of the information available from an indentation test. The applied stress is localised in a small volume, so that any cracks are unable to propagate through the whole specimen, and is mainly compressive in nature. The test is therefore especially useful for investigating the flow, rather than fracture, properties of brittle materials. However the indentation method is increasingly being used as a means of producing controlled cracks for evaluating material parameters (e.g. Lawn, Hockey and Richter 1982). Such practical work is outside the scope of this thesis, which is concerned primarily with indentations in the plastic flow regime, but a brief review is included in section 3.3.

1.2 The History of Hardness Testing and Various Indenters

The first of the modern techniques for measuring hardness was conceived and pioneered by J. A. Brinell, chief technical manager of the Fagersta iron and steel works in Westmanland, Sweden (Brinell 1900). His developmental work covered a wide variety of pure metals and alloys, and even many kinds of wood (Hill, Storakers and Zdunek 1989). Brinell gave a number of requirements for a hardness test to be considered suitable for practical use (Wahlburg 1901):-

1. It must give trustworthy results.
2. It must be easy to learn and to apply.

3. There should be no necessity for costly or time-wasting mechanical treatment of the material prior to testing.
4. The testing medium for forcing into the material should be cheap, easy to obtain, incapable of altering its shape, and of sufficient hardness.
5. The method should admit finished articles for testing without damage to these objects.
6. The testing results should be indicative of the absolute hardness of the material.

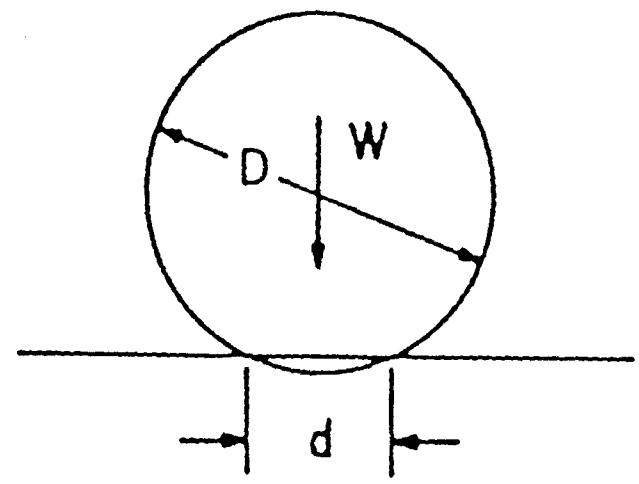
Nearly a century later, and after much development of costly machines and delicate systems, such a list is still relevant and liable to bring a wry smile to the lips of hardness experimenters!

Brinell's initial tests squeezed steel plates together with a steel ball in between the two. In the modern form of the test the indenter in the shape of a hard steel ball, diameter D, is pressed, normally onto the surface of the material under examination, for a standard period of 10 to 15 seconds at full load (British standard 240 : 1986). It is then removed and the diameter, d, of the indentation measured (see figure 1.1). The load is usually adjusted so that d/D is between 0.3 and 0.5 (B.S.240:1986 gives the permitted range as between 0.25 and 0.6). The Brinell hardness number, H_B, is defined as:-

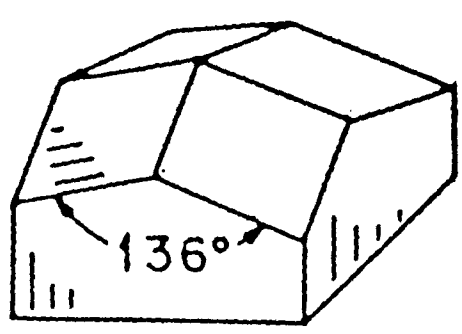
$$H_B = \text{load} / \text{ curved area of indentation}$$
$$= 2W/\pi D(D-(D^2 - d^2)^{1/2}).$$

where W is the load, D the ball diameter and d the diameter of the indentation. Thus the hardness pressure is based on the contact area rather than the area in the plane of the surface.

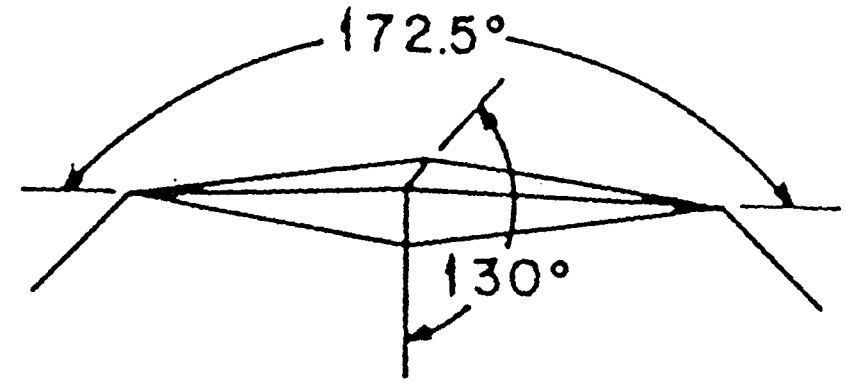
The Brinell hardness number will vary according to the size of the impression because the stress and strain fields change with the amount of the indenting ball "submerged" in the specimen. Smith and Sandland (1925) proposed that a pyramid be substituted for the ball in order to provide geometrical similitude. If the shape of the indentation remains the same as the scale is increased, the stress fields around it should also remain the same shape, so the hardness number should be independent of load, (but see note in section 3.5). Thus in the Vickers test (developed by Smith and Sandland), the indenter is cut fron a diamond or other hard stone into a square based pyramid with an apex angle of 136° since this is the angle subtended when d/D = 0.375 (Shaw 1973), see figure 1.1. The Vickers hardness number, H_V is again defined by the load divided by the contact area of the indentation (B.S. 427: Part 1: 1961):-



(a)



(b)



(c)

Figure 1.1 Indenter geometries; (a) Brinell, (b) Vickers and (c) Knoop.

$$H_V = \text{load/pyramidal area of indentation}$$
$$= 0.5\,W / d^2 \sin(136/2)$$
$$= 1854\ W / d^2\ kg/mm^2.$$

where d is the mean of the two diagonal lengths of the indentation the surface (μm) and W is the load (g). The standard indentation time is 10 to 15 seconds at full load (B.S. 427: 1961).

In the Knoop test (Knoop, Peters and Emerson 1939) an elongated pyramid diamond indenter is used, see figure 1.1. Unlike the other two tests described above, the Knoop hardness, H_K, is expressed in terms of the projected area rather than the contact area:-

$$H_K = 2\,W / d^2\,[\cot(172.5/2) \times \tan(130/2)]$$
$$= 14230.0\ W\ kg/mm^2.$$

where d is the length of the long diagonal (μm) and W the load (g).

It is especially useful for studying hardness anisotropy, since it produces indentations which are seven times as long as they are wide. It is also used with thin specimen or coatings because it gives a shallower impression than the Vickers indenter.

Another pyramidal indenter is the Berkovich indenter, a triangular based diamond pyramid with an angle of 65.3°C between the face and the vertical axis. This geometry was chosen to give the same area-to-depth ratio as the Vickers indenter (Pethica, Hutchings and Oliver 1983). Conical indenters are sometimes used. In the Rockwell test a steel ball is used for soft materials, and a diamond cone with a hemispherical tip, for hard metals. A setting load is first applied, then a test load, before reducing to the setting load again (Wyatt and Dew-Hughes 1974). The hardness is derived from the difference in depth of the indentation between initial and final application of the setting load.

The sharp pyramidal indenters, such as Vickers and Knoop, are more suitable for the investigation of plastic deformation in brittle materials, since spherical and conical indenters develop circumferential tensile stresses around the region of contact, which encourage brittle fracture and chipping.

Brookes and co-workers have pioneered an interesting type of hardness testing, "soft indentation" (e.g. Brookes and Green 1973 - on MgO; and Brookes, Brookes, Howes,

Roberts and Waddington 1990 - on different types of diamond). Here a point load is applied to a "hard" substance with a much softer cone. The soft "indenter" tip spreads until the contact area can support the applied load. Although no visible impression is made on the hard specimen, dislocation arrays are produced and can be analysed, with the advantage that the density of dislocations beneath the indentation is much less than with conventional indentation.

In spite of differences in the details of testing, all the static indentation tests measure largely the same physical property, a materials' resistance to plastic deformation under a complex stress field. Here lies the technological importance of hardness testing, particularly since it is possible to carry out the test at relatively high temperatures. However, the results are only useful when the hardness result can be clearly linked to other physical properties. The various models which attempt to do this are reviewed in chapter 11.

2. OXFORD INDENTATION TESTER DEVELOPMENT

Hardness testing equipment has come a long way since Brinell used two steel balls and a vice. There are a number of micro- and macro- machines available for testing at room temperature, but fewer that can carry out tests at elevated temperatures.

Ideally, for precise hardness data one must know:-
(i) the actual load applied, the loading rate, and the length of time under load,
(ii) the geometry of the indenter and the orientation relative to the sample surface if it has texture or is a single crystal, and
(iii) the environment (including an accurate assessment of temperature) in which the test took place.

This chapter describes the Oxford machine and discusses how nearly these criteria are met by the Oxford system and alternatives.

2.1 Basic Description of the Oxford Machine

All the indentation tests results reported in this thesis were carried out in a machine commissioned by the Department of Metallurgy and Science of Materials at Oxford, and made by Stanton Redcroft, Wimbledon, UK (body-work subcontracted to Leisk Engineering, Burgess Hill, UK). A general view of the machine is shown in figure 2.1 (and the colour frontispiece). It is a development of the Wilberforce microhardness tester. Tests, in the range of 10g to 1kg load, can be made at temperatures up to 1500°C, under vacuum, and it has both an upper furnace (around the indenter) and a lower furnace (around the sample). A thermocontroller is used to maintain set temperatures, but control of the indentation time is purely manual.

Loading is by a dead weight system. The load is applied via a dashpot-damped, counterbalanced arm (see discussion in section 2.2). The load range is achieved with two interchangeable holders for weights, in the ranges 10g to 100g and 100g to 1kg. Each weight holder is fitted into the upper lid of the machine with a thread. Initially the threads were both stainless steel, but this caused thread welding problems, so the female thread in the machine lid was replaced with a brass insert. The accurately machined weights have a centre hole which fits over the indenter loading rod (see figure 2.2a). The inside of each weight holder is stepped, so that the number of weights which rest on the indenter can be altered by screwing the holder in and out of the lid (using the black cap which can be seen in figure 2.1 and the colour frontispiece), thus altering the applied load. This could be done

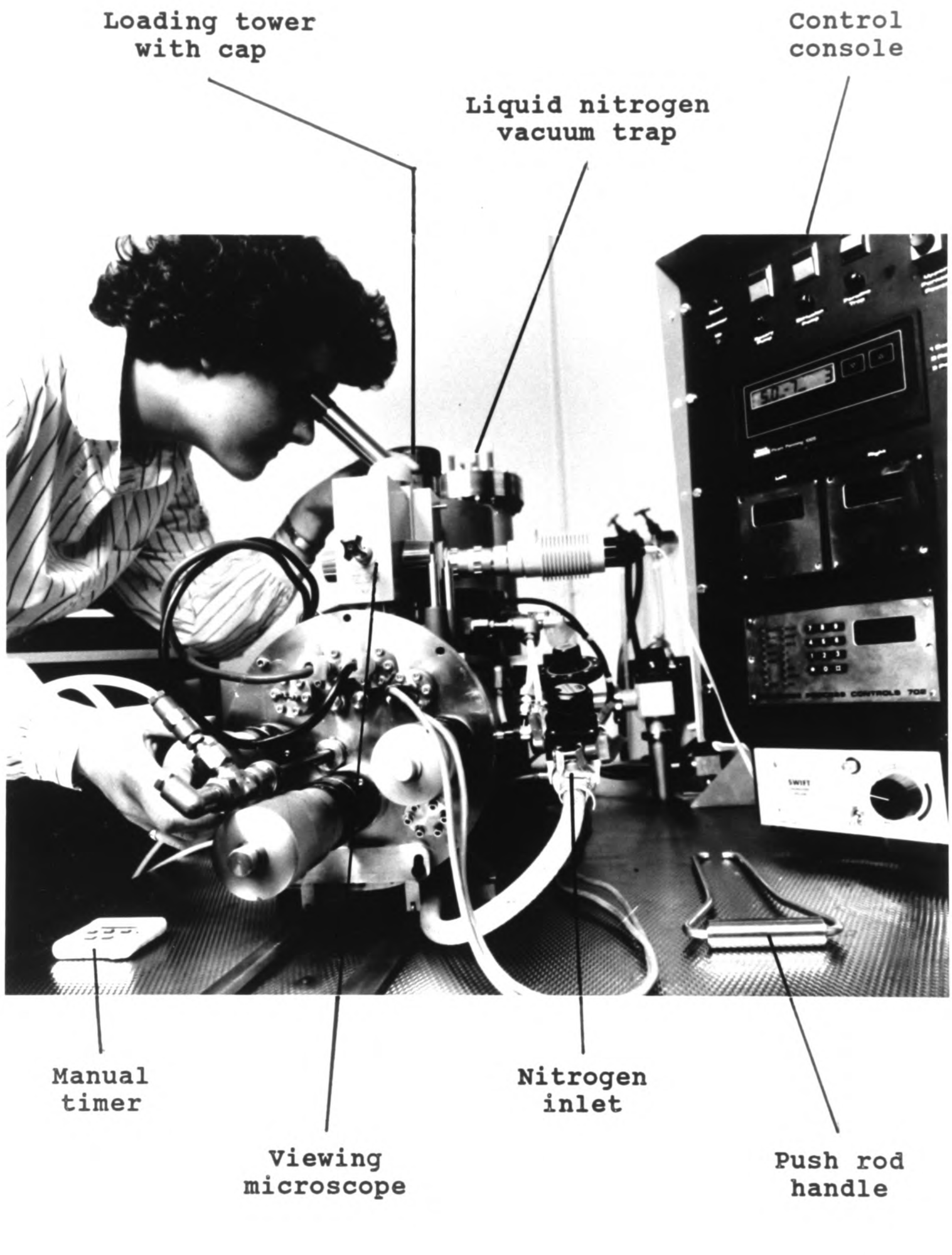
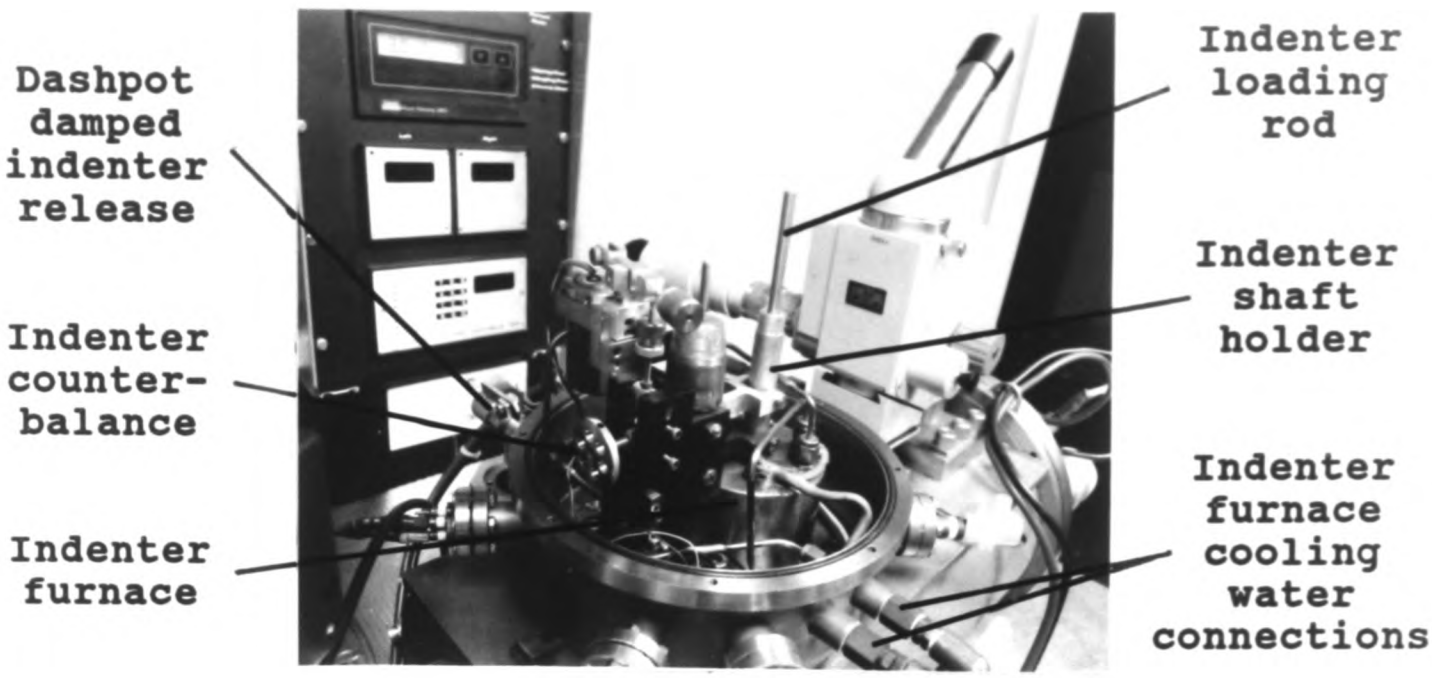
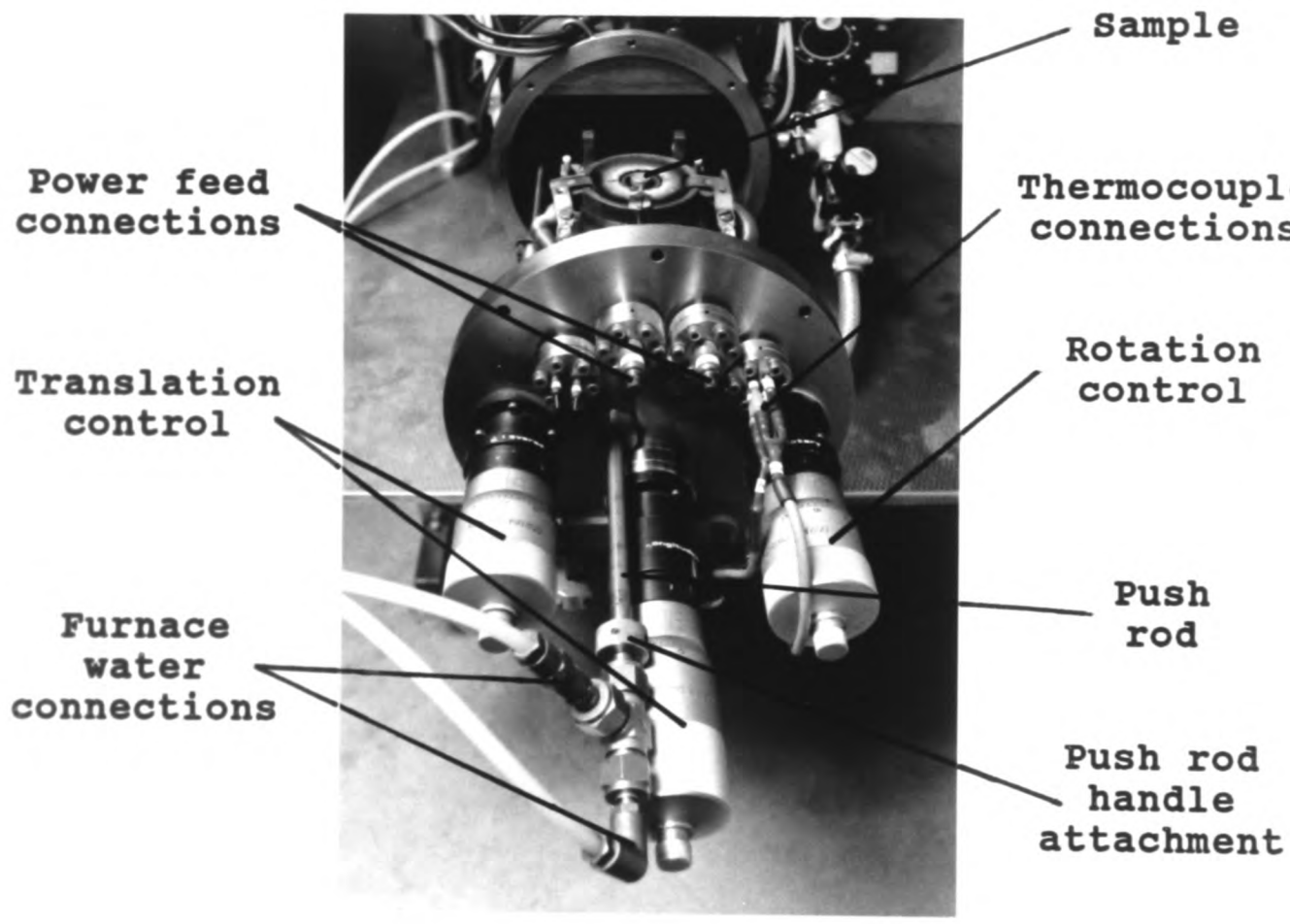


Figure 2.1 General view of the Oxford high temperature indentation tester.



(a)



(b)

Figure 2.2 Detailed views of the Oxford machine
(a) Upper assembly - loading system and upper furnace,
(b) Lower assembly in pulled forward position.

during an experiment (i.e. at temperature), but obviously the machine has to be brought up to atmospheric pressure in order to change between loading towers.

A baffle valve between the diffusion pump and the main chamber enables the diffusion pump to be isolated whenever the vacuum is to be broken. A gas inlet was installed so that the machine could be brought up to atmospheric pressure using dry N_2, in an effort to keep the system as clean as possible. Inevitably, in a system which is constantly brought up to air and then pumped down, and has high temperatures (and currents) in close proximity to water cooling, some problems are experienced with the vacuum. However, after the machine modifications were completed, vacuums in the region of 10^{-6} - 10^{-5} mbar were routinely achieved, and better than this if the system and sample had been "baked out" at medium temperatures and then allowed to cool, prior to higher temperature experiments.

The indenters consisted of single crystal diamond or sapphire stones of approximately 3mm diameter, cut to the Vickers or Knoop profile. Each stone is mounted in a molybdenum head (since 1500°C is too high for the use of the more commonly used steel mounting), and the head is fixed to a 3mm diameter tungsten shaft by Mo screws. The indenter is mounted in the machine by unbolting the top assembly, and inserting the indenter shaft from the bottom of the upper (indenter) furnace, through the centre and up into a holder (labelled in figure 2.2a). The alignment of the indenter is ensured by locating the fixing screws onto flats on the tungsten shaft.

Figure 2.2(b) shows the bottom assembly of the machine pulled forward in the position for installing samples. It would then be pushed forward and bolted to the main body of the machine (with an o-ring seal), after which the machine is ready to be pumped down. The position of the sample can be accurately controlled (to within 50μm) using the micrometer translation controls, and the specimen can be rotated through 360° using the rotation control The specimen / furnace trolley can be in two stations, firstly under the viewing microscope for alignment and mapping of the specimen, and secondly under the indenter assembly. The trolley is pushed from one to the other using the push rod (which also carries the cooling water to the indenter furnace). A stiff spring arrangement keeps the trolley (which runs on linear bearings) pushed up against the end stop in either position. The position of the microscope on the machine could be altered so as to allow indentations to be centred in the field of view. (This was necessary when the indenter was changed).

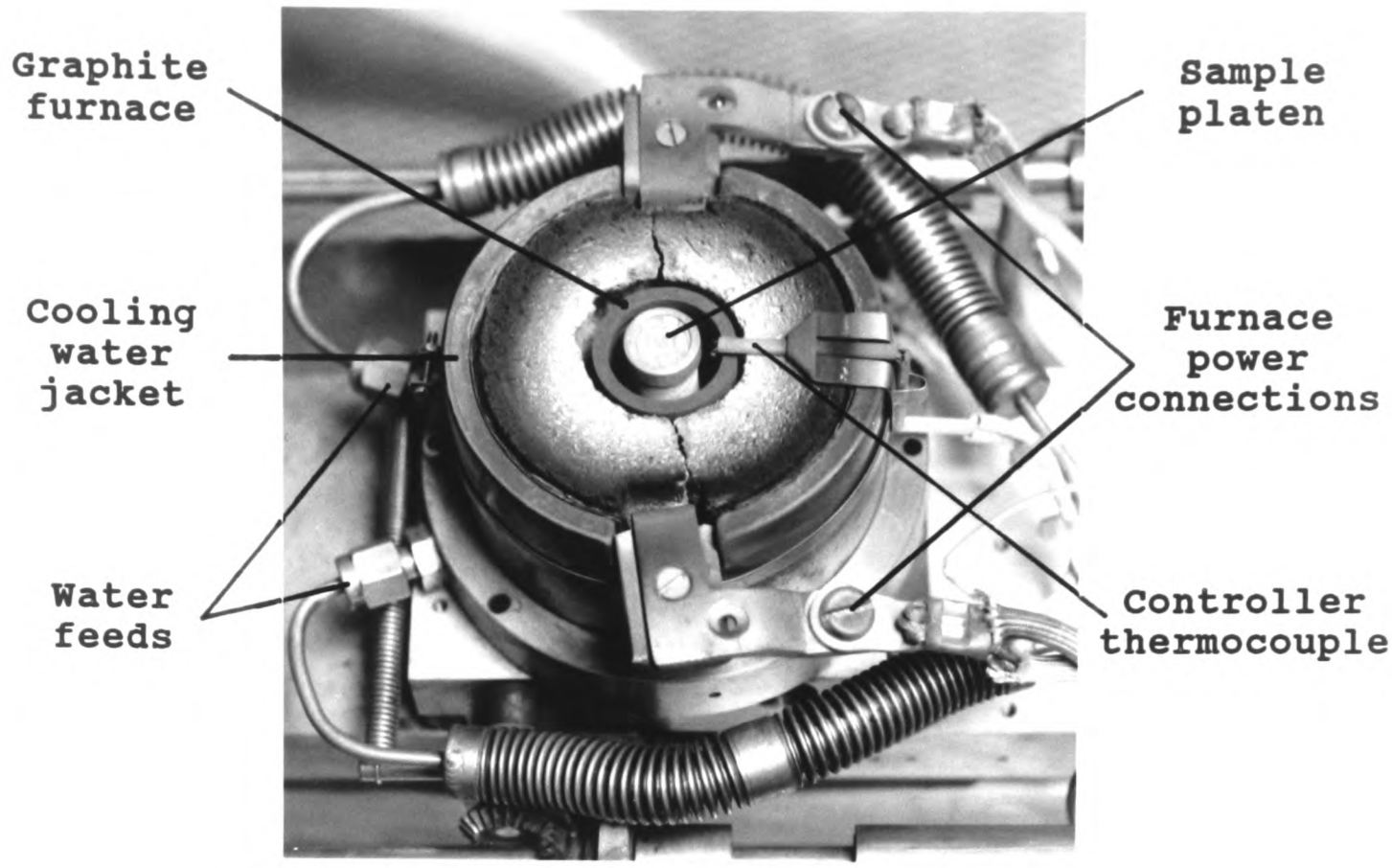
The actual sample is mounted on an alumina platen (12mm diameter) which sits on the top of an alumina column. A Mo ring was supplied with which to secure the alumina

cap (shown in figure 2.3a); but this was not found to be necessary during normal operation. Limited clearance between the sample platen and the roof of the stainless steel chamber means that the height of the sample can not be more than 3mm. The output from the thermocouple visible in figure 2.3(a) is used by the thermocontroller, and, if the reading falls below the set temperature, then current would be supplied to both the upper and lower furnaces. The details of the power distribution and setting are discussed in section 2.3, together with a description of the furnaces.

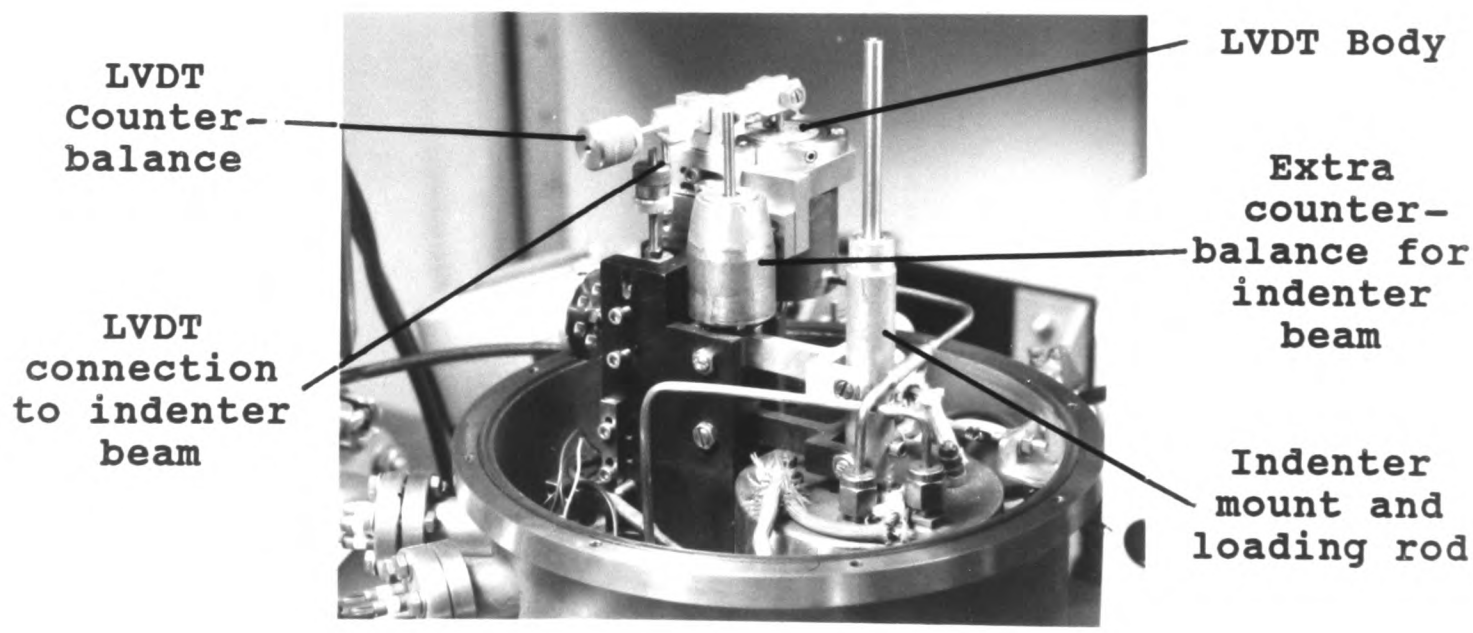
2.2 Load Calibration and Application

Methods of applying the load during an indentation test are often based on a counterbalanced lever mechanism. As briefly mentioned above, the Oxford machine uses a dashpot damped arrangement, see figure 2.2(a). Counterbalance weights at one end of the lever arm cancel out the weight of the indenter, and the load is applied by weights placed directly above the indenter itself. An alternative method is to have direct loading, such as is used in the NPL machine, in which load is applied by a servo motor driven, spring loaded system. A feed-back loop compares output from a strain gauged load cell within the loading chain with the desired load, which is set up via the controlling computer program, and stops the motor at the appropriate point. This type of system depends on the (continued) accuracy of the load cell calibration. Problems which might be encountered include load overshoot, due to time lag in the feedback loop (thus this might vary with loading rate), dealing with voltage spikes in the sensitive strain gauge system, and adequate safety features to prevent the indenter being driven down into the specimen in the event of a program crash, for example.

If absolute hardness values are to be calculated, then not only must the load used be repeatable, it must be capable of reliable calibration. For Vickers hardness tests there are standard (metallic) blocks of a certified hardness available, although the recent VAMAS survey on hardness testing of ceramics (1989) found that there was a considerable need for higher hardness standards to ensure proper calibration for testing harder materials. However, even if the suitability of the standards is accepted, calibration of the Oxford machine gave rise to a number of problems. The standard block normally supplied was too large to fit into the machine; although the top could of course be removed from the body of the machine and externally set up; the dash-pot is fixed to the lower part of the machine and can not be transported. It was therefore not possible to carry out normal hardness tests on the standard block to determine necessary adjustment of the counterbalances. In any case, the standards only apply to Vickers indentations. Knoop testing is carried out on the assumption that the set up of the machine which is correct for the Vickers indentation is also correct loading for the Knoop. In the case of counter-balanced machines, this is only



(a)



(b)

Figure 2.3 (a) Specimen mounting block and furnace, (b) Loading system and displacement monitor.

the case if the weights of the two indenter assemblies differ by insignificant amounts. For the Oxford machine, the weight of different indenters and shafts could vary by as much as 5g, which is significant in a load of 50g for example.

In order to solve the calibration problem, a strain gauged beam system was designed and built to measure the applied load from indenter and given weights. Such readings were then used to adjust the counter balance weights; to allow for the weight of each indenter when it was installed. The design and method of this system is described in appendix A. The accuracy of the system was calculated to be 0.4g. Occasionally, calibrations were checked by comparing indentations made on LiF, with indentations at the same nominal load on a Matsuzawa machine (Seiko Co.), previously calibrated using a standard test block.

In the loading arrangement of the Oxford machine, the vertical position of the sample surface in relation to the indenter tip depends on the sample height (and the length of the indenter shaft). It is therefore important that the load is constant over the possible loading distance. Whilst carrying out calibration tests as described above, and in appendix A, it became apparent that the load applied varied over the indenter height range by roughly 6g per mm of vertical travel. It was thought that this was probably caused by the difference in moment at the two ends of the lever arm, since the counter balance weights are in line with the arm whilst the indenter mass is concentrated in the molybdenum head ~95mm below. The problem was rectified by putting a weight above the pivot point of the lever (see figure 2.3b). The height of this was adjusted until it nullified the change in indenter load caused by movement of the indenter head. Such a problem would not of course occur on machines such as the Matsuzawa for example, which can adjust the sample surface to a certain distance below the indenter tip (usually defined by the focussing distance of the microscope lens). However such an arrangement is not readily compatible with high temperature testing due to thermal expansion etc.

2.3 Furnace System

An important feature of the Oxford machine is the provision of two furnaces with close temperature control, allowing both the sample and the indenter to be held at the test temperature prior to each indentation. Most of the hot hardness and indentation creep experiments at temperatures lower than 400°C use commercial room temperature microhardness testers, equipped with a standard microscope hot stage or similar arrangement (e.g. Gerk 1975, Henshall, Carter and Hooper 1988). Vacuum conditions are necessary to reach higher temperatures and also to prevent deterioration of the indenters, so dedicated apparatus is required. A few specialised machines are in use; the Nikon model QM is available commercially e.g. Hirai and Niihara (1978), machines also exist at the

National Physics Laboratory (NPL) e.g. Kollenberg (1988), at Cambridge e.g. Naylor and Page (1981), and in the USA e.g. Tokar and Green (1973). Okada, Yamanoto and Yoda (1987) also report this kind of test. (For earlier work at higher temperatures, mutual indentation of wedges in a furnace was often used, e.g. Atkins and Tabor 1966).

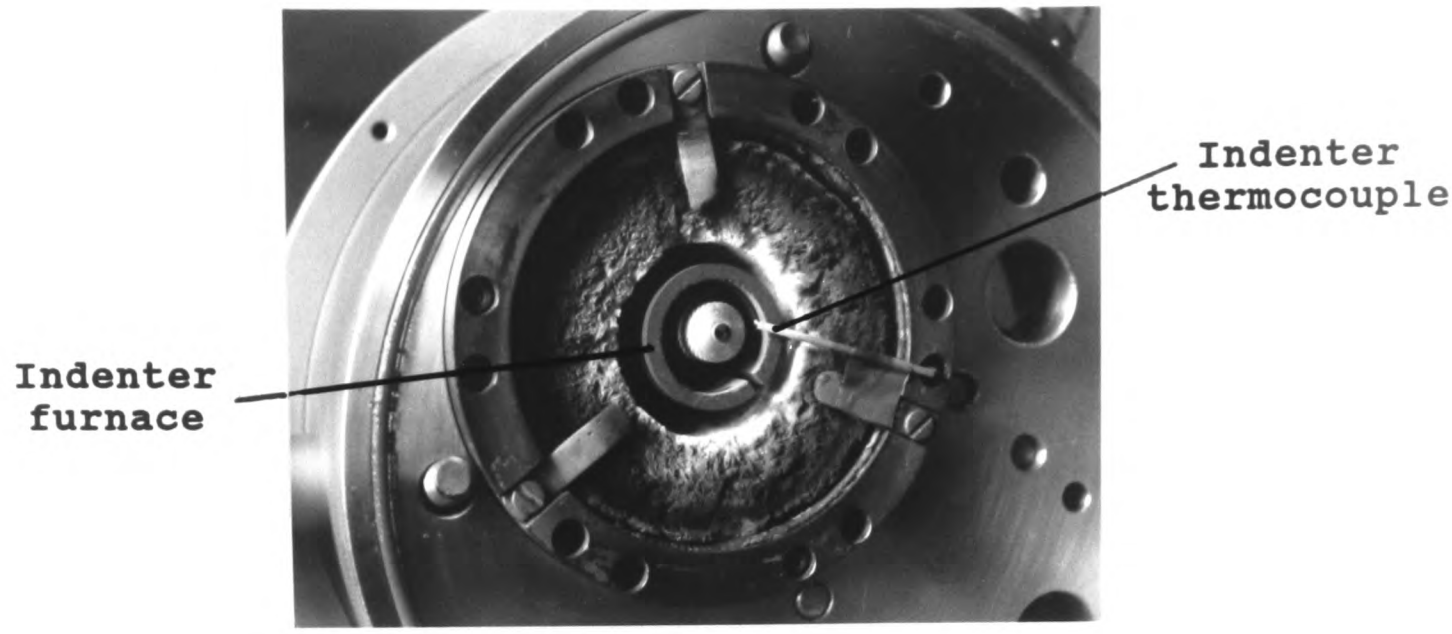
The Oxford machine uses two graphite furnaces (diameter 20 mm), one around the alumina sample platen (see figure 2.3a) and the other around the indenter (when it is in the "up" position). The graphite elements worked satisfactorily, and seemed more durable than the pyropholite / tungsten wire ones on the NPL machine. Very high currents, surging up to 20 amps were recorded during heating cycles. This caused some heating problems (e.g. melting plastic connection covers!), most noticeably on the body of the top furnace assembly, where the live input terminal of the furnace was unwisely put close to the dash-pot assembly causing the heating problem mentioned in section 2.4.

As well as the controller thermocouple shown in figure 2.3(a), the indenter and the sample both have a thermocouple in very close proximity, figure 2.4(a) and (b). The controller thermocouple controls the total power input to the furnaces based on a programmed hold temperature. The power split between the sample and indenter furnace is adjusted manually so that the temperature of the two is equalised. The temperature of both the sample and the indenter can therefore be controlled to within +/- 3°C of the desired value.

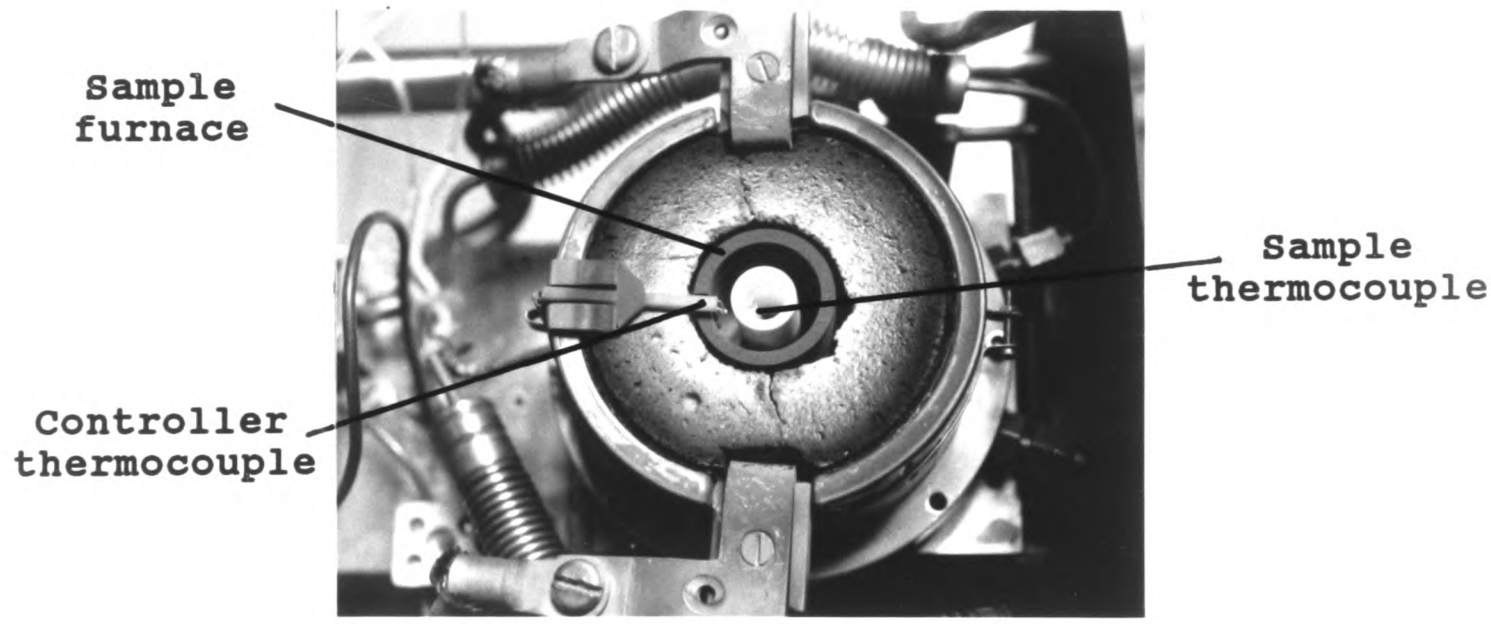
As labelled in figures 2.2 and 2.3, water jackets surrounded each furnace to contain the heated region. The system on the Oxford machine was not without drawbacks. During higher temperature experiments, the water within the jackets became quite hot. Unless purified water was used, scaling inside the thin bore pipes would lead to eventual blockage of the system, with potentially hazardous effects, so a closed temperature controlled water pump and reservoir was installed. It is advisable to have safety features incorporated in the design, so that the power to the furnaces will be automatically turned off in the event of a cooling water failure (blockage within the jackets or leak outside). The original design included a flow switch on the outlet side of the water flow. However, the water pressure was too small for reliable operation of this system. Installation of temperature trips in the form of switches mounted on the outside of the water jackets met with some, if not total success.

2.3.1 Effect of Indenter Heating

In order to investigate the effect of an indenter being at a lower temperature than the sample, some creep experiments were carried out in which no current was allowed in



(a)



(b)

Figure 2.4 Furnaces and thermocouples
(a) Upper (indenter) assembly,
(b) Lower (sample) assembly.

the indenter furnace (i.e. a power split of 0:100), thus mimicking the conditions of test carried out on microhardness testers equipped with only a hot stage. The results were compared with experiments carried out at the same sample temperature, but with a heated indenter. These experiments were carried out on MgO since a "no indentation creep region" had been identified in the temperature range 750°C to 1050°C. (The physical implications of this will be discussed in chapter 7). The results of experiments in the range 600°C to 1175°C with and without a heated upper furnace are shown in figure 2.5 (a) and (b), and give conclusive evidence of the importance of the temperature of the indenter in the first few moments of indentation.

The short time hardness values and creep characteristics of the tests not using the upper furnace correspond quite closely to those obtained for tests with a heated indenter (and sample temperature) at the (lower) temperature indicated by the indenter thermocouple. As the indentation time is increased, the indentation size for most of the samples tends to a value characteristic of the sample temperature hardness, presumably as the indenter and material surrounding it heat up towards the sample temperature.

Quite how the local cooling affects the data obtained will obviously be sensitive to the details of experimental technique and the equipment used, as well as depending on the material in question. Heat exchange between the indenter, the sample and the surroundings will be both radiative and conductive. The temperature of a cooler indenter will be raised by heat radiation coming both from the sample directly below it, and whatever is heating the sample itself. In the Oxford machine, the up position of the indenter holds the tip 7mm above the sample surface and the top of the surrounding furnace. The lateral distance from the sample furnace walls will vary depending upon the position of the sample which is being indented, since the whole bottom section (alumina sample tower, furnace and water jacket) is moved via the micrometer controls. It is probably this which causes the variation in temperature recorded by the indenter thermocouple (see table 2.1).

Once a cooler indenter is in contact with the specimen surface, the indenter (and indenter head) start to heat up and locally reduce the temperature of the sample at that point. The temperature of this region at any particular time during the test will depend on the rate of heat flow to it from the surrounding specimen, compared to the heat flow away through the indenter. Ignoring radiative heating, it would be interesting to investigate the effect of changing the indenter stone from diamond to sapphire which has a heat conductivity $\sim 1/5$ compared to diamond. Indenter heads and shafts are metallic (molybdenum head in the case of the Oxford machine), so that heat will be conducted quite rapidly away from the hot zone by this means.

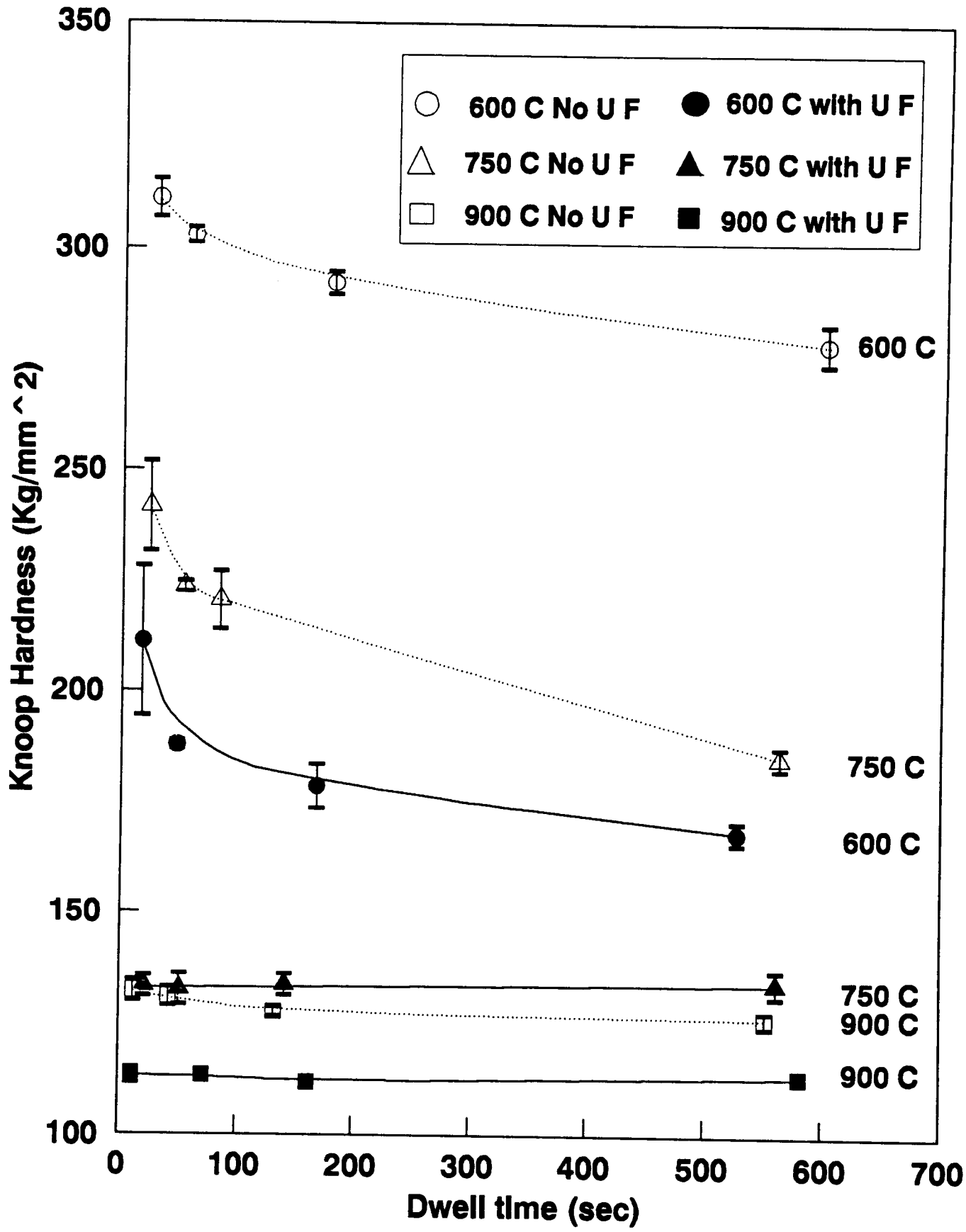


Figure 2.5(a) The effect of upper furnace heating on the variation of <110> Knoop hardness with dwell time, in the temperature range 600 C to 900 C, on (001) MgO.

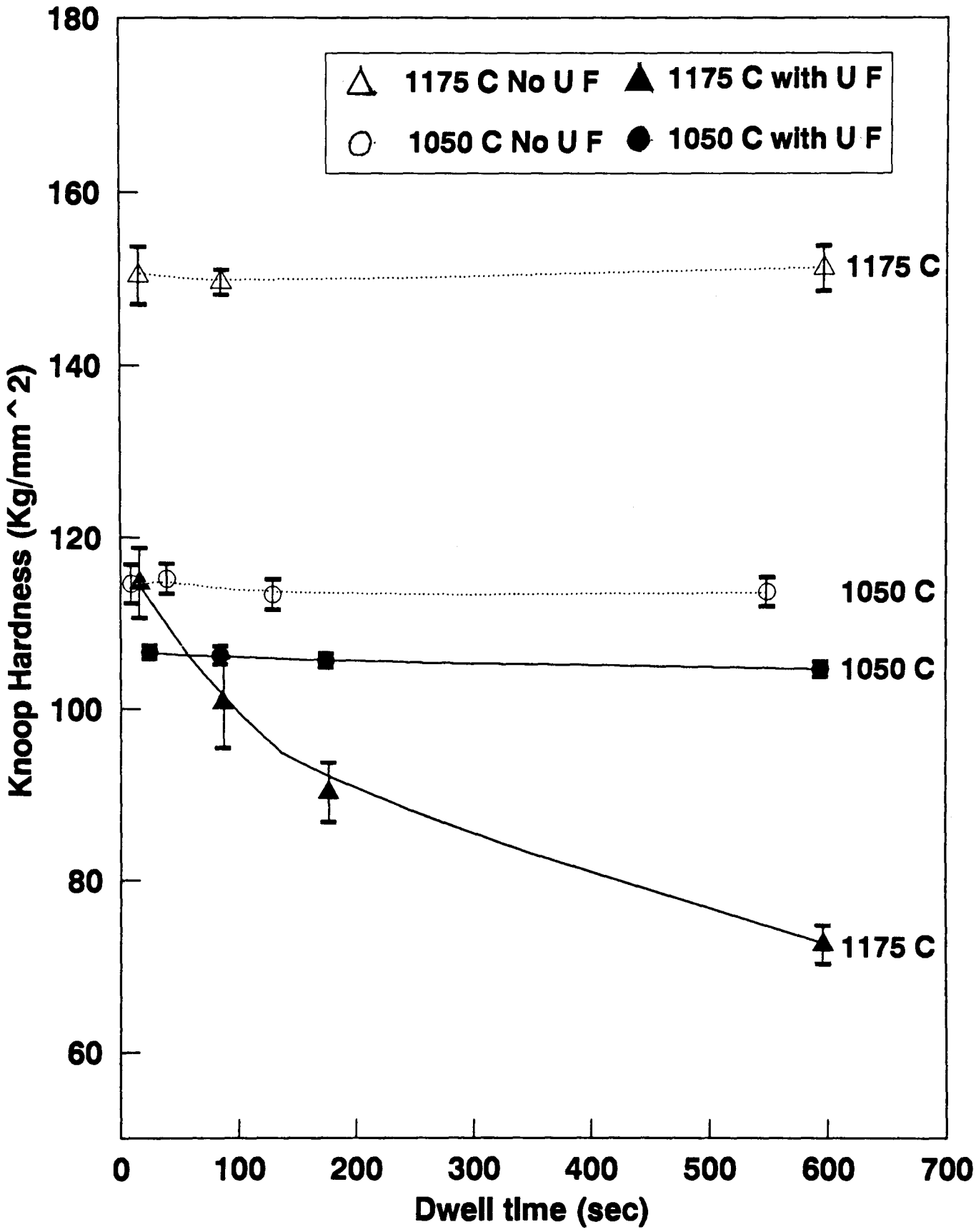


Figure 2.5(b) The effect of upper furnace heating on the variation of <110> Knoop hardness with dwell time, in the temperature range 1050 C to 1175 C, on (001) MgO.

Bulk sample temperature +/- 3°C	Indenter "up region" temperature with with no upper furnace heating (°C)	
	Average	Range
1175	927	915-935
1050	841	837-848
900	715	704-728
750	591	583-600
600	475	464-483

Table 2.1. Thermocouple readings during the experiments without an upper furnace.

Some authors mention that the indenter tip was kept in close contact with the specimen surface before testing began (Henshall et al (1988) - 30 minutes, Okada et al (9187) - 5 minutes). This would have the effect of heating up the indenter assembly and reducing error, but even so, it is unlikely that the indenter will be at the sample temperature when it first touches the surface. Experiments with the sample at 600°C and no upper furnace heating (indenter thermocouple 475°C), showed that after 30 mins with the tip held just above the surface of the specimen, 60 second indentations made straight away were slightly bigger than those made before the 30 min heating, but still a lot smaller than the true 600°C results using a heated indenter.

Results may also be sensitive to the delay between each indentation i.e. how long since the indenter was in contact with the hotter body. A time record of the experiment carried out at a sample temperature of 900°C suggests that intervals of ~ 3 min between indentations (i.e. holding the indenter at ~715°C for that time) may affect the size of the indentation subsequently produced even if the previous indentation was a long one.

The results shown in figure 2.5 have implications for the interpretation of data obtained on microhardness machines equipped with hot stages for the sample but without facilities to control, or at least separately record, the temperature of the indenter. The investigation was prompted by the apparent discrepancy between the Oxford results and the results of apparently similar experiments carried out by Brookes, Burnand and Morgan (1975). That investigation found creep at 727°C and 1047°C for the same Knoop orientation and MgO crystal face as the results shown in figure 2.5. The authors were using a hot plate on a Leitz miniload (temperature control and measurement about ± 20°C), but had introduced a pyrophillite extension to the normal indenter arrangement so as to reduce temperature losses (Brookes 1990). The first indentation in a series made at a given temperature was not used in their measurements. However, whilst material dependent factors can not be ruled out (e.g. differences in impurity influenced behaviour), it seems likely that the "true" creep behaviour was masked by the effect of the progressive heating up of the cooler indenter and surrounding material. Thus the dominant variable during their creep tests, at least for the higher temperatures, was not the variation in loading time, but the variation in local temperature which was the result of varying times of contact. Such effects should therefore be considered when evaluating data calculated from higher temperature hardness tests (e.g. creep activation energies - Atkins and Tabor 1966, Kumashiro, Nagai and Kato 1982, Sargent and Ashby 1989).

2.4 Loading Rate - LVDT and Dashpot

In investigations of indentation creep it would be especially advantageous to have a continuous readout of the indenter position with time during a test, as in the nanoindenter (Pethica 1982). An attempt was made to link an LVDT (linear voltage displacement transducer) to the movement of the indenter via the balance beam. The photographs in figures 2.2 and 2.3 show the LVDT arrangement in place, and figure 2.6 shows a schematic view of the LVDT and indenter beam system. As the loaded indenter was released and travelled down, the counterbalance end of the indenter beam would move up and push up the counterbalance end of the LVDT arm. This would result in the LVDT slug moving down and a displacement being recorded. The output from the LVDT module was processed using an analogue to digital converter system which was interfaced to a BBC computer. (During an indentation, a "fast" subroutine in machine code sampled and stored the LVDT readings). The LVDT had a linear region of travel of 1.27 and the response curve is shown in figure 2.7.

Whilst the system was utilised for a number of experiments (and enabled estimates of loading rates to be made), it was eventually abandoned due to operational difficulties. The short linear stroke of the LVDT meant that the system had to be tuned for each sample (by altering the vertical position of the LVDT / indenter beam connection). At higher temperatures, machine expansion (and thus alteration in the relative height difference between indenter up position and sample surface) sometimes rendered even this tuning invalid. Unless the LVDT slug was accurately aligned, friction between the slug and the LVDT channel walls could give anomalous results.

During work on developing a the LVDT system, it became apparent that the rise in temperature of the top assembly during high temperature work altered the viscosity of the oil in the dash-pot and hence the loading rate of the indenter, producing strain rate variations in experiments at different temperatures. Attempts to find a constant viscosity oil which would have ensured a constant loading rate were not very successful. Initially rotary pump oil was used, but when the problem was discovered this was replaced by Shell Tellus 37 (a hydraulic oil). Extension of the upper cooling circuit to include a coil round the dash-pot alleviated the problem to some extent, but, at medium temperatures, the cold cooling water necessary in the furnace water jacket actually lowered the temperature of the oil, so that the indenter travelled at a slower rate. Not until the cooling coil was on separate cooling circuit (of which the flow could be restricted at will) was some control over the dash-pot temperature and hence loading rate gained.

Little is known of the effect of the dynamics of hardness tests on the motion and final position of the indenter, and hence the perceived hardness. Hutchings (1990) tried to

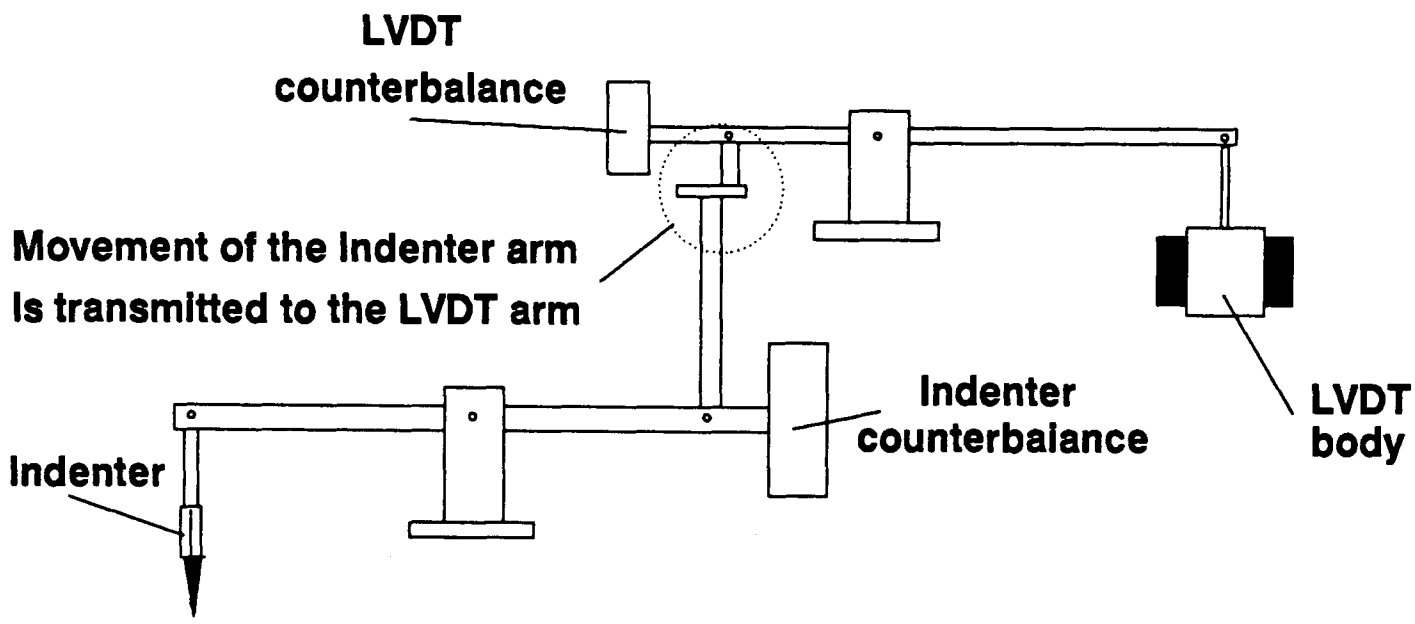


Figure 2.6 Schematic diagram of the LVDT and indenter beam system

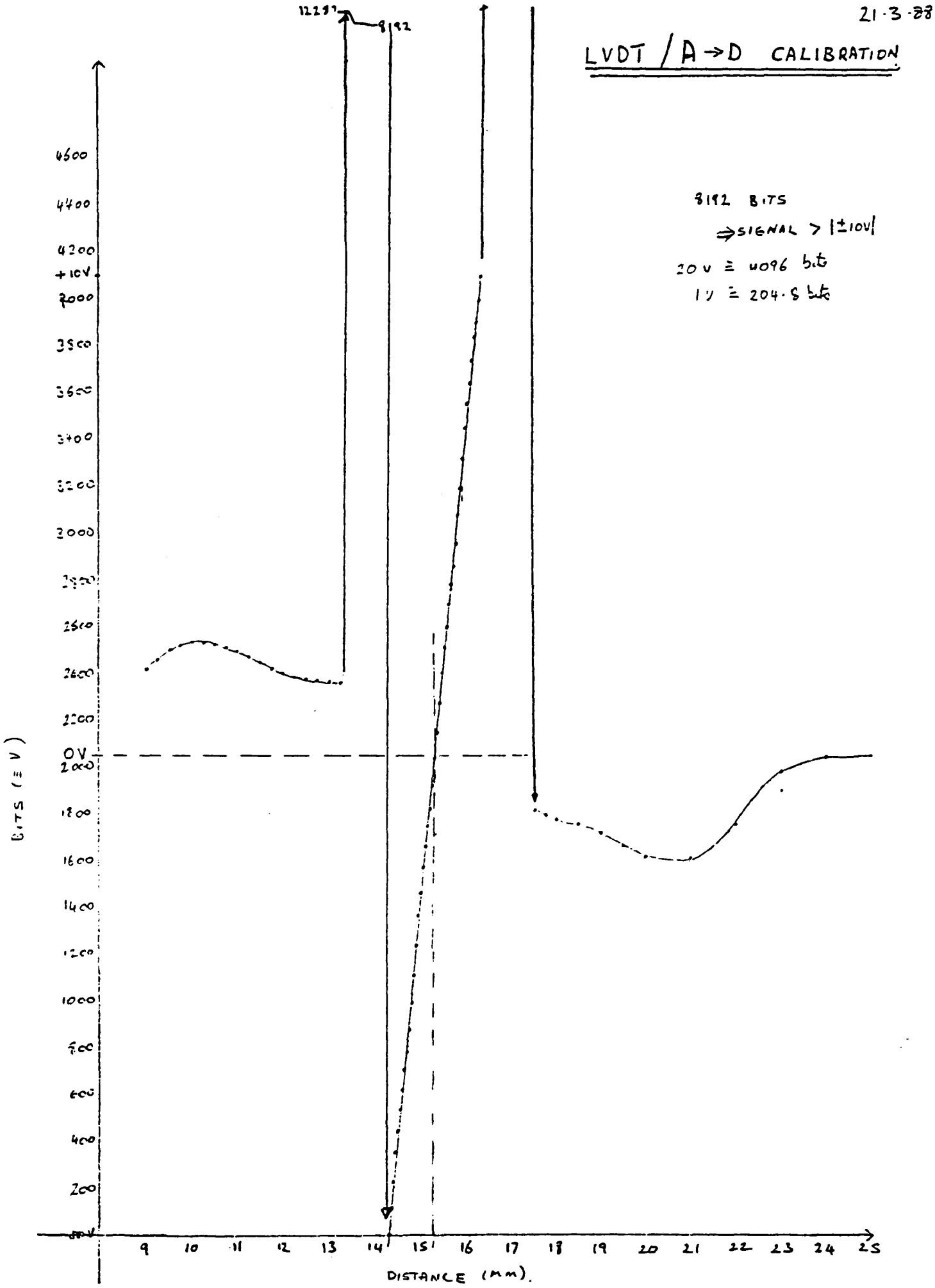


Figure 2.7 A plot of the LVDT response.

investigate the problem by solving the equation of motion for the whole system, assuming the material to be strain rate insensitive throughout. However the model became analytically intractable as the compliances of the various components were added. He concluded that the effects were extremely small for typical realistic loading rates. (The effect on real materials could be checked by indenting a material with a known low rate sensitivity, e.g. a very hard precipitation strengthened alloy, at different loading rates). With the Oxford machine tests at 450°C on an MgO sample with very varied loading times (3 second loading time to 30 second loading time) showed no measurable difference in hardness. It is therefore concluded that any variation in results caused by variation in indenter loading rate is probably insignificant for this work.

3. HARDNESS MEASUREMENT AND TESTING VARIABLES

The hardness values obtained from indentation testing are usually the main, and sometimes the only, result required from the procedure. The basic definition of hardness "number" (which was outlined in first chapter of this thesis), depends upon the measured size of the impression left after the indenter has been removed. It must therefore be a high priority to determine both the optimum methodology, and the limits of accuracy and precision which are implied. At the start of the section 3.1 is a quote from a comprehensive review of Knoop hardness testing on hard brittle substances (Thibault and Nyquist 1947), written soon after the test began to become established. It was an attempt to suggest standard procedures, and thus reduce the lack of agreement on the "true" hardness number of particular substances, whilst suggesting the factors which might have led to these discrepancies. Such matters are still of concern for all indentation testing, particularly for microhardness testing, where the smaller size of indents leads to increased vulnerability to certain measurement errors. Indeed a recent VAMAS report (1989) was still attempting to find and assess the repeatabilty of such measurements for ceramic materials. Whilst self-consistent comparative values within one testing facility are more easily obtained than universally comparable values, it is the latter which must be the overall aim, if the test is to be fully utilized.

This chapter looks first at the optical measuring conditions and presents some investigations into the variation of indent size obtained under different illumination conditions and by different observers. Fracture around indentations is then discussed, before commenting on other factors which might effect the size of impression obtained under the same nominal conditions.

3.1 Optical Viewing Conditions

> "Of this we are certain: The measurement of Knoop indentations, made in hard substances under low loads, is the most exasperating type of microscopy which we have ever experienced. Harassed by the indistinctiveness of the indenter terminations which actually seem to oscillate while being examined, and the realisation that the utmost precision must be obtained, we have never been able to spend more than a few hours a day measuring Knoop impressions."
>
> Thibault and Nyquist (1947)

The quote above, although perhaps a little extreme, graphically outlines the difficulties of measuring optically the size of indentations. These difficulties are most severe with Knoop indentations, but are relevant to other indenters too. In Knoop indentations the angle in the long dimension is very acute, particularly as elastic recovery of the short diagonals may cause the unloaded impression to have an even sharper angle at the long tip. Thus the tip of the long diagonal tends to fade away rather than end abruptly, when examined under high magnification. Using SEM is a possibility but is very subject to measurement errors (scan distortions etc.) (Sargent and Page 1985) . Image analysis was tried by Blau (1983), but not found to be generally useful, although he felt that the system might have potential in the future. As discussed in section 2.5, the only way to avoid the size measurement problems is to directly measure the depth of indentations as they are made. However, this is unlikely to become the standard for some time and has problems of its own, especially detecting the point of contact with the surface. With optical analysis the resolving power used, the visual acuity of the observer and the indentation contrast may affect the measurement of the indentations considerably (Tarasov and Thibault 1947).

The indentations may be measured using the microscope attached to what ever indentation apparatus is being used, (for hot hardness this is usually a long focus, and therefore a lower resolution, lens), or removed and measured using a separate research quality microscope. The latter is likely to provide a more precise measurement of the indentation; but is more time consuming because an accurate record of the sample indentations is required to allow the indentations to be re-located in the new surroundings. Whichever microscope system is used, a micrometer of some sort is used to size the indentations. Early researchers had optical lens of far poorer quality than those now available, and thus they recommend the use of oil immersion (e.g. Thibault and Nyquist 1947). However dry lens are now used, with perhaps monochromatic lighting or differential interference contrast.

Indentations made for the work described in this thesis were carefully mapped onto a sample chart based on the readings of the translation controls (see figure 2.2) as the experiment was carried out. Each sample was then removed and the indentations measured with a curtain micrometer, under conditions of Nomarski interference contrast, and at magnifications of either x1000 or x400, if the indentations were too large to be measured at the higher magnification. The curtain micrometer was calibrated using an inscribed micron scale.

In order to assess the scale of observer errors (i.e. those caused by eye-sight, prejudice or use of interference contrast), a number of sets of indents were measured by

two other observers. So that any any subconscious "adjustment" was avoided, none of the operators knew the results of the other at the time at which they made the measurements. The indentations were on cleaved (001) faces of MgO, thus, as well as visual decisions, judgement was needed in deciding if any of the indentations were unacceptable and should not be included. By the time that these measurements were taken the author had considerable experience in hardness measurement and "case" history as to which indentations were acceptable, but could have been prejudiced towards a "sensible" result (e.g. longer time indentations should be larger). All the indentations were measured with her right eye which is slightly short-sighted. Observer 1 was a 4th year materials science undergraduate project student, with some experience of microscopy techniques and hardness testing. All measurements were taken with his left eye which is short-sighted, needing a lens of strength 1.75D for daily wear (but not close up work). Observer 2 was a graduate research physicist (and therefore trained to observe), but with little experience in microscopy or hardness testing. He is severely short-sighted, needing glasses for reading and writing. The observers were shown how to use Nomarski (and the basis of the hardness test explained as necessary), but not given any explicit instructions as to which indentations should be discarded. A range of indent sizes (i.e. indentation temperatures) in the <110> orientation were included in case size made any difference to the conclusions, and <100> orientation room temperature indentations were considered to assess the effect of the pile up at the ends of the short diagonal on the scatter and/or magnitude of the measured length. The results of this investigation are shown in table 3.1 in terms of mean diagonal and standard deviation associated error for each set of indentations at the same time and temperature. (All the indentations above room temperature had been made on one sample with indentation diagonals ranging from about 200μm at 600°C to 120μm at 150°C. Each orientation of room temperature indents had been made on a different sample.)

The results for each set of indentations were indistinguishable between each observer, suggesting that visual acuity does not play a significant part in discrepancy between sets of hardness results, even for the small more highly fractured room temperature indentations. (The short diagonal measurements did not show any significant variation either). There was occasional variation in the number of indentations within a set which were considered acceptable, but only in two cases did this vary by 1 more or less than those chosen by the author. The investigation thus leads to the conclusion that under identical optical measuring conditions, the measured diagonal lengths are not affected by the observer. This is a more positive result than that suggested by Thibault and Nyquist (1947), and also that of Brown and Ineson (1951) who found considerable differences in measurements of the same indentations by different observers. The VAMAS survey (1989) in which observers at the National Physical laboratory (NPL) measured specific

Sample	Time	Observer 1			The Author		
		D	SD	N	D	SD	N
600°C	90	185	2.4	4	184	7.4	5
<110>	120	193	1.3	5	195	0.5	5
	240	198	2.3	5	200	2.7	5
	600	205	2.2	4	206	1.5	6
525°C	95	163	2.8	6	163	3.3	6
<110>	120	171	2.3	6	173	1.0	5
	240	178	4.1	5	180	3.7	5
	600	187	2.4	5	190	1.6	6
150°C	150	118	3.5	5	120	1.9	4
<110>	180	120	3.7	4	124	1.1	4
	240	124	3.4	3	124	1.2	3
	600	126	3.9	6	127	1.5	5
RT	70	91	5.0	5	95	4.4	5
<110>	120	96	2.6	4	99	1.3	5
	180	97	0.8	3	99	2.6	4
	600	98	1.8	5	101	0.8	4
RT	60	124	3.8	3	126	4.7	4
<100>	120	127	4.3	4	125	5.5	5
	240	129	3.0	4	130	2.7	4
	600	126	6.5	6	132	2.8	3

		Observer 2			
600	90	183	7.6	5	
<110>	120	194	1.6	5	
	240	199	3.2	5	
	600	206	1.9	6	

D is the mean diagonal calculated from N measurements, μm.

SD is the standard deviation of the mean.

Table 3.1 Knoop hardness measurements on (001) MgO, as measured by different observers using Nomarski interference contrast.

indentations in two kinds of alumina ceramic, which were then measured by other laboratories, concluded that individual bias did occur (probably due either to different illumination conditions and/or different criteria for identifying the ends of the indentations), but could not find consistent trends with the eye-sight or age of the observers.

Observer 1 also measured the 600°C, 525°C and 150°C indentations without Nomarski contrast. Although these conditions are more taxing to the eye and look less distinct, it is interesting to note that the results showed no difference compared to the same indentations measured with interference contrast This suggests that, whilst the use of interference contrast is to be recommended since it is less tiring for the operator, the results obtained are not affected if such facilities are not used.

The curtain micrometer is a good measuring device to use since it is not possible to see what length is being recorded whilst looking down the lens and adjusting the position of the "curtains". This helps to prevent knowledge of the expected value affecting the length recorded. Measuring the same diagonal ten times gave a value which varied by 0.16μm (for a diagonal length of 89.34μm) suggesting that this is the approximate precision in measuring a set length for the results quoted in this project (ignoring any other errors).

No investigation was carried out on the effect of the resolving power of lens used for the results quoted in this thesis. All indentations were measured at x1000, or x400 if the indentations were too large to fit in the field of view at the higher magnification. However, if comparing results with those of other authors, it should be noted that Thibault and Nyquist (1947) found that the higher the resolving power of the optical system, the longer a given indent will appear to be. Presumably this was because a thinner part of the tip can be distinguished from the surrounding surface.

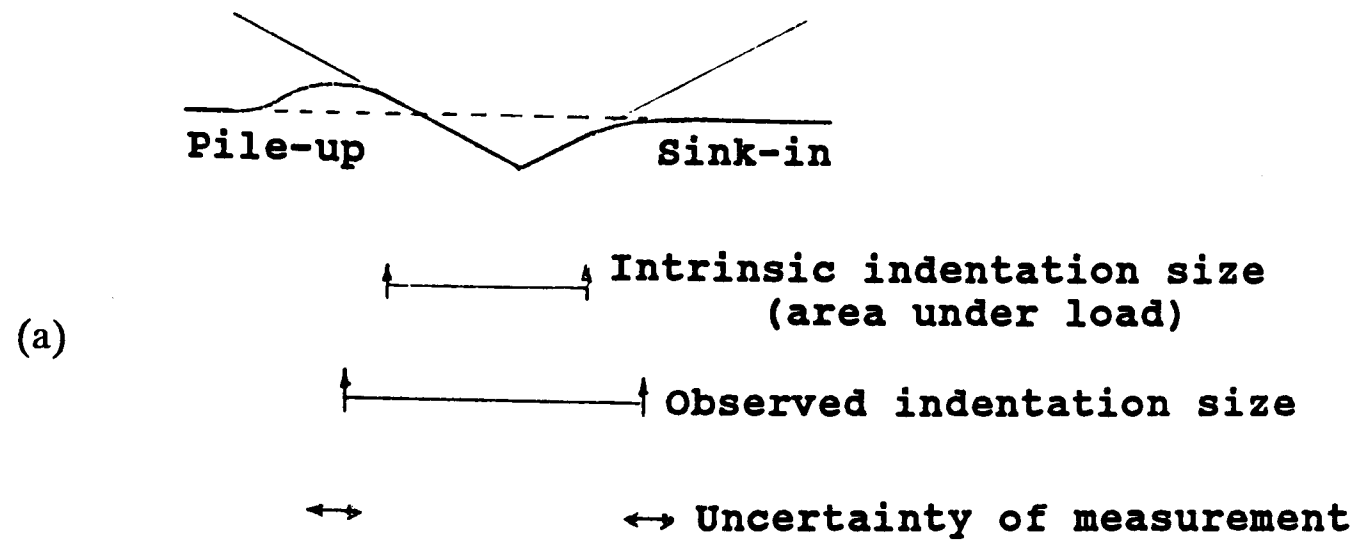
3.2 Pile up, Sink in and Elastic Recovery

"True" hardness is generally taken to be the pressure over the area of contact of the indenter with the specimen whilst the indenter is fully loaded (or projected area in the case of Knoop indentations). However hardness and microhardness measurements are measured from the observed size of the impression (calculated from one or two diagonals) *when the load has been removed.* Thus the measured size depends not only on the response of the material under load as the indentation is made, but also on how the impression changes when the load is removed. Sargent and Page (1985) described effects that change the final measured size and shape of the indent as "extrinsic" factors. These include the surface topography of displaced material, elastic recovery and measurement errors (which have been discussed above).

In ductile materials, material displaced by the indenter often piles up round the edge of the indented area and supports some portion of the load. If the ratio of flow stress to elastic modulus is high, or strong work-hardening occurs, then the material may be displaced radially, sometimes forming sink-in (Sargent and Page 1985). This alters the shape of the indent, so the actual area supporting the load is mo longer that calculated from the diagonal; thus the "intrinsic" hardness is affected. (As reviewed by Rowe, Smethurst and Downing (1982), a number of authors have proposed various corrections to allow for the bulge in hardness impression which is caused by pile up around Vickers indentations). However, there is also an extrinsic effect, since it is often difficult to determine the point at which the pile up (or sink in) no longer supports the load. The measured area is determined by a change in curvature of the surface, and depends on the effective numerical aperture of the measuring system (Tabor 1970). Figure 3.1(a) summarizes such effects (after Sargent and Page 1985).

Elastic recovery is the "spring back" which occurs when the loaded indenter is removed from the surface of the sample. It is caused by the elastic strains around the indent, and will occur in the depth of the indent as well as in the observed dimensions and shape in the surface (figure 3.1(b)). Elastic recovery will be greater for a high flow stress i.e. in the plane of the surface and for a given orientation, θ, of the indenter, the magnitude of the elastic recovery strain is expected to be given by the ratio of lateral compressive stress induced by the loaded indenter, and the effective Young's modulus in the plane of the surface; both quantities vary with θ in anisotropic materials (Sargent and Page 1985). In isotropic materials only the shape of the indenter will effect any differences in response around the indent. In Vickers tests more elastic recovery is expected to take place across the four facets, than in the line of the diagonals. For Knoop indenters very little compressive stress is expected along the line of the long diagonal and therefore little elastic recovery is expected in that diagonal whatever the indenter orientation. However, the short diagonal is much more effected by elastic recovery. Marshall, Noma and Evans (1982, through Sargent and Page 1985) estimated Young's modulus from the width contraction of Knoop indentations and the flow stress from the hardness (i.e. long diagonal).

Blau (1980 and 1983) noted that the Knoop test is particularly structure and orientation sensitive, and is doubtful about the supposed lack of elastic recovery along the long diagonal. He proposed a modified method for calculating the "Knoop hardness" using the lengths of both diagonals to find the projected area. This method seems to be concentrating on the projected area of the *unloaded* indentation, rather than for the material under load, and therefore is not helpful.



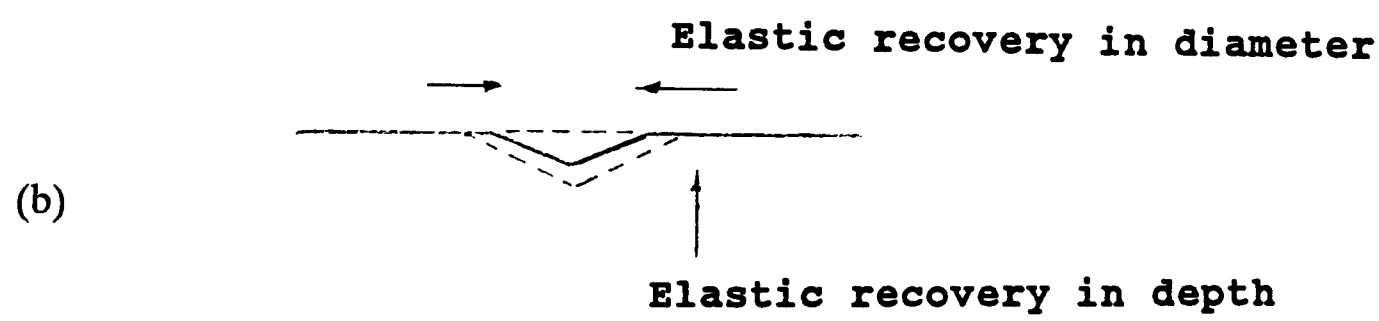


Figure 3.1 Extrinsic effects on indentation size and measurement: (a) Topographic effects due to pile-up and sink-in. (b) Elastic recovery effects shown in the absence of topographic changes (after Sargent and Page 1985).

3.3 Indentation Fracture

The fact that indentation of brittle materials may produce cracks around the indentation as well as a permanent impression has already been touched upon. Indentation fracture studies allow cracks to be viewed not as cause of perturbation of hardness measurements, but as a new possibility for toughness determination (Guille and Matini 1988). Microhardness indentations may also be used as a means of producing controlled localised fracture e.g. Burnett and Page 1984; Hirsch, Roberts and Samuels 1987. This thesis does not contain any work on indentation fracture, but merely comments on the existence of cracks around the indentations in MgO and Ge where appropriate. However, since indentation fracture is an integral part of indentation of brittle materials, a brief review is given below.

The extent of radial cracking around indents made with "sharp" indenters like Vickers and Knoop was first recognised by Palmqvist in 1957 (through Pontons and Rawlings 1989a). Lawn and co-workers published their seminal works on using indentation fracture to find fracture toughness in 1975 (e.g. Lawn and Wilshaw). The types of idealized cracks which might form around an indent are shown in figure 3.2 (after Cook and Pharr 1990). In a comprehensive review of the current Vickers indentation fracture test and theoretical treatments, Pontons and Rawlings (1989a and b), showed that there are two classes of model which are used to calculate the fracture toughness from the measured crack lengths. The first assumes that cracks form are well developed radial-median ("half-penny" shaped) cracks. The second class assumes that radial Palmqvist cracks are formed. However, the "accepted" initiation sequence of indentation cracks has recently been challenged by a paper detailing the direct observation and analysis of indentation cracking in two normal glasses, two anomalous glasses and seven crystalline materials (Cook and Pharr 1990). Using an inverted tester, which allowed simultaneous viewing of the fracture process and measurement of the indenter load and displacement during contact, they found that the initiation sequence of cracks (cone, radial, median, half-penny and lateral) was materials dependent. Importantly, normal glasses (soda-lime), which have previously been used as a model material, behaved differently to many of the crystalline materials and the anomalous glasses. In crystalline materials radial cracks formed almost immediately on loading of the indenter, in anomalous glasses at a somewhat greater load, but in normal glasses during unloading. The authors concluded that simple fracture mechanics models, based on subzone initiation morphology, are able to describe lateral crack extension because the model is correct in its material dependence but in sensitive to the details of the crack morphology. They had direct evidence that surface traces of cracks observed at indentation contacts are those of radial cracks, rather than the median-nucleated half penny cracks, which had previously been proposed (at least for loads < 40N).

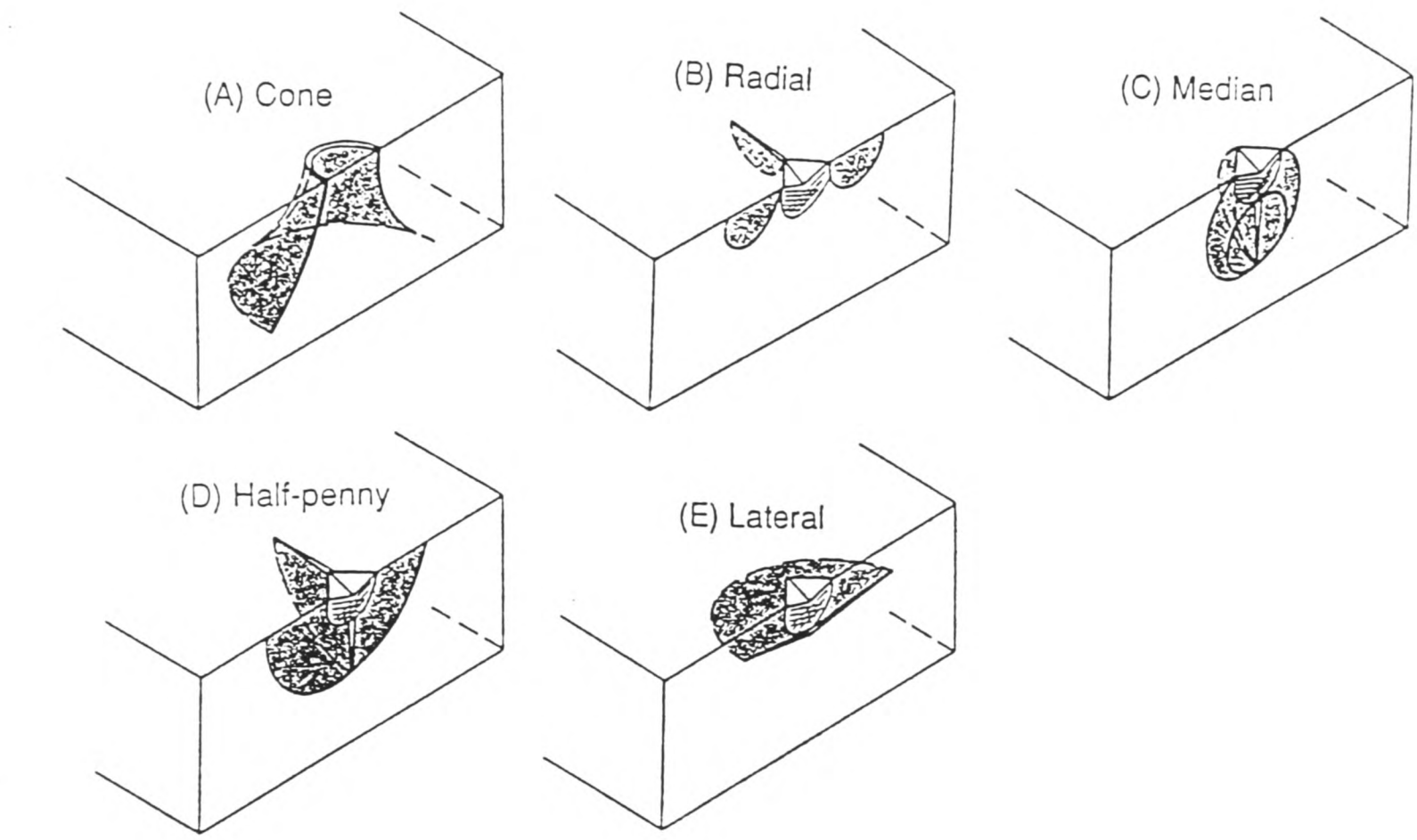


Figure 3.2 Idealized indentation crack morphologies (after Cook and Pharr 1990).

It is worth noting that the VAMAS round robin survey (1989) found that there was considerable error in crack length measurement when the results from different labs were compared. This was perhaps due to lack of skill / experience in adjusting the illumination level, as well as uncertainty in defining the end of the crack.

3.4 Environment and Surface Effects

Numerous studies have shown that the environment can markedly affect the surface mechanical properties of non-metallic materials, but it is a controversial area because of the difficulty of reproducing the effects. The Soviet scientist Rebinder was a pioneer in this field of chemo-mechanical phenomena (1928, through Westwood, Ahearn and Mills, 1981) and such behaviour, paticularly that associated with adsorbed surface active species, is sometimes categorised as being due to "Rebinder effects". Adsorbed water, ζ-potential, prior surface treatments and oxide or other surface layers may all influence hardness, as well as cracking, size effects and/or features revealed by subsequent etching, around the an indentation. These effects are of technological interest because of the implications for wear and drilling of ceramics.

The effect of the chemical environment, and specifically the effect of adsorbed water, is often ignored in indentation studies. In 1965 Westbrook and Jorgensen looked at the effect of water adsorbed from the ambient atmosphere on the indentation hardness of a number of ionic, covalent and metallic solids, including Ge and MgO. The loads used were between 3g and 25g, and were chosen to give indentations of 1μm depth. Comparing the time-dependence of hardness of samples in the "as polished and exposed to air" condition, with that of samples heated, quenched and exposed to Toluene (to prevent re-adsorption of water), all the non-metallic materials gave a time-independent hardness in the "dry" condition, whilst in the "wet" condition they showed a substantially lower value of hardness which was time-dependent. (The most electronegative polar face of zinc blende and wurtzite structure materials showed up to 30% difference between "wet" and "dry" values). Non-aqueous adsorbates gave hardness levels which were the same as those obtained on the dry samples. Tests on LiF showed that the amount of creep decreased with increasing temperature, vanishing at around 50°C, (hence the term "anomalous" creep), but much higher temperatures were required to eliminate the effect on the hardness level. Tests on alumina indicated that "wet" and "dry" values of hardness were the same for indentations of about 1.5μm depth and above. This is further proof that the effects observed are due to surface effects from the water.

In general agreement with the results above, Hirao and Tomozawa (1987) found that various SiO_2 glasses did not show indentation creep when exposed to non-aqueous

liquids but did creep in air and water (Knoop indentations). The load needed to initiate cracks around Vickers indentations was seen to depend on the environment in a similar fashion, i.e. depending upon the environment in which it was measured, and decreasing with loading time, only in the presence of water. It was concluded that these effects were caused by water diffusion into the glass during indentation. (It was also noted that the hardness increased with decreasing load for a given environment). In the same year, work published by Czernuszka and Page (1987) found that the Knoop hardness of two glass-bonded ceramics varied with the number of carbon atoms in the alkyl group of a series of alcohols (N_C) in which the test was submerged. In all cases the maximum hardness was slightly less than that recorded under vacuum, but considerably less than that under water or water-containing environments.

Although it is generally agreed that the chemo-mechanical effects are due to changes in the near-surface plasticity of ionically and covalently bonded materials, the mechanisms are still somewhat unclear. Westbrook and Jorgensen (1965) concluded that the water is present in two states: strongly bonded water which nevertheless affects plastic indentation, and less strongly bound water which is sufficiently mobile to move from one bonding site to another during the time of the experiment and (by some means) permits additional deformation. In a later paper, Hanneman and Westbrook (1968) concluded that three mechanisms survived as possible explanations for the observed adsorption induced changes in microhardness and dislocatation properties in non-metallic materials. Namely, adsorbate-point defect interaction (restricted to crystalline materials), adsorbate alteration of the surface and near-surface bond strength, and lubrication-friction effects. The last of these was considered to be the best possibility. Bull and Page (1989) showed that low load indentation hardness (and friction behaviour) of MgO are dominated by the effects both of chemisorbed and physisorbed water. In a review in 1981, Westwood, Ahearn and Mills concluded that chemo-mechanical effects are a generic type of phenomena without any universal mechanisms but rather several basic mechanisms, depending on the material concerned.

Other reported effects related to hardness testing are the photomechanical effect and the electromechanical effect. The photomechanical effect, first observed by Kuczenski and Hochman (1957, through Westwood and Macmillan 1973), concerns the decrease in hardness of Ge and other semiconductors with increasing intensity of incident light. The electromechanical effect seen by later authors, is the same effect caused by applying an electrical potential between specimen and indenter. Published data on these effects are inconclusive however, and it is possible that adsorbed species are also responsible for these changes in hardness.

Chemo-mechanical phenomena have not been experimentally investigated within this thesis. In order to eliminate water adsorbed surface layer effects as far as possible, all the room temperature hardness values which are reported were obtained on samples which had previously been heated in vacuum. It is not considered that the photomechanical effect would lead to any significant differences in recorded hardness, but in experiments carried out in the Oxford machine, the sample has no incident light apart from red glow from the furnaces at the higher temperatures.

3.5 Effects of Load scaling - ISE

Although the definition of hardness as load per area implies no change of hardness with increased load for pyramidal indenters, deviations from this geometrical similarity has been reported by many authors (Burnand 1974). In general, the measured hardness increases as the load decreases below about 100g. This is often referred to as the indentation size effect, ISE (e.g. Farges and Degout 1989).

ISE can be expressed empirically by the relation

$$L = kd^n$$

where L is the load, d is the indentation diagonal, k and n are constants. n may be regarded as the ISE index. If n = 2 then the hardness is independent of the indentation size. For metals, n lies between 1.92 and 2.00, thus hardness weakly increases as the size of the indentation decreases. Ceramics typically have a sligthly smaller n, e.g. Si ~1.8 and SiC ~1.7 (Sargent 1979). The reasons behind the size effect are still subject to debate, although it is now established as a "real effect". (It should be remembered however, that surface effects as detailed in the preceding section could confuse investigations into ISE. For example, n>2 is very unusual, and is probably due to softer superficial layers on the specimen surface (Sargent 1989)). Such instruments as the nanoindenter enable the phenomena to be investigated by measuring both the depth of the indentation and the area (Pethica, Hutchings and Oliver 1983).

The implication of an ISE index which is not 2 is that the deformtation has a definate scale. The simplest explanation (as described by Sargent (1989) is one that was originally advanced by Mott, that finer slip on more closely spaced slip planes requires higher glide stresses. Work-hardening may be more intense in small volumes (Pethica, Hutchings and Oliver 1983). Upit and Varchenya (1973) concluded that the ISE in ionic and metallic single crystals results from the size dependence of the properties of dislocation

loops formed by the indentation deformation, (hence the disappearance of ISE in polycrystals since the grain boundaries provide a barrier to the movement of dislocations).

It is possible to propose geometrical correction factors to compensate for the ISE with pyramidal indenters (e.g.Tarasov and Thibault 1947, Farges and Degout 1989), but until the mechanisms are more fully understood, it would seem wise only to compare results made at similar depths if attempting quantified conclusions. Interpretation of spherical indentations is even more complex since the amount of strain alters as the size of indentation increases. As the load is increased, both work-hardening and size effects are introduced (Sargent 1989).

3.6 Vibration and Other External Effects

Vigilance is necessary if hardness results are to kept free of unconscious errors from external factors. Movement of the indenter relative to the sample, by vibration for example, will obviously affect the size of indentation produced to some degree. Thibault and Nyquist (1947) concluded that "building" vibration did not have any measurable effect, but knocking the table on which the indenter was mounted did. In a paper specifically investigating the effect of vibration using a specially supported Leitz machine, Brookes, Hooper and Morgan (1987) found that the measured hardness was decreased by vibration of the specimen, especially for amplitudes above 10^{-4} cm. The effect was more pronounced at low load, but reduced if the vibration was only applied after the indenter had actually come to rest. Surprisingly, the rate of indentation creep was not significantly influenced by the amplitude or frequency of imposed vibrations. The amplitude of incidental vibrations transmitted to a well supported hardness tester are $< 10^{-5}$ cm (Brookes et al 1987), so the results of the paper suggest that vibration should not significantly affect microindentation creep investigations such as are described in this thesis.

However, the condition and mounting of the "diamond" indenter has been shown to have a significant result on the quality of hardness measurements obtained (Thibault and Nyquist 1947, VAMAS 1989 and the author's results at Oxford). For reproducible results it is necessary that the pyramid facets are cut with a high precision. The required dimensions, accuracy and stone orientation are laid down in the relevant British and American standards, but it is recommended that the stones are carefully inspected, both on first arrival and at intervals throughout their working life, in order to check for chips, incorrect cutting and wear. High temperature hardness testing needs especial care, since the relative hardness difference between specimen and indenter may diminish as the temperature is raised, depending on the temperature / hardness characteristic of each material. Chemical erosion may also be a problem in spite of the vacuum conditions, perhaps exacerbated by

the high pressures involved. Tests on SiC (Fenwick 1988) and MgO at Oxford at 1200°C resulted in progressive blunting of the tips of a diamond indenters until a re-grinding was necessary.

Even if the indenter stone is correctly dimensioned, the correct hardness value will only be obtained if the indenter is applied perpendicular to the sample surface. This requires the indenter to be correctly mounted and the sample to be held flat and perpendicular to the direction of loading. The amount of asymmetry of a Knoop indenter can be estimated by measuring one half of the long diagonal as well as the whole diagonal length. Thibault and Nyquist (1947) found that a significant lowering of the measured Knoop hardness occurred if asymmetry exceeded 20% i.e. the smaller half diagonal was less than 80% of the longer diagonal. Such measurements were made for all the indentations described in this thesis and the skew ratio (defined by $(R_1 + R_2)/ R_1$) calculated. If the asymmetry of indentations exceeded this 20% limit (i.e. a skew ratio less than 1.8 or more than 2.2) the indentations were usually discarded. They formed a very small proportion and were normally caused by incorrect sample mounting, although occasionally an indenter stone shifted in its mounting (or was incorrectly mounted).

4. EXPERIMENTAL WORK

This chapter details the composition of the materials used and the way in which they were prepared. Etching techniques and treatment of experimental results are then described.

4.1 Magnesium Oxide Analysis and Sample Preparation

All the MgO samples were taken from the same block supplied by Koch chemicals Ltd. The stated purity was 99.99%. Analysis was carried out at the Inorganic Chemistry Laboratory, Oxford, and the results are shown in table 4.1. The block was aligned along the <100> axis by X-ray Laue diffraction patterns, and cut into bars 5 by 5 by 30 mm, using the high speed saw. Samples for indentation testing were freshly cleaved from these bars, using a steel wedge held along the <010> direction.

This cleaving technique produced a surface fairly free from plastic deformation, but with varying concentrations of slip steps. Polishing with orthophosphoric acid was investigated but it was found that this technique produced a wavy surface by simply smoothing out the edges of the slip steps. Such a surface led to increased error in measuring indentation sizes since, whilst an indentation falling on a slip step is obviously suspect, undulations on the surface are not readily visible with the optical measuring techniques used, but still effect the size of indentation produced.

4.2 Germanium Analysis and Sample Preparation

Most of the germanium samples used were cut from a boule of slightly N doped material. Analysis at Imperial College found the carrier concentration to be 7.1×10^{14} cm^{-3} at 300K. A few of the later samples were cut from a boule obtained from the University of Essex. The doping of this material was found to be 2×10^{17} cm^{-3} P type impurity. In terms of dislocation velocity these two dopings are essentially the same.

The Ge boule was aligned using X-ray diffraction patterns to within 1 degree of the crystallographic pole required. The materials was then cut into 700μm slices, using a high speed diamond wheel saw. The slices were lapped using alumina slurry from 15μm to 1μm, then the polishing continued on hard and soft cloths with diamond paste to 0.25μm particle size. Finally a chemomechanical polish ("Syton 2360") was used to remove any remaining plastic deformation.

	Weight (ppm)		
The Oxford crystal	Al,	Cr,	Fe
(Koch chemicals Ltd.)	200	70	180

Table 4.1 Results of the chemical analysis of the MgO crystal, carried out by M. Bown, Inorganic Chemistry Laboratory, Oxford.

The slices were cleaved to the required size for indentation testing along the <110> direction.

4.3 Etching

The use of etchants to reveal the position of dislocations on a crystal face is a well established and useful technique. The atoms (or ions) at the core of a dislocation line dissolve in a suitable solvent more rapidly than the normal crystal surface, because it provides a high energy site. The etch pit technique is particularly convenient for revealing dislocations in brittle crystals, which can be cleaved to produce a dislocation free face suitable for etching, and harder materials which can be polished without producing damage deep below the surface. It is a simple and speedy method for workers interested in determining dislocation densities and distributions, rather than in studying the details of dislocation Burgers vector etc. (Johnston 1961). The most serious limitation is that observation is restricted to the crystal surface, but this can be largely overcome by step-by-step removal of material, re-etching after each step.

Other techniques can be used for revealing dislocations. Electron microscopy has high resolution, but needs thin foil with the accompanying problems of preparation, and doubts as to whether the dislocations viewed are typical of the bulk situation. Xray diffraction is a possibility, but it takes a long time to process results.

4.3.1 The History of Etching

Although the history of dislocation etching might be considered to have begun in 1949 with Shockley and Read, for over 130 years prior to that mineralogists had been producing etch figures on minerals (Johnston 1961 - useful review).

Work in the early 1950's produced etch pits at growth spirals on SiC and other materials. In perhaps the most important single piece of work in establishing the validity of the etch pit technique, Vogel et al (1953) used a pure tilt boundary in germanium to establish a one-to-one relationship between etch pits and dislocations (under his specific conditions). This also demonstrated that etch pits could form at edge dislocations as well as the screw dislocations previously studied since a pure tilt boundary consists only of edge dislocations. The general applicability of the etch pit method for studying plastic deformation became apparent, as it was shown that the individual dislocations in glide bands (Johnston 1961), and the dislocation network substructure, could be revealed. Further refinement of the etch pit techniques, particularly by Gilman and Johnston (1956),

have made it possible to trace individual dislocations and measure quantitatively their properties.

4.3.2 Formation of Etch Pits

A dislocation has an elastic energy of several electron-volts, and a core energy of several tenths of an electron-volt, per lattice spacing. It is this localised energy which leads to the formation of an etch pit at a dislocation. Pits are formed as long as the rate of solution normal to the surface is large enough compared to the rate of solution parallel to the surface (Gilman, Johnston and Sears 1958).

Dislocation etch pits are generally pyramidal with the apex of the pyramid lying on the dislocation line, and the centre of the base located at the original intersection of the dislocation with the surface (Johnston 1961). If the energy of the crystal-solution interface is isotropic the pit will be circular, otherwise the shape of the pyramidal base will tend to reflect the crystal symmetry. If the pit has sufficient symmetry the orientation of the dislocation with respect to the surface can be inferred; an imaginary line drawn from the base of the pyramid to the apex will be parallel to the dislocation (Amelinckx 1956).

The etching behaviour of a crystal may depend critically upon the orientation of the surface. Dislocation etch pits are produced most readily on close-packed crystallographic faces (Johnston 1961), and a study on Ge by Holmes (1959) found that the orientation range within which etch pits appeared depended upon the specific etchant.

The question of whether there is a one-to-one correspondence between etch pits and dislocations arises for each new etchant, and the question may be broken into three parts: (a) Is there some correlation between etch pits and dislocations? (b) Are all dislocations etched? (c) Do all etch pits correspond to dislocations? All the etches used in this thesis work are established systems, and the reader is referred to the referenced papers for reassurance on the first two questions; the answer to the third is probably no, and is commented upon in succeeding sections.

4.3.3 The MgO Etch

Stokes, Johnston and Li (1959) established that a solution consisting of five parts saturated ammonium chloride in water, to one part concentrated sulphuric acid and one part distilled water reveals dislocations on the {100} cleavage face of MgO, and this solution has been the most frequently used etchant in MgO studies. (A 3:1:1 mix is also quite commonly used). Boiling orthophosphoric acid is used to polish MgO, the rate of

dissolution depending on the crystal face concerned. The shape and size of etch pits is time and temperature dependent. Several authors have also used orthophosphoric acid at temperatures between 50°C and 100°C to etch deformation-induced dislocations on (110) faces which do not respond to the Stokes et al etch.

In a specific study on etching and polishing of MgO single crystals, Ghosh and Clarke (1961) confirmed that the Stokes etch revealed both edge and screw dislocations, but found that not all etch pit arise at dislocations. They decided that equal parts of NH_4Cl solution and concentrated H_2SO_4 gave the best defined pits. However, for work in this thesis, the Stokes 5:1:1 etch was found to give the best results, at least for the lower temperature samples. The results from samples which had been indented at 750°C were less satisfactory. On the surface of some 750°C samples, the Stokes etching reagent failed to show up any dislocation patterns at all. Prolonged etching in orthophosphoric acid at 80°C revealed only the dislocations with edge components at the surface, but after polishing in boiling orthophosphoric acid, the Stokes etch would show up dislocations with screw components at the surface.

4.3.4 The Germanium Etch

One of the reasons for choosing germanium as a model material was the ease of etching. The etch used was 10 ml nitric acid, 5 ml hydrofluoric acid and 11 ml acetic acid, with 30 mg iodine dissolved in it (Tuck 1975).

An etching time of a few seconds gave the best results for most of the (001) faces. However, samples indented at 700°C seemed to thermally etch, producing square based etch pits whose sides were orientated in the <110> directions, which enlarged under the influence of the chemical etch. Figure 10.13 shows the surface of a sample indented at 700°C. The surface of these higher temperature samples seemed more resistant to the chemical etch, and "normal" etching times etched both the background dislocations and those produced by the indentation deformation. Prolonged etching times were required to successfully show up the indentation rosettes against the background structure. This contrast was probably made possible by the different relative rates of solution parallel and perpendicular to the crystal surface (see mechanisms of pit formation, section 4.3.2).

4.4 Sectioning

Two kinds of sectioning were carried out at Oxford to investigate the dislocation arrays beneath indentations. Both involved a serial polish and etch technique, but one

polished from the surface of the sample down, and the other (used on a few Ge specimens) removed material in a plane perpendicular to the indented surface.

For Ge samples in which material was removed from the indented surface, an automatic polisher (Prepamatic) at NPL was used. This gave a reasonably repeatable polishing rate so that the depth removed at each stage could be more closely controlled than with a conventional polisher. The sample to be sectioned was mounted in resin with the sample surface being held flat. Pan W cloths with diamond pastes followed by a chemical polish gave quite a good surface finish for etching, although particles breaking away from the sample edges could produce surface scratching which was revealed when the sample was etched. Once etched, the array from each indentation was photographed before a further polishing stage was carried out. (Examples of this technique are shown in figures in chapter 10).

MgO samples were analysed in a similar way, but the polishing was achieved with boiling orthophosphoric acid. The effective polishing rate was not easy to control. Figures in chapter 7 show sections obtained in this way.

The vertical sections of a few Ge samples were made by mounting the specimen between two 5 mm wide glass strips (cut from microscope slides). The "sandwich" was held up against the side of a channel cut in the centre of a brass block. The block was mounted to a rigid plate which could be held against a polishing wheel. Since the top of the brass block (40mm by 25mm) was only fractionally lower than the edge of the sandwich, it prevented any gross tipping of the sample as it was held against the rotating polishing plate. Material was polished off until the desired position of section was reached (as monitored by looking through the glass face of the sandwich, at the indented face of the specimen). The sample could be etched and photographed before re-polishing.

4.5 Treatment of Hardness Results

The experimental details concerned with the operation of the Oxford indentation tester, and physical condition of the samples inside, have been described in chapter 2.

The sample was fixed to the alumina platen using colloidal silver, and then installed under vacuum; it was correctly orientated using the rotate control. The <110> cracks around 300g Vickers indentations were used to align the indenter diagonal with the chosen direction for the MgO sample. (In the case of Knoop indentation the Vickers indentations were made on another machine before the sample was installed). The Ge samples were aligned either by using the <110> cleavage edge, or the direction of lines of dislocation pits

round an etched indentation in the corner of the specimen. The latter method was found to be more accurate, but could not be used for the lower temperature tests, since the sample had to be heated above 200°C to get sufficiently extended dislocation arrays. The sample coordinates were then mapped.

The machine was then heated up to the chosen test temperature and allowed to equilibriate for at least 20 min before indentation testing began. (For the high temperature MgO specimens the temperature was reached in a series of stages).

At least 5 indentations were made at each chosen dwell time, and the indentations were spaced as far apart as possible to ensure an individual hardness response at each point. In order to guard against any effects from different portions of the sample (or long term heating effects, but see section 9.5 for specific investigation), the indentations of each dwell time were made out of sequence; (i.e. a 20 second indentation, next to a 600 second indentation, next to a 300 second etc.). A typical full experiment (at one particular temperature) would take 4 to 5 hours. Approximately half way through this time, the furnaces were switched off; and, once the sample had returned to room temperature, it was brought back under the viewing position and checked for any shift in orientation and/or indentation asymmetry. The experiment was then continued as before.

For experiments carried out with LVDT monitoring the movement of the indenter (see section 2.4), the time for the indenter to reach the sample surface could be calculated from a change in the rate of descent of the indenter. More generally a series of indentations with difference of 5 or 10 second total time were made during the first half of the experiment. When the sample was cooled down and brought into the viewing position, a narrow range of time could be identified and accurately identified with a series of indents with 1 or 2 second difference in loading times. The dwell times for the indentations on that particular specimen could then be calculated by subtracting the time which the indenter took to reach the surface, from the overall time allowed for each indentation.

Once the experiment had been completed, the specimen was removed from the machine and the indentations measured on a Nikon research microscope with Nomaski contrast (see section 3.1) and a curtain micrometer. The mean diagonal lengths and standard deviation for each dwell time set of indentations were calculated. (All the raw data was entered into computer data files and manipulated using Nag routines). Since the hardness is calculated from the inverse of the square of the diagonal, the error in the

hardness was calculated from

$$\frac{\pm 2\,C\,L\,SD_D}{D^3}$$

where C is the indenter geometric constant for the indenter used, L is the load, D is the mean diagonal measurement and SD_D the standard deviation associated with that mean.

5. PREVIOUS WORK ON MAGNESIUM OXIDE

MgO is often considered a model ceramic material because of its simple rocksalt structure, elevated melting point (2800°C) and general availability (Wolfenstine and Kohlstedt 1988). It was chosen as a material for this study because, although, like Ge, it is easily etched and shows considerable hardness anisotropy, there are significant differences in dislocation behaviour and slip systems compared to Ge. However, understanding of the mechanical properties is complicated by their sensitivity to even small amounts of impurities, since this tends to obscure effects related to the structure of the pure crystals. A succinct review of the application of indentation testing to MgO and other semi-brittle materials of the rock-salt structure is contained in Hockey's "Use of the hardness test in the study of the plastic deformation of single crystals" (1973).

5.1 Slip Systems and General Features of Deformation

The bonding in rock-salt (NaCl) structured oxides is largely ionic but, despite similarity with the alkali halides, the oxides form a distinct isomechanical group with high melting points and moduli (Frost and Ashby 1982). (MgO has a particularly high melting point, see Table 5.1). The structure is a f.c.c. array of the larger oxygen ions, with the metal ions occupying the octahedral interstices.

The primary slip system of the rock-salt structure is on {110} planes and <110> directions, but slip on {100} <110> may also be found (Haasen, Barthel and Suzuki 1985). The direction of gliding <110> is the shortest distance between lattice points in the crystal structure, hence it requires the smallest amount of displacement across the glide plane to restore the structure (Figure 5.1). Also this translation does not require any nearest neighbour ions of the same polarity to become juxtaposed during the process of gliding. It is consideration of these electrostatic forces which accounts for the choice of glide plane. The {100} planes are the most closely packed (and hence most widely spaced apart), yet the primary glide planes are {110} (Gilman 1961). The reason for this is probably that gliding on {100} is accompanied by electrostatic faulting (figure 5.2). When a crystal has glided **b**/2 in a {100} plane, the positive and negative ions are brought into neutralised nearest neighbour positions. There are just as many ions in repulsive positions at planes A, B, C and D as are in attractive positions, as shown in on the right of figure 5.2. Thus there is no net binding between the nearest neighbours ions across the glide plane. However this does not happen for gliding on {110} planes (left hand side, figure 5.2).

Material	MgO	CoO	FeO
Melting point (K)	3125	2083	1643

Table 5.1 Melting points of some rocksalt materials.

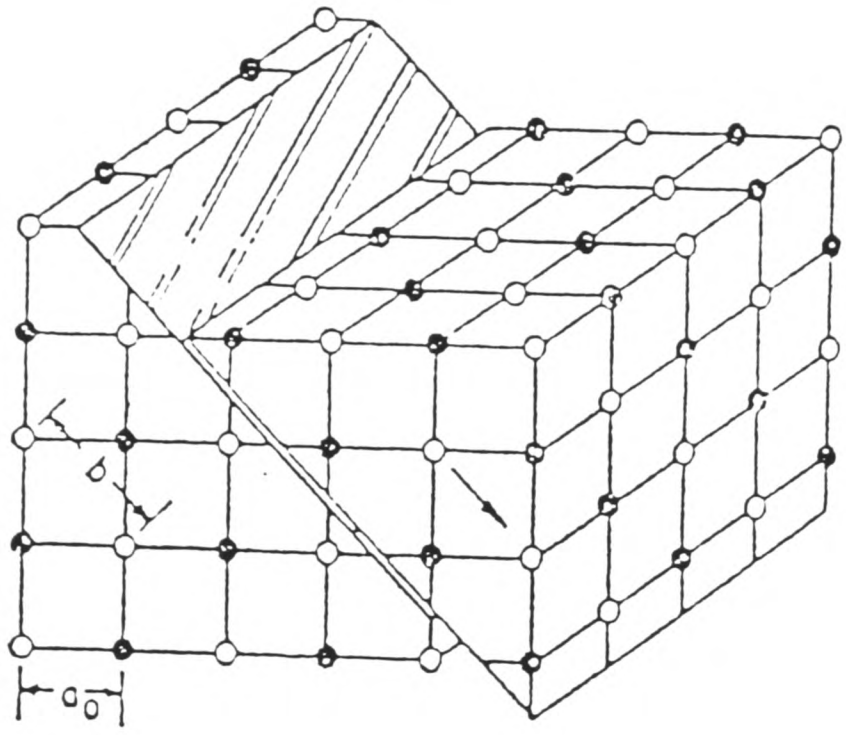


Figure 5.1. The two gliding planes in the rocksalt structure (Gilman 1961).

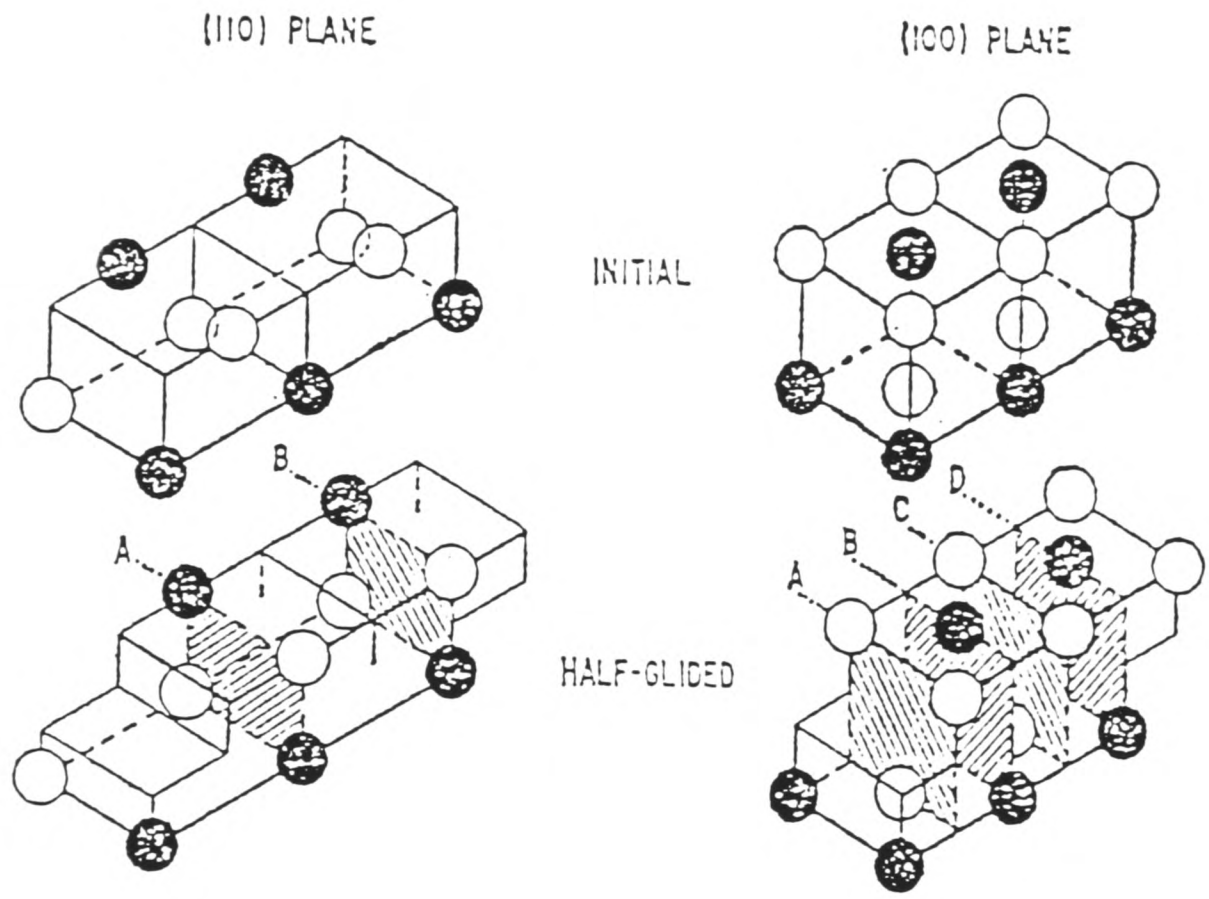


Figure 5.2. Structures of glide planes in rocksalt crytals for half glided positions (Gilman 1961).

In a review of the choice of slip systems and Peierls stresses in materials with this structure, Haasen, Barthel and Suzuki (1985) found that the plane selected depended on the ionicity of bonding, orientation of stress, temperature and doping. The first variable mentioned echoes earlier work of Gilman (1959) who developed some results by Buerger (1930) exploring the "anomalous" behaviour of rocksalt crystals with respect to their glide planes. (His results and those of Gilman are summarized in table 5.2 reproduced from Gilman's paper). {100} glide is favoured by increasing polarisability of the ions (i.e. as the ionic character of binding decreases) and is an example of the important role played by the core structure of the dislocations in the plastic behaviour of crystals (Gilman 1961).

5.3 Flow Stresses and Impurity Effects

Methods employed to look at the flow stresses on the rocksalt slip systems include subjecting single crystals to tensile testing, compressive testing or bend testing, torsion, and indentation methods. The dislocation activity produced has been studied by observation of slip lines, etching techniques, electron microscopy and X-ray topography. The mechanical properties of MgO are sensitive to even small amounts of impurities, even at relatively low temperatures (e.g. 600°C), because of dislocation impurity interactions and dislocation pinning (Groves and Fine 1964).

Four processes determine the yield stress in MgO - interaction between dislocations and localised obstacles, the Peierls stress (lattice friction), jog-dragging and long range dislocation interaction (Moriyoshi et al 1978). Aliovalent impurities, mainly Fe but also Mn and Cr, are regarded as the main barriers to the motion of screw dislocations (Nadgornyi 1988). In "impure" MgO most authors agree that the dislocation mobility and hence flow stress in determined by dislocation/impurity interaction (e.g. Singh and Coble 1974b, Valkovski and Nadgornyi 1975).

For "pure" single crystals the question is whether the flow stress of the crystal is controlled by the Peierls mechanism for dislocation movement, i.e. the friction stress required to move a dislocation through "perfect lattice", (particularly for low temperature deformation), or the dislocation/dislocation interaction, or interaction between dislocations and the small amount of impurity centres which are still present (typically about 100 ppm of aliovalent impurities - see table 5.3 listing crystal analysis). Woo and Puls (1977) concluded that dislocation velocity results may be explained on the basis of a Peierls mechanism when the applied resolved shear stress (RSS) is greater than 5 MPa and the crystal contains less than 20 ppm Fe^{3+}. They point out the large discrepancies between values of Peierls stress estimated by different experimental techniques. Singh and Coble's value of 60 MPa for the Peierls stress (1974a) is in good agreement with that of Woo and Puls (70 MPa), but the

Crystal	Primary Glide System	Secondary Glide Systems	References
MgO	(110) [110]	—	Mugge
LiF	(110) [110]	(100) [110]; > 200°C	Gilman
NaF	(110) [110]	(100) [110]	Buerger
NaCl	(110) [110]	(100) [110]; (111) [110]	Buerger
NaBr	(110) [110]	(100) [110]; (111) [110]	Buerger
NaI	(110) [110]	(100) [110]; (111) [110]	Buerger
KCl	(110) [110]	(100) [110]	Buerger; Gilman
KBr	(110) [110]	(100) [110]	Buerger; Gilman
KI	(110) [110]	(100) [110]	Buerger; Gilman
RbCl	(110) [110]	—	Johnsen
NHI (high)	(110) [110]	—	Johnsen
AgCl	(110) [110]	(100) [110]	Stepanov
AgBr	(110) [110]	(100) [110]	Stepanov
PbS	(100) [110]	(100) [001]	Buerger
PbTe	(100) [110]	(100) [001]	Rachinger; Gilman

O. MUGGE, *Neues Jahrbuch*, 29 (1920).
J. J. GILMAN, *Acta Met.*, 7, (1959).
M. J. BUERGER, *Amer. Mineralogist*, 15, 1, 21, 35(1930).
A. JOHNSEN, *Neues Jahrb.*, 147, (1902).
A. W. STEPANOV, *Phys. Z. Sowjet.*, 6, 312 (1934).
W. A. RACHINGER, *Acta Met.*, 4, 647 (1956).

Table 5.2 Summary of the results of Gilman and Buerger (after Gilman 1961).

	Al,	Ca,	Cr,	Fe
The Oxford crystal	200	-	70	180
Brown, Khan, Chaudhuri (1988)	50	500	20	50
Stokes, Johnston and Li (1958)		96-99% pure		
Val'Kovskii and Nadgonii (1976)	30	30	-	300
Kim and Clifton (1984)	1	3	1	70
Singh and Coble (1974)	35	20	-	19
Wolfsteine and Kohlsted (1988)	45	280	-	-
Sato and Sumino (1980)	30	10	<10	30
Scrinivasan and Stoebe (1973)	70	50	-	50
Haasen Barthel and Suzuki (1985)			< 300	
Woo and Puls (1977)			20 Fe^{3+} or 5 Fe^{3+}	
Copley and Pask (1965)	50	100	10	100 or
	50	1200	20	60
Hulse and Pask (1960 and 1968)	500	100	-	200
Chaudhuri, Wells and Stephens (1981)	15	100	10	50

Table 5.3 List of analysis of MgO crystals used in the works referred to in the text, as given by the authors, p.p.m.

double kink nucleation energy expression used by Singh and Coble to calculate the Peierls stress is rather crude, and has been superseded by later theories (Woo and Puls 1977).

Srinivasen and Stoebe (1973) used strain-rate cycling methods to study the thermally activated flow parameters of MgO single crystals. Above room temperature the authors identify the interaction of dislocations with dislocation dipoles as the rate-controlling factor, since the activation volume decreased as the dipole density increased with strain. Dislocation intersection mechanisms are ruled out by Kumar (1968) in favour of impurity mechanisms. Applel et al (1984) concluded that interaction between dislocations and point obstacles is the dominant mechanism controlling dislocation mobility, but Peierls stress, jog dragging and long range interaction between dislocations are also active.

The variation of the CRSS for MgO on the {100} and {110} planes is shown in figure 5.3 (after Haasen et al 1985). The {100} planes remain unfavourable at all temperatures, but the difference in CRSS is greatly reduced at higher temperatures. The authors conclude that the Peierls region is not observed down to 4K on the {110} planes, but is operative below 1200K on the {100} planes.

5.4 Creep and Work Hardening

Hulse and Pask (1960) carried out compression creep tests on the <100> axis and found that the MgO crystals showed considerable ductility even at -196°C. At room temperature, samples deformed plastically to about 6% before fracture, and tests in the range 800°C to 1000°C showed large instantaneous plastic deformations followed by slow constant-rate creep. They attributed the increased ductility at higher temperatures to the relief of the interaction stress between dislocation stress fields afforded by diffusion of dislocations. Using the same experimental technique, Wolfenstine and Kohlstedt (1988) concluded that, above 0.5 T_M, the creep of MgO single crystals is controlled by dislocation climb, rather than by dislocation glide.

Srinivasen and Stoebe (1973) have also examined the temperature dependence of yielding and work-hardening in MgO single crystals. Depending on the temperature and purity of the crystals they resolved the stress-strain curve of MgO single crystals into two work-hardening stages which were athermal in nature. At and below room temperature there were two contributions to stage I hardening; a temperature dependent one arising from dislocation-point defect interactions, and a temperature independent one arising from the dislocation-dislocation dipole interactions. After 3-4% strain, work-hardening increases slightly to stage II, probably caused by dislocation interaction with dislocations on intersecting slip systems and blocking obstacles. At higher temperature only stage II was

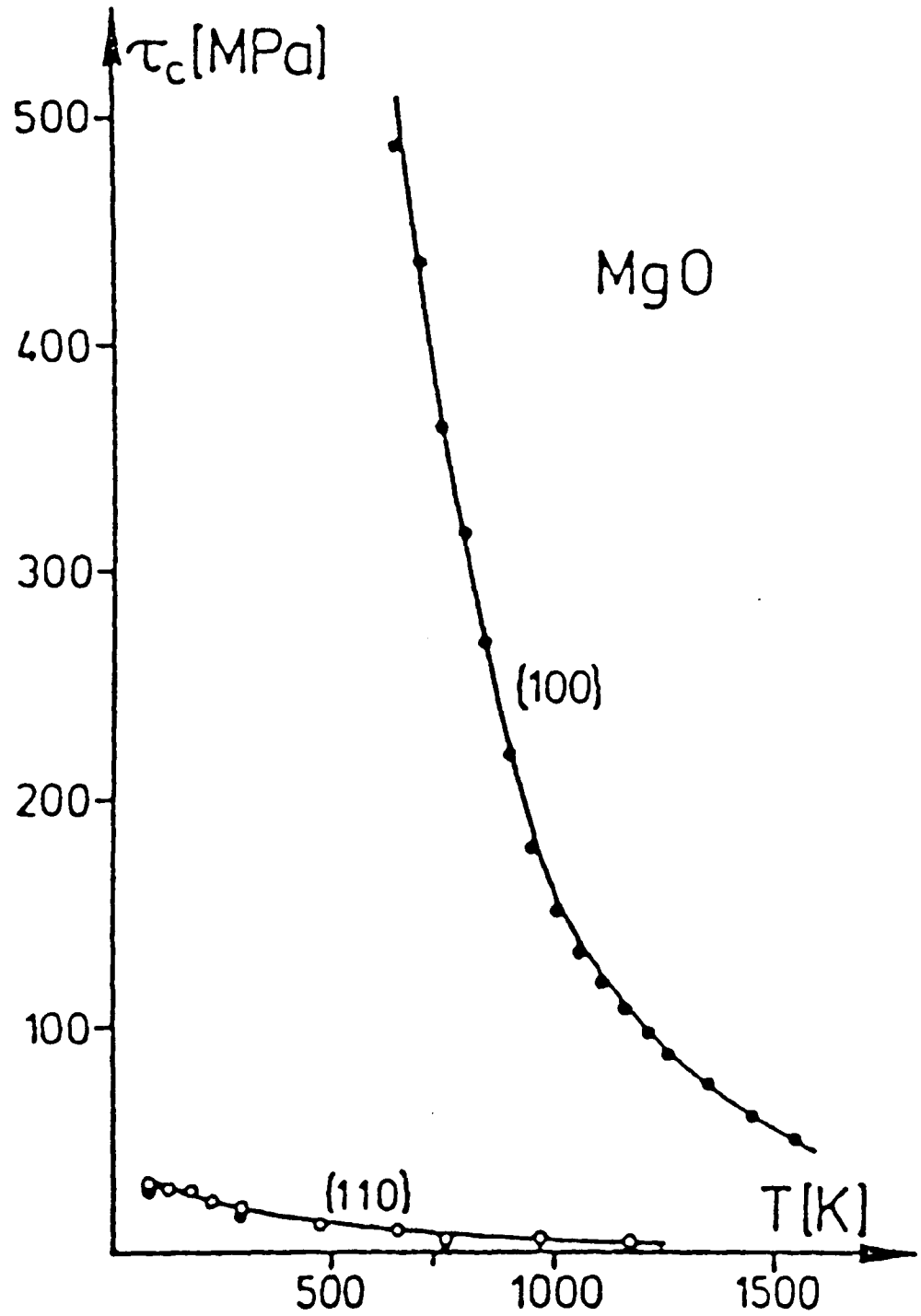


Figure 5.3 Variation of CRSS for MgO on the {100} and {110} planes (Haasen et al 1985).

present. The two stage behaviour was only observed in the "pure" i.e. 99.97% crystals, not in crystals of 99.93% or less purity. The less pure crystals showed single stage work-hardening with a hardening rate higher than that of purer crystals, particularly at room temperature. Strain rate had little influence, such that an order of magnitude change in strain rate caused practically no change in work-hardening rate.

5.5 Dislocation Mobility

Copley and Pask (1965) obtained stress-strain curves for single crystal MgO in <100> and <111> orientations. They found that below 1200°C the experimental results indicated that the yielding behaviour is determined primarily by the dislocation mobility, but at higher temperatures, the dislocation density may become less stress sensitive, and the length of the dislocation line therefore plays a greater part in determining the yield behaviour.

Johnston and Gilman (1959) studied dislocation movement in LiF and determined that it was the dynamic resistance to dislocation motion that determined the yield stress of the crystals. Whenever the applied stress was sufficiently high to cause dislocation motion, profuse dislocation nucleation and multiplication occurred. At low velocities the motion of the dislocations was jerky. Dislocation velocities were extremely sensitive to applied stress, particularly at the lower velocities encountered during normal testing. Such behaviour is confirmed by later work and is similar to that of MgO. As in alkali halides, edge dislocations in MgO always move faster than screw dislocations at a constant stress, but the difference at room temperature and above is more pronounced than in the alkali halide crystals (Nadgornyi 1988).

Nadgornyi (1988) summarises the range of data now available and concludes that the dependence of dislocation velocity, V, on applied stress, σ, in MgO can be described by

$$V = \sigma^m$$

for all temperatures. The exponent, m, is temperature dependent and varies from 33 at 393K to 62 at 203K for edge dislocations and 67 for screw dislocations at 77K. Such high values of m confirm that dislocation movement puts MgO into the class of a "bowing out" mode crystals.

5.6 Indentation Cracking

A schematic diagram of the cracks and "picture frame" of slip lines which are typically found around a Vickers indentation on an (001) surface are shown in figure 5.4 (after Armstrong and Wu 1978). The $\{110\}_{45}$ cracks are thought to be a result of

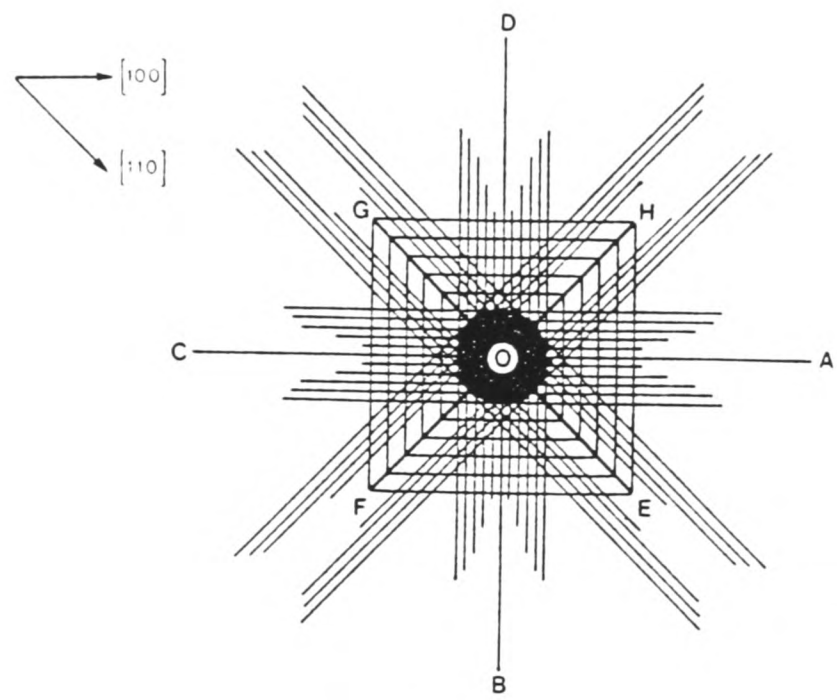


FIgure 5.4 Schematic diagram of the cracks and slip lines typically found round an indentation on (001) MgO. The extent of the $\{110\}_{90}$ cracks OE,OF,OG and OH is limited by the outermost square-shaped slip trace EFGH (after Chaudhuri 1986.)

dislocation interactions on the $\{110\}_{45}$ planes (Keh, Li and Chou, 1959, Armstrong and Wu, 1978, Hagan 1979, Chaudhuri, Wells and Stephens 1981). Cracks on {100} planes which are seen around spherical indentations are caused by dislocation interaction and/or simple cleavage under tensile circumferential stresses around the indentation produced as a consequence of local plasticity (Chaudhuri 1986).

6. MAGNESIUM OXIDE INDENTATION RESULTS

A series of indentation experiments have been carried out on a magnesium oxide crystal. This chapter describes the results of these investigations, includng some important findings on a temperature range in which no indentation creep takes place and changes in the indentation morphology.

6.1 Indentation Creep and Anisotropy

The variation of Knoop hardness (at 500g load) with dwell time between room temperature and 1175°C is shown in figure 6.1(a) and (b). The error bars were calculated using a mean diagonal value and 1 standard deviation error as described in chapter 4. Four or more indentations were used for each hardness value quoted except where indicated. All tests were carried out on cleaved (001) faces using a diamond or sapphire indenter in the Oxford machine (described in detail in chapter 2). The long diagonal of the indenter was aligned along either a <100> direction or a <110> direction. For easy analysis, table 6.1 shows the fraction of the melting point which each temperature represents.

The hardness values in figure 6.1(a) all come from samples which were heated to 600°C and cooled to room temperature before heating and testing (without the vacuum being broken). This was to avoid any distortion in the relative hardnesses caused by precipitation hardening, as discussed in section 6.5. (The room temperature hardness values in figure 6.1a compare well with those of Roberts (1988) at 100g, namely 4.5 ± 0.5 for the <110> orientation and 11.0 ± 0.5 for the <100> orientation).

Figure 6.2 shows the variation in Vickers hardness with dwell time at a limited number of temperatures, for 500g and 100g indentations. The 500g indentations, like the Knoop tests, were all carried out on cleaved (001) faces. However, the majority of the lower load indentations were performed on chemically polished surfaces (see section 4.1).

As might be expected, the hardness decreases with temperature throughout the range studied. At room temperature the <110> Knoop orientation is considerably harder, but the difference in hardness between the two orientations decreases as the temperature is raised and the situation becomes more complicated. The anisotropy between the two orientations decreases and finally reverses from the room temperature (and resolved shear stress predicted) pattern. At the high temperatures <100> is the hardest orientation for all dwell times. As detailed by Brookes, Burnand and Morgan (1975), the anisotropy of crystals of the rocksalt structure seems to be particularly sensitive to the homologous

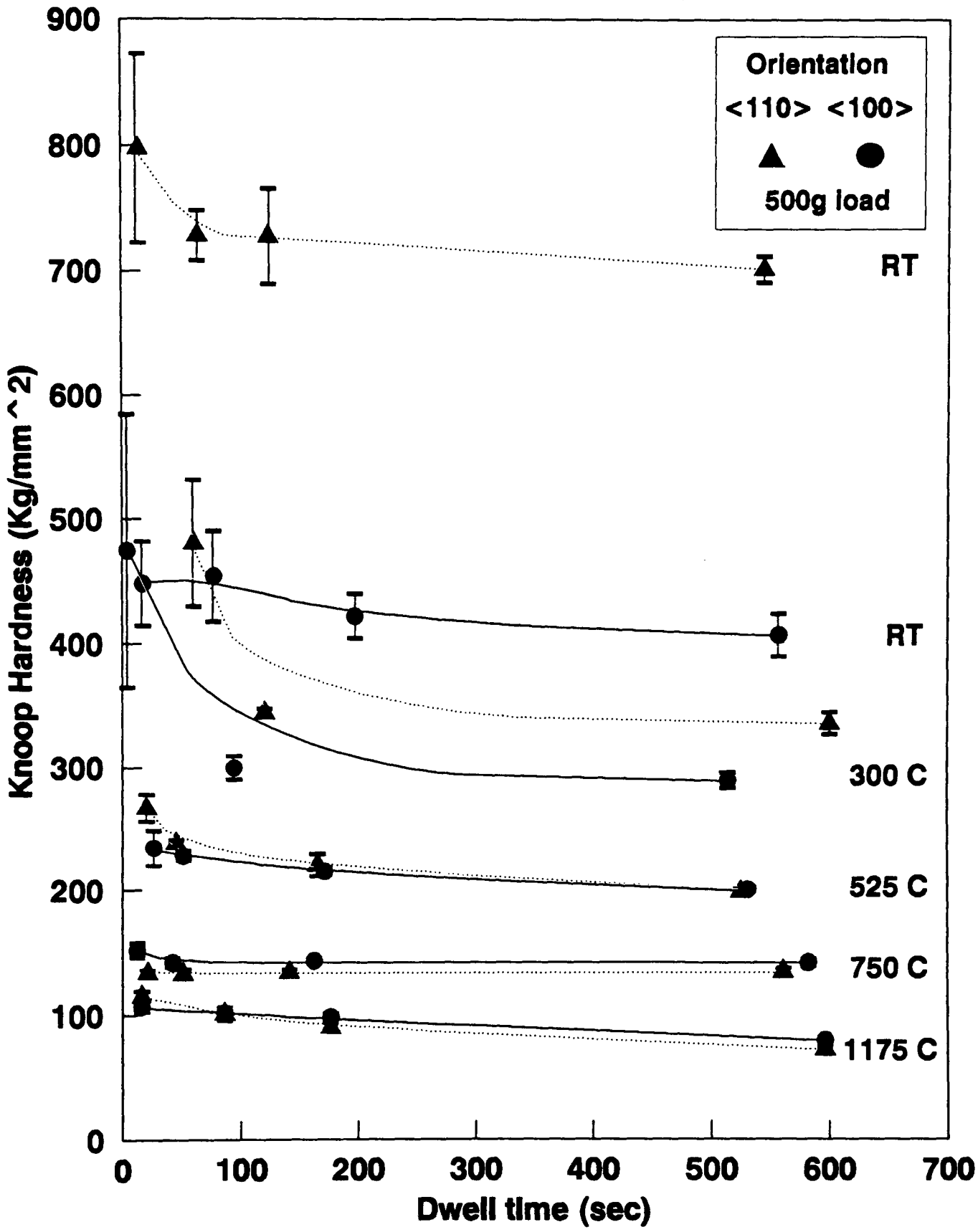


Figure 6.1(a) Variation of Knoop hardness with dwell time between room temperature and 1175 C, on (001) MgO.

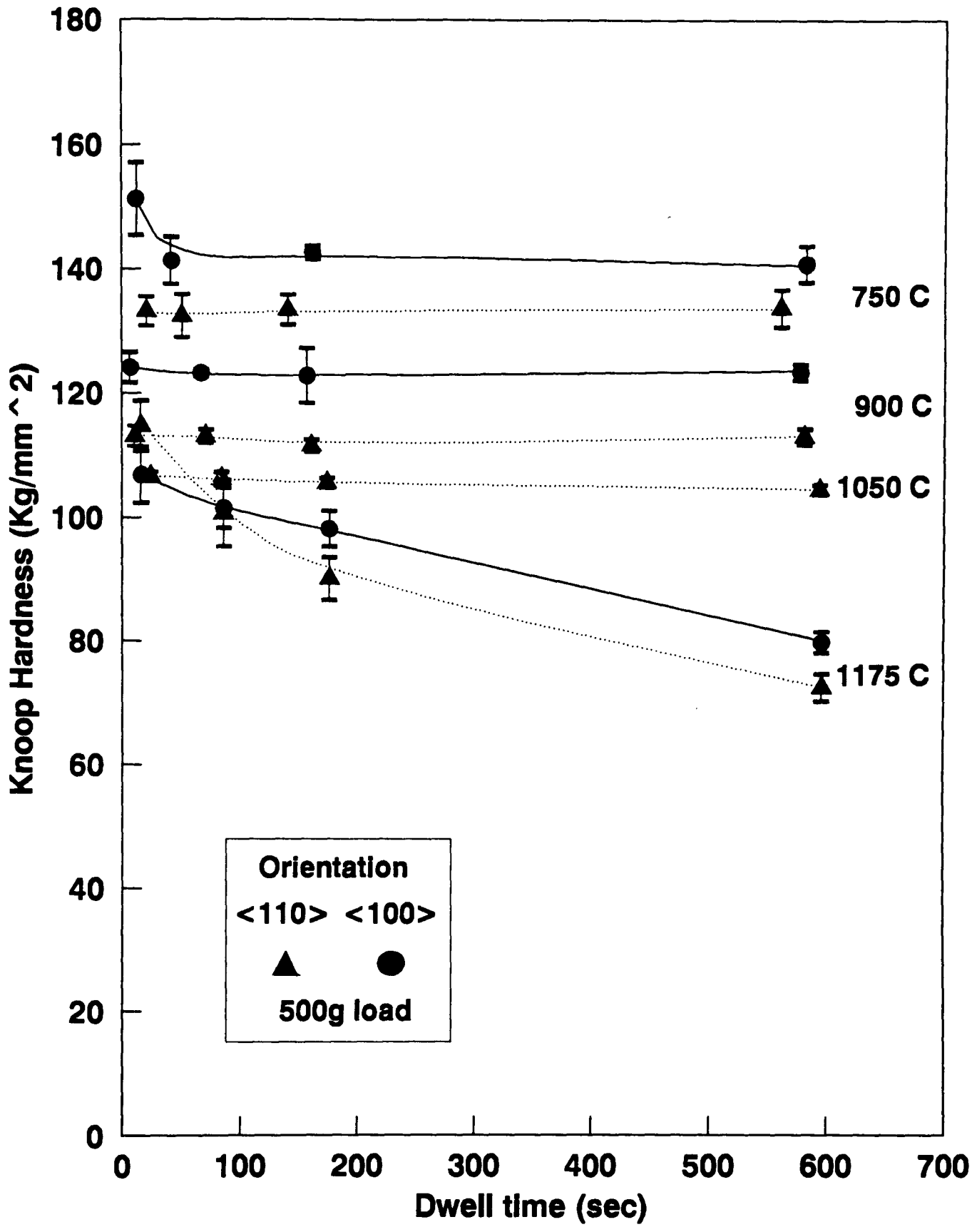


Figure 6.1(b) Variation of Knoop hardness with dwell time between 750 C and 1175 C, on (001) MgO.

°C	K	T/T_M
20	293	0.10
150	423	0.15
300	573	0.20
450	623	0.26
525	798	0.29
600	873	0.31
750	1023	0.37
900	1173	0.42
1050	1323	0.47
1200	1473	0.53

The melting point (T_M) of MgO is 3073K (2800 °C).

Table 6.1 Various temperatures in °C, K and T_M for MgO.

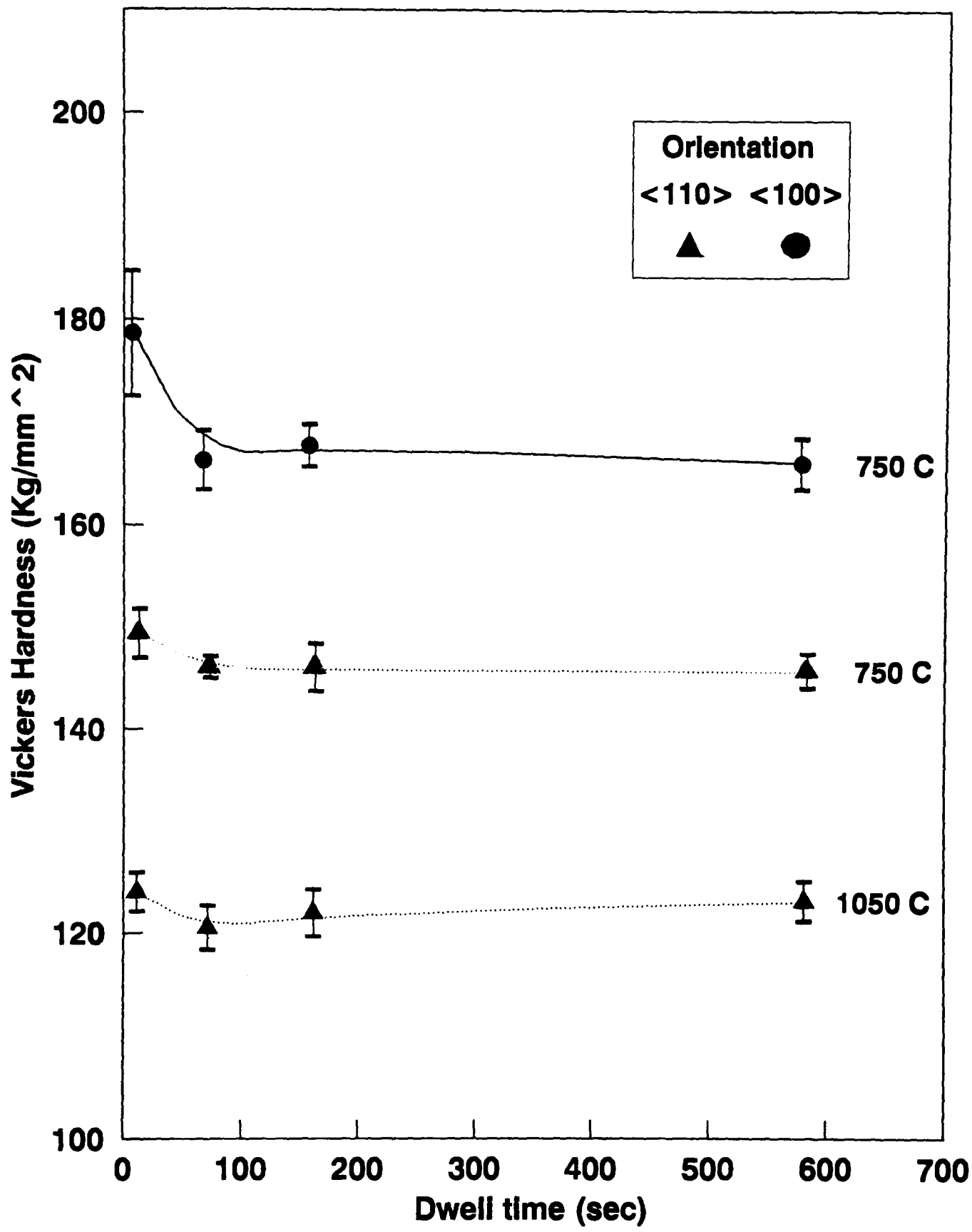


Figure 6.2(a) Variation of Vickers hardness (500g) with dwell time at higher temperatures, on (001) MgO.

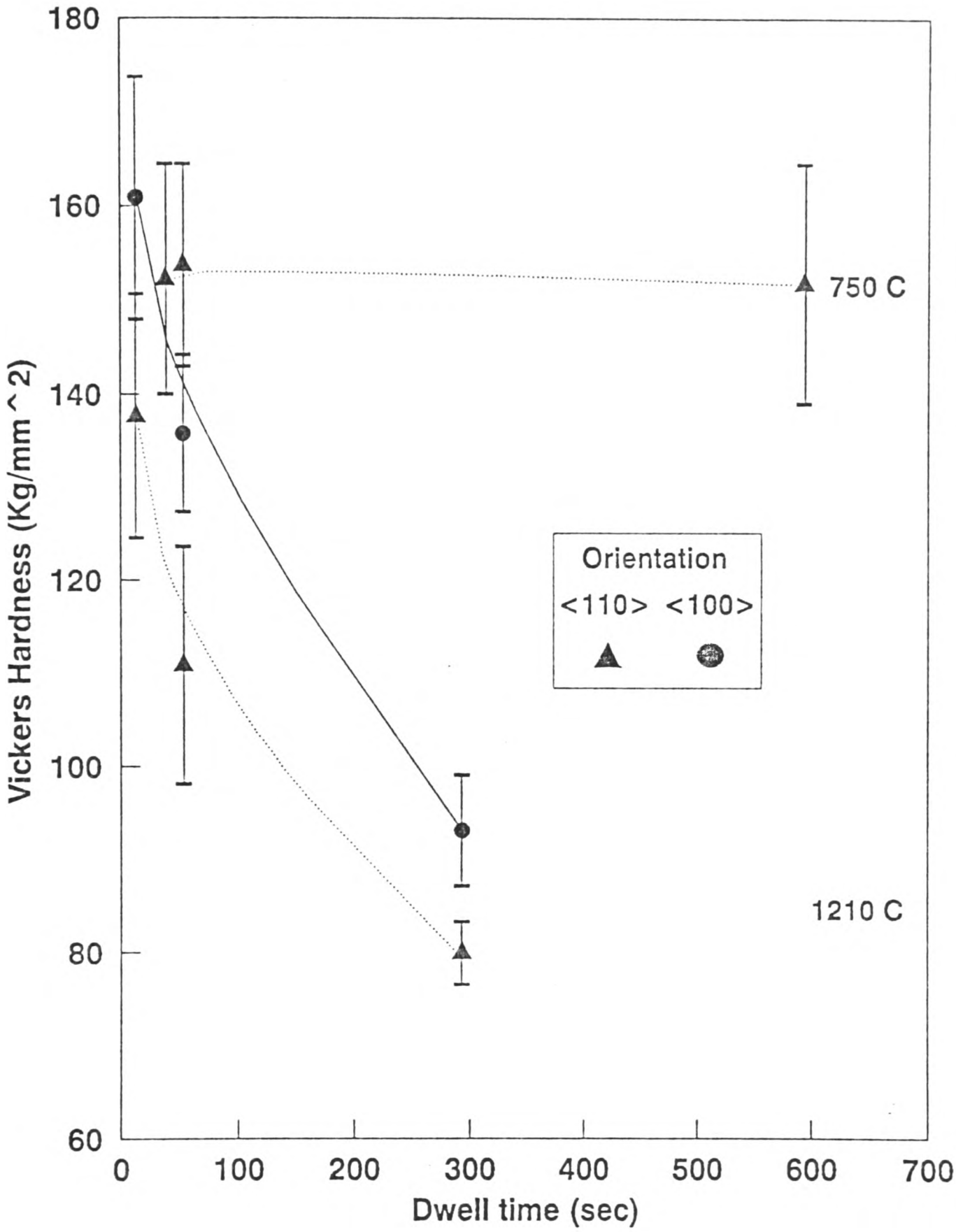


Figure 6.2(b) Variation of Vickers hardness (100g) with dwell time at higher temperatures, on (001) MgO.

temperature. They demonstrated that, at T/T_M of about 0.15, NaCl has the same type of anisotropy as MgO at room temperature (i.e. $0.15T_M$), although at room temperature, which is $0.27T_M$ for NaCl, the anisotropy is the opposite. For the Vickers indentations at 750 and 1200°C, the <100> orientation was always the hardest.

Between room temperature and 750°C both orientations creep. (The <100> Knoop orientation did not creep within experimental error at room temperature, which was confirmed by a 3600 sec indentation). The harder orientation (<110>) appears to creep faster than the other, see the 525°C or 600°C results for example.

The surprising results lie in the temperature range 750°C - ~1050°C, since the material showed no measurable indentation creep for Knoop indentations. (Some 1200 sec indentations at 750°C were carried out to confirm this). This is in direct conflict to results previously published (Brookes et al 1975). It seems likely that the reason for this discrepancy is the difference in indenter heating arrangement, as discussed in section 2.2. The no creep region was manifested at various loads and with both Knoop and Vickers indenters, and with varying sample heights. (Vickers <100> orientation just showed creep within the one standard deviation error range. Otherwise, like the Knoop indentations, none of the tests between 750°C and 1050°C showed measurable creep). It has therefore been proved to be a "real effect". By 1175°C indentations were again showing indentation creep. A mechanism for this behaviour is proposed in chapter 7, partly based on the change in indent morphology which is described below.

6.2 Aspect Ratio of Knoop Indentations

If the impression left after Knoop indentation conforms perfectly to the profile of the indenter, the shape of the indentation should be 7.11 times as long as it is wide (see section 1.2). Since both the long diagonal (length) and the short diagonal (width) of each indentation had been measured, it was possible to calculate the actual aspect ratio (long diagonal length/short diagonal length) for each of the indentations whose hardness is shown in figures 6.1(a) and (b). There was no significant variation in the aspect ratio of indentations for each orientation at a particular temperature, so a mean aspect ratio (and standard deviation) was obtained for each set of 20-30 indentations (i.e. all the indentations of various dwell times for one orientation under a given set of conditions). The variation of aspect ratio with temperature is shown in figure 6.3. The standard deviations were larger for the room temperature measurements, which might be expected, since the indentations are the smallest and have more surface cracking than at higher temperatures.

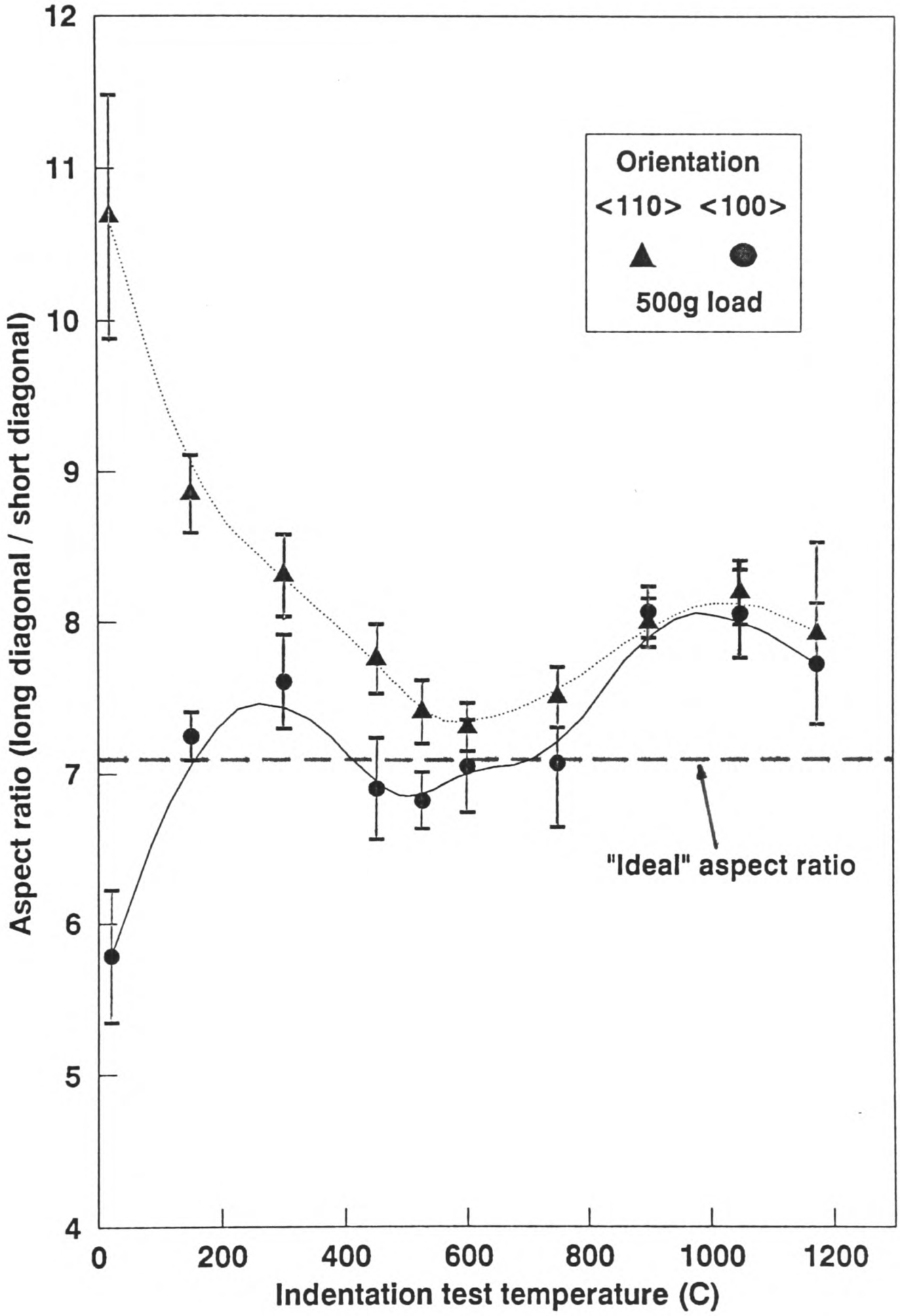


Figure 6.3 Variation of Knoop indentation aspect ratio with the temperature of indentation, on (001) MgO

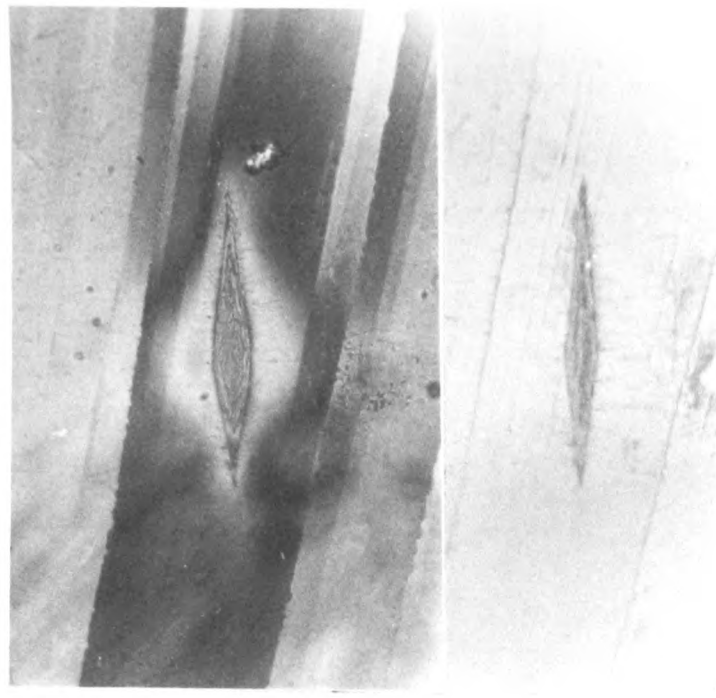
A high aspect ratio (i.e. > 7.11) indicates that indentations were thinner (or longer) than the original indenter profile which created them (and on which the calculated hardness is based). This is the case for room temperature indentations in the <110> orientation and is attributed to elastic recovery of the short diagonal. As the temperature is raised, the <110> aspect ratio decreases from its room temperature high to just above the 7.11 "ideal" ratio at 750°C, after which it begins it rise again.

The <100> orientation gives a room temperature aspect ratio which is very low, (i.e. fatter, or shorter, than the original profile); but as the temperature is raised, quickly returns to around the ideal value until 750°C. At this temperature it begins to rise above that value in a similar fashion to the <110> orientation.

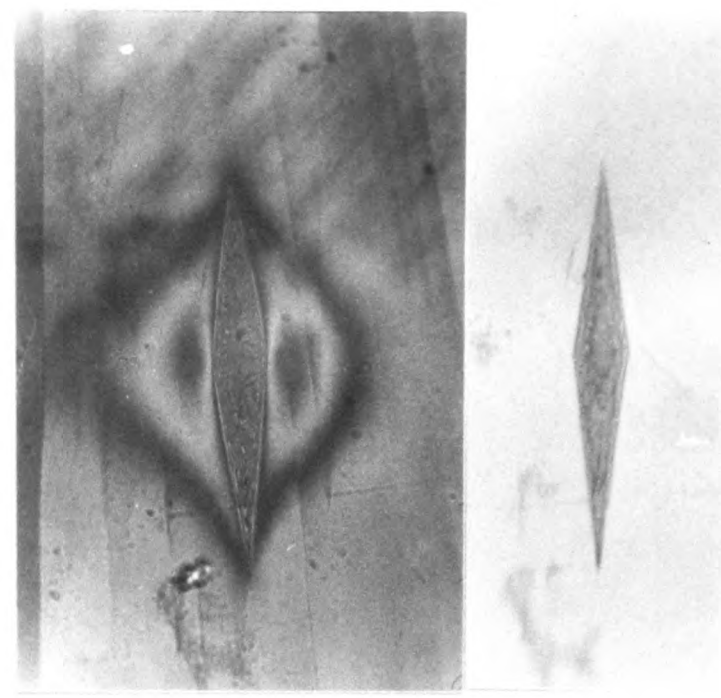
6.3 Indentation Morphology

Sodium light interferometry was used to investigate the morphology of the surface surrounding the indentations (fringe spacing 0.591 μm). Figure 6.4(a) shows interference fringes around <110> Knoop indentations (each indent has an identical photo, but without interference fringes placed beside it for easy identification of the indentation profile). No interference fringes could be seen around <110> room temperature indentations, but as the temperature of indentation is raised, raised areas begin to appear each side of the indentation, suggesting movement of material up to the surface as the indentation is formed and creeps. These "rounded hills" either side of the indentation do not cause a very steep height variation immediately adjacent to the indenter sides, thus affecting the aspect ratio very little. (The aspect ratio decreases from its room temperature high as the amount of elastic recovery decreases). However, in the no creep temperature region, 750°C to 1050°C, closely spaced fringes indicate the presence of a steep, roughly elliptical valley close around the indenter. A schematic surface profile is shown in figure 6.5. The hollow beneath the short diagonal of the indentation causes a higher than ideal aspect ratio. At the highest temperature investigated, 1175°C, the indentation morphology begins to change again. Not only is the average aspect ration lower than for the 1050°C indentations, but it significantly decreased with increasing dwell time. (Figure 6.4(e) shows a 20 second indentation). The sides of the hollow under the short diagonal have become less steep. The fact that the valley beneath the indenter is closely connected with the rate of indentation creep, is confirmed by the interference fringes around an indentation with a sample temperature of 1175°C but an unheated indenter (average temperature 927°C) (figure 6.4(f). The hollow around the indentation is very pronounced, although the rounded hills either side of the indentation seem to be diminished in size.

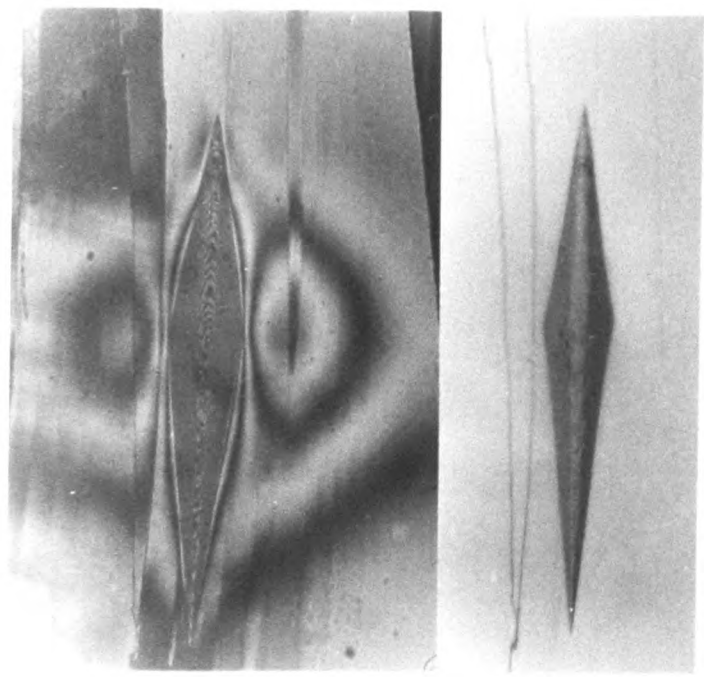
Figure 6.4 Interference fringes (and accompanying image without fringe contrast) for <110> Knoop indentations on (001) MgO: (a) 150°C, (b) 525°C, (c) 750°C, (d) 1050°C, (e) 1175°C and (f) 1175°C sample temperature but unheated indenter (927°C).



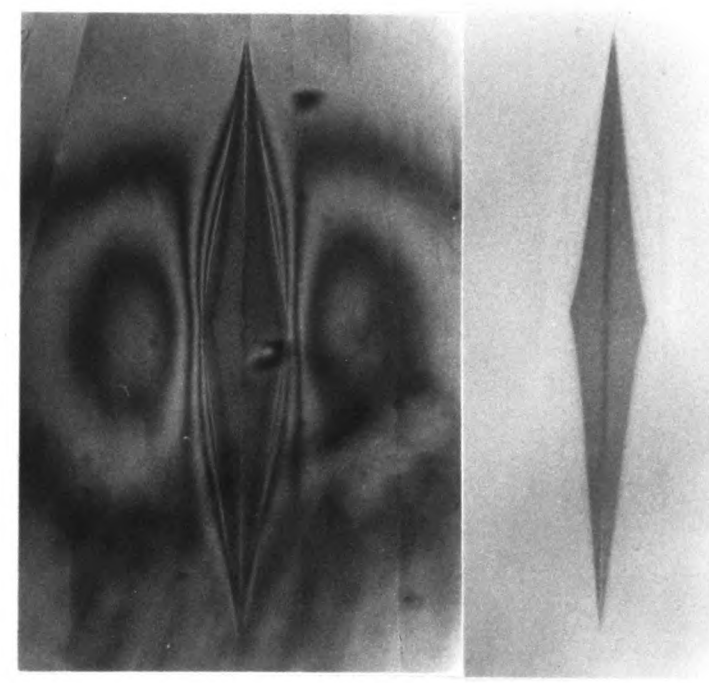
(a)



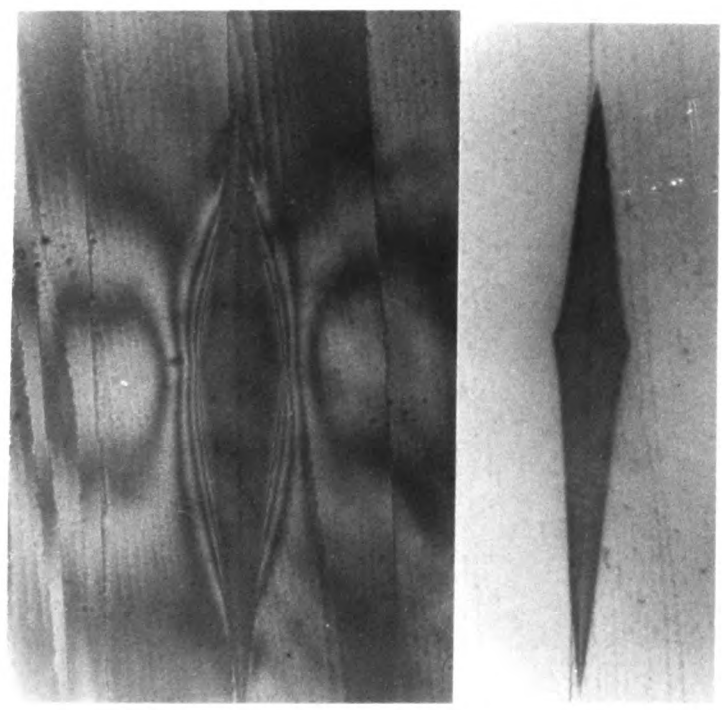
(b)



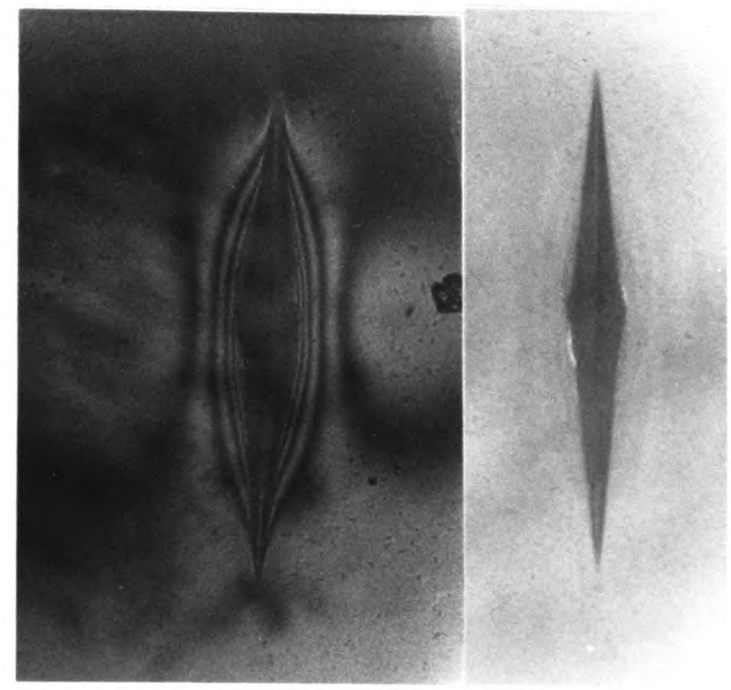
(c)



(d)



(e)



(f)

100 μm

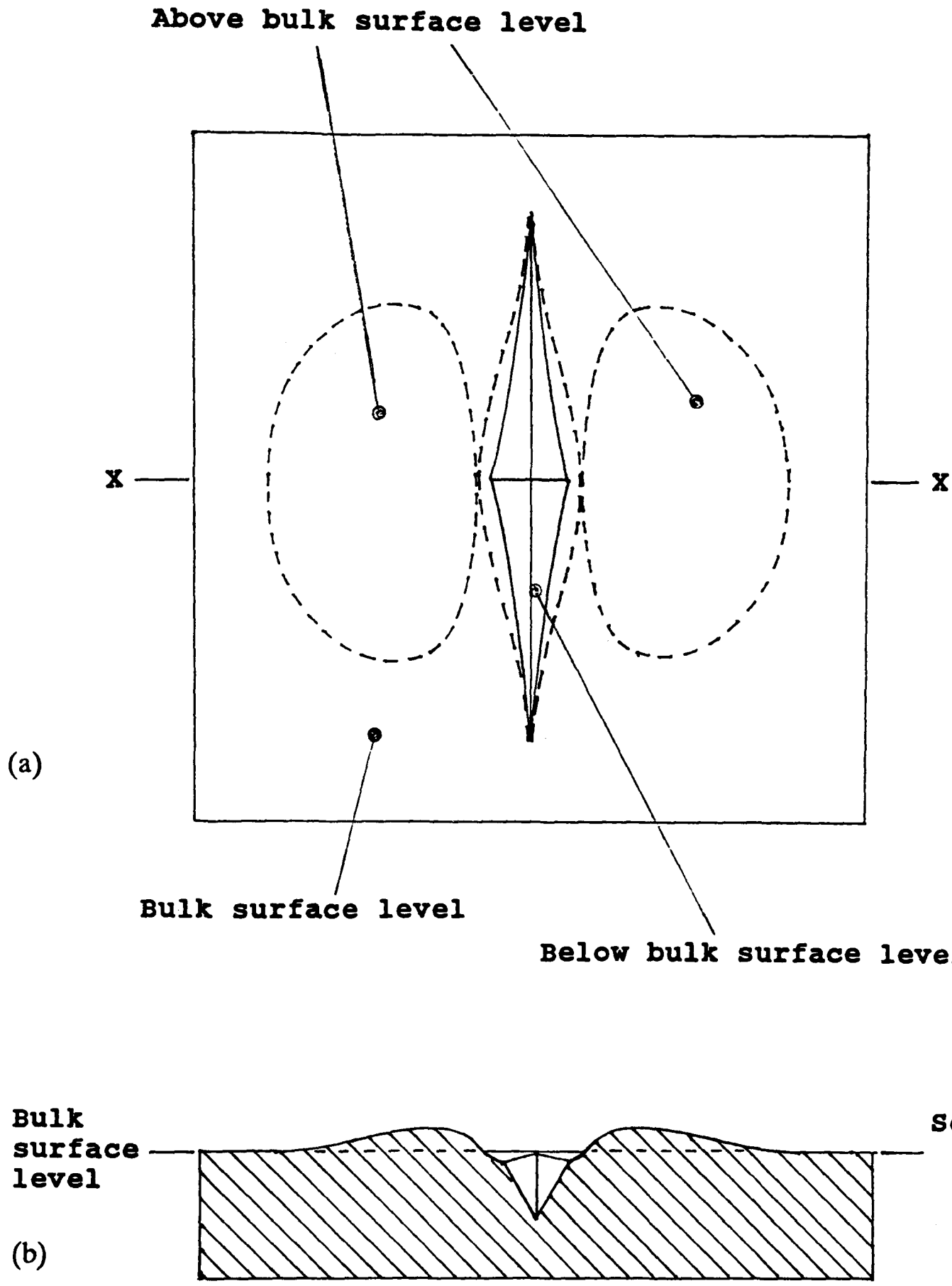


Figure 6.5 Schematic view of the surface morphology aound a <110> Knoop indentation on (001) MgO: (a) Sketch of fringe pattern indicating the position of various regions relative to the bulk sample surface, (b) Vertical section across the short diagonal of such an indentation.

Figure 6.6 shows interfermometry fringes around <100> Knoop indentations. At room temperature, very steep and localised pile up either side of the short diagonal can be seen. It is this which causes the increased length of the measured short diagonal compared to the long diagonal and hence the low aspect ratio. As the temperature of indentation is increased, the pile up of material around the indentation is still concentrated in two ridges, running parallel to the long diagonal of the Knoop indent, but spread over a larger lateral area, not so close to the short diagonal tips. The aspect ratio therefore tends more towards the ideal. In the no creep temperature range the aspect ratio began to rise for the same reasons as outlined above, although the extent of pile up around the <100> indentations (and therefore the aspect ratio) was always less than for the <110> orientation.

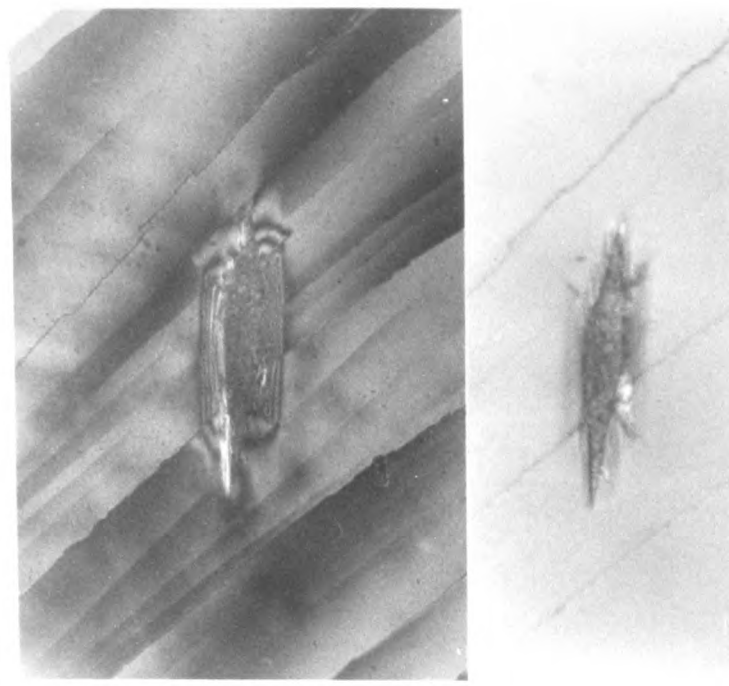
Pile up around the Vickers indentations was, as would be expected, more symmetrical (figure 6.7). The <100> indentation at 750°C shows clearly the hills of pile up opposite each facet and the dip at each diagonal tip which gives rise to the barreled appearance (figure 6.7a and b). By contrast, the <110> indentation has pile up at each tip, giving a starred appearance (figure 6.7c and d), even more pronounced at 1050°C (figure 6.7e and f).

6.4 Cracking and Slip Steps

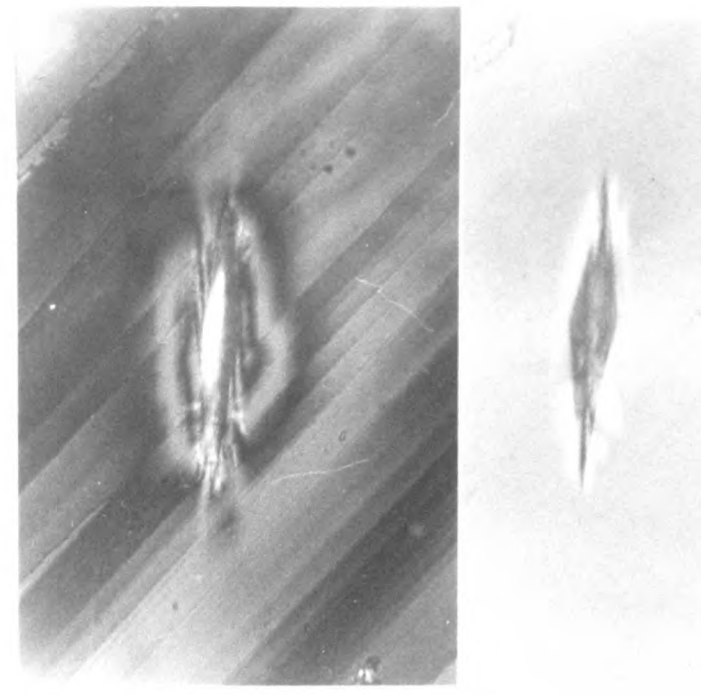
Some surface cracking occurred round the room temperature <110> Knoop indentations, although the cracks were variable in number (sometimes none at all), and ran at 90° to the direction of the long diagonal From the relatively small number of indentations at each loading time (five) it would appear that the long time (600 second) indentations have fewer cracks. On <100> room temperature indentations cracks formed at 45° to the long diagonal. "Angels' wings" composed of slip steps or very small cracks could be seen on each side of the indentation (figure 6.8a). Sometimes extra cracks had formed near the tips of these wings, and occasionally end cracks extending from the indentation tips. Thus both Knoop orientations showed cracks in the <110> directions which are formed by dislocation interactions (as discussed in section 5.5).

Figure 6.8 shows how the pile up, cracks and slip steps effect the morphology around room temperature Vickers indentations, both before and after annealing at 600°C. Cracks are in the <110> direction and lie across the top of the four pile up hills. The <100> indentation which is in an as made state (figure 6.8a and b) shows angular pile up patterns, clearly illustrating the picture frame of slip steps. As mentioned by Chaudhuri (1986), the <110> cracks stop at the corner of the picture frame. There is evidence of subsurface fracture activity for both orientations. The <110> orientation is noticeably starred.

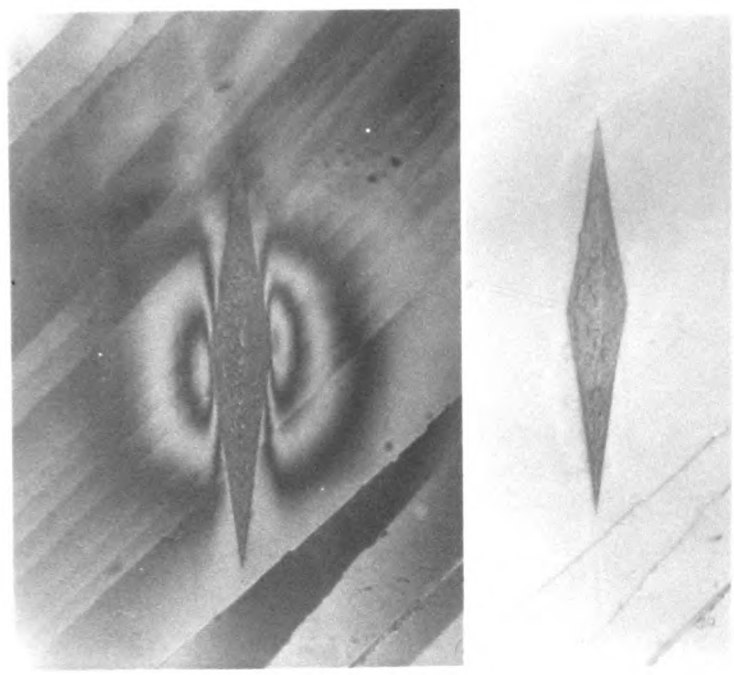
Figure 6.6 Interference fringes (and accompanying image without fringe contrast) for <100> Knoop indentations on (001) MgO: (a) room temperature, (b) 150°C, (c) 525°C, (d) 750°C, (e) 1050°C and (f) 1175°C.



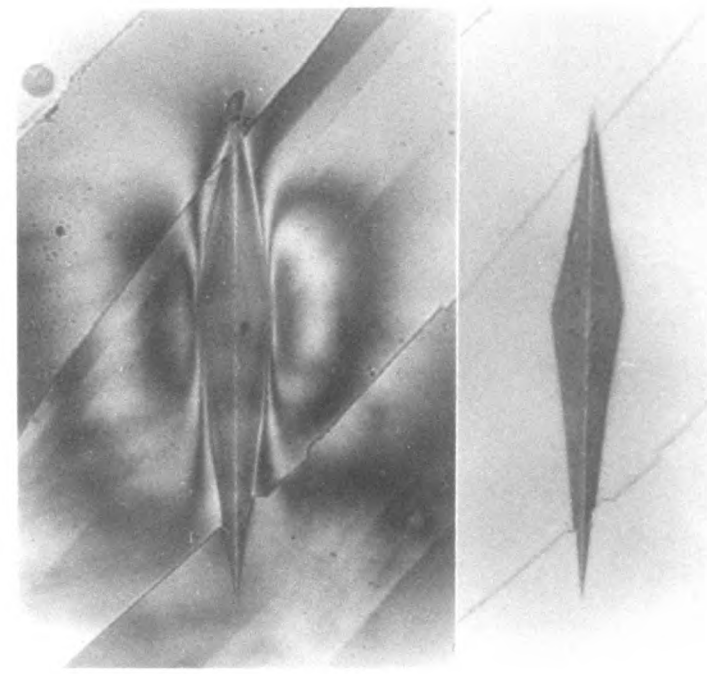
(a)



(b)



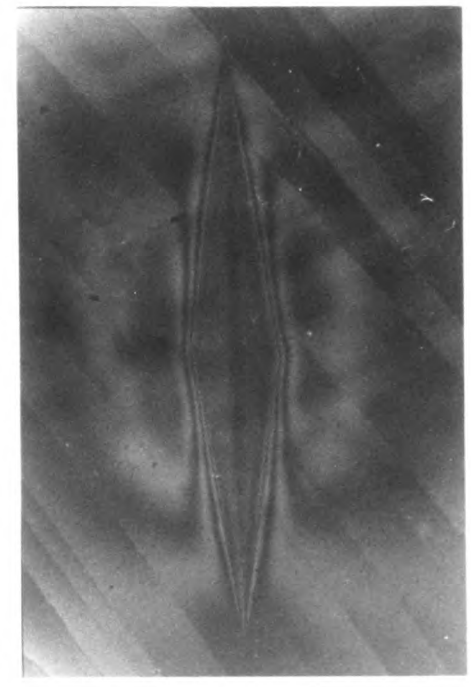
(c)



(d)



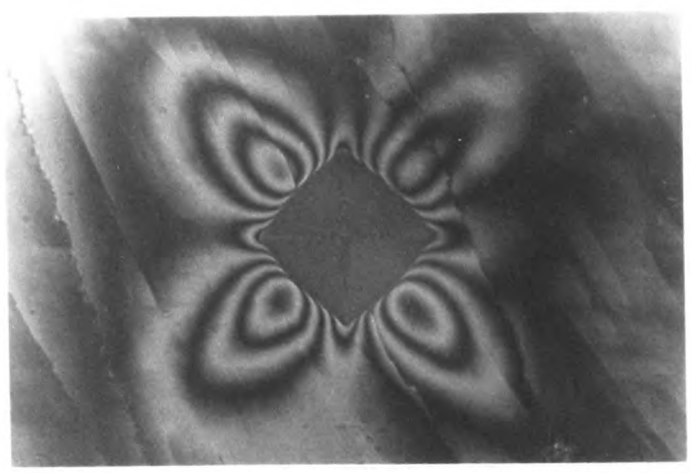
(e)



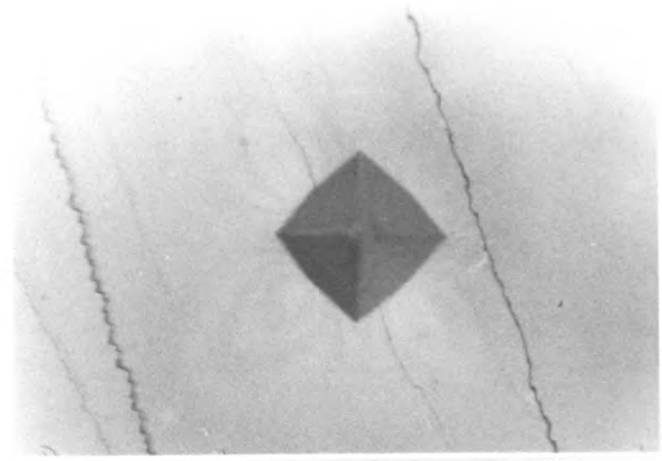
(f)

100 μm

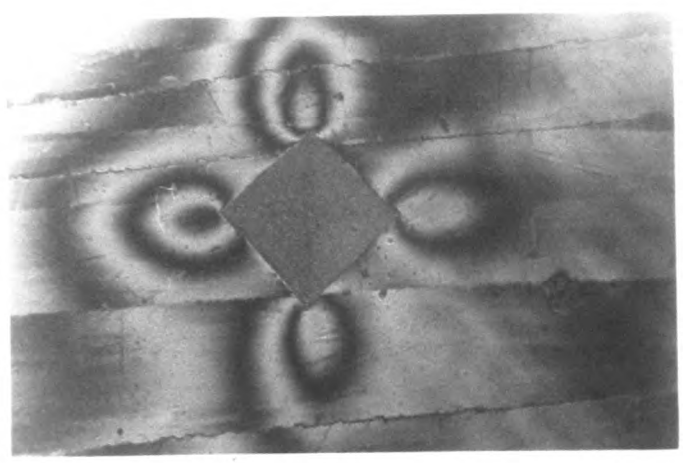
Figure 6.7 Interference fringes (and accompanying image without fringe contrast) for Vickers indentations on (001) MgO: (a) and (b) <100> orientation at 750°C, (c) and (d) <110> orientation at 750°C, (e) and (f) <110> orientation at 1050°C.



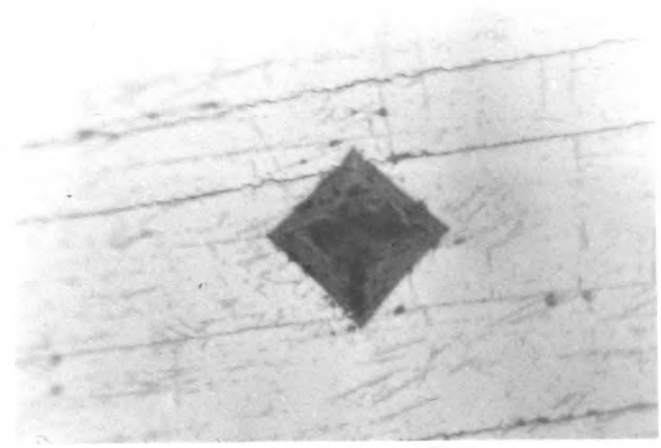
(a)



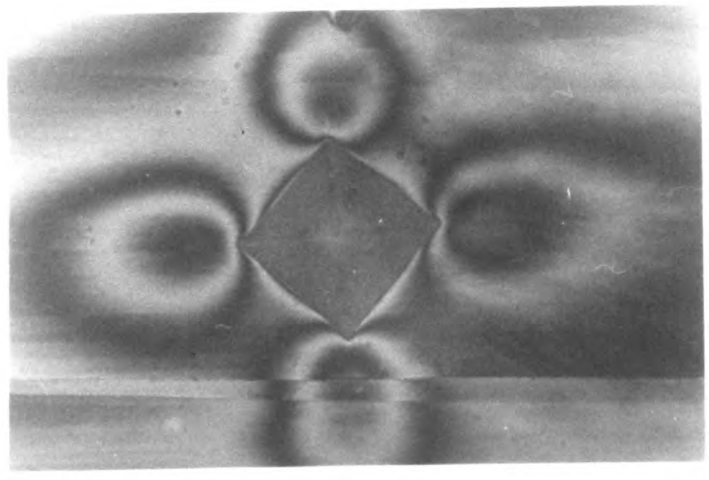
(b)



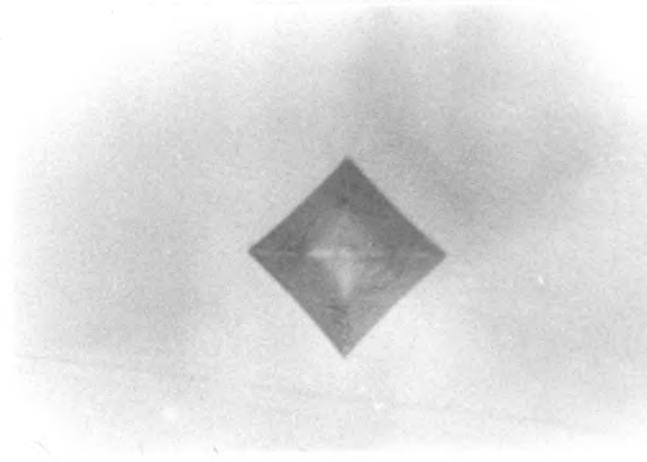
(c)



(d)



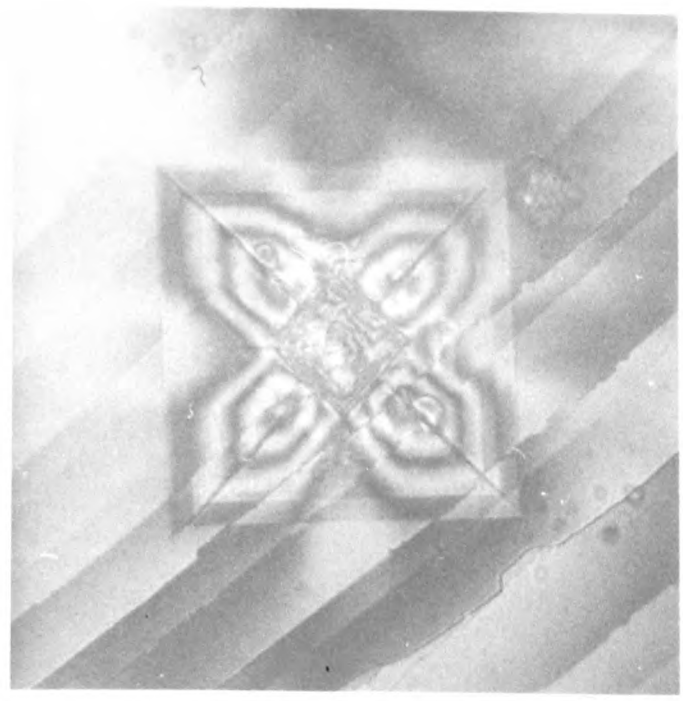
(e)



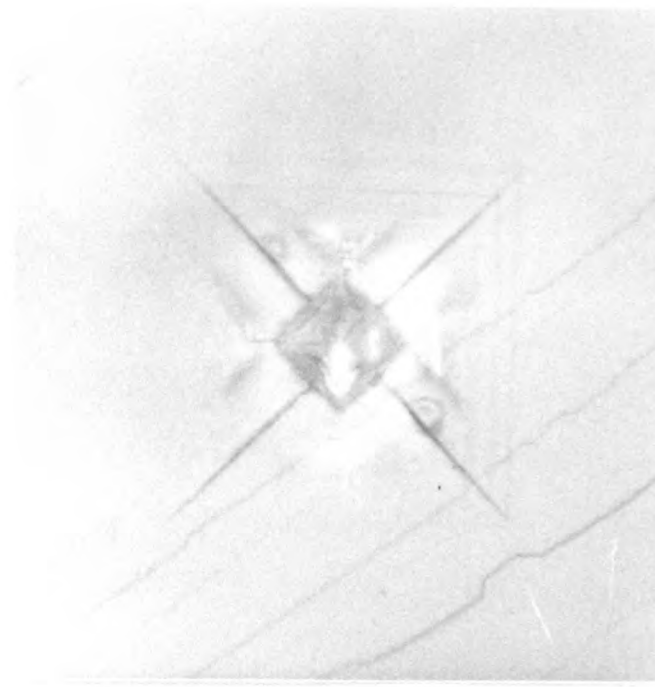
(f)

100 μm

Figure 6.8 Interference fringes (and accompanying image without fringe contrast) for room temperature Vickers indentations on (001) MgO: (a) and (b) <100> orientation indentation made after the sample had been pre- annealed at 750°C for 3 hours, (c) and (d) <100> orientation indentation post-annealed at 750°C for 4 hours, (e) and (f) <110> orientation indentation, post annealed at 750°C for 4 hours.



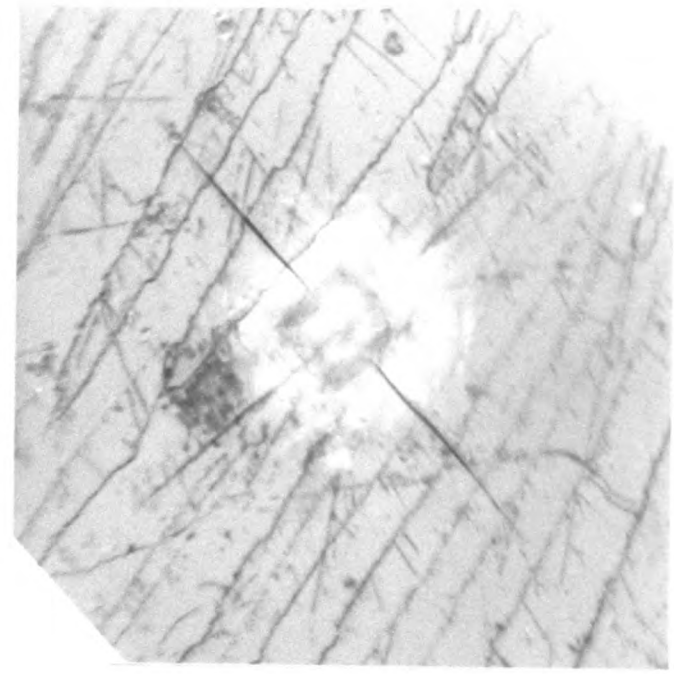
(a)



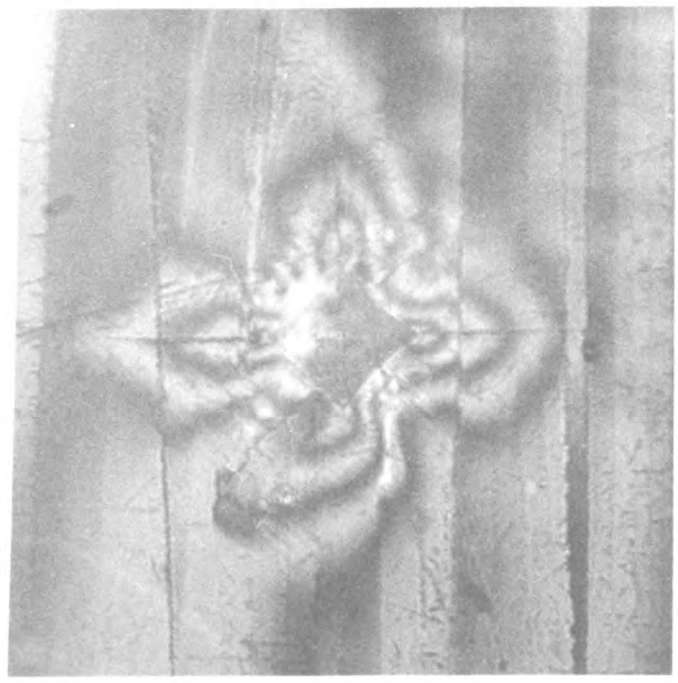
(b)



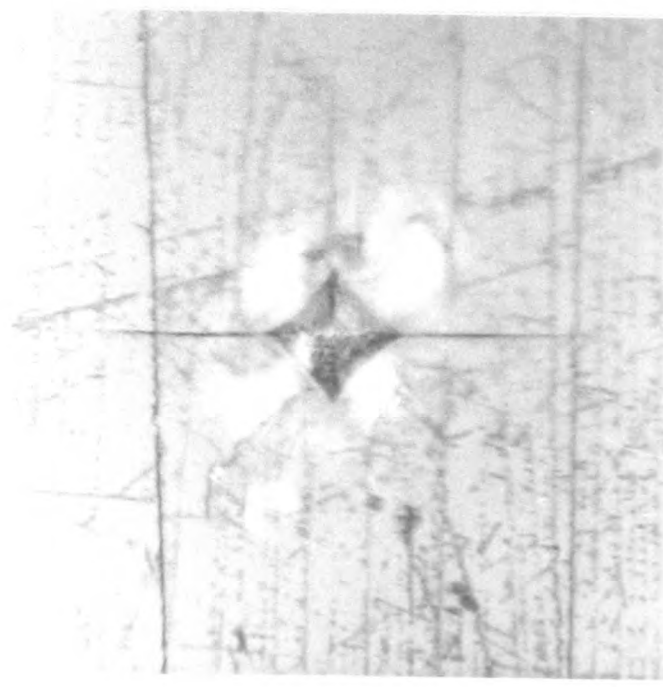
(c)



(d)



(e)



(f)

100 μm

6.5 Effect of Pre- and Post-Annealing

Pre-anneal (i.e. at least 2 hours) at 750°C or 450°C did not alter the hardness, creep behaviour or aspect ratio of room temperature Knoop indentations at either orientation within experimental error.

However for indentation tests carried out at 600°C the values of hardness were effected as shown in figures 6.9. For both orientations, samples pre-annealed at 750°C gave a lower value of hardness when tested at 600°C, (and showed a higher, more distorted aspect ratio) than samples had not been annealed. The affect on 450°C hardness values was less, although generally pre-annealing seemed to lower hardness. The hardness anisotropy was preserved between the two orientations at any equivalent conditions.

The measured dimensions of room temperature Vickers indentations were not changed by an anneal after indentation. Figure 6.8 shows that the amount of pile up was also unchanged, although some rounding of outline occurs indicating that some dislocation re-arrangement may take place.

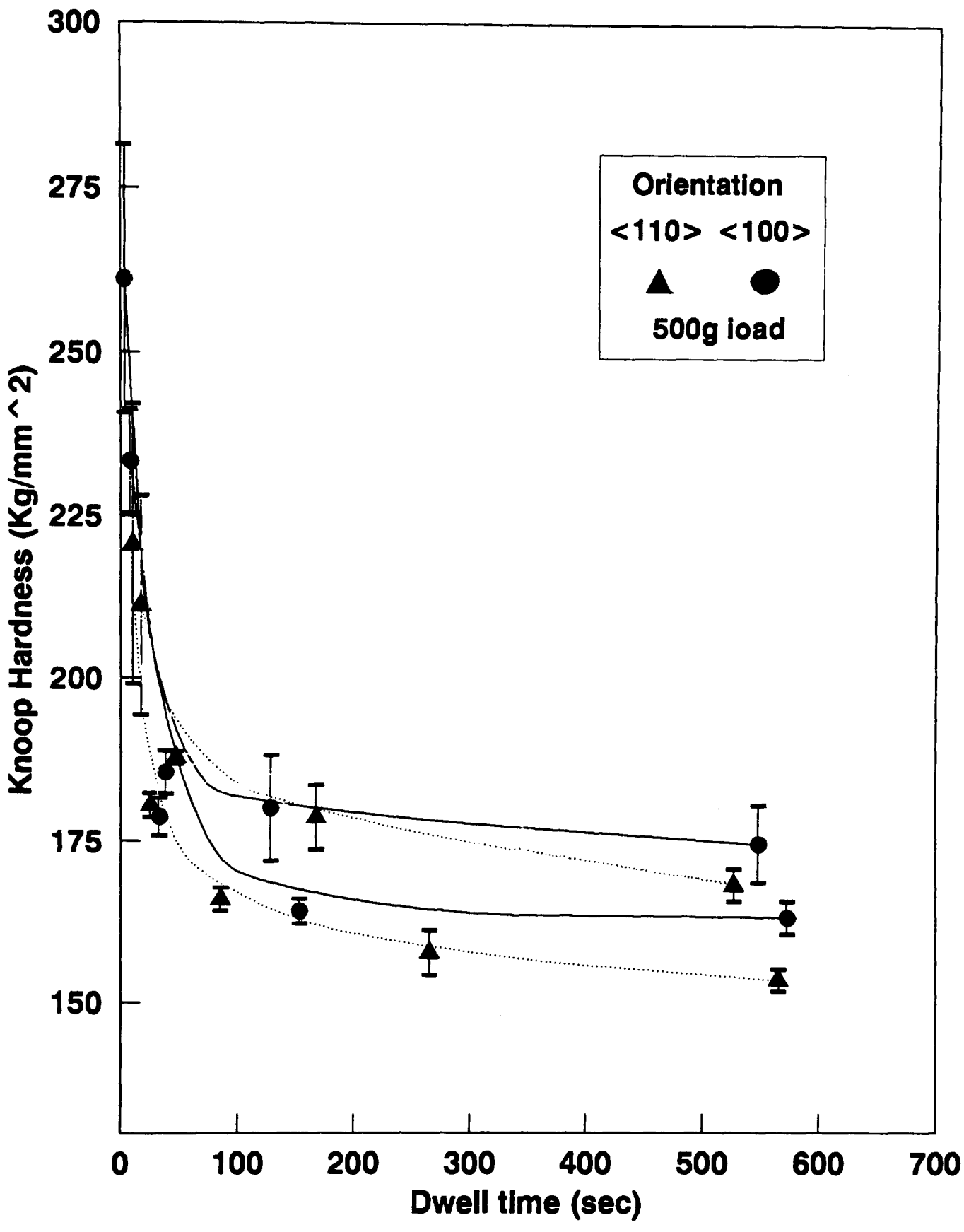


Figure 6.9 The effect of pre-anneal on Knoop hardness at 600 C on (001) MgO.

7. MAGNESIUM OXIDE DISLOCATION ANALYSIS AND CONCLUSIONS

Many authors have shown that the indentation behaviour of MgO is determined by the indenter morphology and the temperature of testing. This is not surprising since the indenter morphology will affect the stress distribution to which the material is subjected and, as the temperature is raised, the relative importance of various deformation mechanisms will alter.

This chapter details the dislocation arrays around indentations from etched samples and discusses the mechanisms which might lead to the observed creep and anisotropy behaviour.

7.1 Slip Systems

Most indentation testing has taken place on the {100} cleavage planes, and the arrangement of the primary slip systems ({110} [110]), which might be activated, are shown in figure 7.1.

{110} planes may meet the surface at an angle of 45° or 90°, referred to as $\{110\}_{45}$ and $\{110\}_{90}$ respectively. By etching spherical and pyramidal indentations, Keh (1960) identified pits on the $\{110\}_{45}$ planes (i.e. forming traces along the [100]) directions as being screw components at the surface, since the segments are parallel to the Burgers vector. Conversely those on the $\{110\}_{90}$ planes meet the surface with edge components.

7.1.1 <100> Knoop Indentations

The ERSS type model (Brookes et al 1971, Roberts 1988) predict that Knoop <100> orientations on the {001} face of rock-salt structures will be the hardest, since this corresponds to the minimum value of the effective resolved shear stress on the <110> {110} slip system. Such anisotropy at room temperature has been well documented (e.g. Brookes et al 1971 and 1975), and can be seen in figure 6.1. The <110> Knoop hardness is nearly twice that of the <100> hardness, which is in good agreement with results published by other authors (e.g. Brookes et al 1971).

The room temperature etched dislocation pattern around a <100> Knoop indentation is shown in figure 7.2(a). The dislocations are dispersed along definite crystallographic directions. The <110> orientation indentations showed a dense array, from which separate directions could not be distinguished. It seems probable that all slip

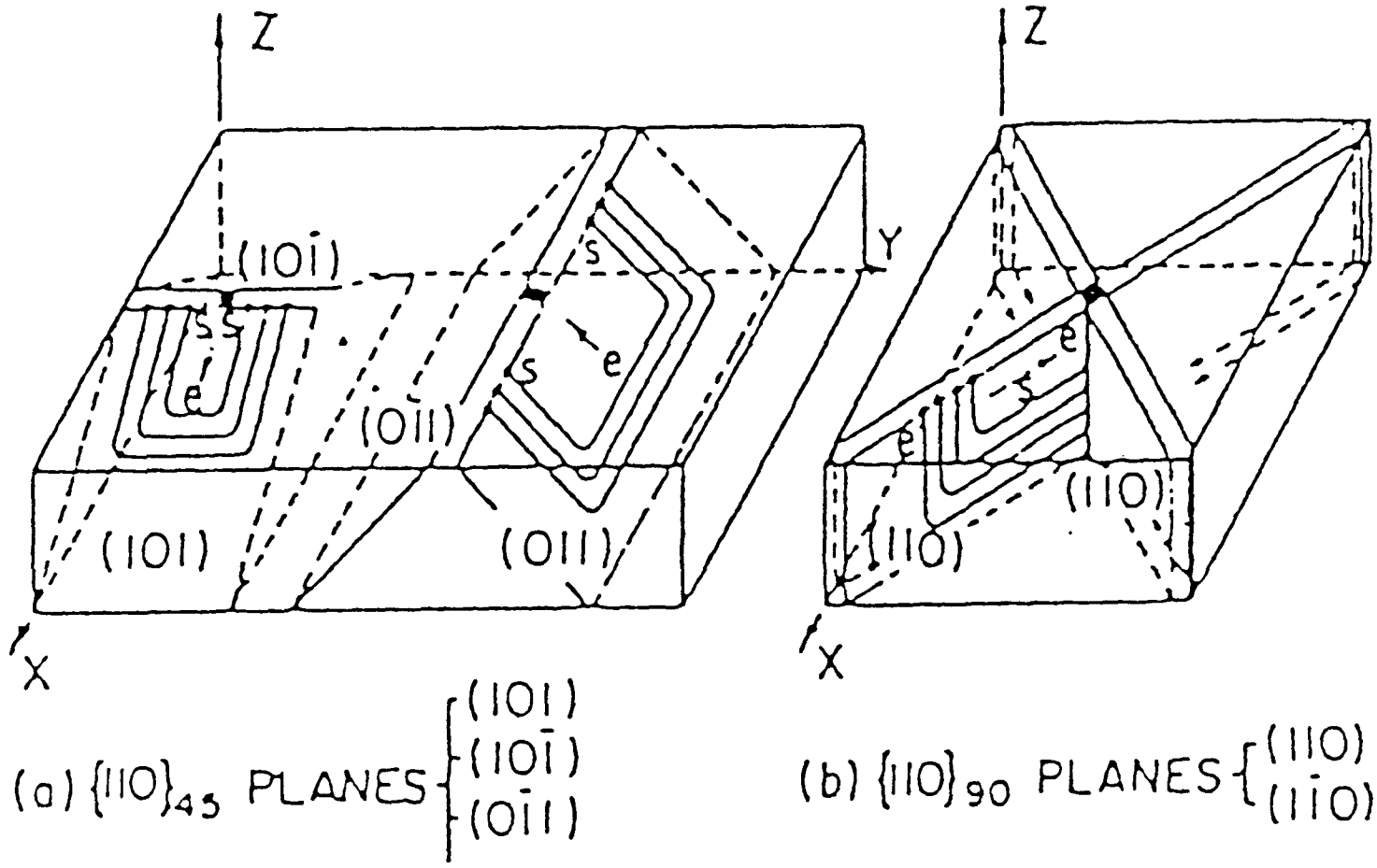
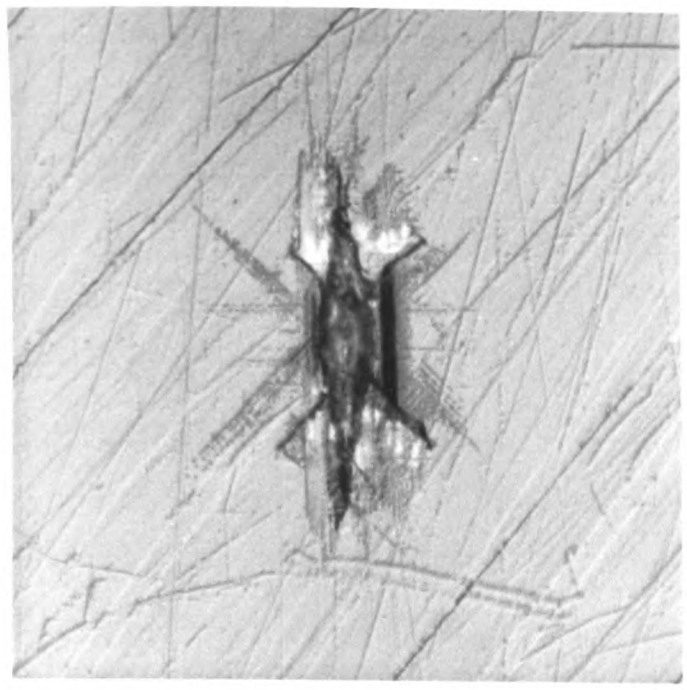
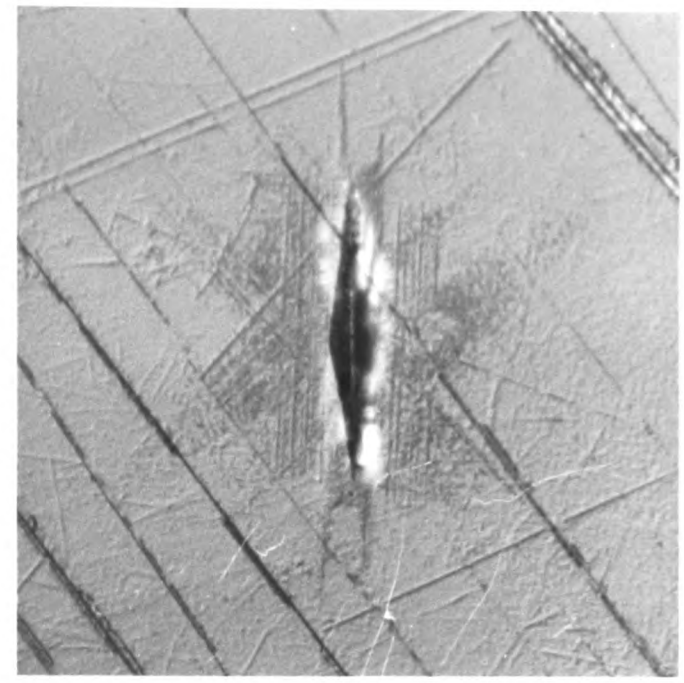


Figure 7.1 Primary slip system which might be activated by indentation on (001) MgO:(a) $\{110\}_{45}$ planes, (b) $\{110\}_{90}$ planes (after Keh 1960).

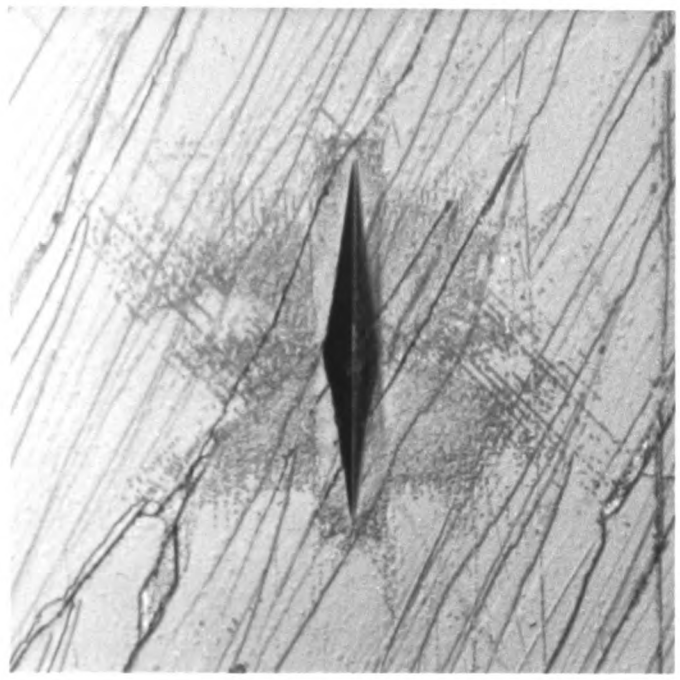
Figure 7.2 Dislocation patterns around <100> Knoop indentations on (001) MgO: (a) Room temperature, (b) 150°C, (c) - (f) 400°C indentations with dwell times of 60, 120, 240 and 600 seconds respectively.



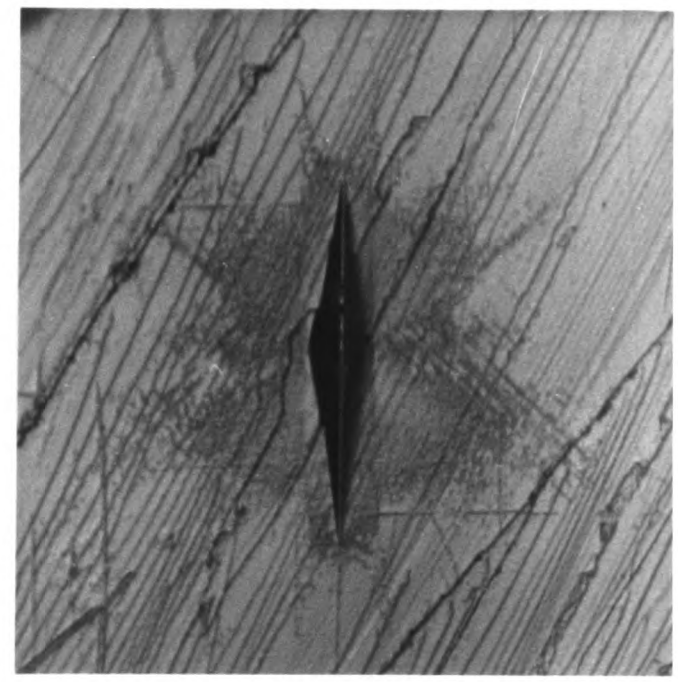
(a)



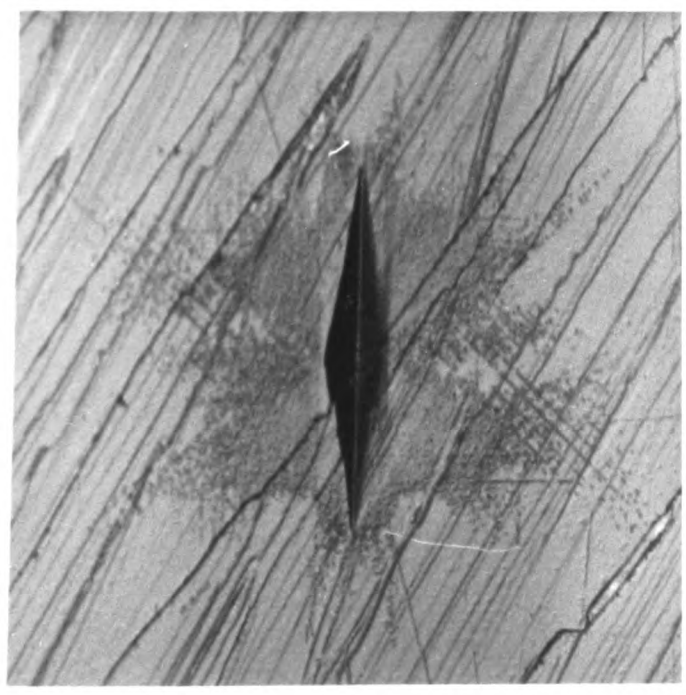
(b)



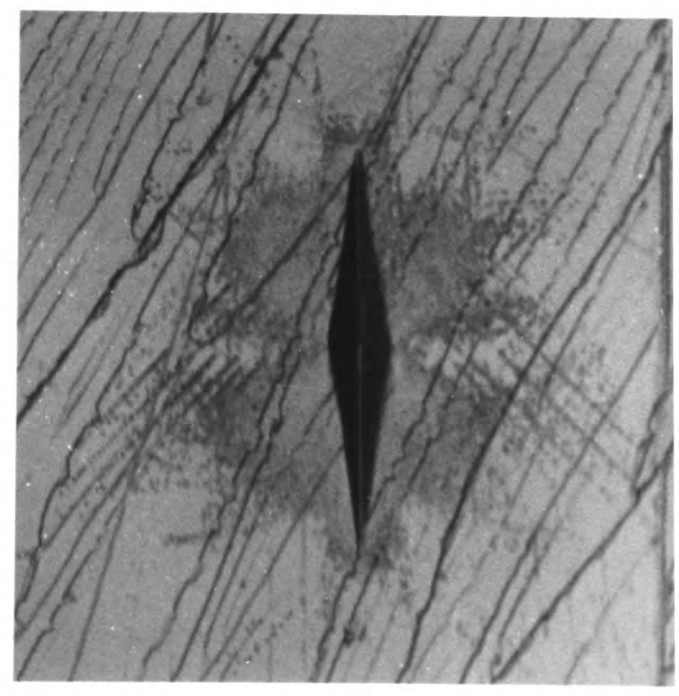
(c)



(d)



(e)



(f)

100 μm

modes in the primary system are present in both orientations. Roberts (1988) did not identify any "rosette" slip ($\{110\}_{90}$) normal to the indenter long axis in the <110> orientation, (the RSS models predict zero stress on this system for this orientation), but the density of the pattern makes it difficult to tell. Serial sectioning and etching allowed Roberts to identify the dominant slip mode for the <100> orientation at room temperature, as punching in of material on two sets of parallel slip planes, inclined at 45° to the specimen surface, with the traces of the planes parallel to the long diagonal. Extending down to approximately the same depth was less intense dislocation activity on the other set of inclined planes which crossed over beneath the indenter. Some shallower slip also occurred on $\{110\}_{90}$ planes, with traces on the surface at 45° to the indenter diagonals.

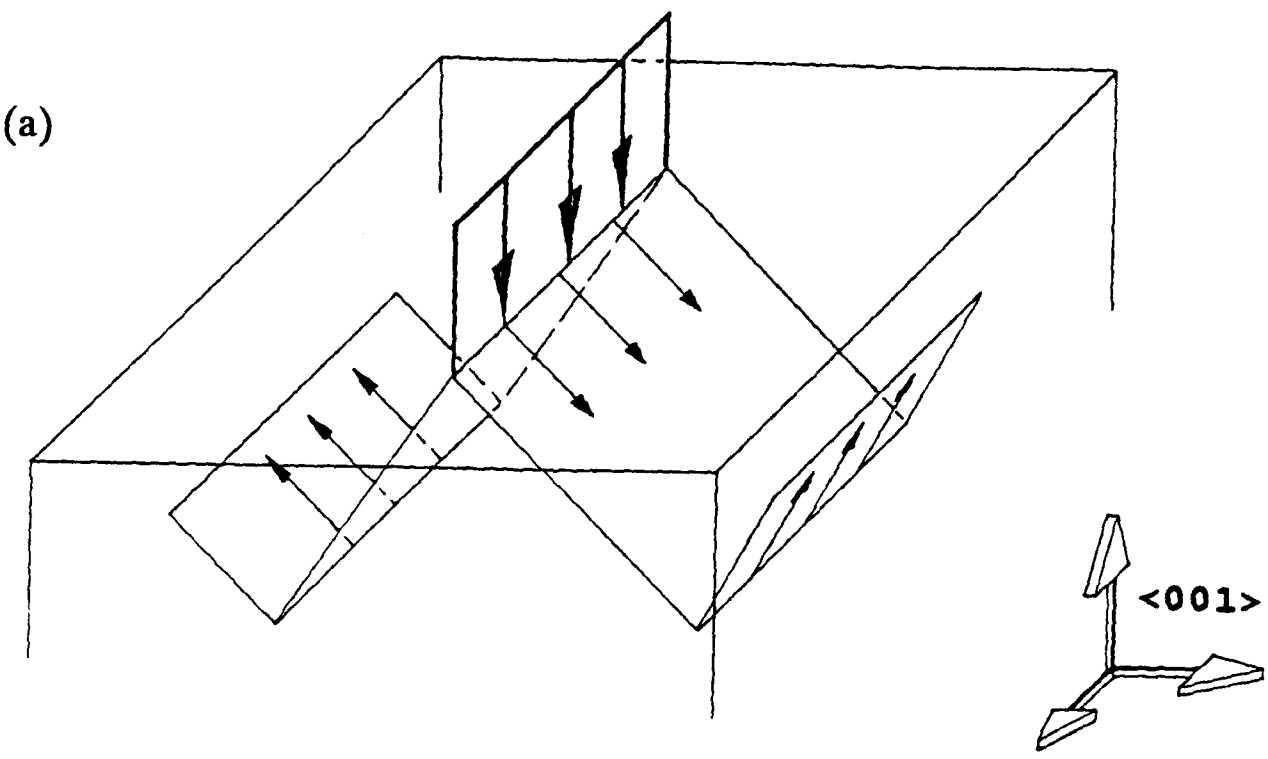
At higher temperatures, the lines of dislocations parallel to the long diagonal of the <100> indentations (which were concentrated in the "angel wing" areas) become more widely spaced. Such lines are visible beside the 150°C indentation shown in figure 7.2(b) running the whole length of the indentation, and corresponded well to the slip lines observed on the unetched sample. Suggested material movement which would cause these slip lines (and the pile-up illustrated in section 6.3 is shown in figure 7.3(a) (after Boyarskaya, Grabko and Purich 1979). It has been calculated (Roberts 1988) that most, if not all, of the material displaced by the indenter in room temperature <100> orientations is compensated for by amount of material which has moved to the surface to form the pile up. He comments that the slip which is responsible for the pile up, can be assumed to result from pre-existing dislocations in the bulk of the sample moving to the surface on the appropriate slip planes, activated by the stresses moving dislocations in the outer $\{110\}_{45}$ slip band.

The time sequence at 400°C (figure 7.2c - f) indicates that, at longer dwell times, some dislocation movement takes place on the $\{110\}_{45}$ planes with traces perpendicular to the long diagonal of the indenter, opening up a "space" by the ends of the short diagonal. At 400°C and above, a rectangle of dislocations approximately the length and (widest) breadth of the impression surrounds the indent (figure 7.4). The main dislocation area does not extend the whole length of the impression.

7.2 <110> Knoop Indentations

Dislocation patterns around <110> indentations are shown in figure 7.5. As noted in the interferometry results (section 6.3), the surface around <110> room temperature indentations was almost flat. This suggests that displaced material was accommodated by elastic compression of a large volume, rather than by upward plastic flow (Roberts 1988), which would provide a large driving force for elastic recovery once the load was removed

(a)



(b)

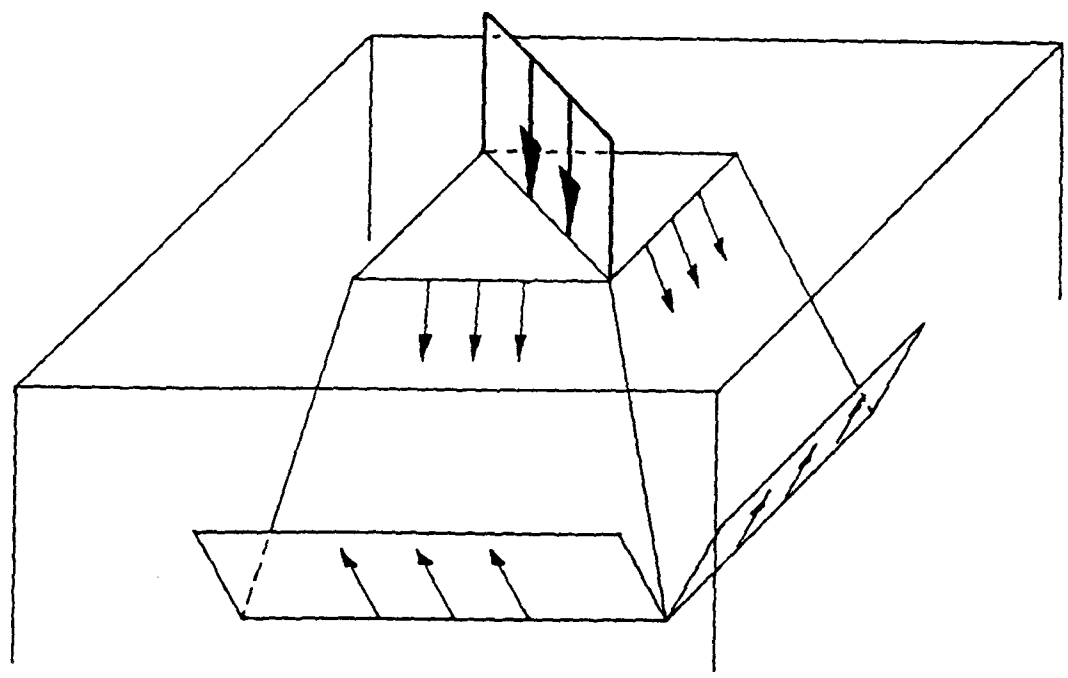
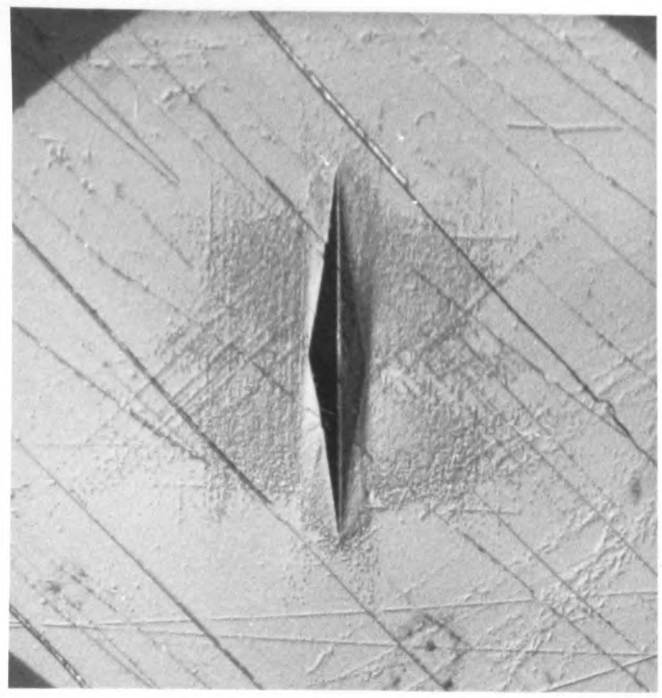
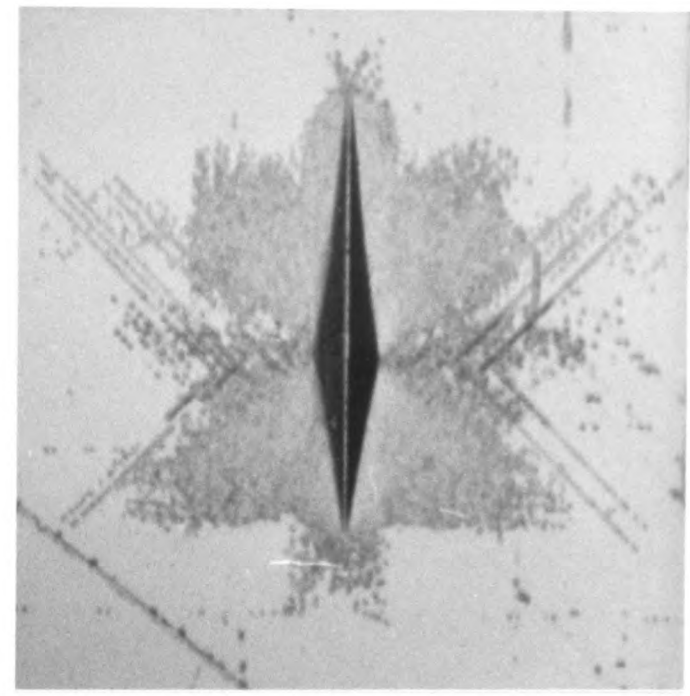


Figure 7.3. Arrangement of the most active $\{110\}_{45}$ slip planes for a) <100> orientaton, b) <110> orientation.

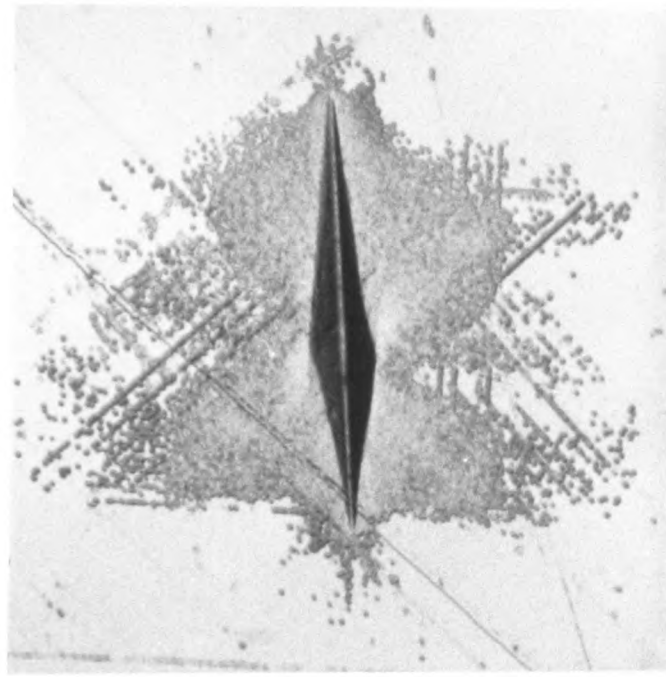
Figure 7.4 Higher temperature dislocation patterns around <100> Knoop indentations on (001) MgO: (a) 600 second indentation at 525°C, (b) and (c) 60 and 600 second indentations at 600°C, (d) 600 second at 750°C, (e) 600 second indentation at 1050°C.



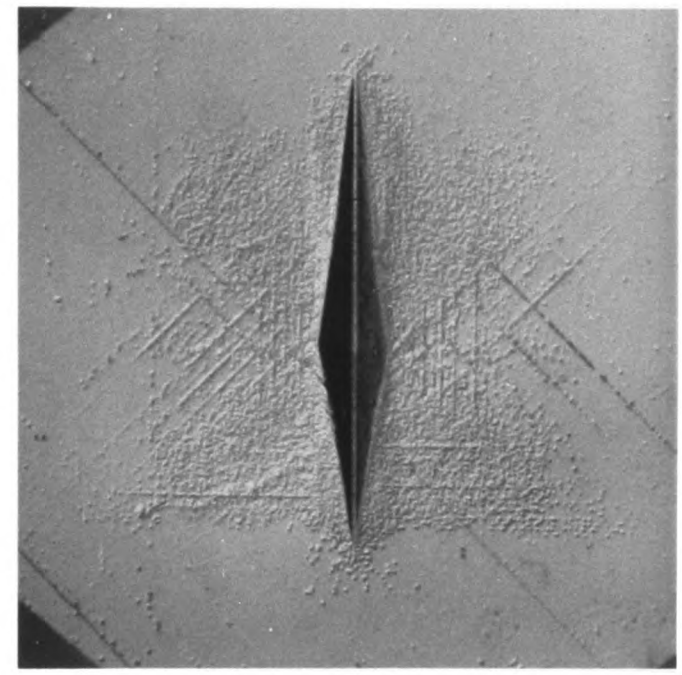
(a)



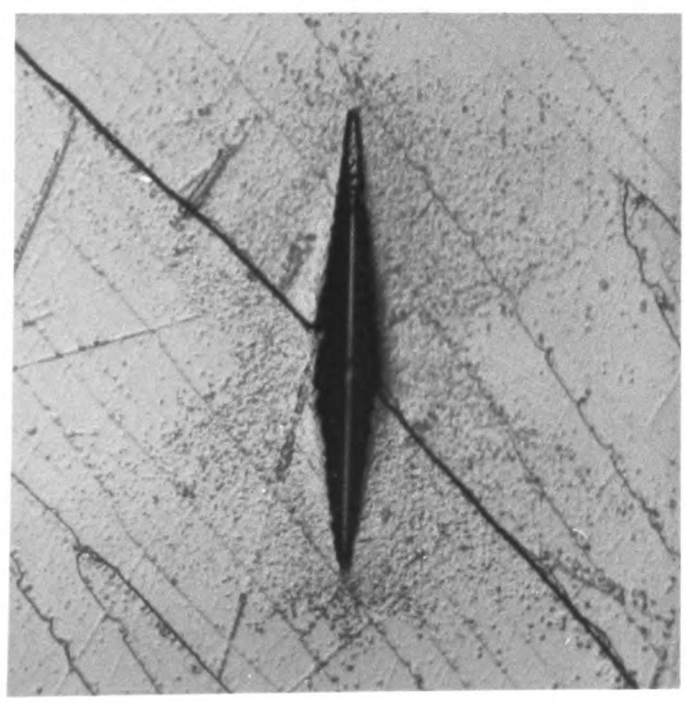
(b)



(c)



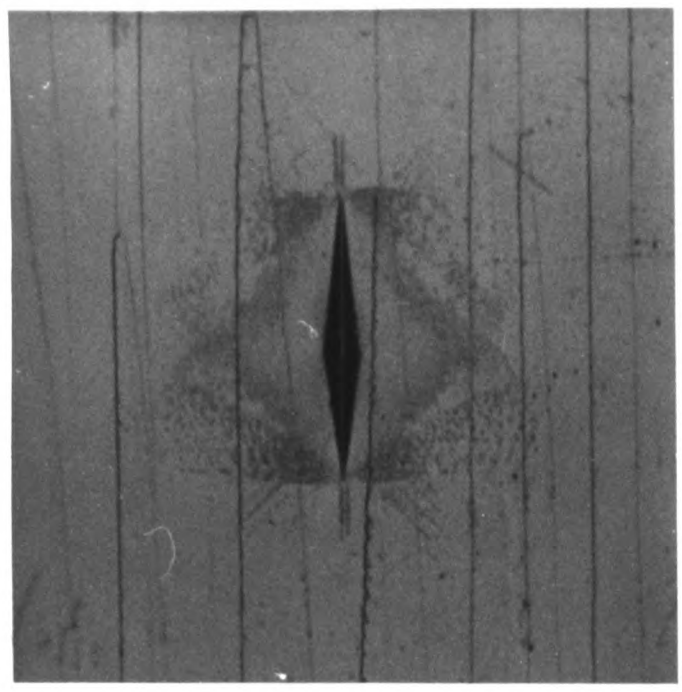
(d)



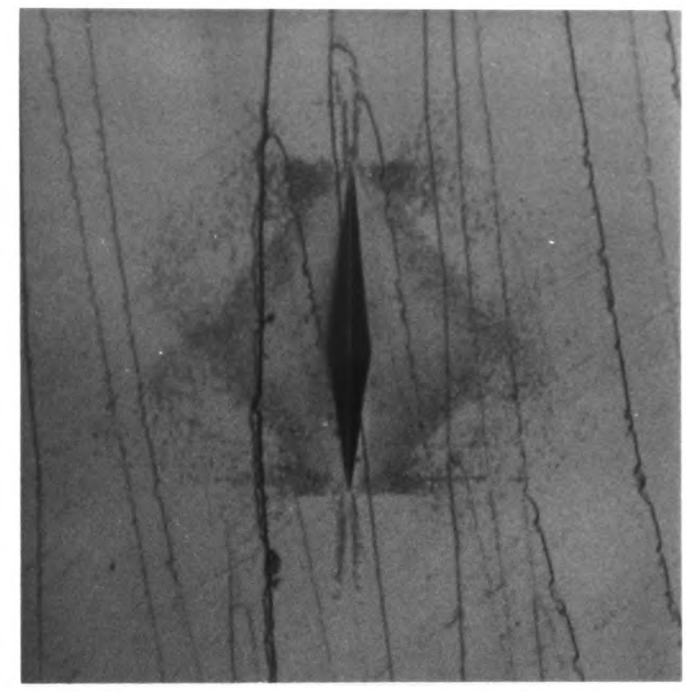
(e)

100 μm

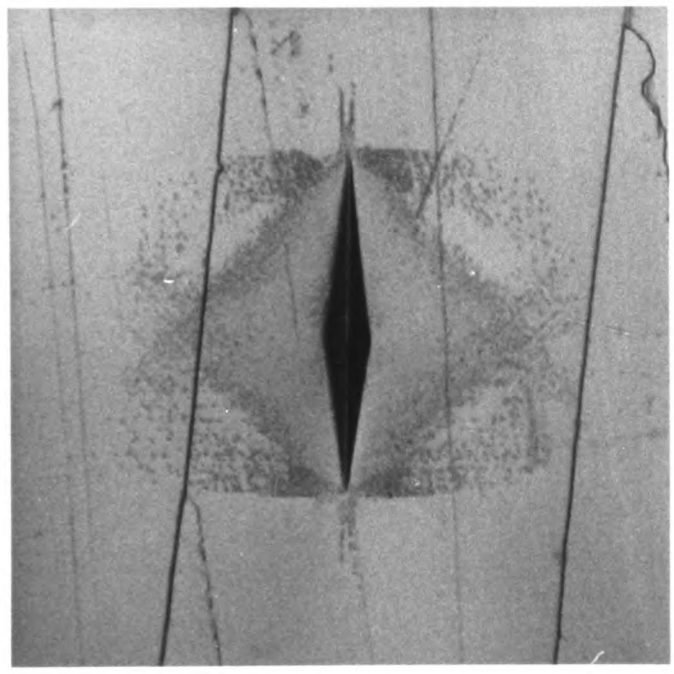
Figure 7.5 The dislocation pattern around <110> indentations on (001) MgO: (a) and (b) 60 and 600 second indentations at 300°C, (c) and (d) 60 and 600 second indentations at 450°C, (e) and (f) 60 and 600 second indentations at 600°C.



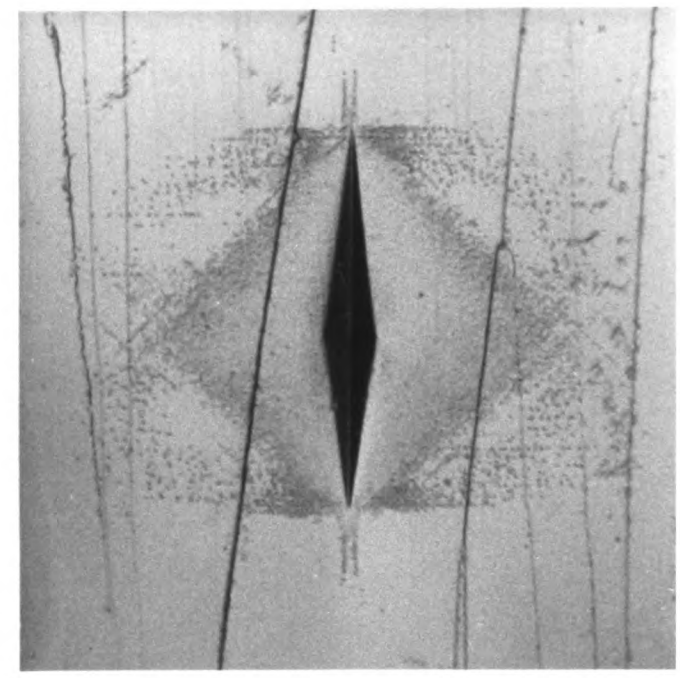
(a)



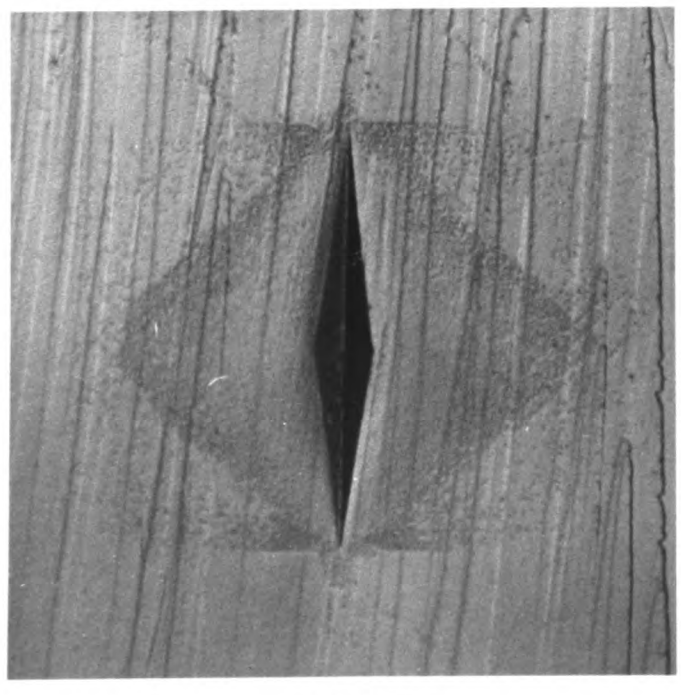
(b)



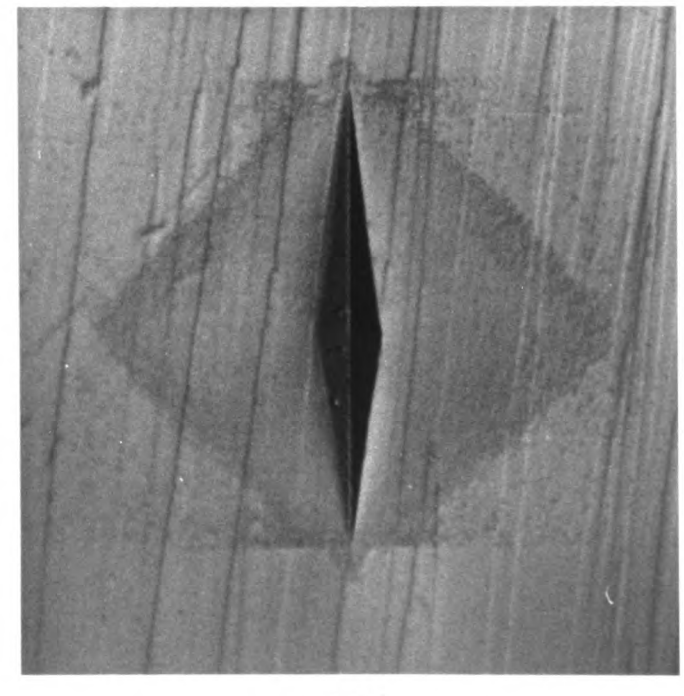
(c)



(d)



(e)



(f)

100 μm

leading to the high aspect ratio noted. Serial sectioning (Roberts 1988) found that, below the surface, the deepest activity had again extended down on the $\{110\}_{45}$ planes, this time with fourfold symmetry. Activity on planes with traces parallel to the indenter long diagonal went down deeper than for the <100> orientation.

No definable difference in pattern or scale could be seen between the dislocation arrays of indentations made at a particular temperature, but at different dwell times. The 300°C pattern shows clearly that all the primary slip system planes are being activated, including the $\{110\}_{90}$ planes which show traces running normal to the indenter. The fourfold symmetry of $\{110\}_{45}$ planes which form a diamond shape (with the indentation long diagonal forming the diagonal of the diamond), probably indicate the same diverging set of planes as noted in the serial section of room temperature indentations (Roberts 1988). The $\{110\}_{90}$ planes' traces extending from the indentation tips in the same direction as the long diagonal were always in two distinct rays, which was also often the case for the traces at 45° to the indenter diagonal and 90° to the diamond shape mentioned.

At 450°C the two rays extending from each tip are still there, but there is little sign of traces running perpendicular to the sides of the intensely packed diamond shape in the middle. The patterns also show pits outside the diamond area which appear to be arranged in a four curved bands, each starting and ending at a point of the diamond, but enclosing an area with out dislocations. (Such areas were visible, but less densely populated in the 300°C patterns. Examination at higher magnification suggests that they mainly consist of rows of dislocations, whose traces are perpendicular to the long diagonal (i.e. $\{110\}_{90}$ if on the primary slip system), but that, near the tips of the diamond which are adjacent to the short diagonal, the rows are at 45° to the long diagonal in the same direction as the side of the diamond area from which they extend. (Surface etching which only revealed the dislocations with an edge component at the surface on 750°C samples confirms this analysis if the dislocation distribution can be taken to be essentially the same).

By 600°C the very dense diamond shape area has extended out beyond the end of the long diagonal. It is therefore not possible to tell if the dislocation arrangements producing the rays from the indentation tip, and the curved bands mentioned above, are still activated, but it seems likely. Traces perpendicular to the long diagonal from $\{110\}_{90}$ planes are still visible.

It is interesting that, as reported in chapter 4, Stokes etching reagent failed to show up any dislocation patterns at all on the surface of some 750°C samples. A typical pattern for the $\{110\}_{90}$ dislocations etched by orthophosphoric acid at 80°C is shown in figure

7.6(a). It is possible that keeping the specimen at 750°C for several hours causes some change in the impurity / dislocation relationship, which means that the etching mechanism no longer works. It would seem to indicate that between 600°C and 750°C some rearrangement of impurities can take place. There was no difference in the dislocation patterns from short and long time indentations (30 and 570 seconds respectively). Nor did indentations at different made at 100g, 200g and 500g show any difference apart from scale.

The results of serial sectioning (figure 7.6) shows that the traces running parallel and perpendicular to the long diagonal are the shallowest feature for <110> Knoop indentations. The traces running in the <100> direction perpendicular to the sides of the central diamond pattern go deeper. The etch pits of these arrays could be distinguished from those in the central diamond under interference contrast conditions and someimes extended across the centre of the indentation. As more crystal is removed the density of pits decreases, until only the outline of the central diamond is left, with an area of pits lying across the diagonal which was directly below the indenter.

7.3 Vickers Indentations

For Vickers indentations, all four $\{110\}_{45}$ planes are activated in both orientations, but more intensively for <110> orientation (Boyarskaya et al 1979). (<110> is the softer Vickers orientation corresponding to Knoop <100>).

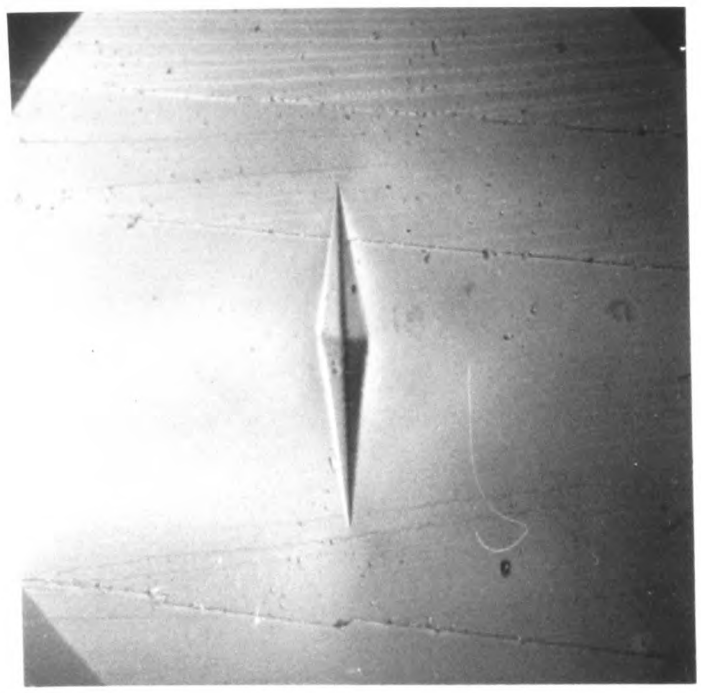
7.4 Indentation Creep

It is necessary to look closely at the creep mechanisms which might be available, to understand the indentation creep behaviour which is exhibited by MgO.

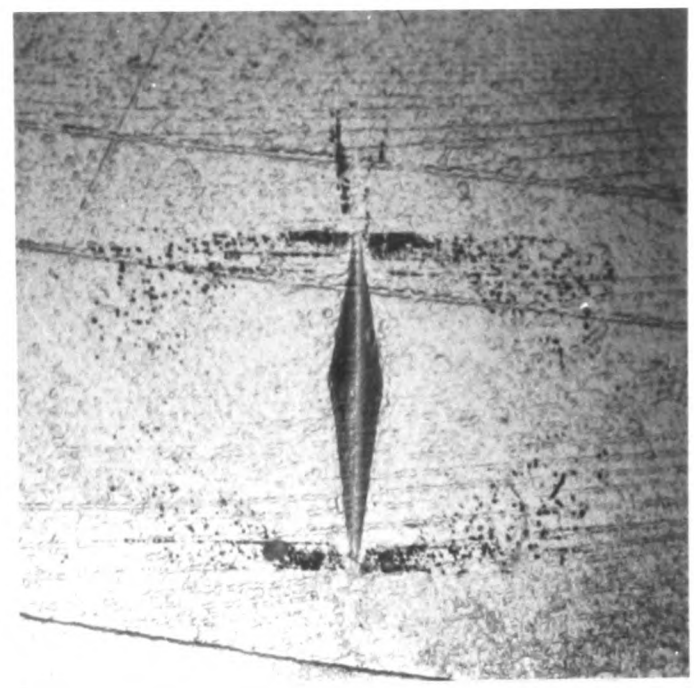
At temperatures from room temperature to over 600°C the results presented in this thesis agree with those of Brookes et al. The <110> orientation is hardest at room temperature for all indentation times; but does show slow creep (Brookes et al used dwell times up to over 16 hours), whilst <100> is of lower hardness with no measurable creep. The short time hardness of <110> decreases more rapidly than that of <100> and continues to show more rapid creep so that the anisotropy is reversed at longer time indentations for tests carried out at or above 0.3 T_M (600°C). (See figure 6.1 for fuller results).

Brookes et al (1975) suggest that it would be advantageous to consider the indentation in two parts. A first stage consists of initial penetration which occurs at fairly high strain rates, and is accommodated by slip on the primary slip system. A second stage

Figure 7.6 Serial sections of <110> 60 second indentation on (001) MgO:(a) Unetched, (b) surface etch, (c) ~4μm depth with orthophosphiric acid etch, (d) ~4μm depth with Stokes etch, (e) ~10μm depths with Stokes etch.



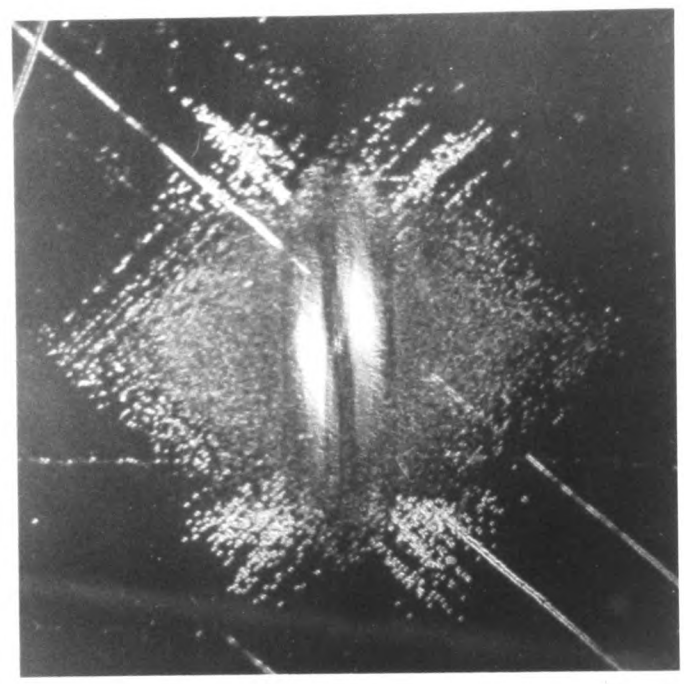
(a)



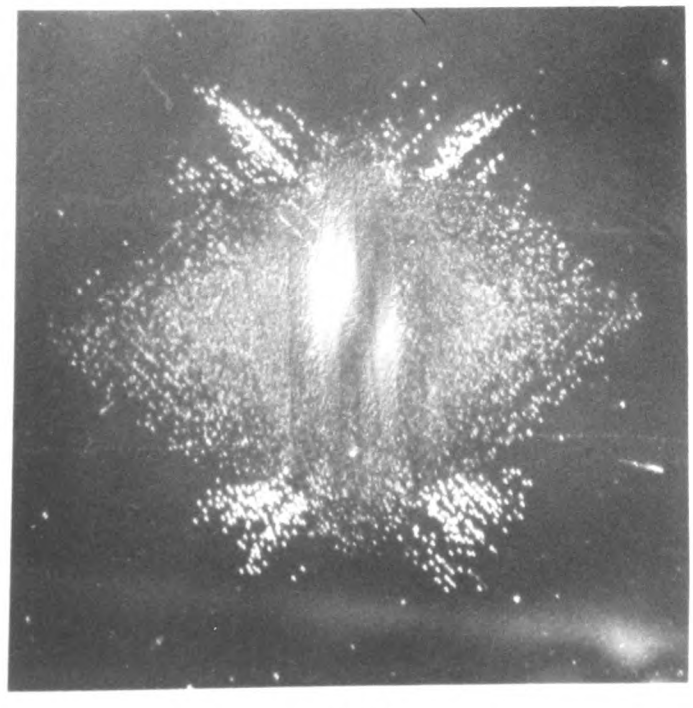
(b)



(c)



(d)



(e)

100 μm

of continued (time-dependent) penetration of the indenter, that is controlled by creep mechanisms at lower rates of strain, then follows the first. They suggest that it is in this second stage that the availability of secondary slip systems may be important, but that the predominance of one mechanism over the other would depend on the homologous temperature. Whilst primary slip should be more important than indentation creep at low temperatures, the converse would hold true at higher temperatures.

Whilst it may be helpful to consider the indentation tests in two stages; an initial stage right at the beginning, and a time dependent stage following on, it is less clear that the initial stage will be the part of the indentation for which only primary slip systems apply. When the indenter first meets the surface the stresses will be very high, since the load is applied through a very small surface area. The stresses directly below the indenter are enough to homogeneously nucleate dislocations, as well as activate existing dislocations and heterogeneously nucleate others. Considering only the applied force/area (rather than stresses which build up from dislocation arrays), the RSS on any particular slip system will be at their highest value right at the beginning.

The rate of deformation will presumably decrease rapidly as the indenter is brought to rest, or near rest, by the resistance of the material. At this point most of the material which will be displaced during the hardness test has been displaced. For a given load on a single crystal, how much material has been pushed aside will depend on the ease with which dislocations are moved along the various slip systems, and the way in which they themselves instantly affect the stress state existing in the specimen. This is perhaps the measure of "resistance to deformation" which the intrinsic hardness of a material is supposed to convey.

The intensity of activation on any one slip system will be heavily dependent on the RSS (or perhaps more correctly the ERSS as calculated in the Brookes et al type model; since this allows for the constraints on deformation introduced by the indenter and the elastic hinterland) and the CRSS needed to move dislocations on that system. Thus, if there is a primary slip system with a low CRSS compared to the others available, the RSS models will provide a reasonable estimate of hardness anisotropy, providing that the stress state or field used is realistic. However, in trying to predict the behaviour of the material under continued load (stage 2), the effect of internal constraints arising from the existence of a dense array of dislocations must not be forgotten.

As stated before, the lower temperature anisotropy was as predicted by the resolved shear stress models, but this anisotropy was eroded by longer time indentations and as the temperature was raised. The aspect ratios of the hardest (<110>) orientation indicated

considerable elastic recovery on removal of the indentation load, which continued to take place until 600°C or 700°C, when the aspect ratio finally decreased to the "ideal" of 7.11. The flatness of the area surrounding the room temperature indentations confirmed the lack of pile up, and slip line patterns did not become visible until 300°C. By contrast, the softest (<100>) orientation showed considerable pile up on the specimen surface after room temperature deformation. This suggests activation of dislocation systems pushing material up to the surface. Although between 150°C and 600°C the aspect ratio of this orientation indicated indentations of approximately ideal shape, the concentration of slip lines parallel to the long diagonal and extending out into the surrounding area suggest that upward material movement remained, but spread over a larger area. For creep to occur (i.e. the size of the indentation to increase) either dislocations must move downwards on $\{110\}_{45}$ planes which have all ready been activated;, or new arrays must be activated. In either case such slip is likely to be obstructed by dislocation systems created by slip up to the surface.

It seems reasonable to conclude therefore that the <100> orientation creep rate is slowed by the obstruction of dislocations on slip systems moving material down into the body of the crystal, by systems moving material up towards the surface. The <110> indentations show greater room temperature creep, because slip occurs almost exclusively down into the crystal, with elastic compression of the hinterland contributing far more to the accommodation of displaced material. Creep occurs, as stress from the high density of dislocations in the region below the indenter, pushes the dislocations at the edge of each array further out along the slip plane. The ability of the material to respond in this way will depend on the mobility of the dislocations, hence the decrease in hardness with increased temperature. The relative amount of elastic deformation also decreases since more plastic deformation is taking place.

The relationship between the amount of strain and the upward movement of dislocations was also commented upon by Chaudhri (1985). Looking at displacement of material and formation of cracks around spherical indentations, he found that at low and moderate strains, material is pushed downwards, whilst at high values of strain dislocations move towards the indented surface as well. These observations seem to accord with the model proposed above.

7.5 Region of Zero Indentation Creep

By 750°C the <110> orientation does not show any creep, and the <100> orientation practically none (this is now the hardest orientation). This region of zero creep extends to indentations made at 900°C and 1050°C. The author's results shown in figure 6.1 used a load of 500g, but 750°C tests using 100g and 200g Knoop also failed to show creep.

Having accepted that zero indentation creep is a real effect, the question remains as to the cause of this distinctive mechanical behaviour. It could be either (i) that the dominant dislocation mechanism is fundamentally changed by changes in the impurity distribution as the temperature is raised, or (ii), the combination of the dislocation arrays and the applied stress control the creep behaviour.

7.5.1 Impurity Effects

The MgO single crystal used was for this work was 99.99% pure, i.e. the best that was available. Chemical analysis showed that it contained small amounts of impurities as listed in table 4.1, and at the top of table 7.1 which lists the analysis of the MgO used (where given) in other investigations which are referred to in this thesis. It can be seen that the levels of Fe, Al and Cr were found to be above those of many of the "pure" MgO specimens which have been used in other experimental programs.

Stokes (1965) showed that the the distribution of impurities known to be present in commercially pure crystals is changed by heat treatment, and the interaction of dislocations with these impurities is dependent on past thermal history. He found that both precipitation hardening (dynamic dislocation - impurity reaction) and dislocation locking (static dislocation - impurity reaction) were present above 600°C. It was suggested that the yield behaviour of as-received crystals is controlled by a fine distribution of precipitation particles. As the temperature was raised above 700°C, the particles started to agglomerate and precipitation hardening effectiveness started to decrease. Above ~1000°C precipitates begin to return to solid solution and by 1300°C solid solution was complete. Davidge's investigation of CRSS in Fe doped MgO crystals (1967) showed features which agree with conclusions of precipitation hardening mechanisms. A crystal successively annealed for 1 hour at increasing temperatures showed maximum CRSS at just over 700°C. At 800°C, the maximum hardness was obtained in ~20 minutes; for longer times the crystal got softer due to overaging. (Keh (1960) found that dislocations around indentations in MgO could be pinned by annealing between 750°C and 1000°C for a period of 1/2 hour; above ~1000°C recovery effects were observed). Sato and Sumino (1980) found that the presence of iron (probably in the trivalent state) decreased the mobility of both screw and edge dislocations. Although they identified a peak critical resolved shear stress at 700°C, they concluded that this was associated with the development of some internal structure during deformation at that temperature, and not with the temperature dependence of the mobility of individual dislocations.

Static pinning would have little effect on indentation creep since once the dislocations have away from the pinning points, they are free to move; (and in any case the

	Al,	Ca,	Cr,	Fe
The Oxford crystal	200	-	70	180
Brown, Khan, Chaudhuri (1988)	50	500	20	50
Stokes, Johnston and Li (1958)		96-99% pure		
Val'Kovskii and Nadgonii (1976)	30	30	-	300
Kim and Clifton (1984)	1	3	1	70
Singh and Coble (1974)	35	20	-	19
Wolfsteine and Kohlsted (1988)	45	280	-	-
Sato and Sumino (1980)	30	10	< 10	30
Scrinivasan and Stoebe (1973)	70	50	-	50
Haasen Barthel and Suzuki (1985)			< 300	
Woo and Puls (1977)			20 Fe^{3+} or 5 Fe^{3+}	
Copley and Pask (1965)	50	100	10	100 or
	50	1200	20	60
Hulse and Pask (1960 and 1968)	500	100	-	200
Chaudhuri, Wells and Stephens (1981)	15	100	10	50

Table 7.1 List of analysis of MgO crystals used in the works referred to in the text, as given by the authors. (Reproduced from table 5.3 for easy reference).

high stresses under the indenter are such that new dislocations will play a large part in the deformation). Dynamic hardening by clusters of impurities raising the stress needed to move dislocations is a possible effect, as discussed above. However, although pre-annealing at 750°C had some effect on 600°C Knoop hardness (see section 6.5), room temperature hardness was unaffected by pre-annealing of specimens, suggesting that this is not a large effect. Evidence for the premise that the no creep effect is caused not by impurity effects, but by the dislocation structure set up at the start of the indentation process, is given by the results with unheated indenters. In spite of a bulk sample temperature at 1175°C (i.e. above the no creep region), indentations made with an indenter at 927°C did not show creep, even though the indenter and material in contact with it must have warmed up throughout the indentation. Therefore, after reviewing the experimental evidence, it is concluded that the no creep results reported in this thesis are not caused solely by impurity effects.

7.5.2 Mechanism for Zero Indentation Creep

In the no creep temperature range both orientations have intense activity on all of the $\{110\}_{45}$ planes (and probably the $\{110\}_{90}$ planes). Dislocations are more mobile to travel through the lattice, due to higher temperature and perhaps decreased precipitation hardening, but can still be obstructed by other dislocations (locking). The interferometry results show that both orientations have pile up formed by material moving up to the surface at either side of the indentation (on $\{110\}_{45}$ planes). It seems likely that once an indentation has formed (within the first few moments of the indentation), the stresses from the indenter are not able to drive new dislocations out through the network of dislocation arrays and dislocation locks which are formed as material being driven down into the specimen meets material moving up towards the surface (see figure 7.3). A shell of work-hardened material forms and causes sink in very close to the indenter. The depth of this shell increases with increasing temperature, causing a decrease in the length of the measured short diagonal compared to the long diagonal of each indentation, and hence the observed rise in aspect ratio. The slower creep rate of <100> Knoop indentations (compared to the <110> orientation) at lower temperatures is also caused by conflicting dislocation systems, due to upward movement of displaced material in response to material shoved "down and out" on the $\{110\}_{45}$ planes. (The upward movement planes are concentrated much nearer to the indenter, (and hence newly created dislocation loops on the downward plane), in the <100> orientation than they are in the <110> orientation). The Vickers indentations in the no creep region also showed signs of a work hardended shell around the impression (especially the <100> orientation).

Indentation was once more observed at temperatures above 1050°C. It seems likely that this is facilitated by the fact that dislocations can climb at this temperature, and bulk diffusional flow can occur. The secondary slip systems, {100} <110>, become more favourable at these temperatures too, so that once away from any workhardened shell close to the indenter, dislocations could cross slip onto {100} to avoid locks. (Haasen et al (1985) showed that the critical resolved shear stress for dislocation movement on {001} planes is over 100 times that needed on {110} at room temperature, but that the difference has decreased by an order of magnitude by 1200°C. Also the high stresses that exist directly beneath the indenter may mean that the secondary slip system is activated at lower temperatures than are observed during "bulk deformation".)

7.6 Effects of Increased Temperature

Sargent (1979) has pointed out that, in addition to facilitating flow by secondary slip, increase in temperature affects the flow of MgO in a number of other ways. Firstly, the Youngs modulus, E, decreases with increasing temperature, although at a slower rate than the flow stress, the overall effect being to increase the E/Y ratio. The change in modulus also affects the strain fields of individual dislocations, and hence the work hardening rate, because of the effects on the multiplication and interactions of the dislocations. Secondly, the increase in temperature increases the strain rate dependence of slip - hence the indenter velocity becomes a more important parameter. Thirdly, one would expect diffused creep mechanisms to increase in importance at higher temperatures.

An increase in the E/Y ratio might lead to lower elastic strains in the hinterland and hence less driving force for elastic and plastic recovery. This agrees with the the decreasing aspect ratio results for the <110> orientation between room temperature and 600°C (see previous section).

7.7 Comparing Vickers and Knoop Anisotropy

For some time the apparent anomaly between Vickers anisotropy (<100> hardest) and Knoop anisotropy (<100> hardest) of rocksalt structures was a cause of concern. However this can be explained if one considers the difference in indenter shape and the effect that this will have on the slip systems activated. The indentation "direction" is defined as the direction along which the diagonals of the indenter lies. However, the faces of the Vickers indenter which, simplistically, provide the "push" to displace material, are at 45° to the diagonal direction in the horizontal plane whereas the Knoop faces are nearly parallel to it. As Sargent (1979) and also Rickerby (1979) have pointed out, this is accounted for in a theoretical sense by ERSS models such as that by Brookes et al (1971) which include a

geometrical constraint factor based on the orientation of the indenter facet with respect to the crystallographic slip system. Armstrong and Raghuram (1973) considered that an orientation dependent workhardening term must be added to the CRSS to get the resolved shear stress, which determined the size of an indentation. The DPHN of a direction was defined as the average of two orthogonal KHN values aligned along the same crystallographic direction:-

$$DPHN_{\theta} = (1/2)\,[KHN_{\theta} + KHN_{\theta+\pi/2}]$$

This worked for Niobium single crystal, but not for MgO. They considered that was due to"a change in deformation mode" shown by the extensive cracking around the indentations. It is possible that work-hardening does play an important part in determining the hardness of MgO, but there seems little justification for the equation above.

8. PREVIOUS WORK ON GERMANIUM

Semiconductor materials are suited to the investigation of the controlling factors of indentation because their slip systems are well defined, and there is a lot of data available on the nature of their dislocation velocities under various conditions (reviewed Alexander and Haasen 1968, Nadgornyi 1988). Germanium is a useful material for this study because it etches relatively easily and, with a melting point of 938°C, the temperature dependence of hardness could be investigated from 0.24 T_M (at room temperature) up to the melting point on the Oxford machine. The hardness test allows the plastic (rather than the fracture) behaviour to be studied down to 0.2 T_M where fracture becomes a problem here also (Ashby and Jones 1982).

This chapter looks at the work on Ge of previous authors including conclusions on the deformation behaviour under conventional stress strain testing, and the effects of doping and increased temperature on dislocation dynamics. The existing work on indentation of Ge is reviewed.

8.1 Crystal Structure

The mechanical behaviour of Ge (and Si) is dominated by their localised, strongly directional, covalent bonding (Ashby and Jones 1982). It creates an exceptionally large lattice resistance for slip on all systems, including the primary {111} [110] slip system of the diamond cubic structure (Alexander and Haasen 1968). The high Peierls stress compared to metallic and ionic crystals of comparable melting points leads to the characteristic behaviour of Ge. For example, pure silver has a melting point (962°C) close to that of Ge, but Ag is soft and malleable at all solid temperatures, whilst Ge is brittle (under normal conditions) below the brittle-ductile transition temperature, which is usually found to be in the region 300°C to 400°C depending on the test method used. However there is a similarity between the plastic properties of Ge and fcc metals which stems from the fact that the translation lattice of the diamond structure is fcc, therefore the glide systems are the same in both structures (Alexander and Haasen 1967).

8.2 Disiocations in Germanium

8.2.1 Dislocation Generation and Multiplication

Patel and Chaudhuri (1961)a noted that the dislocation generation stress is very low and well defined, depending on the temperature and strain rate. In tensile tests (1963) they found that dislocations were generated at very low stresses in the initial linear region of the

stress stain curve. They concluded that their observations were consistent with the idea that the yield behaviour is controlled by the numbers and velocities of dislocations generated early in the deformation process. "Dislocation free" Ge and Si deformed at stresses which were orders of magnitude below the theoretical value, probably due to the presence of condensed vacancy loops formed during crystal growth.

At low temperature, the velocity temperature relation can be divided into two stress regimes with different exponents that varied with temperature (Patel and Freeland 1971). At high stresses single loops always multiplied during motion, but at low stresses the single loops always remained single throughout. The region of stresses around which the transition from no observable multiplication to multiplication occurred was around 1-2 kg/mm^2. If it is assumed that multiplication occurs by a double cross slip mechanism, dislocation glide segments on a cross slip plane might be expected to have a retarding effect on dislocation motion on the primary plane, resulting in a lower stress-dependence of velocity at high stresses (Patel and Freeland 1971).

8.2.2 Dislocation Velocity and Disposition

Kink mode dislocation motion occurs in crystals like Ge, where the lattice glide resistance (characterised by the Peierls energy and Peierls stress) is an essential and predominant feature (Nadgornyi 1988). The dislocation lines advance and lengthen by the generation and motion of double kinks (Hirth and Lothe 1982). (The operation of such double kink motion has now been shown experimentally, Nikitenko and Farber 1989).

As in other materials with a high Peierls energy the glide dislocations are observed to lie straight along crystallographic directions (Celli, Kabler, Ninomiay and Thomson 1963), (this in contrast to dislocations in metals and ionic crystals). However, high temperature annealing may cause this to disappear (Patel and Alexander 1956, Tyler and Dash 1957).

With the dislocations lying along the [110] directions, two types of segment can be distinguished. One type with is identified as "60°" since the line of the dislocation lies at 60° to the [110] Burgers vector. The other type of segment has screw characteristics since it moves in the same [110] direction as the dislocation line.

The relationship of the velocity, V, of dislocations with stress may be described by an equation of the form:

$$V_{dis} = (\tau/\tau_0)^m . V_0$$

where V_0 is a temperature dependent constant found by experiment, and τ_0 is an arbitrary stress, usually 1 MPa. The strain rate may then be defined as the product of the density of dislocations, the velocity of dislocations and the burgers vector.

The stress is near to one, as predicted by the Hirth and Lothe model for the double kink mechanism. (In ionic crystals and metals, very small increases in stress lead to large changes in dislocation velocity, i.e. the stress exponents are much higher. Therefore a larger strain rate is accommodated with small increases in applied stress). *In situ* observations show that dislocation movement is smooth and continuous, even on the scale of electron microscopy (e.g. Louchet et al 1988) as would be expected in materials with high Peierls potential.

Chaudhuri et al (1962) produced curves showing dislocation velocity as a function of resolved shear stress for a range of temperatures between 420°C to 700°C. The velocity of dislocations at a resolved stress of about 1 kg/mm^2 varied between 1 x 10^{-2} μm/sec at 440°C to 1 x 10^3 μm/sec at 700°C. Velocity activation energies were found to be about half that of self diffusion, and there was greater resistance to dislocation movement than for LiF or SiFe. Nadgornyi (1988) reviews the data available, and agrees that Ge has the characteristic of different stress and temperature dependence of activation energies for low and high temperatures. Johnson (1965) didn't find any consistent differences between the velocity of grown in dislocations and those resulting from surface or bulk growth. Long dislocations have been observed to move faster than short ones, because the short dislocations lines are shorter than the kink mean free path (Louchet et al 1988). However above a certain length (in excess of 0.4μm - Louchet et al) the velocity is independent of the dislocation length.

8.2.3 Screw Dislocation Velocity Versus 60° Velocity

It has already been mentioned that glissile dislocations in Ge show a strong tendency to lie along the <110> directions. According to Kabler's data (from double etch experiments), the difference in velocity between screw and 60° dislocations is dependent on the magnitude of stress experienced. At higher stresses (6 - 12 kg/mm^2), there were strong indications that the 60° dislocations moved faster than the edge, although at ~500°C, velocities became nearly equal at all stresses. At stresses of about 6 kg/mm^2 both types of dislocation moved at the same velocity, independent of temperature. At temperatures below 500°C and reduced stress (below 5 kg/mm^2), the velocity of 60° dislocations decreased faster than that of the screw dislocations, so that the screw dislocations move faster than those at 60°. However, at low stresses and above 500°C, the screw dislocations were slower than those at 60°. This agrees well with the work of Tyler and Dash (1957).

Louchet et al (1988) and Haasen (1966) also found that screw dislocations were faster than 60°, especially at high temperatures (Haasen 1966). (Johnson (1965) didn't find any consistent differences between 60° or screw dislocations but wouldn't have detected a difference less than 20%. Generally his results agreed with those of Kabler (1963) although the stress levels of the two studies do not quite overlap.)

For strains as low as 0.1%, the fraction of mobile dislocations (for a given orientation of tensile test) is largely a function of the stress acting on the crystal (Louchet et al 1988). The higher the stress, the lower the fraction of dislocations in the crystal which are mobile. The greater mutual interference at high stresses appears to be related to the activation of slip on systems other than the primary system.

8.3 Generai Features of Deformation

The high Peierls potential leads to relatively immobile dislocations at lower temperatures, and hence brittle behaviour. The temperature at which Ge is described as ductile depends not only on the doping of the material (see next section) but also the testing conditions. Gallager (1952), testing Ge and Si in bending and in tension, found that Ge was ductile above 500°C (Si above 900°C). (Feltham (1978) quotes 350°C - 420°C for conventional bending or compression testing). In microscopic terms, the change from brittle to ductile behaviour can be considered as the temperature at which significant dislocation movement can take place (so that flow precedes fracture) and might be expected to be around 0.5 T_M (350°C). Using Vickers indentation, etch figures produced by dislocation movement first appear at 250°C (Trefilov and Mil'man 1964) or 300°C (Sumino and Hasegawa 1968). Roberts, Pirouz and Hirsch (1985) defined a brittle/ductile transition when the radial cracks surrounding Vickers indentations became rapidly shorter with increasing temperature. This occured at 350°C +/- 50°C depending on the doping. At a higher temperature there existed a further transition temperature at which cracks, as seen on the surface, disappeared entirely but lack of data prevented this being defined, Roberts and Pirouz (1985). Naylor and Page (1983) noted that indentation fracture may persist up to temperatures substantially in excess of the temperature at which the plastic flow mechanisms change.

Patel and Chaudhuri (1963) subjected dislocation free Ge crystals to tensile testing, and found a strong drop between the yield point and flow stress, which diminished as the initial density of dislocations in the crystal increased. (Most previous work was carried out on crystals with initial dislocation densities in the range 10^3- 10^4 cm^{-2} Patel et al 1963)). The lower yield stress is well defined; the yield drop is due to dislocation multiplication,

helped by a low stress exponent, since at a fixed strain rate, as the dislocation density rises the average dislocation velocity, and hence the stress needed, must drop.

At high temperatures, i.e. > $0.6T_M$, Ge (and Si) show power law creep often complicated by an inverse transient (in creep tests) or a yield point drop (in constant strain rate tests - see above) during which the dislocation density increases towards a steady state (Ashby and Jones 1982). This steady state is rarely reached in the small strains of most published experiments. Creep mechanisms (steady state, or at sufficiently low stresses, diffusional flow) are diffusion controlled and therefore slow, since diffusion rates are low (Ashby and Jones 1982). From hot hardness experiments, Gerk (1975) suggested an exponent of n=3 for the power law creep in Ge, but Ashby and Jones used an exponent of n=5 (as for Si) leading to better agreement with the data of Trefilov and Mil'man (1964).

Patel and Alexander (1956, compression tests) found that at lower temperatures Ge has a very high strain hardening coefficient, which then decreases rapidly, until at temperatures approaching the melting point, it is only slightly temperature dependent. (As the paper pointed out, unlike Al and Mo, the strain hardening coefficient of Ge does not tend to zero at the melting point). The stresses required to cause 0.10% strain varied from 350 g/mm^2 at 550°C to 75 g/mm^2 at 800°C.

8.3.1 Doping Effects

The variation of dislocation average velocity with temperature is shown in figure 8.1 (from Patel and Freeland, unpublished work). At 350°C (the approximate brittle transition temperature for intrinsic Ge), the velocity of dislocations in n-type is roughly 40 times that in p-type. The maximum effects from doping are observed at or below 400°C (Nadgornyi 1988). Neutral impurities usually show no effects on dislocation velocity, but Bondarenko (1981, through Nadgornyi) found that at low stresses (below 20 MN/m^2), the velocity of dislocations is significantly diminished by oxygen doping. This is a specific example of impure crystals showing a "starting-off" stress. Moving dislocations can show a continuous gathering of obstacles with periodic breakaway (Nadgornyi 1988).

Doping also changes macroscopic properties (Roberts and Pirouz 1985). Donor and acceptor impurities have been shown to have a large effect on the behaviour of dislocations during mechanical deformation, when the impurity concentration is larger than the intrinsic carrier concentration at the test temperature (Patel and Chaudhuri 1966). Doping with Ga (i.e. p-type) raises the maximum stress at the upper yield point, whilst doping with As (n-type) lowers this stress. This equates with the effect of doping on dislocation velocity and, as the authors concluded, it is more likely to be the influence of doping on dislocation

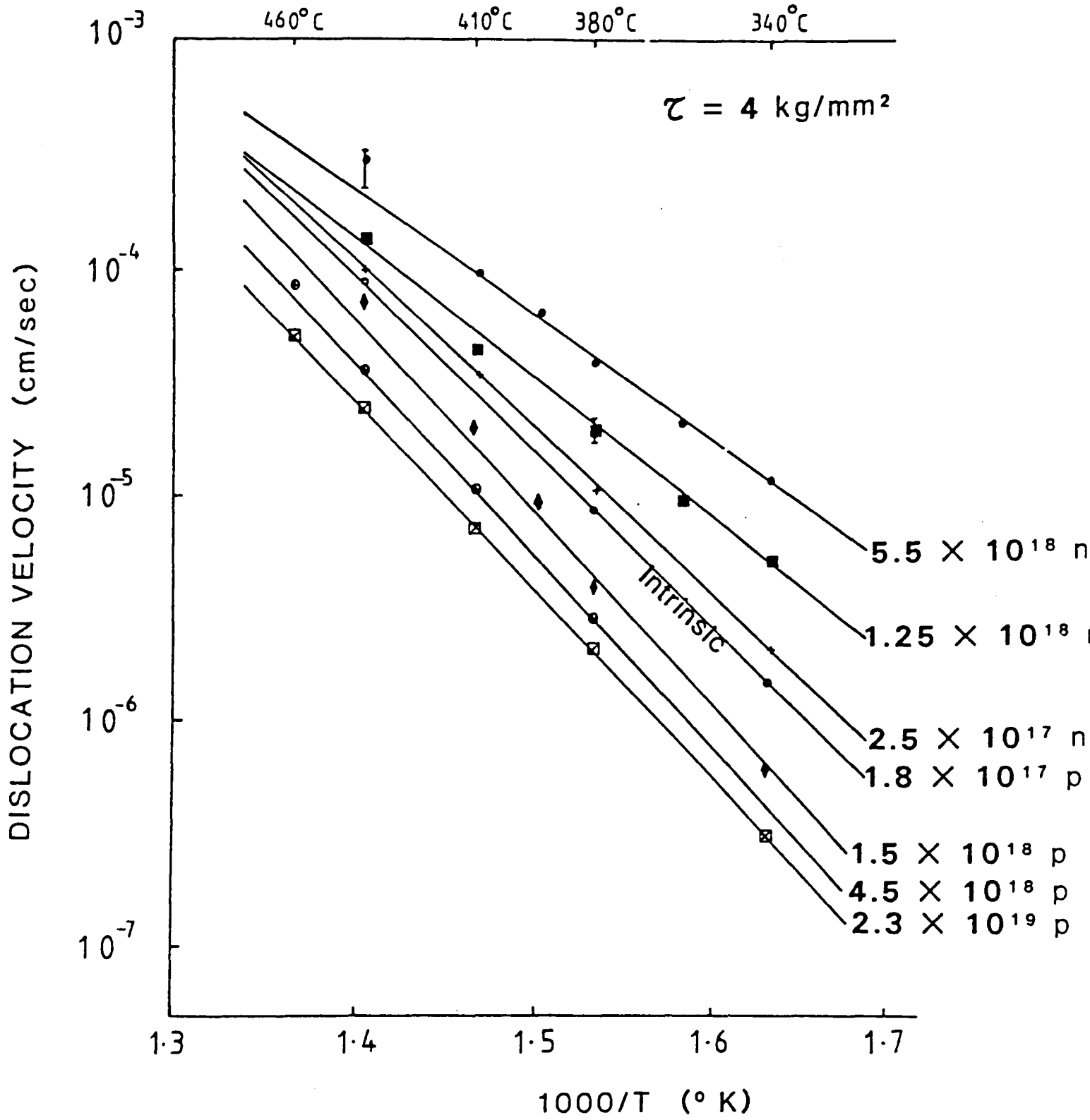


Figure 8 1. Variation of dislocation velocity with inverse temperature for various doping (Patel and Freeland unpublished work).

velocity that causes the yield behaviour than any influence on the number of dislocations generated as the specimen is deformed.

8.4 Deformation by Indentation

The use of semiconductors as model high Peierls barrier materials, and also interest in their mechanical properties (often linked to doping effects), has been the basis of a number of indentation studies. Most of these have been carried out with Vickers indenters, but a few have used Knoop indenters.

8.4.1 Effect of Temperature on Hardness

The hardness of Ge varies slowly with temperature until the transition temperature is reached (which is dependent on doping), then decreases more rapidly as the temperature is increased further, until at about 600°C the low hardness is relatively insensitive to temperature; e.g. Trefilov and Mil'man (1964) found a rapid decrease in Vickers hardness above 200°C; Sumino and Hasegawa (1968) using Vickers indentation on (111) demonstrated a rapid decrease above 300°C. Roberts, Pirouz and Hirsch (1985) using Vickers indentations on (001) Ge found that hardness values below 300°C were not dependent on doping, but then diverged until about 500°C, which is the temperature at which the intrinsic carrier concentration approaches that due to the doping levels.

8.4.2 The Deformed Region

Wagatsuma et al (1971) studied the size of the deformed region around Vickers indentations (100g load) on the (110) plane using X-ray topography. He reported that throughout the temperature range studied (20°C - 700°C) a highly deformed region, with linear dimensions approximately ten times that of the indentation diagonal, surrounded the indentation. Annealing the samples brought about configurations of dislocations lying parallel to the [110] directions. The shape of the deformed region at 700°C was different from that made at 550°C and 600°C in that the dislocations were not in regular lines. The authors suggested that this might result from the climbing motion of dislocations which was able to occur at the higher temperature i.e. dynamical recovery.

8.4.3 Anisotropy and Creep

Knoop hardness data (50g load) on Ge of various dopings (Roberts et al 1986) showed that the temperature at which hardness anisotropy was first detectable varied on the doping; about 380°C for p-type, 250°C for intrinsic and about 100°C for n-type. In a study on GaAs, Qin and Roberts (1988) concluded that the main effect producing hardness

anisotropy was the difference in workhardening rates for dislocation slip in convergent and divergent slip planes.

Gerk (1975) has investigated Vickers indentation creep on {111} Ge surfaces. Creep occurred above 200°C and the rate of decrease in hardness with time increased with temperature. Gerk postulated that the creep rate, although not the initial "zero time" hardness, could be explained in terms of the stress and temperature dependence of dislocation velocity by the growth of a plastic zone of mobile dislocations into an elastically strained hinterland.

8.4.4 Rosettes and Dislocation Arrangements

Dislocations are generated on the crystallographic slip planes in the immediate vicinity of the indenter and move outwards, pushed by the stress from the indenter and succeeding dislocations generated behind them. The loops which intersect the surface form the rosette pattern which is revealed by etching. As discussed above (section 8.2.2.) the etch pits at the surface will be from dislocations with 60° or screw character at the surface. Figure 8.2 shows some of the possible dislocation loops around a Vickers indentation on {001} Ge (from Roberts et al 1985). Sumino et al (1968) concluded that a regular alignment of pits represents an array of 60° dislocations whilst a sequence with a disturbed alignment is that of screw dislocations.

Roberts and Pirouz (1985) found that trends in Vickers hardness behaviour and rosette size with doping were as would be expected; i.e. the hardness decreased and the rosette size increased with increased mobility. Sumino et al (1968) considered the relationship of the distance from the centre of the indentation to the etch pit at the top of the rosette pattern (L) with that of the indentation diagonal (D). The variation of L/D with temperature corresponded to the variation of hardness with temperature up to 600°C. (Above 600°C the dislocation etch pits were randomly distributed).

It is usually assumed that (due to the high Peierls potential) the high temperature dislocation configurations are "frozen in" when the temperature is returned to ambient (e.g. Alexander and Haasen 1967b). However, the results from Wagatsuma et al (1971), using X-ray topography to compare the three-dimensional distribution of strain and dislocations round indentations cooled under loaded and unloaded conditions, found that these were not necessarily the same, and warned against the effect of annealing the specimen during cooling. (The size of the deformed region showed no appreciable change, so it is unlikely that the effect involved long range motion of a large number of dislocations, but rather the

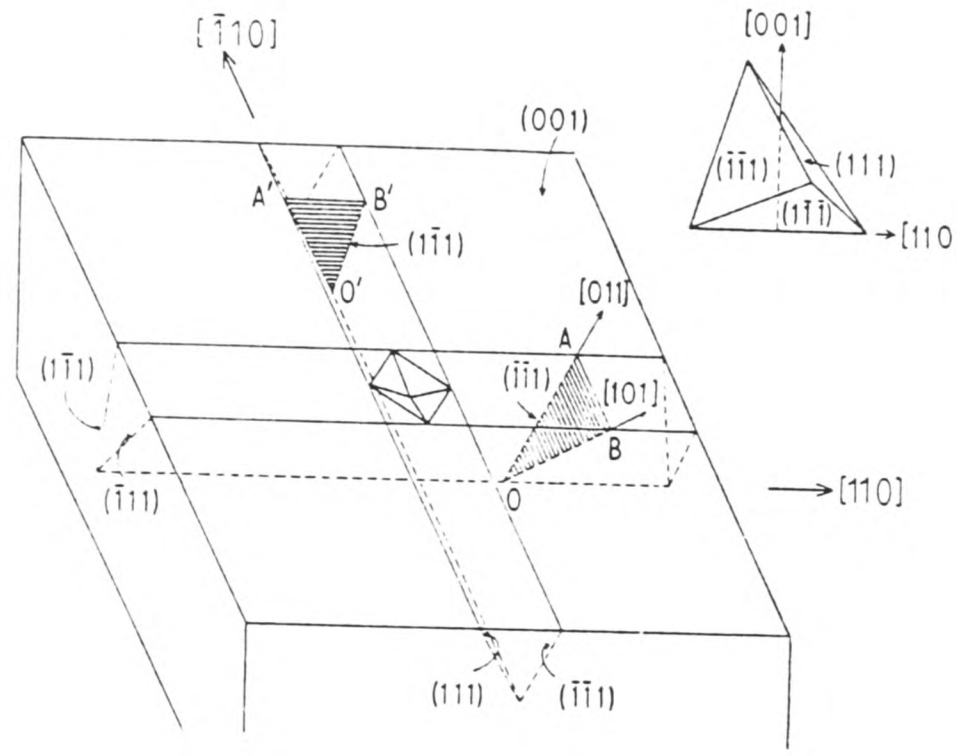


Figure 8.2. Possible arrangement of loops around a Vickers indentation on (001) Ge (after Roberts et al 1985).

re-arrangement of dislocations by the motion and annihilation of kinks along the dislocation line).

The observed rosettes of indentations cooled with the indenter resting on the surface of the specimen were examined by Sumino et al (1968). There was no difference in the dislocation arrangements between these indentations and those cooled in the (normal) unloaded condition. This is an important result as far as modelling the rosettes is concerned, since it is evidence that the indenter did not extend (much) stress directly upon the positions of leading dislocations in the rosette arms. Thus the leading dislocation may be assumed to be predominantly affected by the sum of the stress exerted by the dislocations around it.

It has been found experimentally that in GeAs the slip lines on the surface ([110] direction) are formed after the indenter was removed (Roberts et al 1986). (The specimen was cooled rapidly to room temperature after the indenter was removed, then "annealed" at the indentation temperature in several stages while photographs were taken). It is possible that holding "annealing" indentations at a particular temperature (but zero load), whilst other indentations are made, could affect the measured hardness and observed dislocation arrays. This question is addressed in chapter 9.

8.4.5 Indentation Cracking

Quite severe cracking is seen around room temperature indentations in Ge. Sumino et al (1968) found that the corners of Vickers indentations showed some cracking (using optical microscopy) up to 550°C. Indentations at 550°C showed up small cracks when etched. As discussed in chapter 3, a recent paper by Cook and Pharr (1990) concludes that indentation fracture models, based on the crack sequence seen in glass, are only appropriate for brittle materials with no long range dislocation interactions, which does not include materials above the brittle ductile transition. An investigation by Roberts and Pirouz (1985) showed that the dislocations which affect cracking are those at the crack tip, not those in the bulk of the material.

8.4.6 Transformed Phases Under Indentations in Ge

One topic of interest in the indentation studies of Ge and Si is the question of the formation of an amorphous phase directly beneath an indenter, due to the large pressures involved. Clarke et al (1988) used TEM to study room temperature Vickers and Knoop indentations on Ge and Si (10g-50g loads, loading rate 16.67 N s^{-1}). This showed an amorphous region under the indentations, which crystalised to form a fine grained diamond

cubic structure, if subsequently annealed at temperature above 550°C. Other crystalline solids (sapphire, MgO and GaAs) did not show the amorphourisation. Menoi et al (1986) carried out a study on high pressure phases of Ge using a diamond anvil cell; the results of which tie in with the paper by Clarke et al (1988) described above. Eremenko and Nikitenko (1972) observed diamond hexagonal phase under indentations in Si after unloading had occurred. Pirouz et al (1990) analysed experimental observations of the cubic to hexagonal phase transformation in silicon, describing it in terms of a martensitic nature.

8.4.7 Dispute about Plastic Deformation at Room Temperature

A subject which was until quite recently at the centre of intense debate was whether *plastic* deformation was possible beneath indentations at room temperature in diamond cubic materials (e.g. Rinder and Tramposch 1965). Room temperature indentations were annealed and then etched by Sumino et al (1968) to reveal rosettes. They concluded that these were produced by the generation and motion of dislocations to relieve the elastic strain stored around the indentations. They did not believe that plastic deformation by the motion of dislocations was possible at room temperature. The question has now been resolved since room temperature plastic deformation has even been observed in diamond (Humble and Hannink 1978).

9. GERMANIUM INDENTATION RESULTS

All the results shown and discussed in this chapter were carried out on the Stanton Redcroft hardness tester which was described in Chapter 2. The experimental details and error bar calculations (based on 1 standard deviation away from the mean diagonal) are described in chapter 4. The load used was 50g and indentations carried out on the polished (001) face.

After looking at the variation of hardness with temperature (section 9.1), indentation creep and anisotropy results are presented. Most of the experiments concerned intrinsic Ge, but a little work was done with p-doped material, and the effect of doping is discussed later in the chapter.

9.1 Variation of Hardness with Temperature

Figure 9.1 (a) and (b) shows the variation of Knoop hardness with temperature for the <110> and <100> orientations respectively ((001) face and 50g load). All the indentations (5 for each value quoted) were on the same sample starting with room temperature and increasing the indentation temperature in order to avoid altering the initial state of dislocations by pre-annealling. (The room temperature results may therefore be effected by adsorbed water, see section 3.4 but this would not be a big effect compared to the overall variation). Indentations with a dwell time of 20 sec and 300 sec were made at each temperature at each orientation. (No 300 sec indentations at room temperature for the <110> orientation). Table 9.1 shows the fraction of the melting point which each temperature represents.

For both orientations the hardness at a given (arbritary) dwell time decreases slowly with temperature until about 200°C, then decreases much more rapidly until 400°C or 500°C, when the rate of decrease slows down again. Early experiments using a Vickers indenter in the <110> orientation (only up to 430°C) also showed rapidly decreasing hardness as the temperature was increased to about 400°C, perhaps beginning to decrease less rapidly above this temperature (figure 9.2).

9.2 Anisotropy and Creep Rates

Figure 9.3 contrasts the variation of Knoop hardness with dwell time for both orientations at various temperatures. Part (a) shows the lower temperature results (the 200°C results are from a sample that had been preannealed at 300°C which may slightly

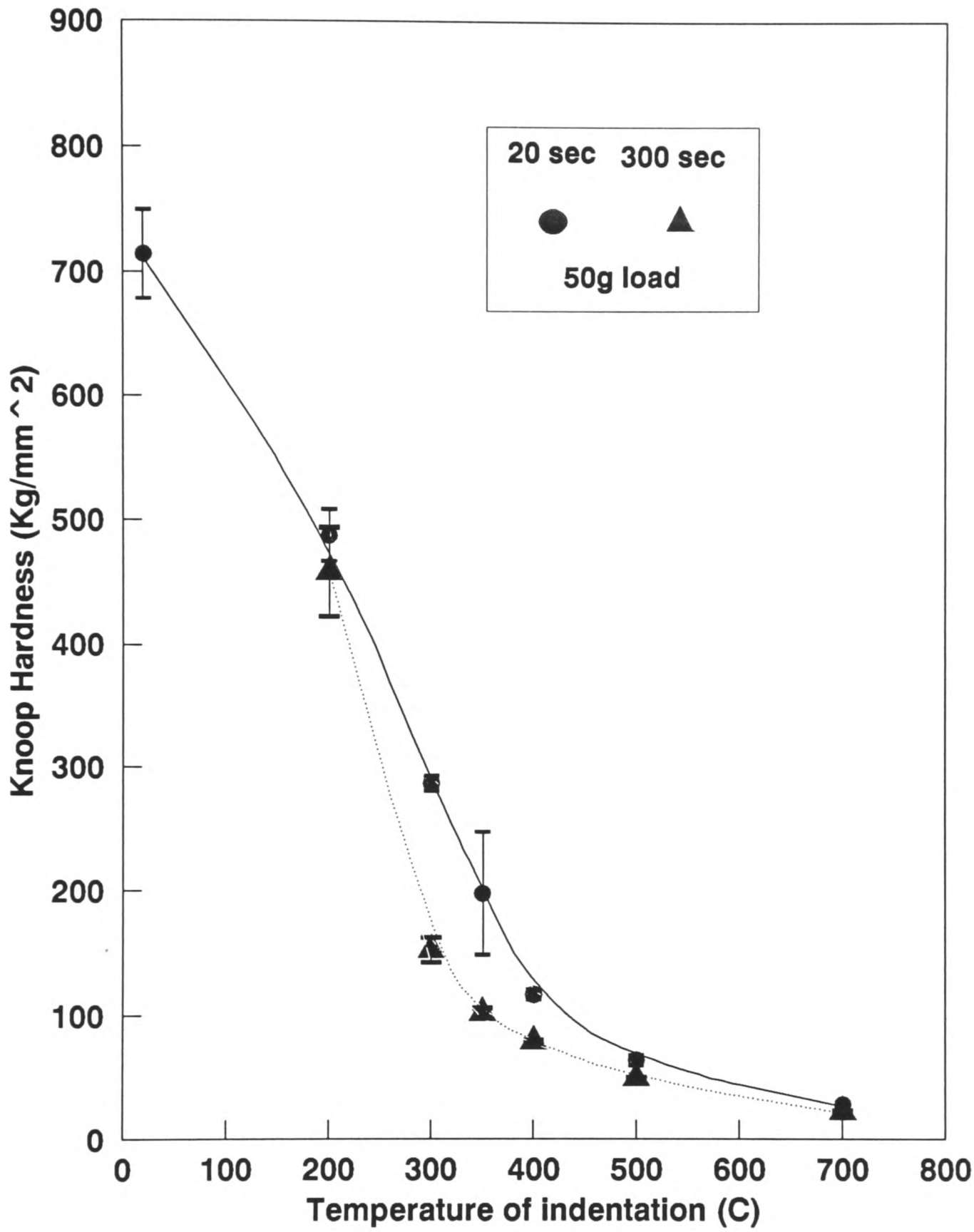


Figure 9.1a Variation of <110> Knoop hardness with temperature on (001) Ge, 20 and 300 second indentations.

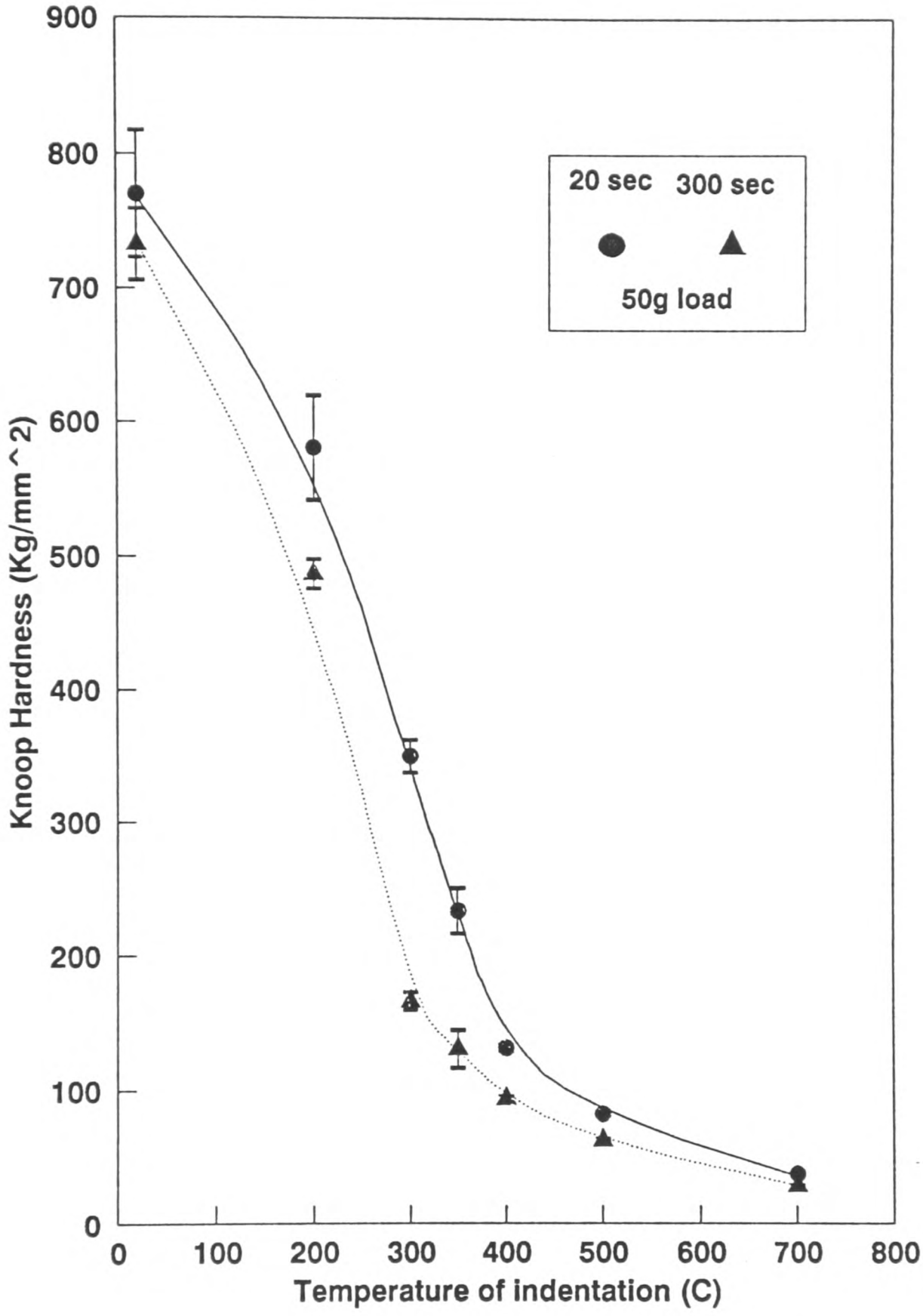


Figure 9.1(b) Variation of <100> Knoop hardness with temperature on (001) Ge, for 20 and 300 second indentations

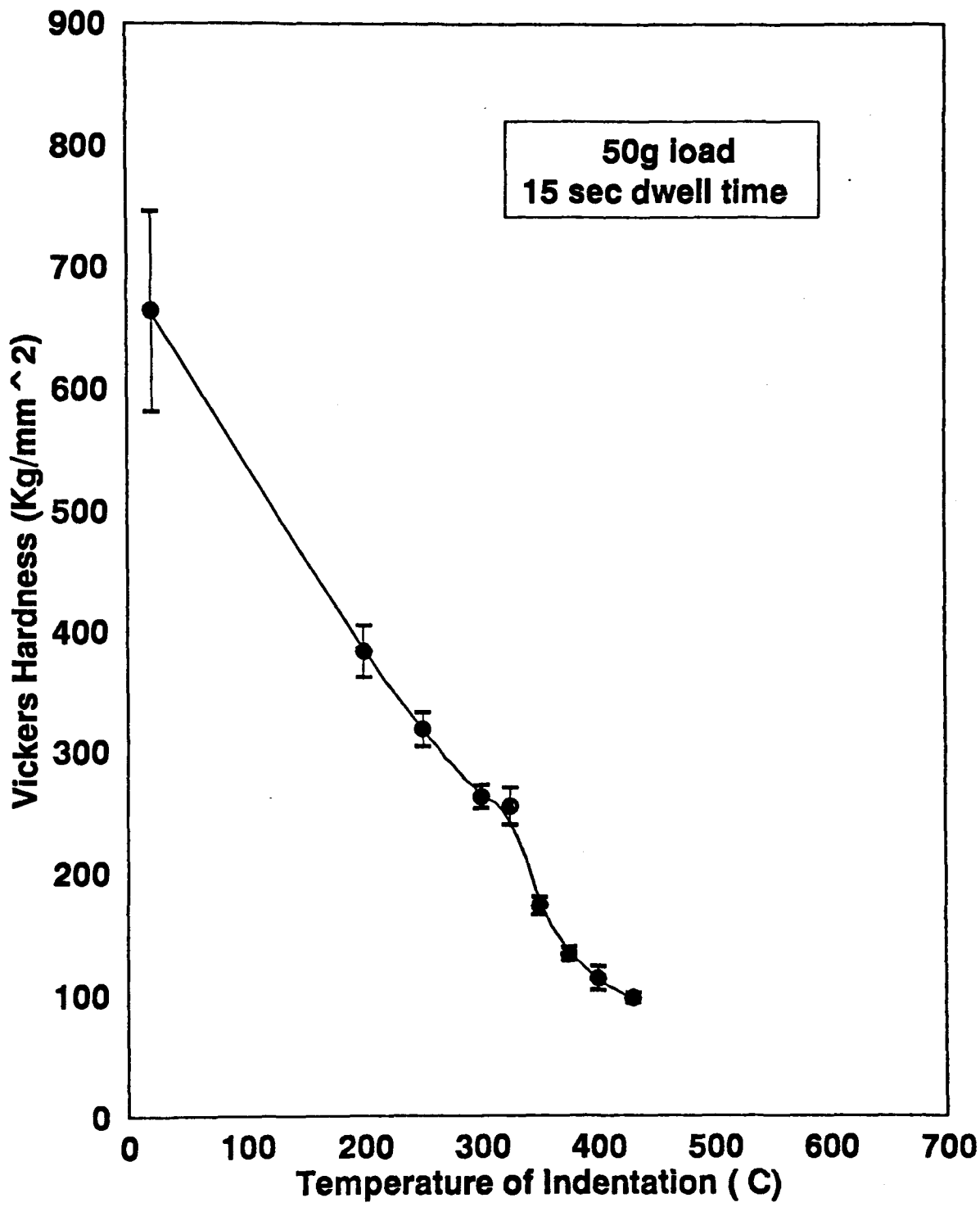


Figure 9.2 Variation of <110> Vickers hardness with temperature, on (001) Ge.

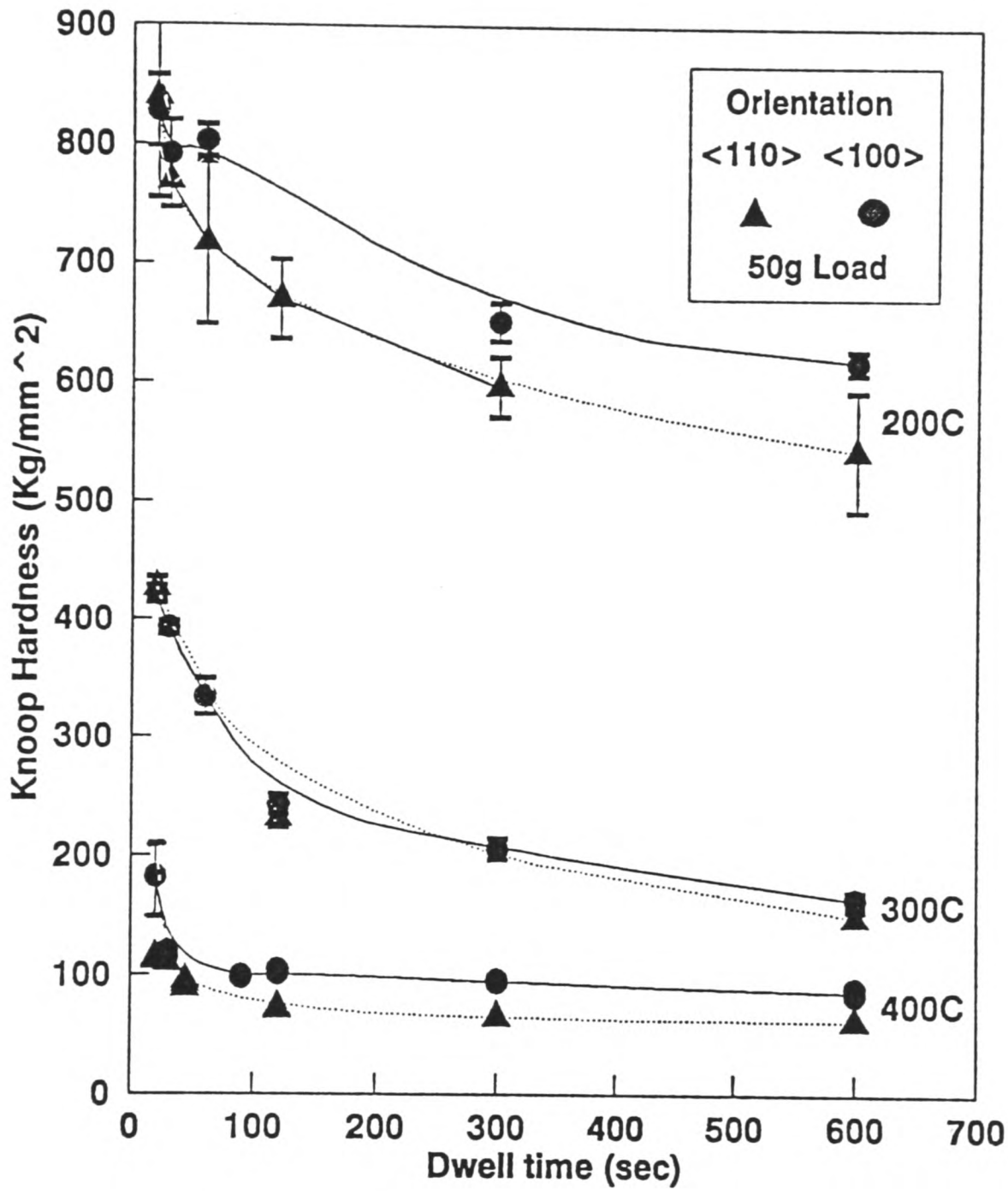


Figure 9.3(a) Variation of Knoop hardness with dwell time, between 200C and 400C, on (001) Ge.

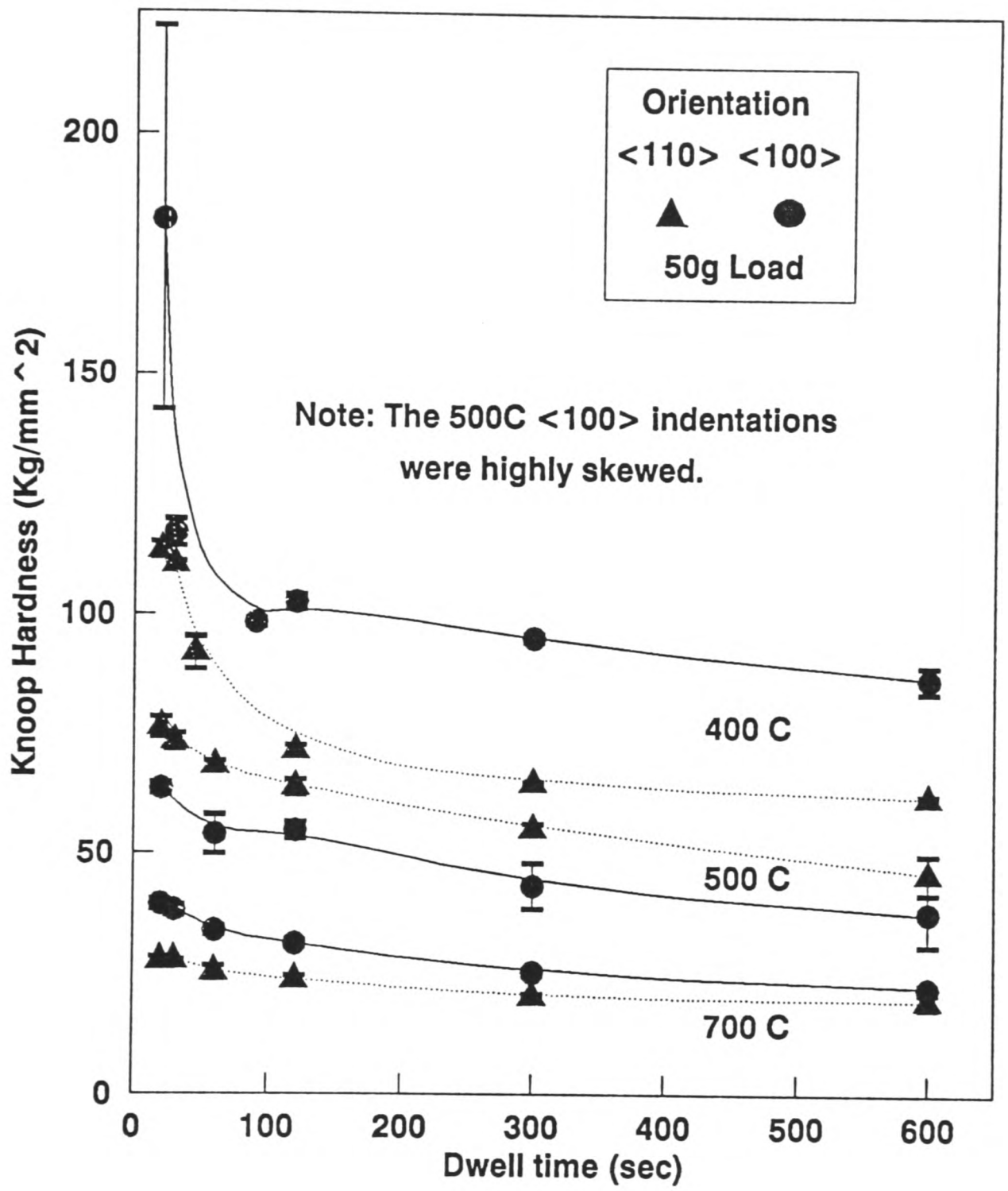


Figure 9.3(b) Variation of Knoop hardness with dwell time between 400C and 700C, on (001) Ge.

°C	K	T/T_M
20	293	0.24
200	473	0.39
300	573	0.47
350	623	0.51
400	673	0.56
500	723	0.60
700	923	0.76
800	1023	0.88

The melting point (T_M) of Ge is 1211K (938 °C).

Table 9.1 Various temperatures in °C, K and T_M for Ge.

effect the absolute value of hardness obtained, see section 9.5). The n-doped Ge showed no measurable anisotropy at room temperature. However by 200°C the results show anisotropy at dwell times of 60 second or longer, with the <100> indentations becoming harder than equivalent <110> orientations. The trend of a faster creep rate for the <110> orientation than for the <100> orientation is continued as the temperature is increased so that by 400°C, anisotropy is evident at all dwell times.

Thus in figure 9.3(b), which shows the higher temperature results, the <100> orientation is always harder than <110> under the same conditions. (See note on the skewed nature of the <100> 500°C results which probably accounts of the anomalous anisotropy). However the 700°C results suggest that at higher temperatures the <100> orientation starts to creep faster than <110>. This is supported by an additional experiment carried out on some p-doped material (figure 9.4). At dwell times of 30 minutes the hardness of both orientations is not distinguishable within experimental scatter.

9.3 Effect of Doping

Figure 9.5 compares the variation of Knoop hardness with temperature for n-doped and p-doped material for (a) <110> and (b) <100> orientation. (Note: the two types of sample are not exactly comparable since in the case of the p-Ge the sample was taken to 400°C first and the temperature decreased. Thus the lower temperature p-Ge results represent 400°C annealed material, whereas the n-Ge results are "first-time-at-that-temperature" values). These results appear to show that at lower temperatures, the p-doped material is harder (which is what one would expect from the decrease in dislocation velocity, see section 8.1), but perhaps creeps faster. This is supported by figure 9.6 which shows the variation of Knoop hardness with dwell time at 700°C for both dopings. The p-doping starts off harder, but at longer dwell times gives a hardness which is not measurably different from that of the n-doped material.

9.4 Aspect Ratio and Pile up

The hardness is calculated using the long diagonal only. As with the MgO samples, the short diagonal of each indentation on Ge was also measured and the aspect ratio, long diagonal/short diagonal, calculated. However, the results were not as clear cut as in the MgO case.

The scatter in the aspect ratio results is quite wide because the widths involved were small (between 4μm and 19μm on the sample which produced the results shown in figure

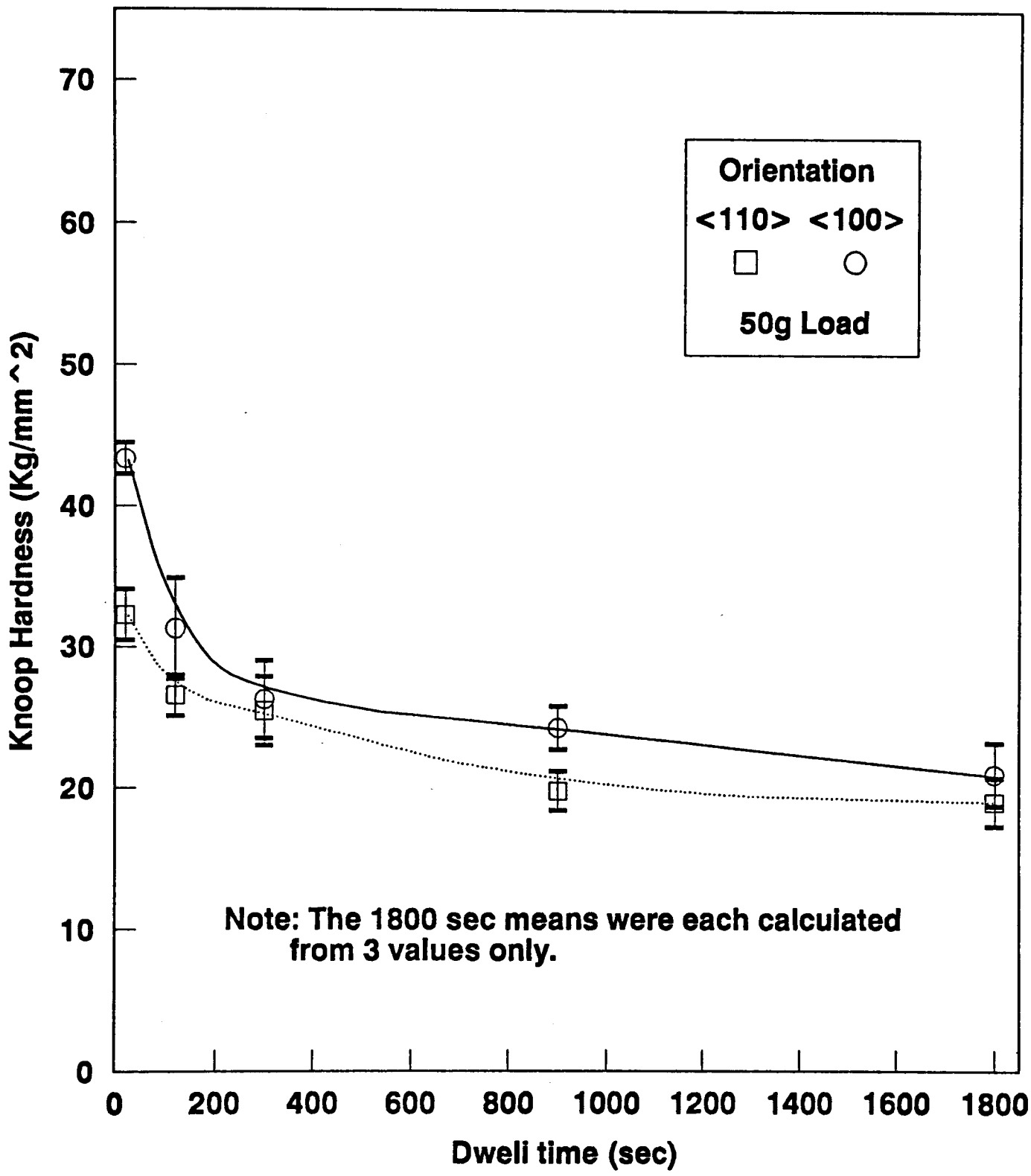


Figure 9.4 Variation of Knoop hardness with dweli time up to 1800 seconds, on P-doped Ge at 700C.

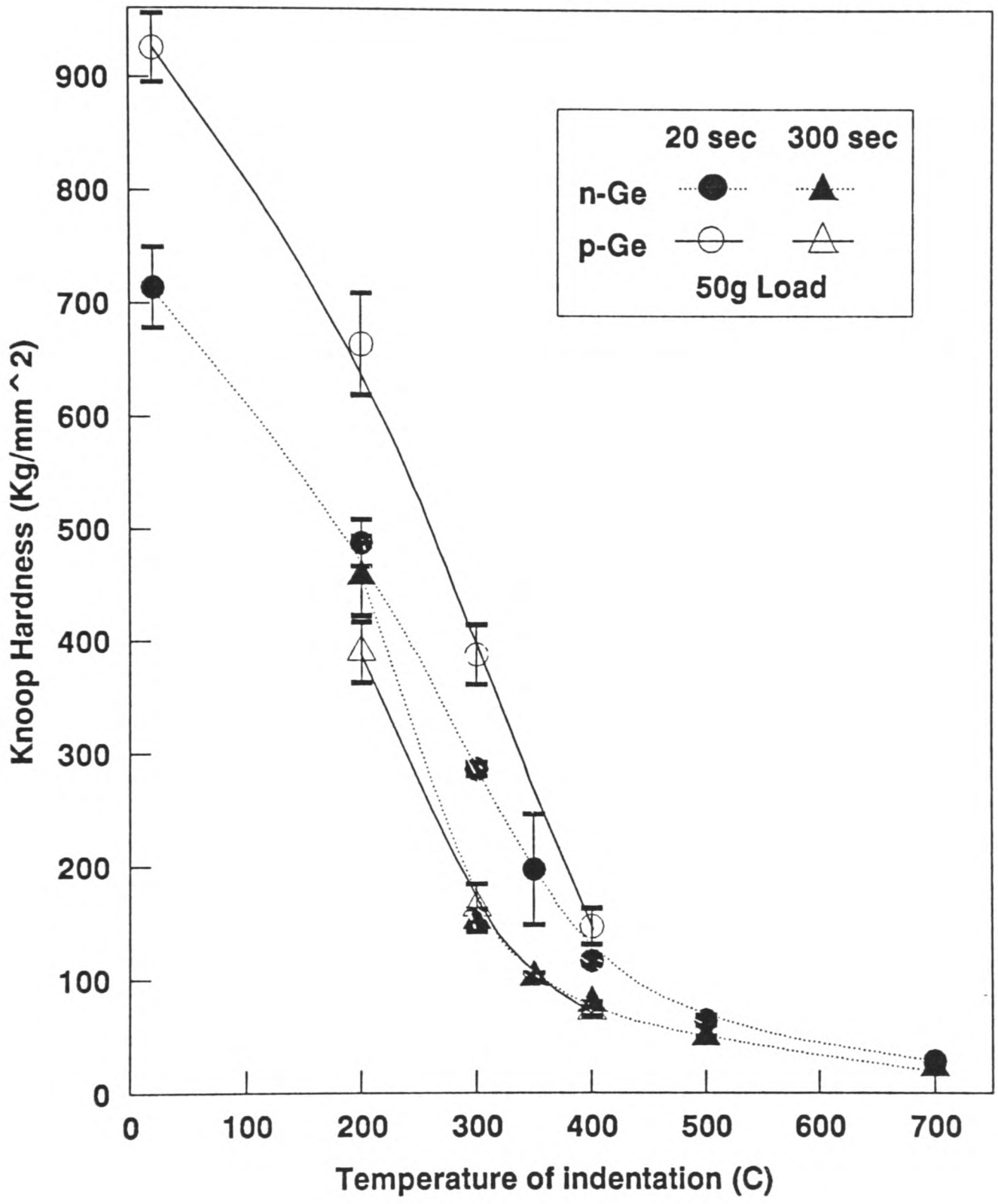


Figure 9.5(a) Variation of <110> Knoop hardness with dwell time, on n- and p-Ge.

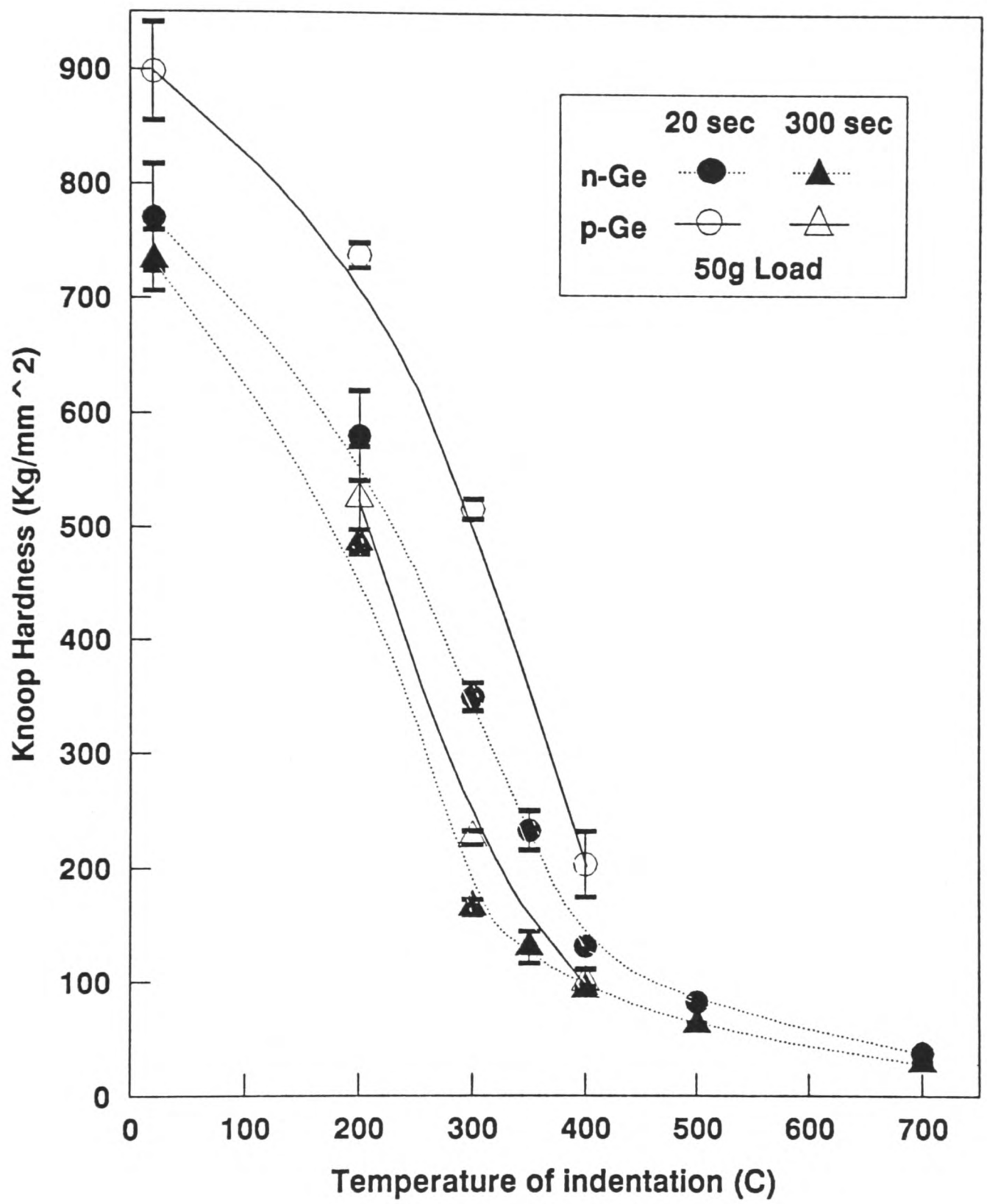


Figure 9.5(b) Variation in <100> Knoop hardness with dwell time, on (001) n- and p-Ge

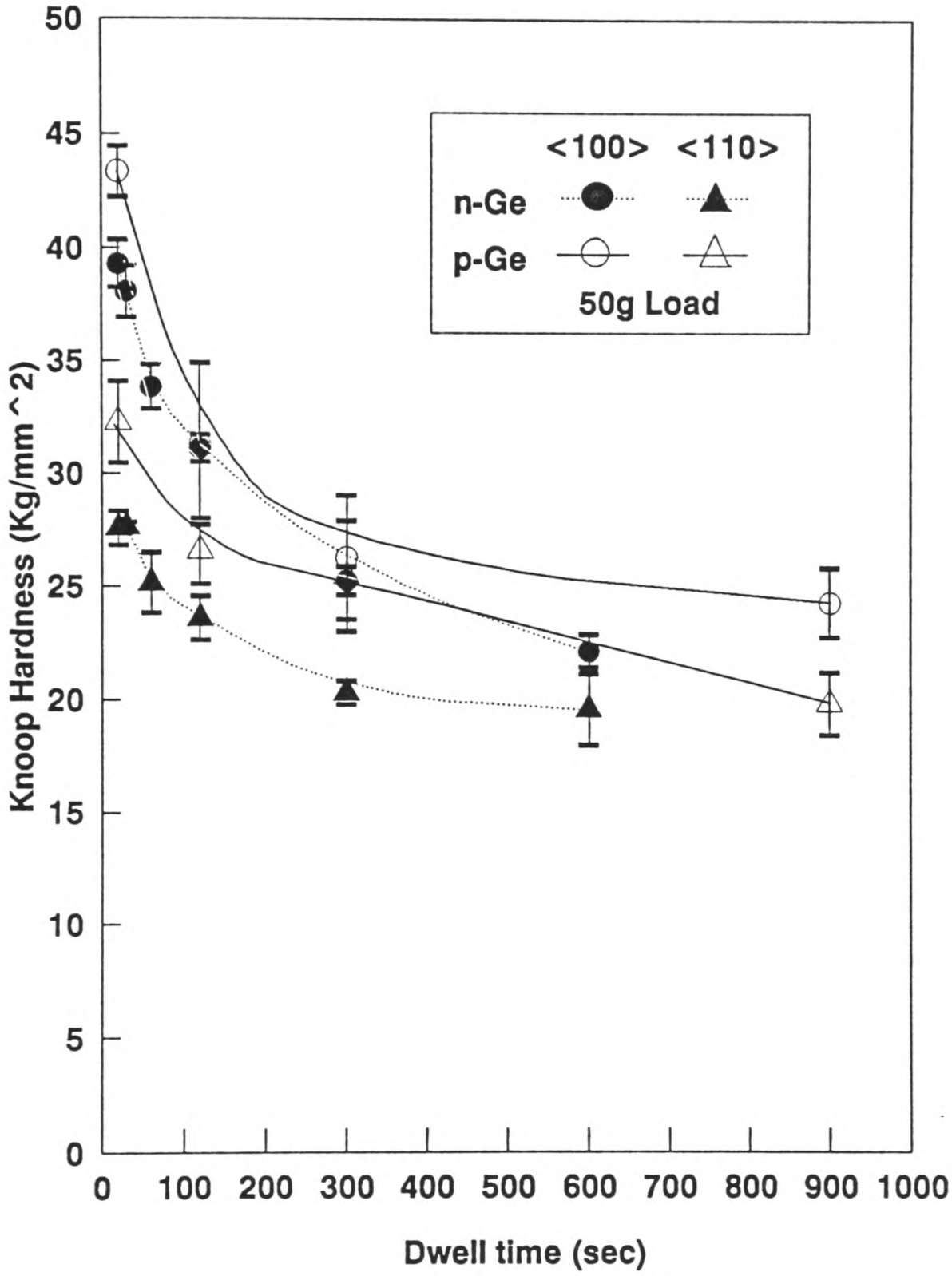


Figure 9.6 Comparison of indentation creep at 700C for (001) n- and p-Ge.

9.1 for example) so that the relative error from the graticule measurements is greater than for the hardness measurements which are based solely on the long diagonal. Also, as some of the figures in the following chapter show, experimental difficulties with the mounting of the indenter head meant that there was a greater variation of in the skew ratio (length of one tip to centre of the indentation along the longest diagonal, divided by the full length of that diagonal). However results did show definite trends. Figure 9.7 shows the change in aspect ratio with increasing indentation temperature for the same <100> Knoop sample whose hardness results are described in figure 9.1. The aspect ratio rises above the ideal Knoop profile in the temperature region in which the fastest creep rates were observed, i.e. 300°C to 500°C. The results at 300°C and 350°C show a significantly larger aspect ratios for the longer time indentations. The change in aspect ratio with temperature for <100> Knoop indentations was much less definite than for the the other orientation. However, by 700°C the aspect ratio (for <100>) had risen to about 9, i.e. of the same order as the <110> orientation aspect ratio at that temperature.

Slip lines were visible (using Nomarski interference contrast) on the surface around at least some of the indentations made at all temperatures, except room temperature. The general form of slip lines for the <110> orientation were lines parallel to the long axis of the indentation and roughly the same length. At longer load times at 350°C and at higher temperatures, a few lines perpendicular to the long diagonal also occurred at the tips of the indentations. The <100> indentations also showed slip lines around each indentation, in the <110> directions, but shallower (and therefore less distinct) than those for the <110> orientation. (This is not in agreement with the results of Roberts, Warren and Hirsch (1986) who reported slip lines parallel to the Knoop indenter axis for both the <110> and <100> orientation).

9.5 Effect of Post- and Pre-anneal

Since an average experiment took 4-5 hours it was necessary to investigate the effect of holding at temperature (but zero load), indentations which had been made at or near the start of the experiment, i.e the effect of post-annealing. In order to test this, indentations which had been made at room temperature were measured and then returned to the machine and annealed for 8 hours at 700°C, before being re-measured. This post- anneal did not affect the measured size of the indentations. Nor did it affect the results from indentations made at 700°C, cooled measured and then post-annealed before further measurement. (Table 9.2 shows the sizes of room temperature indentations both before and after annealing at 700°C.)

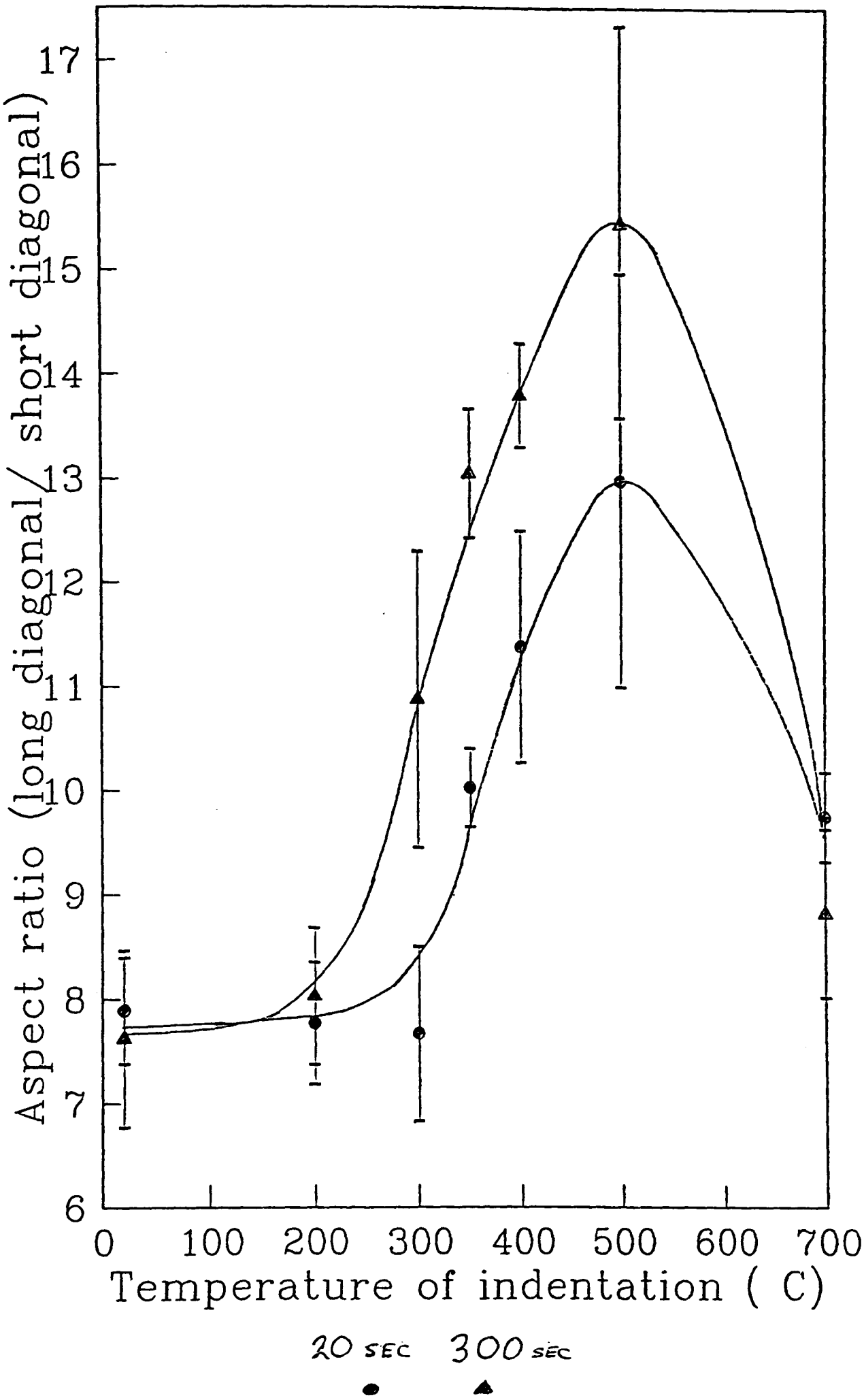


Figure 9.7 Variation of <100> Knoop indentation aspect ratio with indentation temperature on (001) Ge, 20 second and 300 second dwell times.

	Measured size of indentations			
Conditions of the indentation at room temperature	Before 8 hr anneal		After 8 hr anneal	
	D (μm)	SD(μm)	D(μm)	SD(μm)
Straight onto an unheated surface	33.0	0.4	33.4	0.4
After 700°C pre-anneal	29.9	0.3	30.1	0.9

D is the mean diagonal from 6 indentations,
SD is the standard deviation of the mean.

Table 9.2 The measured sizes of straight and pre-annealed room temperature indentations before and after an 8 hour anneal at 700°C.

Table 9.2 also illustrates the change in measured room hardness caused by a pre-anneal at 700°C - compare rows 1 and 2. This effect can be attributed to the removal of surface water since same pre-anneal did not measurably effect the subsequent 500°C hardness compared to that obtained on a virgin Ge sample (intrinsic). A pre-anneal at 800°C did not affect the 400°C hardness of p-doped Ge either.

Thus it seems reasonable to assume that neither the measured size of the indentations, or the hardness response of a sample, are significantly affected by the anneal caused by holding at the test temperature for the duration of an experiment.

10. GERMANIUM DISLOCATION ARRAY ANALYSIS AND CONCLUSIONS

This chapter looks at the dislocation arrays produced by indentation experiments on the (001) surface of intrinsic Ge with the indenter axes parallel to the <110> and <100> directions. Having established the form of array for each orientation, consecutive sections explain how the structure of these arrays changes with time and temperature, and considers how this relates to the observed hardness and indentation creep results which were detailed in the last chapter.

Samples which had been indented at various temperatures were etched to show the structure of the dislocation arrays on the sample surface. The sub-surface dislocation arrays were also observed for some moderate temperature samples, using a serial polish and etch technique for sections both parallel and perpendicular to the sample surface (both orientations). The experimental methods were described in chapter 4. It proved much harder to successfully etch the {110} planes (in the vertical sections of <110> orientations) than the {001} planes.

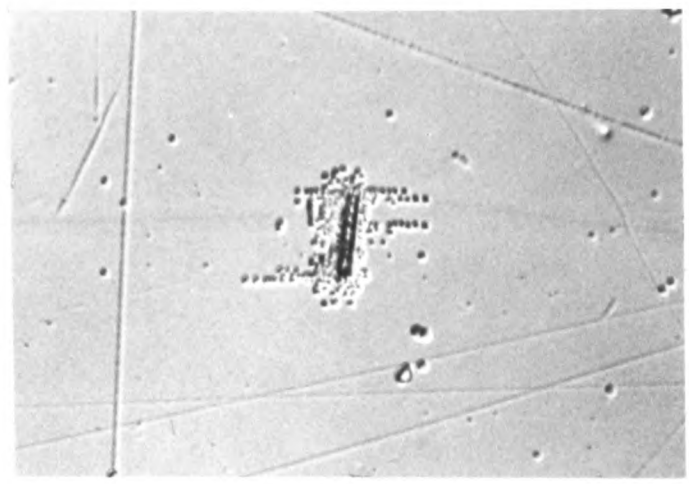
10.1 The <110> orientation dislocation arrays

10.1.1 Rosette Arms - <110> Indentations

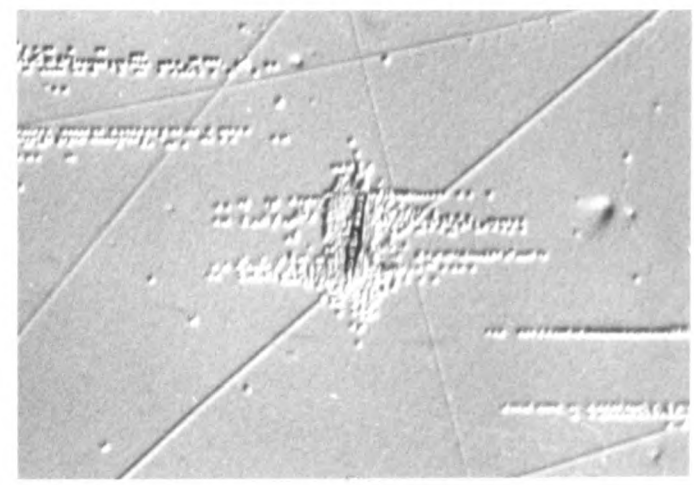
The basic form of the surface dislocation array for a <110> orientation at moderate temperatures is shown in figure 10.1. At this temperature (350^{o}C), a striking aspect is the long rosette arms which emanate from the immediate proximity of the impression in the <110> directions. These lines of pits often extend out a considerable distance from the indentation in a direction perpendicular to the long axis of the indenter, although the pits are not regularly spaced along the line. The rosette arms get longer with dwell time. Figure 10.2 compares the mean rosette length (i.e. from five or more indentations) for each loading time with the mean long diagonal length. There is some degree of correlation between the length of the rosette arm parallel to the long axis and the length of the diagonal, but the long arms (perpendicular to the axis) increase at a faster rate at least for the first two minutes.

In the case shown in figure 10.1, the indenter was orientated at a slight angle to the true <110> direction. It is interesting to note that the characteristic pairs of long rosette arms do not form from the usual symmetrically placed points until the longer dwell times (larger indentations). The 20 second indentation shows arms starting only from the "quarters" nearest the indenter tips. The distance between each pair of long arms is roughly

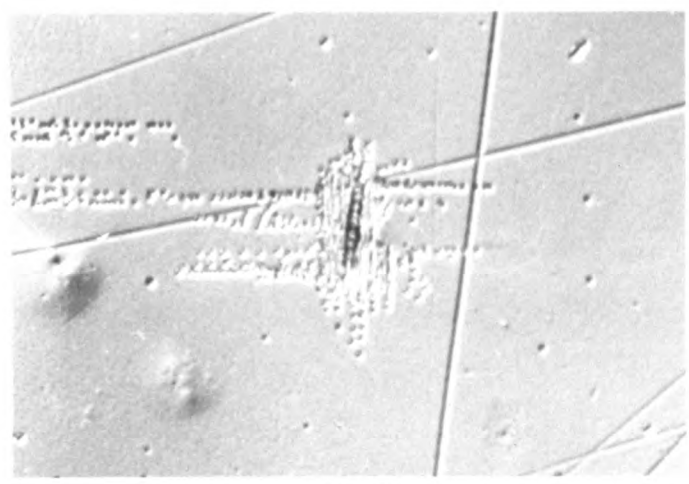
Figure 10.1 Dislocation surface arrays from <110>> indentations on (001) Ge at 350°C showing the effect of increasing dwell time, (a) - (e) 20, 30, 60, 120, 300 and 600 seconds respectively.



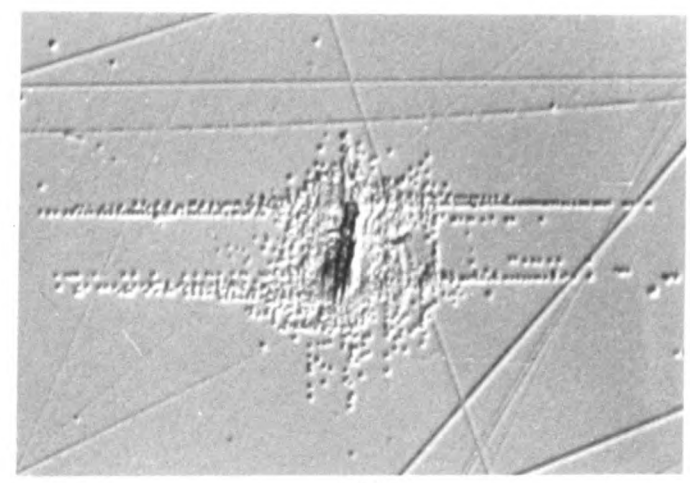
(a)



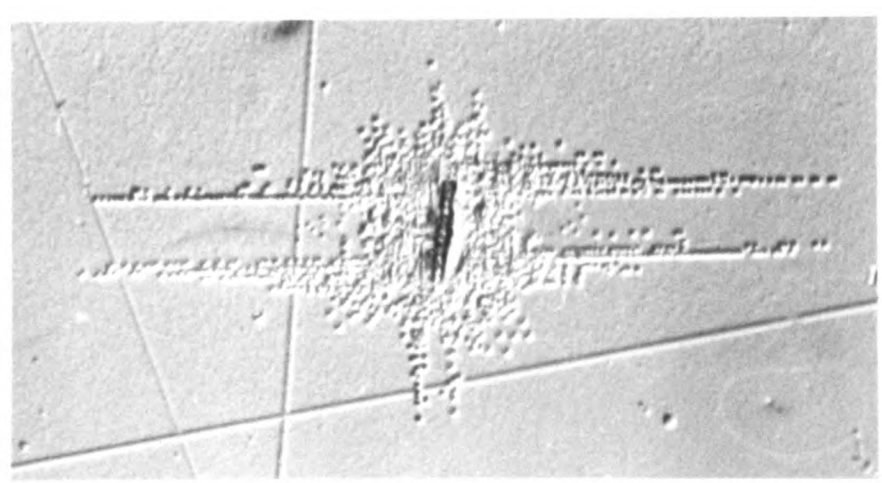
(b)



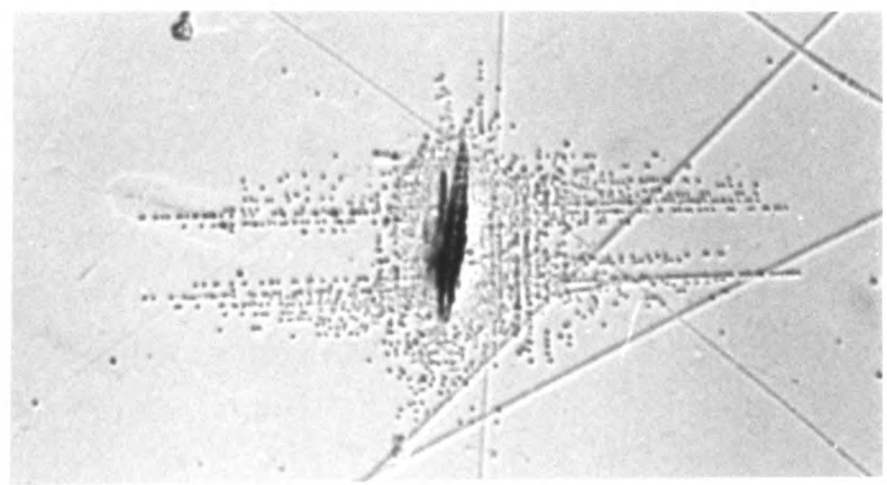
(c)



(d)



(e)



(f)

100μm

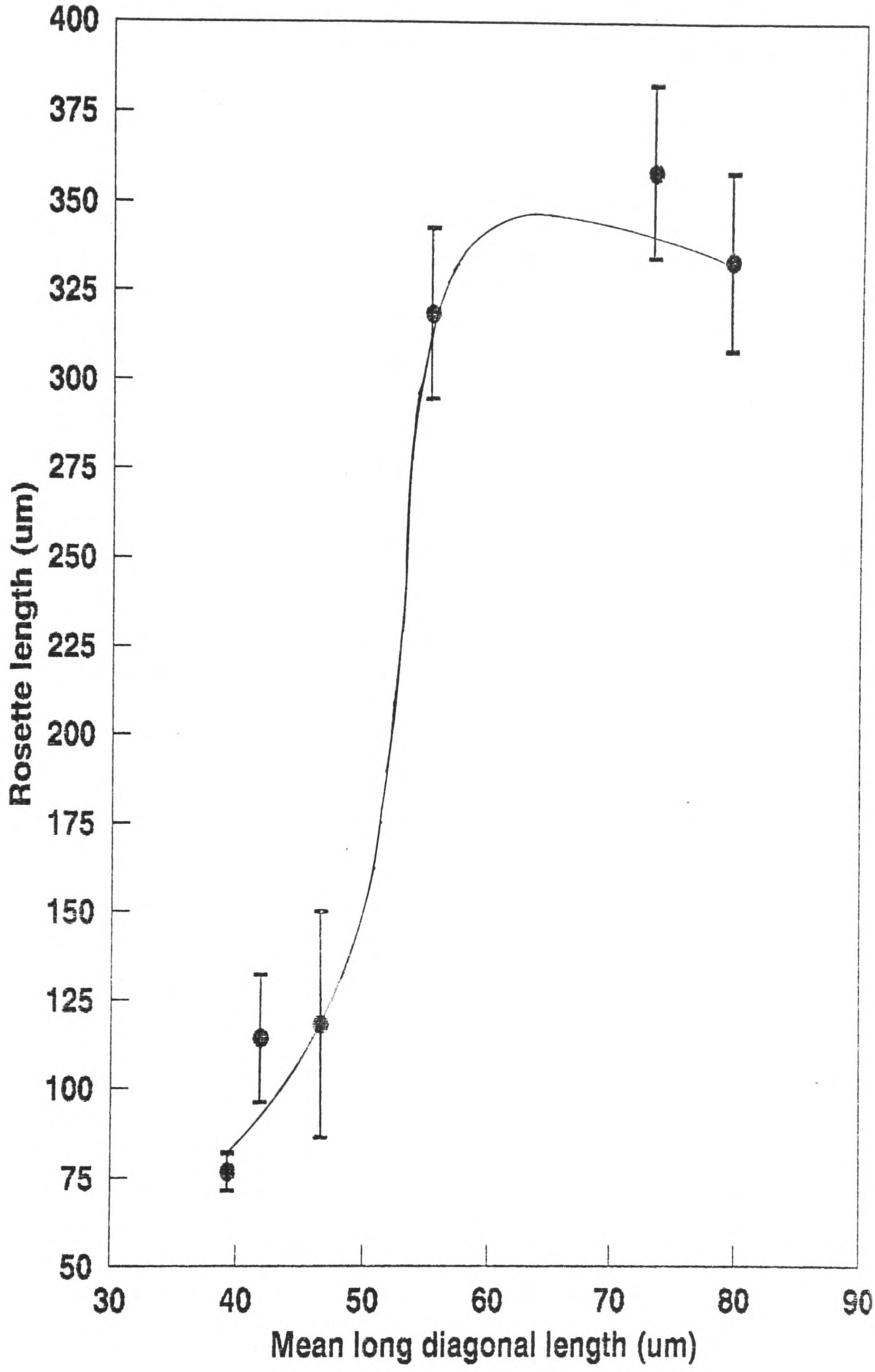


Figure 10.2 Variation in rosette length with the length of long diagonal, for <110> 50g indentations at 350C.

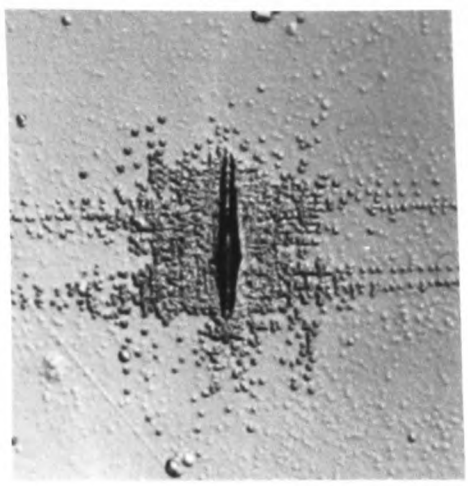
constant (about 30 μm) for all the indentations, once the normal pattern is established, suggesting that loops are first formed at the stress conditions, which occur at this particular spatial point within the stress field (from a 50g load and in this orientation) and then continue to travel outwards with dwell time. At 400^{o}C the same phenomenon occurred, but the distance between the arms was larger. The patterns confirm that the first rosette arms formed travel farthest since they have more time for movement. However, as the indentation increases in size and the arm in length, the resolved shear stress, i.e. the driving force decreases, so at the longest times the longest arms are expanding under the influence only of interaction stress, but the shorter arms are still being driven out at a faster rate. Hence the thickening of the rosette arms.

10.1.2 <110> Indentations Subsurface Information

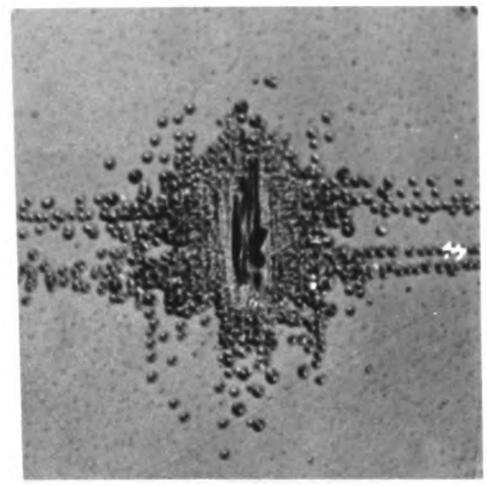
The three dimensional structure of the dislocation activity is perhaps most accurately investigated by the serial polish and etch technique. Figure 10.3 shows a series of etch pit structures under a 20 second indentation (made at 400°C) as surface material was stripped away from the specimen. This shows that the rosette arms consisted of dislocation loops on converging {111} planes since the lines of etch pits moved together and then disappeared entirely as material was removed. This can be seen for a 20 second indentation at 400°C in figure 10.3(a) to (f).

Apart from the rosette arms, most of the dislocation etch pits are concentrated in an elliptical area around the indentation impression. As described above, the lines of etch pits from the rosette arms perpendicular to the long axis move together and then disappear by about 30μm depth. Part (c) and (d) show that the rounded top and bottom of the dense ellipse of pits reduce to an oblong, suggesting that this part of the array is also formed by slip parallel to the surface. (The dimensions of the original indentation were 79.5μm long and 8.7μm wide). The dense area increased in width as material was removed, but stayed a constant length, and then began to decrease. Detailed measurements were made of the clearer dislocation patterns in the later sections (i.e. at greater depth). These showed that, generally, dislocation pits in the long sides of the oblong stayed the same distance apart from neighbouring pits in a direction parallel to the long axis, but moved apart from the corresponding lines on the other side of the oblong (i.e. in a direction perpendicular to the long axis). The pits in the middle of the array moved away from the centre of the indentation in a direction parallel to long axis, causing the observed clear patch in the centre of the oblong array to develop. Eventually only a few lines of pits are left from loops which intersect the surface in a direction parallel to the long axis of the indenter, plus perhaps a few perpendicular lines defining a pit free region in the center of the array (figure 10.3k).

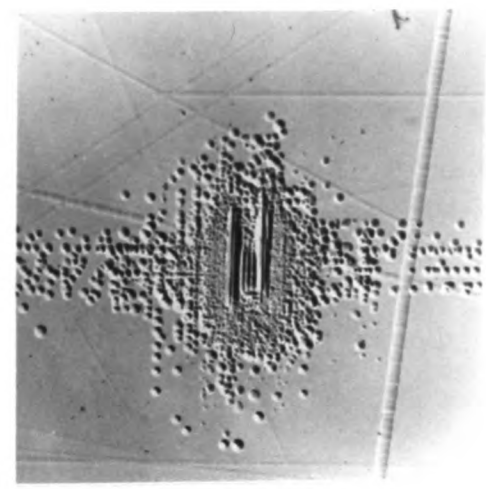
Figure 10.3 Series of etched arrays around a typical indent as the surface was stripped away, 20 second <110> orientation on (001) Ge at 400°C: (a) surface array, (b) 6μm depth, (c) 12μm, (d) 19μm, (e) 26μm, (f) 31 m, (g) 34 m, (h) 41 m, (i) 52 m, (j) 64μm: (k) 30 second <110> indentation also at 64μm depth.



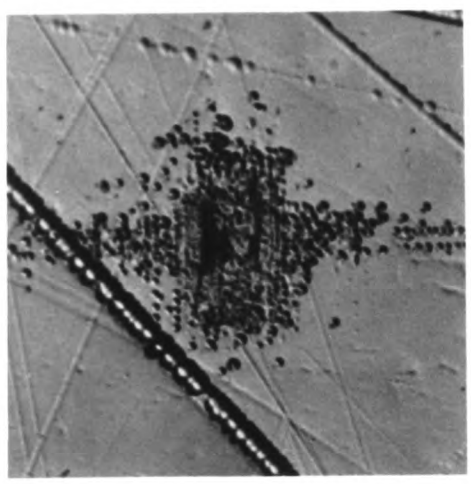
(a)



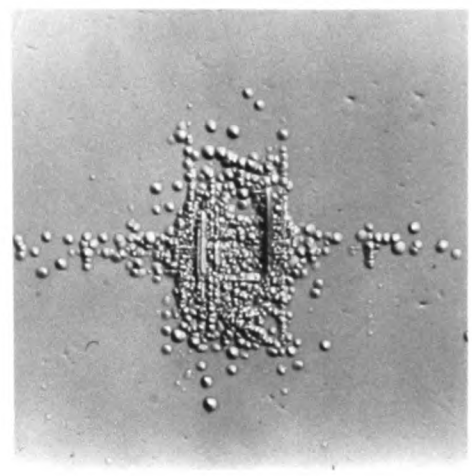
(b)



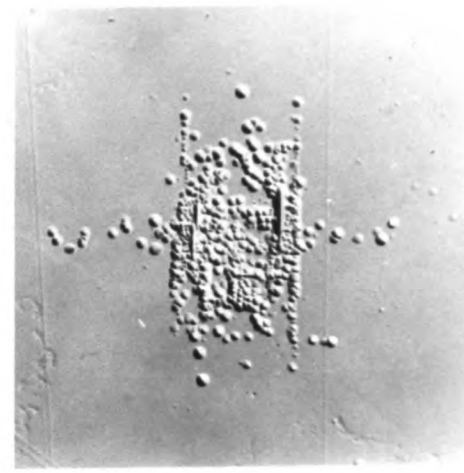
(c)



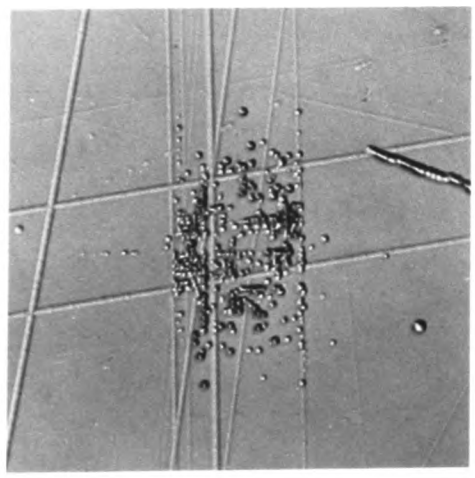
(d)



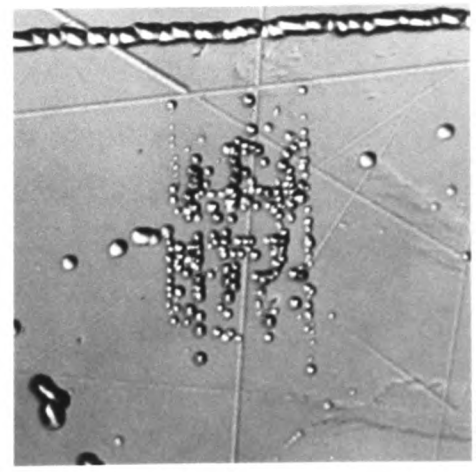
(e)



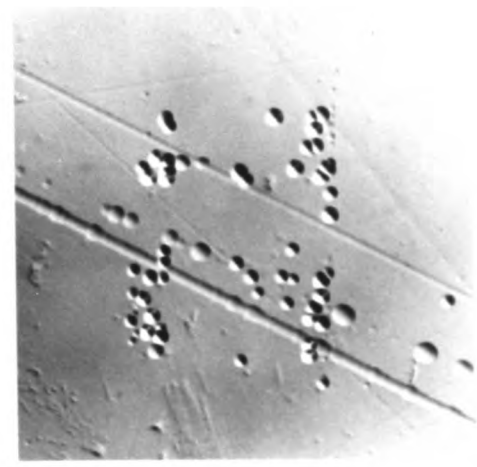
(f)



(g)



(h)

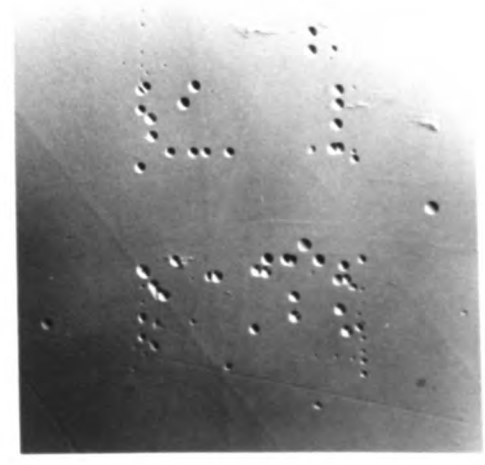


(i)



(j)

100 μm



(k)

Thus most of the dislocation activity, which penetrates to any depth, appears to take place on planes with slip directions inclined to the surface of the specimen, specifically on diverging planes which carry material away from the highly stressed indentation area into the body of the sample. An etched section across the centre of a 120 second (figure 10.4) illustrates the sets of parallel {111} planes each side of the indentation.

An interesting feature is the etch lines which develop in the zone directly beneath the indentation. The trough formed along the spine of the indentation when the surface is first etched, disappears, and is replaced by two or more etch lines which move apart as the surface is removed. These lines disappear at about the same depth as the rosette slip (see figure 10.3f).

10.1.3 Progression of slip with time

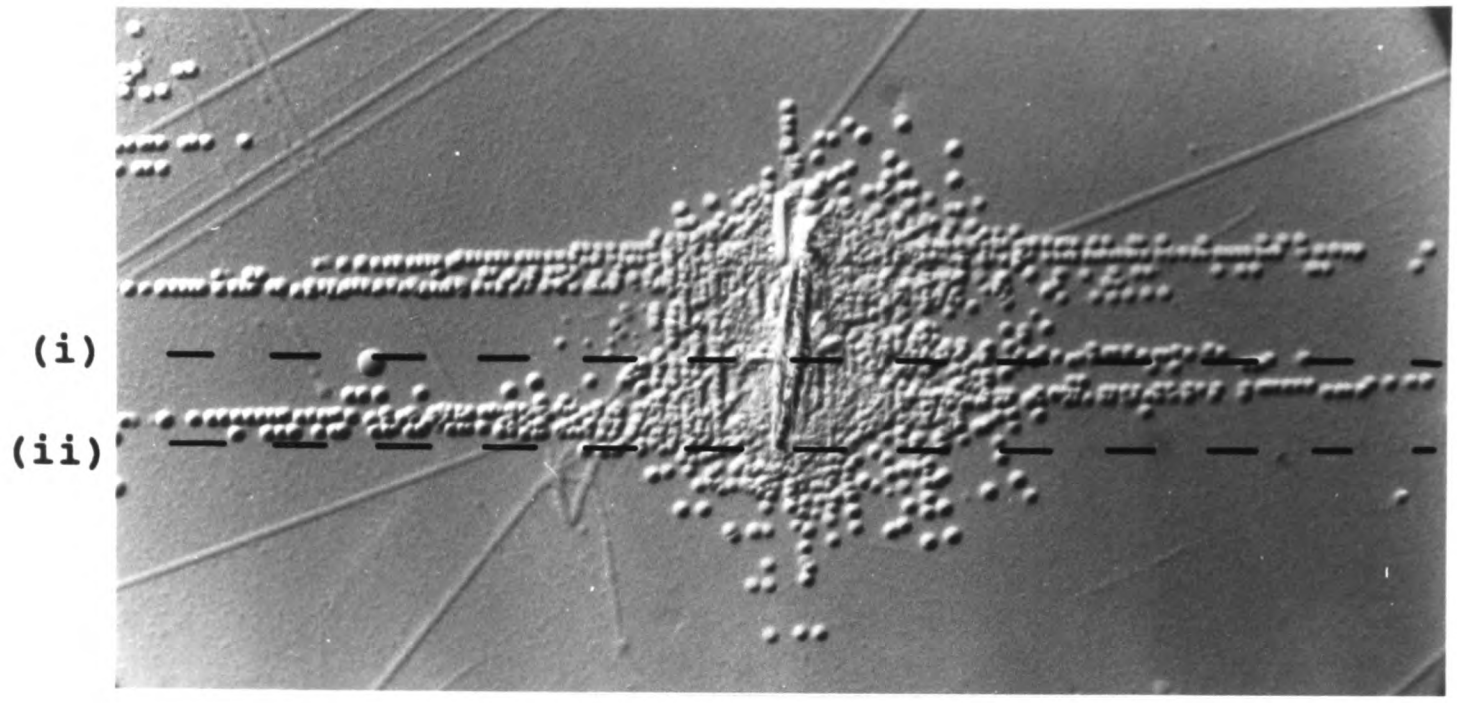
Figure 10.3 considers a 20 second <110> indentation at 400°C. In order to discuss the processes of creep it is necessary to analyse the changes in the dislocation structure with time. Figure 10.5 shows a series of etch pit structures from sections of a 600 second indentation. Comparing figure 10.3(i) and 10.5(i) (and also figure 10.4) illustrates that the surface dislocation arrays of longer time indentations show an increased number of etch pits, and more "far-flung" dislocations. The dense area of pits surrounding the impressions spreads out so that by 600 seconds it is more oblong than elliptical. Lines of pits running parallel to the long axis extend out perpendicular to the long axis to obscure the roots of the rosette arms. Comparing this with figure 10.3 it can be seen that the general three dimensional structure is similar to that of shorter time indentations but dislocation loops not only extend far deeper into the crystal but give a more random pattern in the bottom section.

10.2 Dislocation arrays around <100> Indentations

10.2.1 Rosette arms - <100> Indentations

The basic form of the surface dislocation array for a <100> Knoop indentations at moderate temperatures is shown in figure 10.6. Eight rosette arms can be seen radiating out in the <110> directions. Again, these extend out a considerable distance from the dense area of dislocations which surround the impression, and get longer as the time of loading increases. Figure 10.7 shows the increase of average rosette length with dwell time. Each rosette arm is composed of one or more lines of pits; the pits are not regularly spaced along each line. The serial sections of a 20 second indent at 400°C (figure 10.8) clearly show that the adjacent lines of pits in a rosette arm move together as the surface is stripped

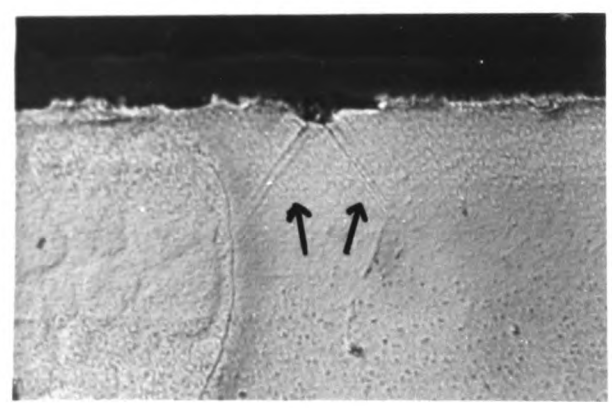
Figure 10.4 <110> Knoop indentation, 120 seconds on (001) Ge at 400°C; (a) Surface array, (i) and (ii) Etched vertical sections across the chords indicated.



(a)



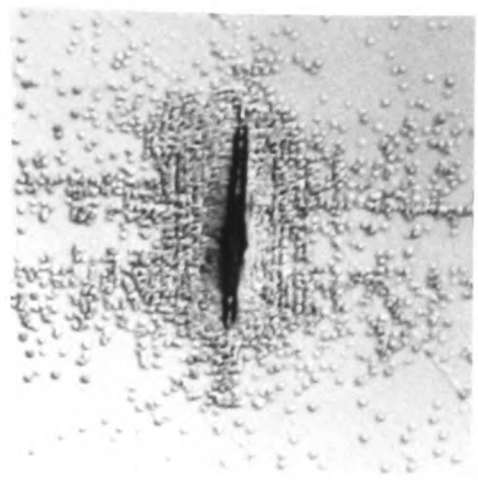
(i)



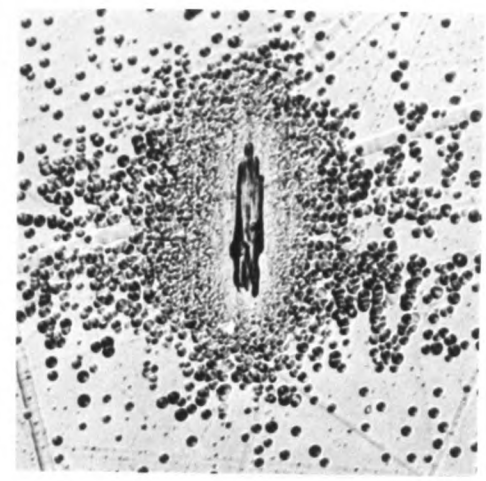
(ii)

100 μm

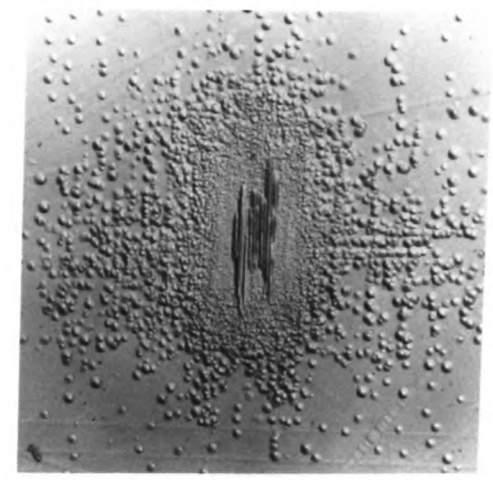
Figure 10.5 Series of etched arrays at the sample surface as it was striped away, 600 second <110> orientation on (001) Ge at 400°C: (a) surface array, (b) 6μm depth, (c) 12μm, (d) 19μm, (e) 26μm, (f) 31μm, (g) 41μm, (h) 52μm, (i) 64μm, (j) 75μm (k) 100 m.



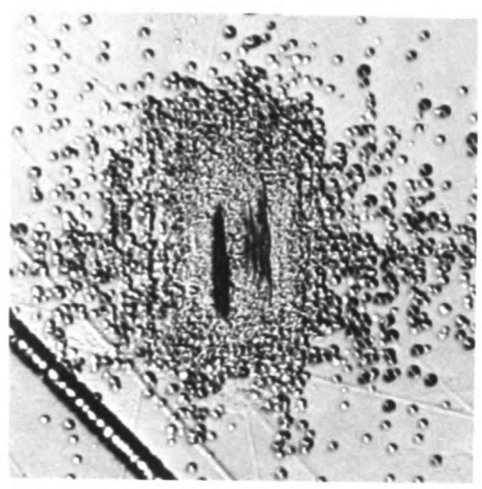
(a)



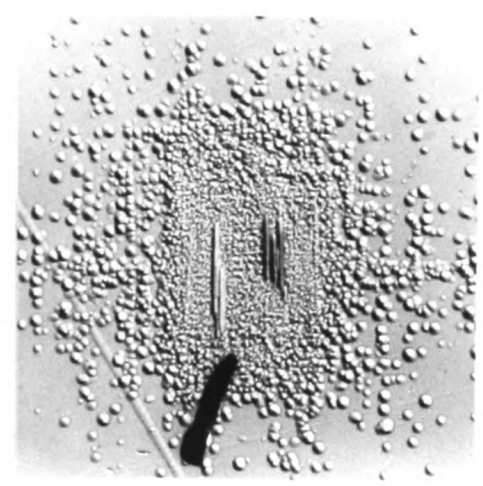
(b)



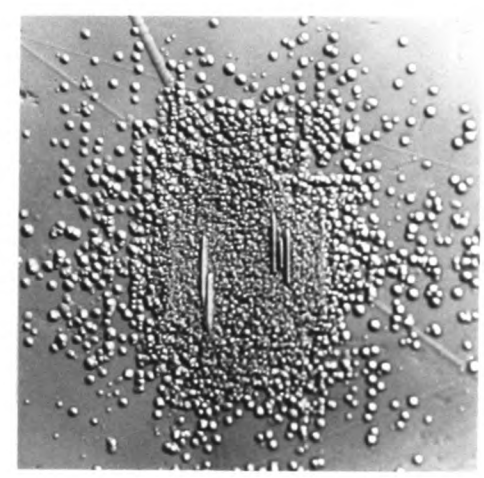
(c)



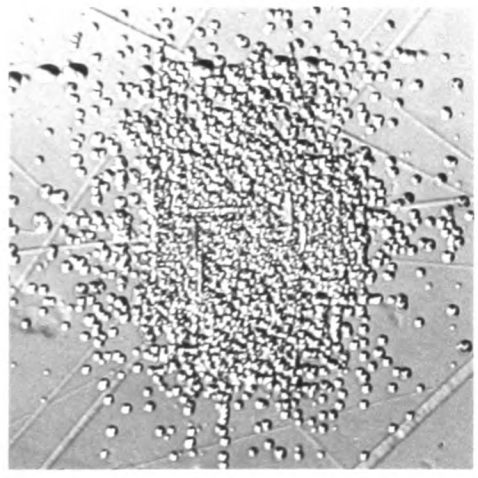
(d)



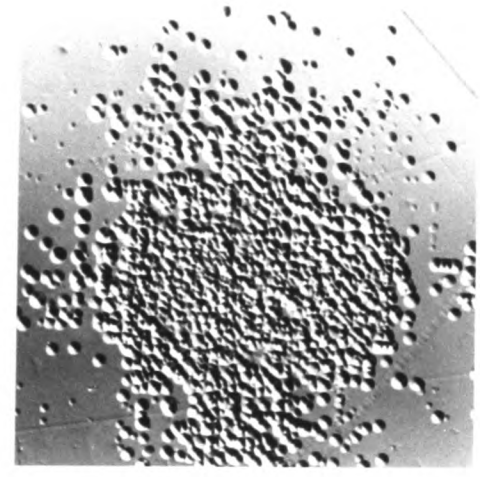
(e)



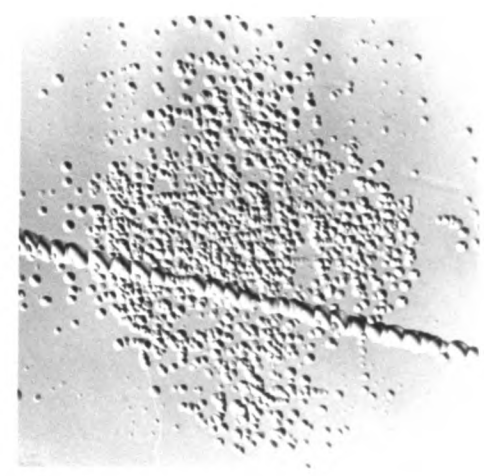
(f)



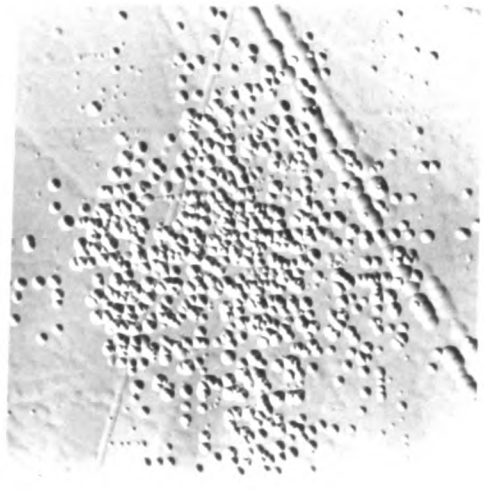
(g)



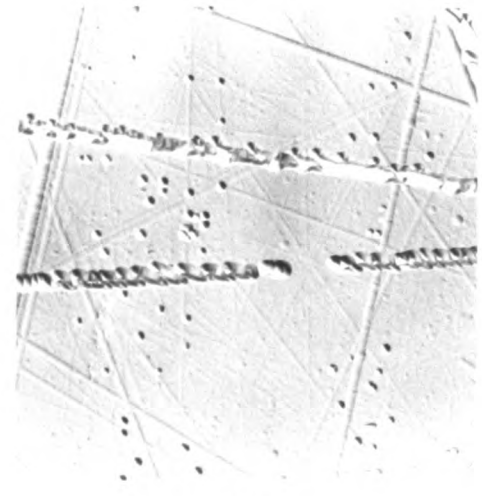
(h)



(i)



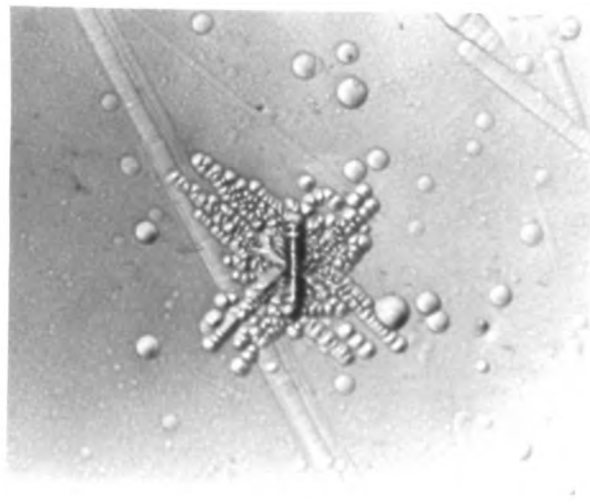
(j)



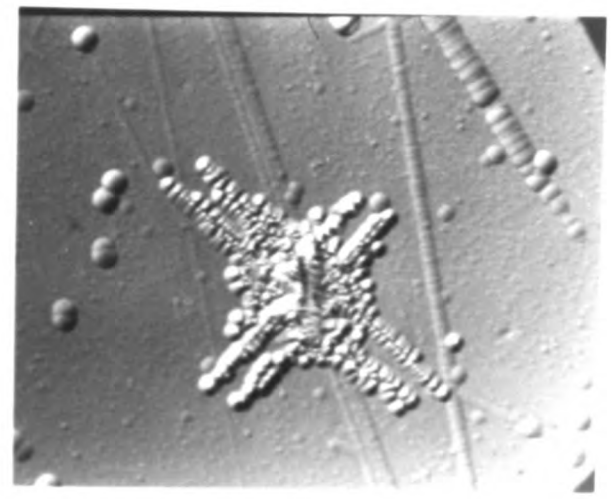
(k)

100 μm

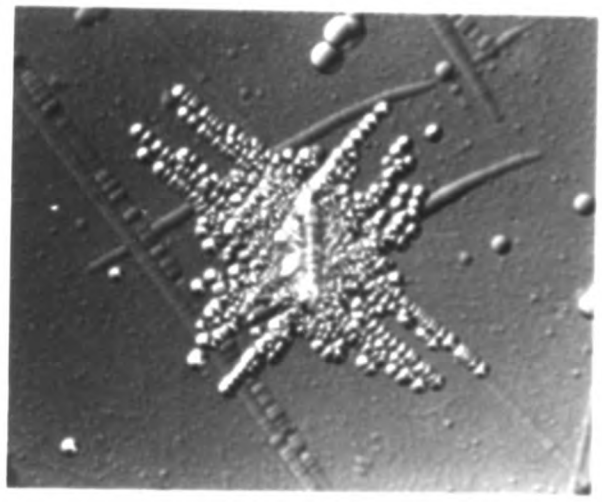
Figure 10.6. Dislocation arrays from <100> indentations on (001) Ge at 350°C showing the effect of increasing dwell time: (a) - (e) 20, 30, 60, 120, 300 and 600 seconds respectively, and (f) a vertical section through a 60 second indentation.



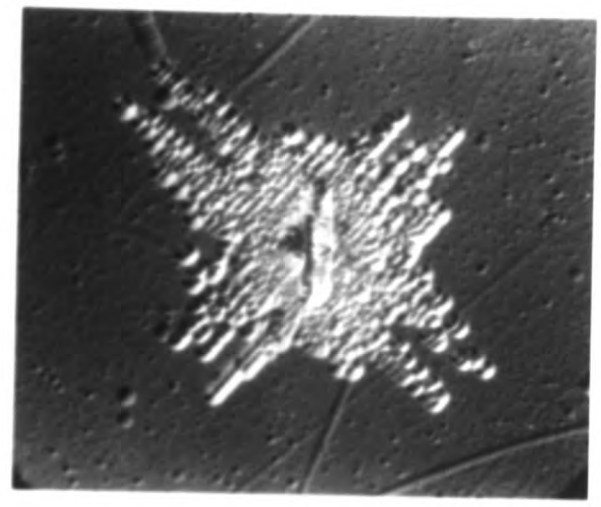
(a)



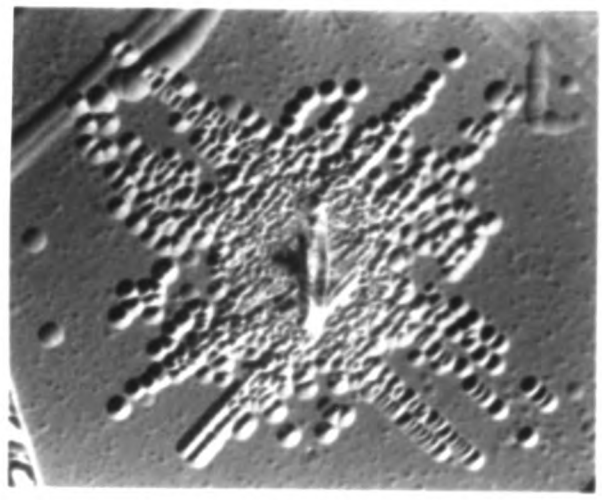
(b)



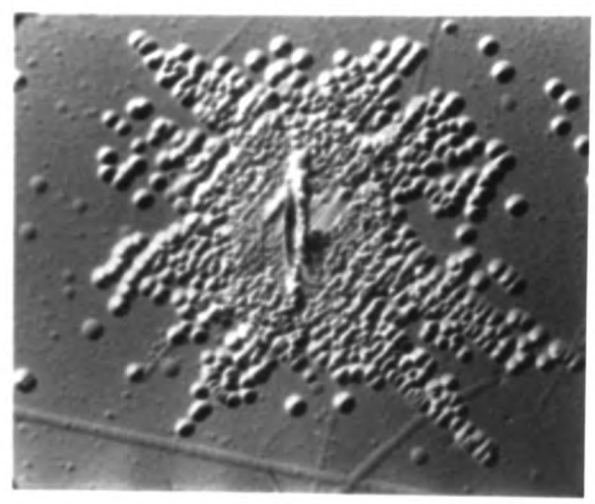
(c)



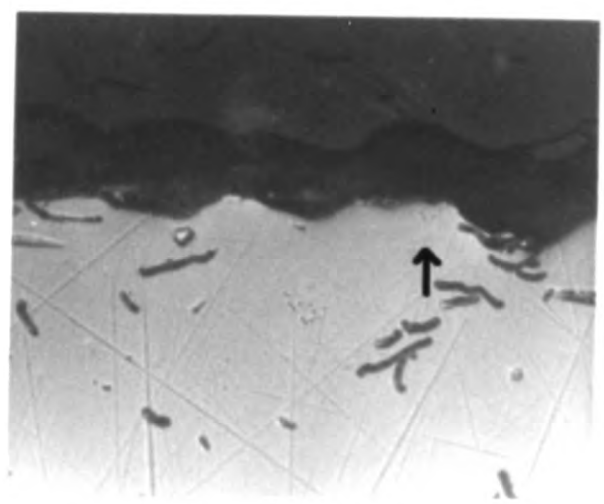
(d)



(e)



(f)



(g)

100 μm

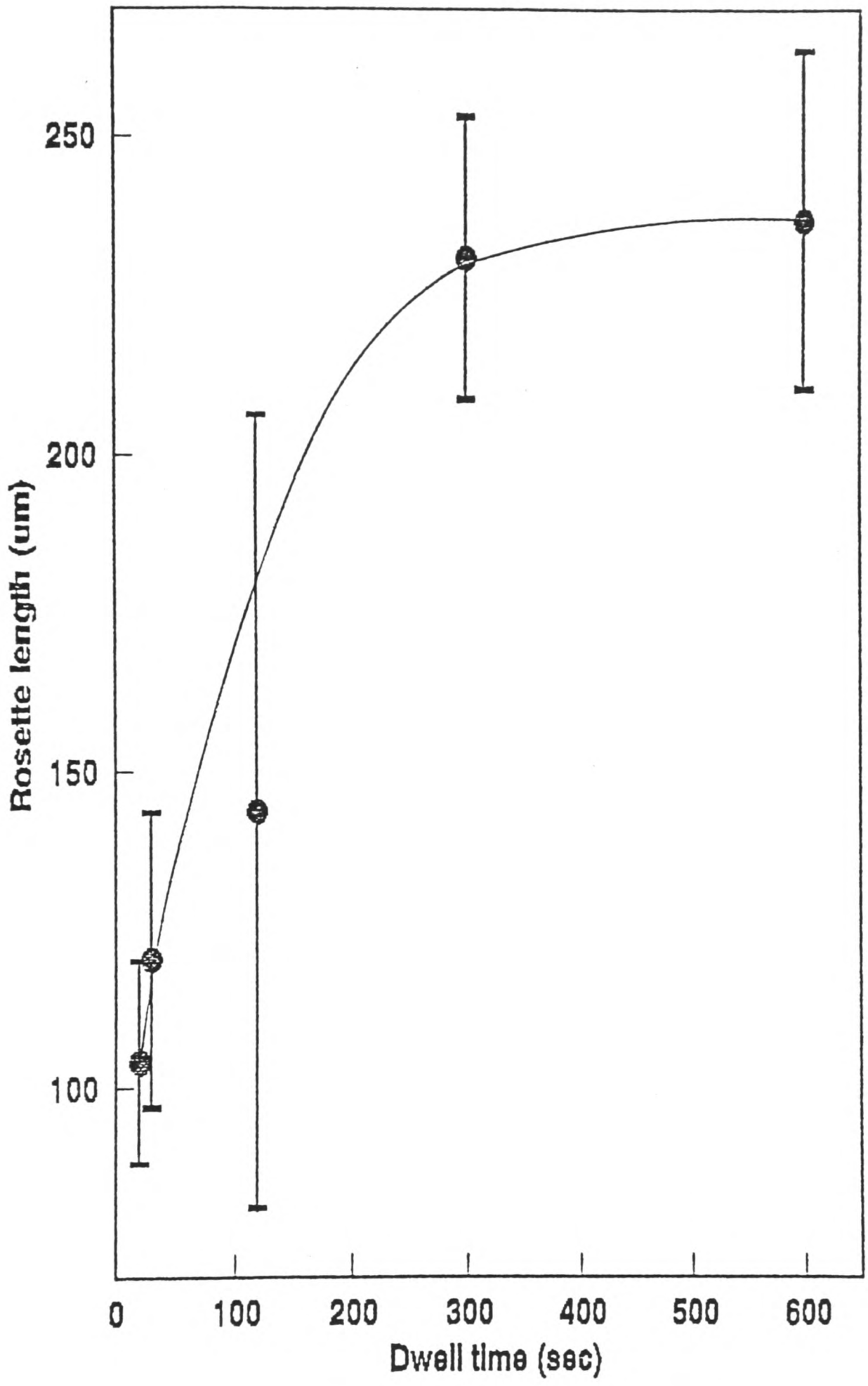
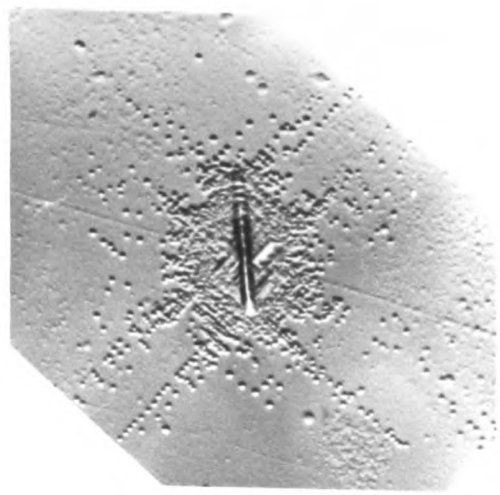
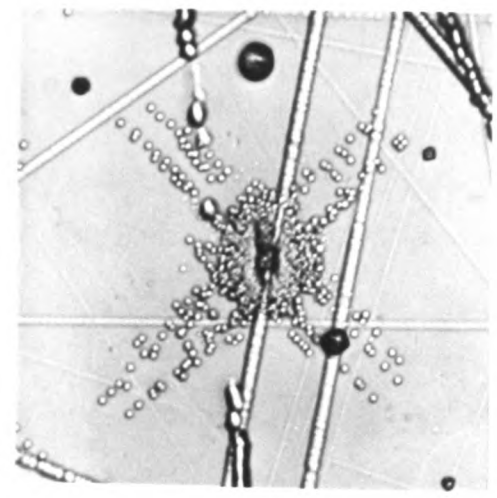


Figure 10.7 Variation of mean rosette length with dwell time, for <100> Knoop indentations, on (001) Ge at 350°C.

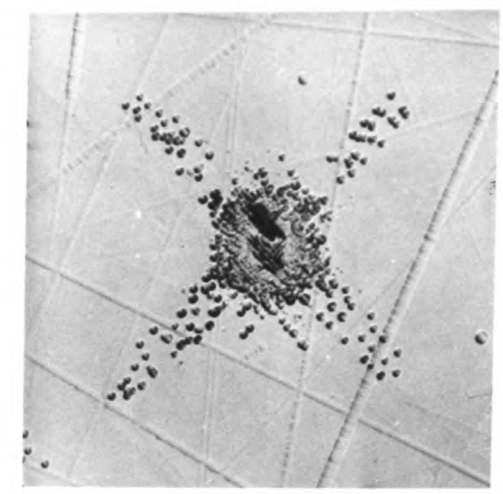
Figure 10.8 Series of etched arrays at the sample surface as it was stripped away, 20 second, <100> orientation on (001) Ge at 400°C: (a) Surface array, (b) 6μm depth, (c) 12μm, (d) 26μm, (e) 31μm, (f) 34μm, (g) 41μm, (h) 48μm, (i) 64μm, (j) 75μm, (k) 30 second indentation at 12μm depth.



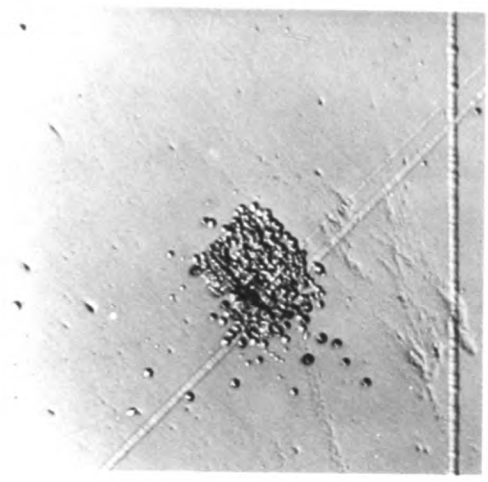
(a)



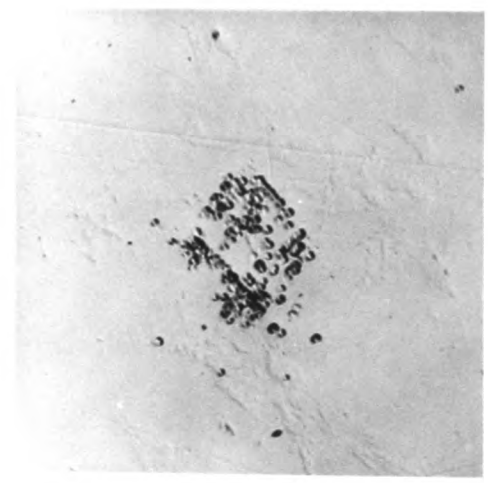
(b)



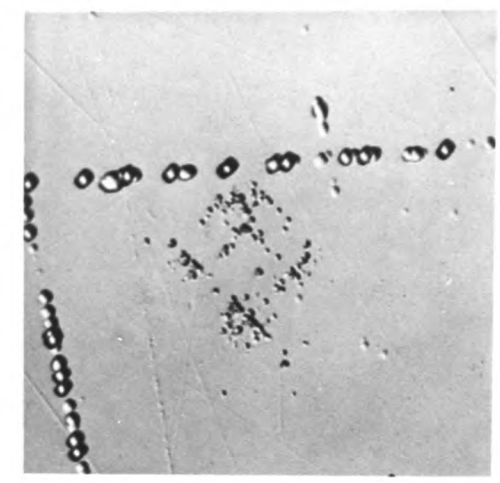
(c)



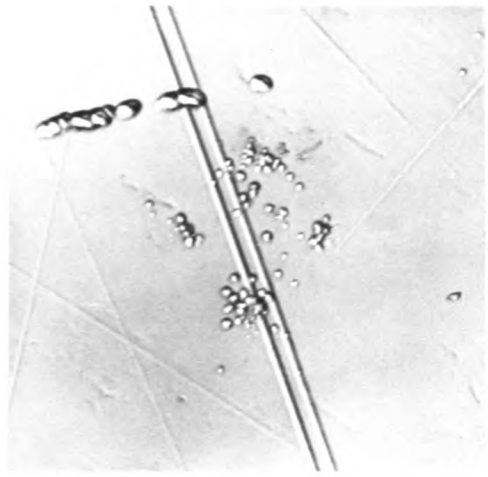
(d)



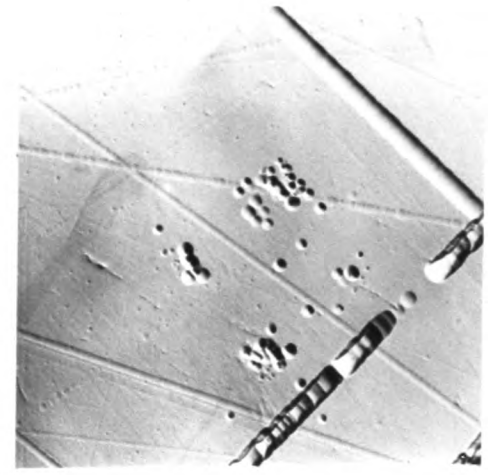
(e)



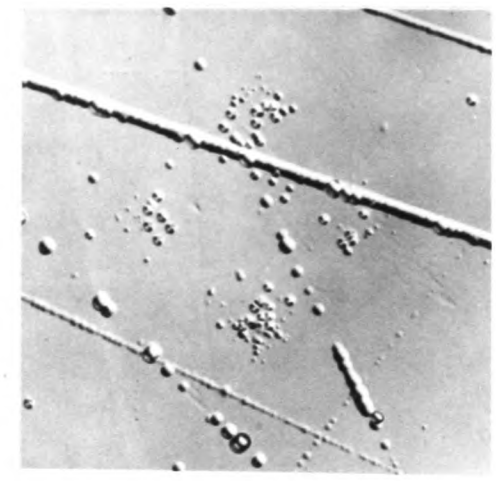
(f)



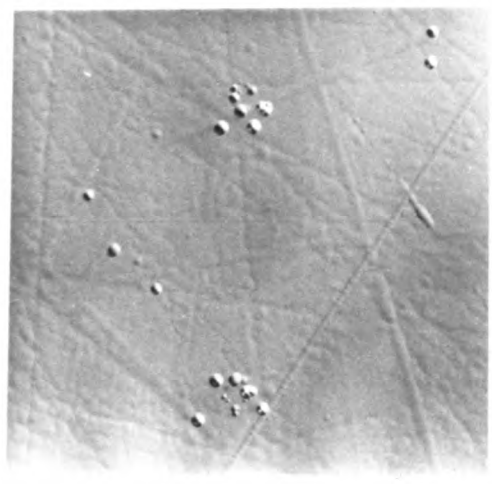
(g)



(h)

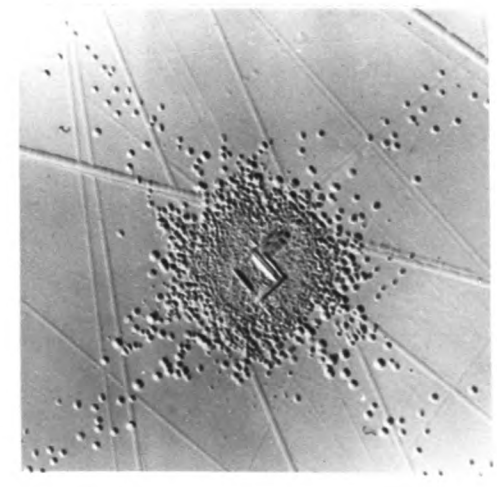


(i)



(j)

100 μm



(k)

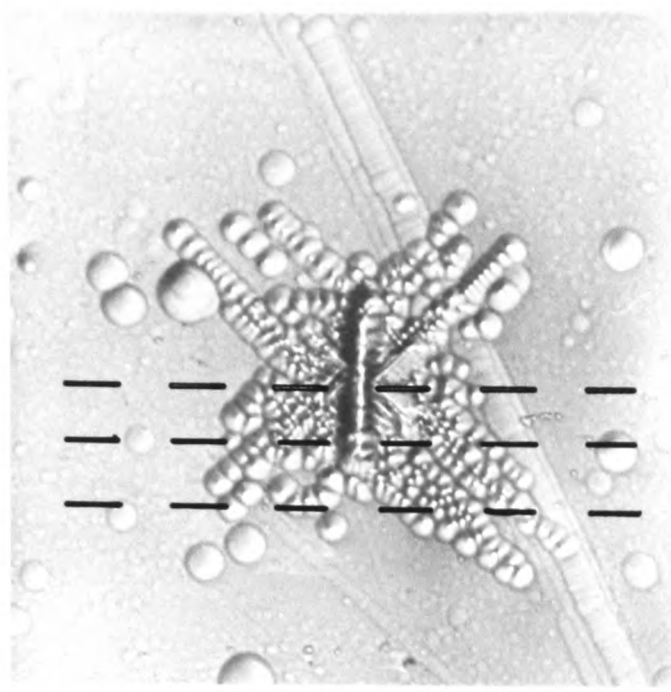
away, until just a few then none remain. This suggests that, as in the <110> orientation, they are on converging planes, which is confirmed by a vertical section of a 60 second indentation at 350°C (figure 10.6g) which shows the V shaped detail of pits which would be expected if the rosette arms being intercepted (see top view) were on converging planes.

10.2.2 <100> Orientation Subsurface Information

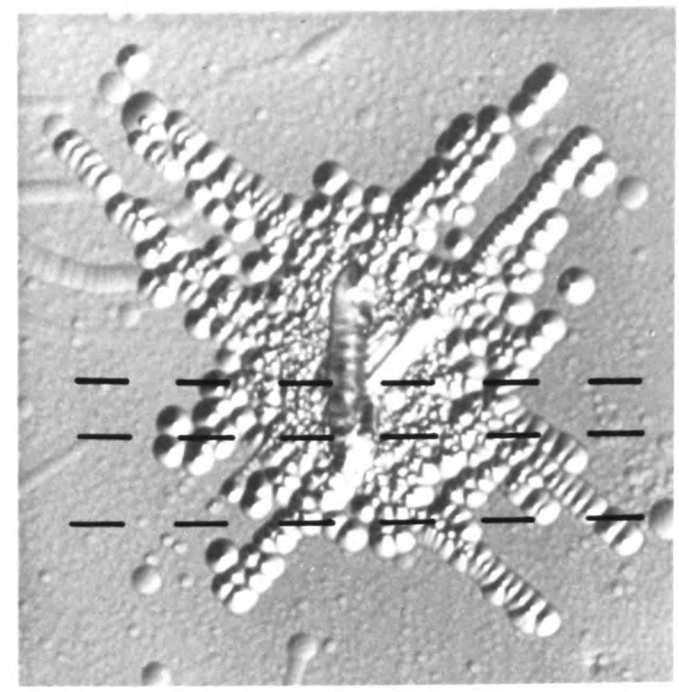
As shown in figure 10.8(a), at first the dense mass of pits around the indentation impression is shown to form a roughly octagonal (or sometimes hexagonal) figure with a rosette arm at each corner. (This is less clear for the 350°C indentations where the rosette slip dominates the surface array). Below the surface this reduces to a square, suggesting that some of the some of dense area of pits around the tips comes from relatively shallow loops. The dislocation density in the square decreases, until finally a few pits clustered at the corner of the indentation are left, as shown by the indentation detailed in figure 10.8. Although the square dimensions do increase as the surface is removed, comparison with the data from the <110> indentation dimensions (from which section depths were calculated) showed that the increase was much less than it would be from a single set of diverging planes which started from e.g. 10.8(c). Therefore the sections suggest that the dislocation structure beneath the indentation consists of a series of "stacked" planes containing loops which intersect the etched surface in lines which run in all the <110> directions contained in that surface. By identifying individual dislocation lines it can be seen that these are on planes that diverge from the impression. The planes do, of course, intersect each other, but since the loops have the same burgers vector this is not a problem. Vertical sections as one approaches the centre of a 20 and a 60 second indentation can be seen in figure 10.9. The deep dislocation structures are not easy to visualise from the patterns since the "slice" is through the corner of the pyramid formed by {111} planes (see figure 10.10). However the fact that the section beneath the tip of the indentation shows planes confined within a certain width across the section, is further evidence of the stacked planes mentioned earlier. This arrangement suggests the existence of a stress envelope beyond which the total force, pushing the loop down and away from the centre of the indent, is not enough to cause further expansion. The isolated triangle of pits in the vertical section away from the indentation tip corresponds to the corner groups of the deep horizontal sections in figure 10.8. It is not clear why these form an inverted triangle for one would intuitively expect the triangle to be the other way up. It might be due to some prismatic loop arrangement at the bottom of the deformed region as shown in Wagatsuma and Sumino's X-ray topography results (1971).

In a similar way to the <110> indentations, short etch "troughs" appear at the centre of the indentations as the section goes down below the depth of the actual

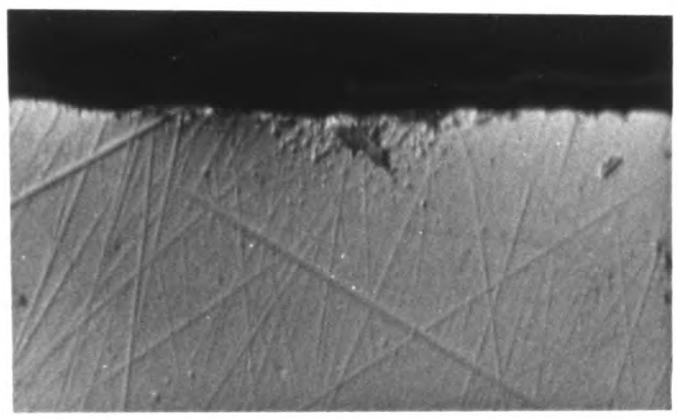
Figure 10.9 Typical dislocation arrays for <100> indentations on (001) Ge at 350°C, (a) 20 second and (b) 60 second, sections (i), (ii) and (iii) as shown.



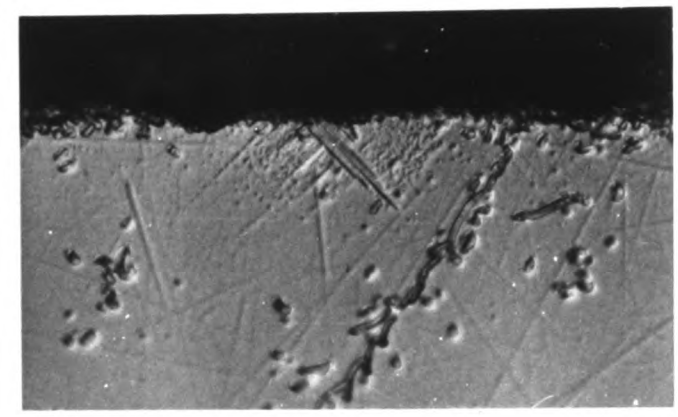
(a)



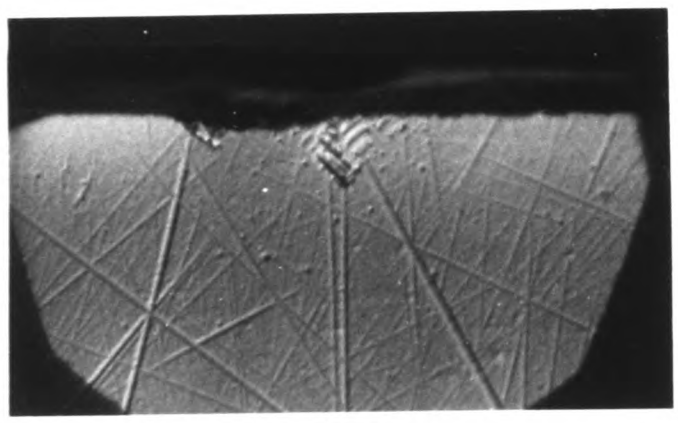
(b)



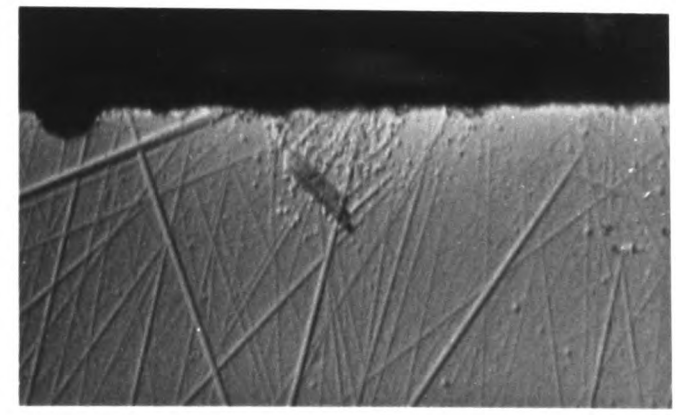
(a.i)



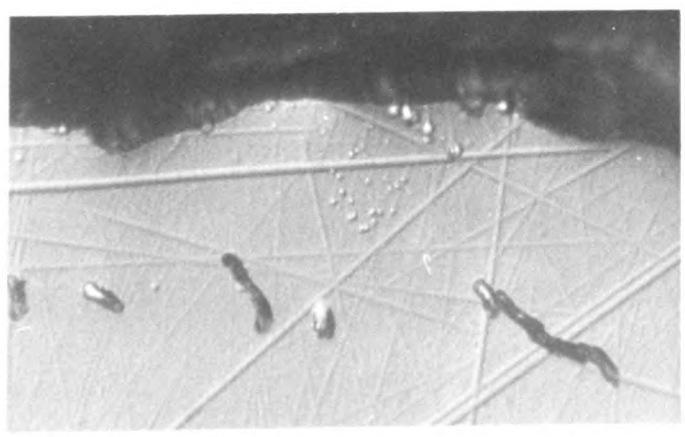
(b.i)



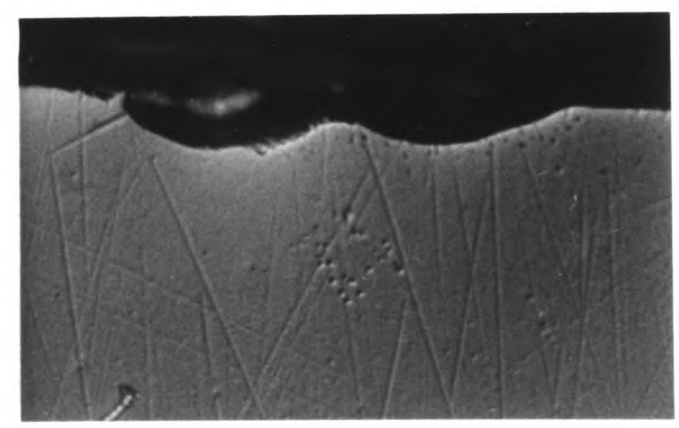
(a.ii)



(b.ii)



(a.iii)



(b.iii)

100 μm

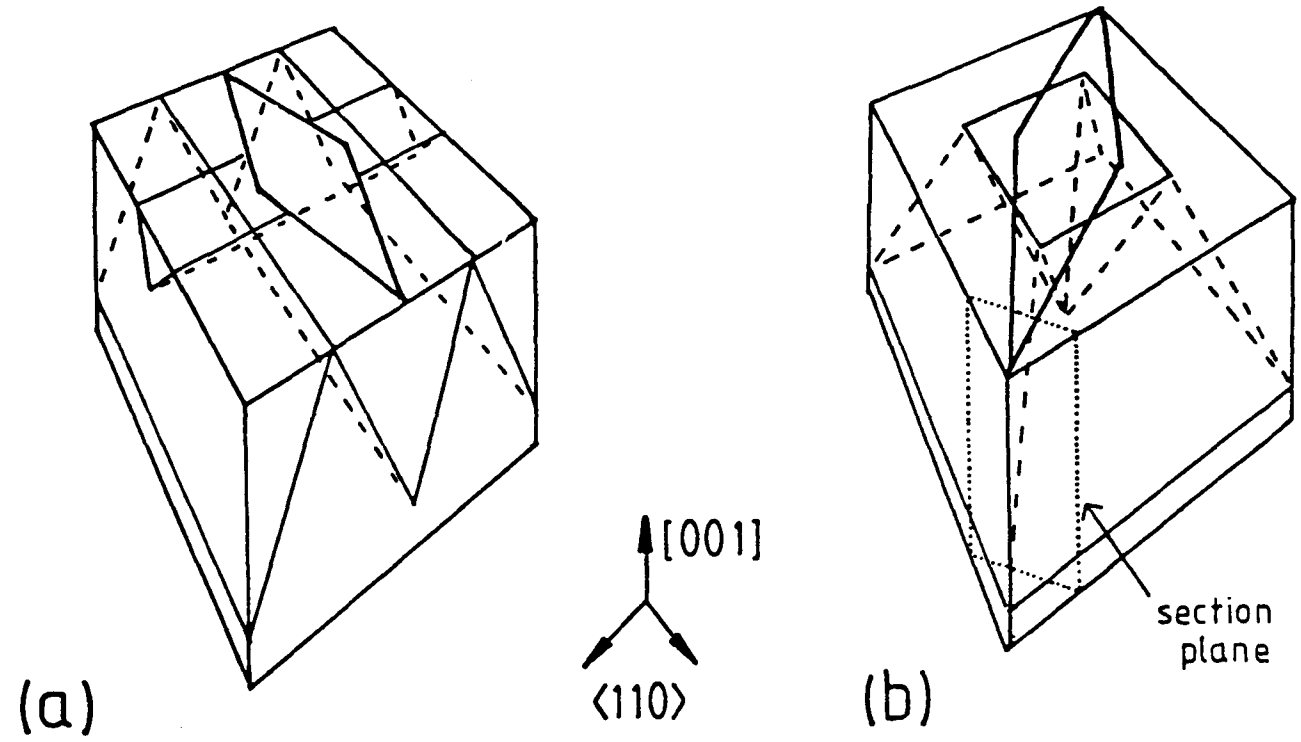


Figure 10.10. Slip geometry under Knoop Indentations on the (001) face of Ge; (a) <110> and (b) <100> orientation.

impression (e.g. figure 10.8 (c) and (k), and 10.11(c)-(e)). Unlike the <110> figures, these features lie along both {110} directions and often criss-cross or form squares.

10.2.3 Progression with time - <100> Orientation

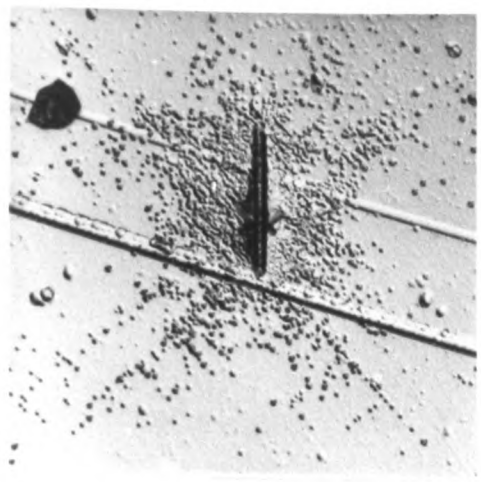
The time sequence of <100> surface arrays at 400°C can be deduced from part(a) of figures 10.8 and 10.11. The dimensions of the dense area of pits increase with longer dwell time, both in absolute terms and relative to the measured long diagonal. Measurements of the dimensions of the square outline left at the bottom of the deepest sections for the 20 second and 60 second indentation at 400°C (10.8j and 10.11k), revealed that the square gets smaller relative to the indentation diagonal. This implies that loops generated as the indentation size increases with time do not extend down to the same depth as those formed earlier on in the deformation (in a similar fashion to the <110> orientation rosette arms as described above). This conclusion is substantiated by comparing vertical sections underneath the tip of the indentation as in figure 10.9. Although the depth of the dislocation structure is obviously deeper, as a fraction of the indentation diagonals (41μm and 87μm respectively) the depth is proportionally less for the longer time indent. However, the horizontal sections (figure 10.8 and 10.11) show that the number of loops reaching the last few horizontal sections are substantially more for the long time indents.

10.3 Variation of Dislocation Structure with Temperature

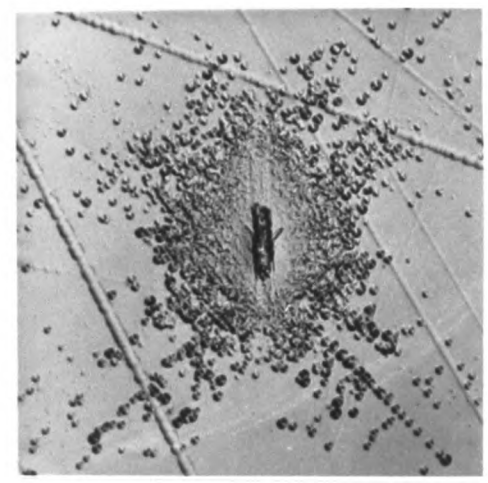
10.3.1 Rosettes

As the temperature was increased above room temperature and dislocation mobility increased, the rosette lines increased in length, but became less dense. (At 200°C the <110> indentations did not show any rosette lines). However due to indentation spacing on some samples it was not possible to define the relationship between the relative rosette length / diagonal length and temperature. (Sumino and Hasegawa (1968) found that the ratio of rosette length to indentation diagonal for Vickers indentations varied with temperature in a way that showed a good correspondence with the hardness variation. The ratio began to increase sharply at the same temperature at which the rapid decrease in hardness began). By 500°C no distinct rosette formation could be seen for the <100> orientations and only vestiges for the <110> orientation. (Sumino and Hasegawa reported that they could not see rosettes above 550°C). It appears therefore that the stress conditions favouring rosette formation become less dominant as the temperature increases.

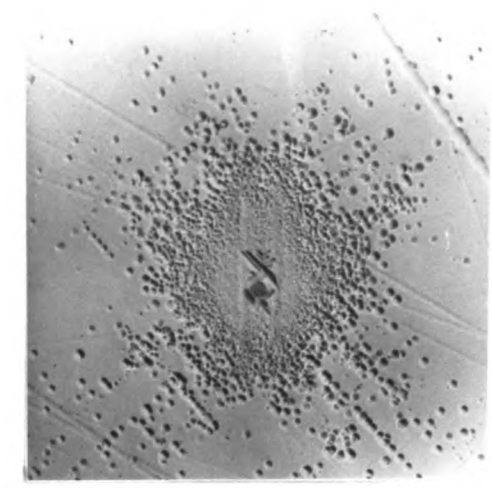
Figure 10.11 Series of etched arrays at the sample surface as it was stripped away, 600 second, <100> orientation on (001) Ge at 400°C; (a) Surface array, (b) 6μm depth, (c) 12μm, (d) 19μm, (e) 26μm, (f) 31μm, (g) 34μm (h) 48μm, (i) 64μm, (j) 75μm, (k) 93μm, (l) 100μm.



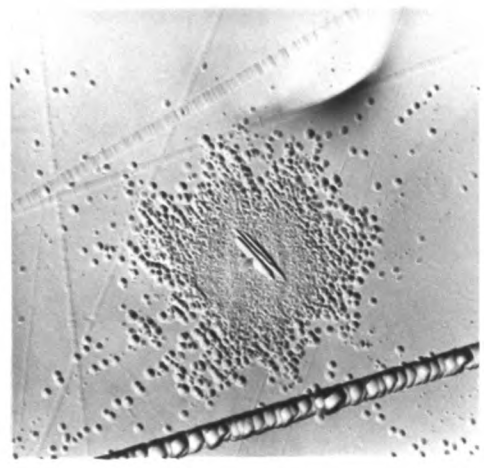
(a)



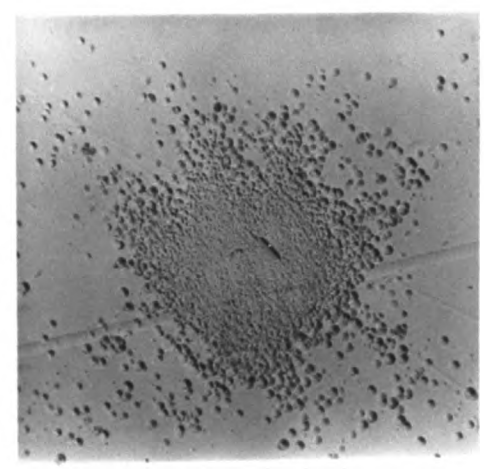
(b)



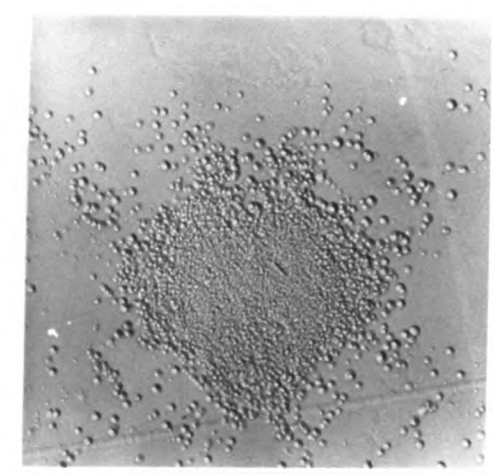
(c)



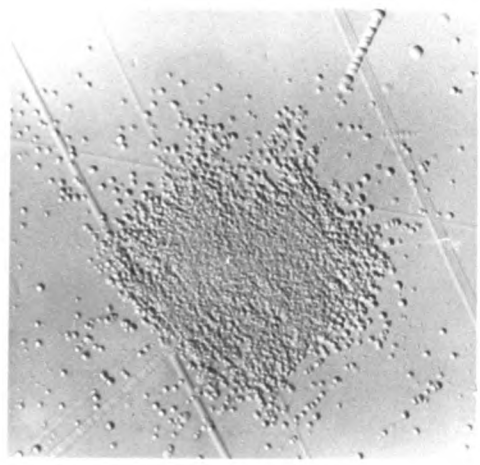
(d)



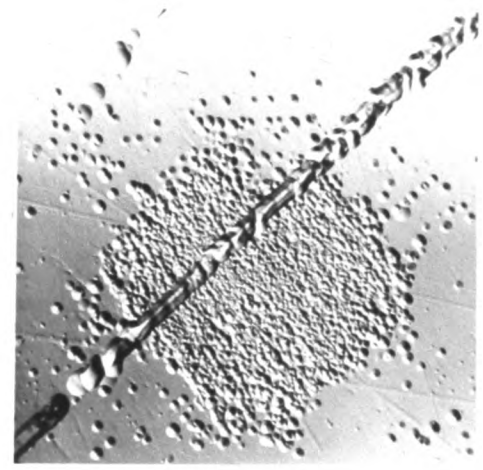
(e)



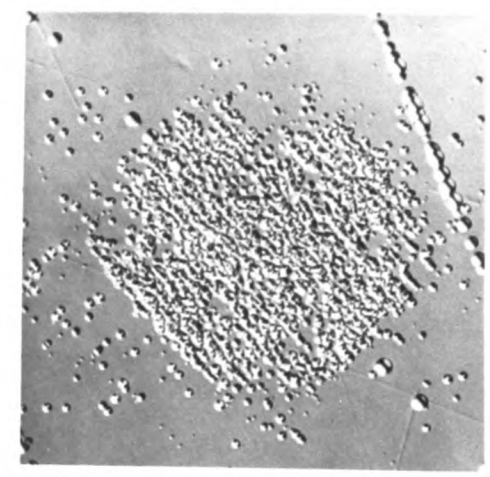
(f)



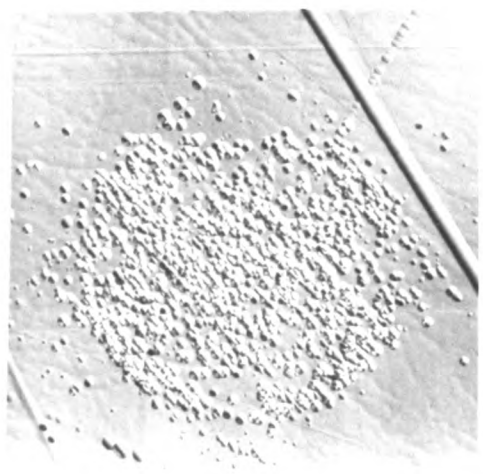
(g)



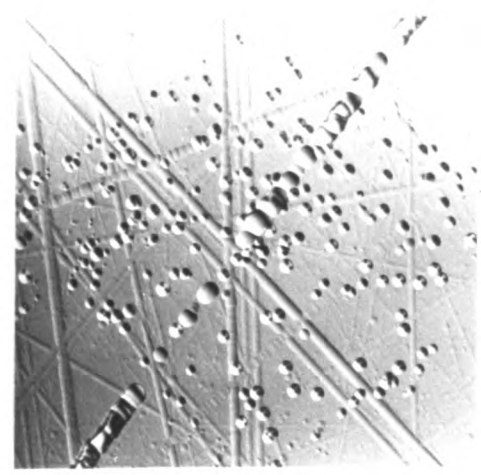
(h)



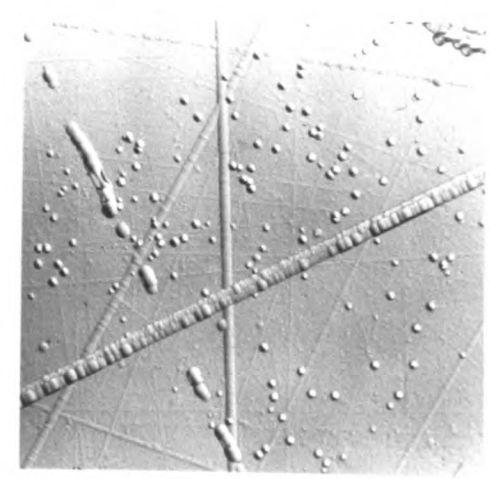
(i)



(j)



(k)



(l)

100 μm

10.3.2 Three Dimensional Dislocation Structure at Higher Temperatures

The 700°C samples etched very differently from lower temperature samples but after long etching did show dislocation arrays (see section 4.3.4). Figure 10.12 shows the surface arrays from <110> 700°C indentations. These are surprisingly different from the lower temperature patterns. The distinctive rosette arms have all but disappeared (see above), and the dense area of pits is no longer an oblong. Without subsurface information it is difficult to be sure of the dislocations mechanisms which give rise to this pattern. (It was not possible to get serial information on many specimens in the time available). The width at the waist of the pattern increases slightly with time, as does the length along the long axis of the indentation. However, most of the change with time occurs in the spread of the four "corners" expanding out, leading to the clear crescent each side of the indent. By contrast the <100> surface arrays (figure 10.13) are geometrically similar to the lower temperature arrays, although the dimensions of the dense area of pits relative to the long diagonal length is larger than at 400°C.

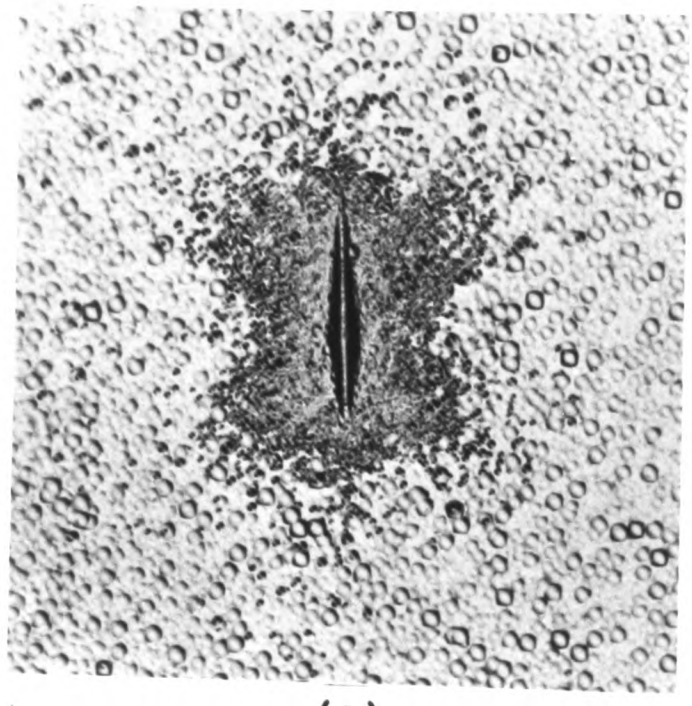
10.4 The micromechanisms of creep

The data presented above, and the creep results reported in the previous chapter, suggest the following sequence of events during an indentation test at temperatures around $0.5\ T_M$.

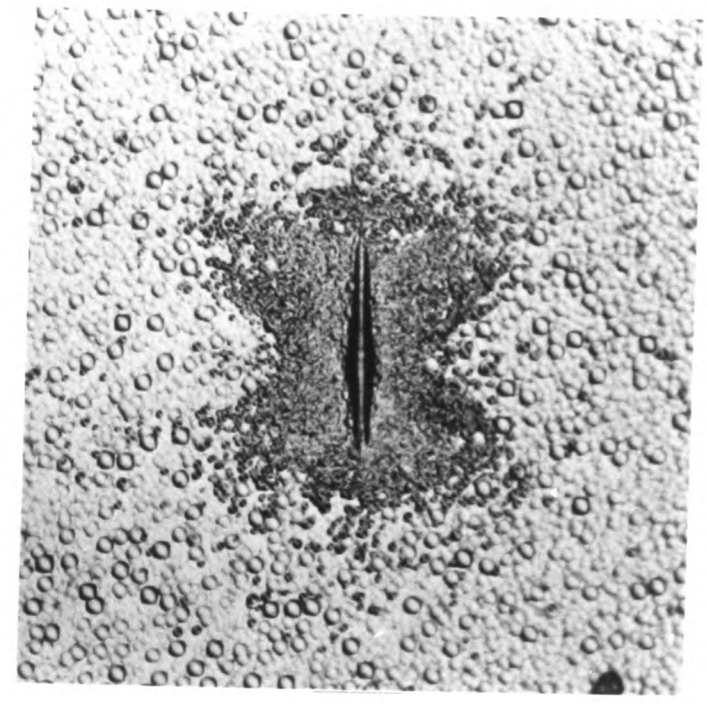
As the indenter first touches the specimen, the very high stresses from "point loading" of the tip generate dislocations on all the {111} [110] systems. Plastic deformation takes place by slip on these systems as dislocations are driven out away from the indentation centre. The initial strain rate (i.e. at "zero time") is very high, but the rate of indenter descent is soon retarded by the energy needed to produce the plastic and elastic deformation which accomodates the indenter impression. How much strain takes place within the first few moments of the indentation test will depend on the material's resistance to deformation, to echo Tabor's phrase (1986). This short time impression will have a characteristic stress field depending on the strain already produced and the applied load. Hence the spatial distribution, Burgers vector and density of dislocation activity on each slip system, is determined by the indenter morphology and orientation for given testing conditions. If the temperature / stress conditions are such that dislocation movement can occur, then this three dimensional dislocation arrangement will develop with time and creep will occur.

In the case of a indentations on the (001) surface of Ge my results suggest that rosettes arms are formed by dislocation loops on converging {111} planes, perhaps with the

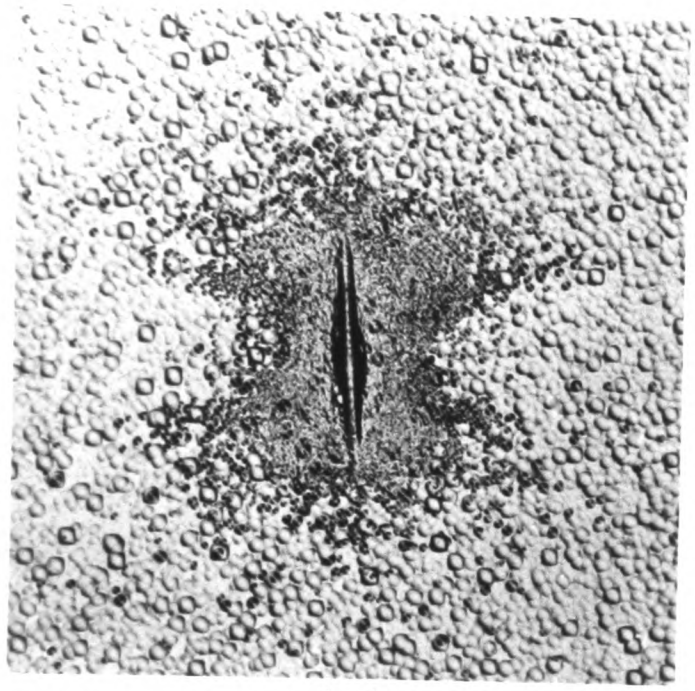
Figure 10.12 Surface dislocation arrays from 700°C <110> indentations: (a) 20 second, (b) 30 second, (c) 60 second, (d) 120 second, (e) 300 second, (f) 600 second.



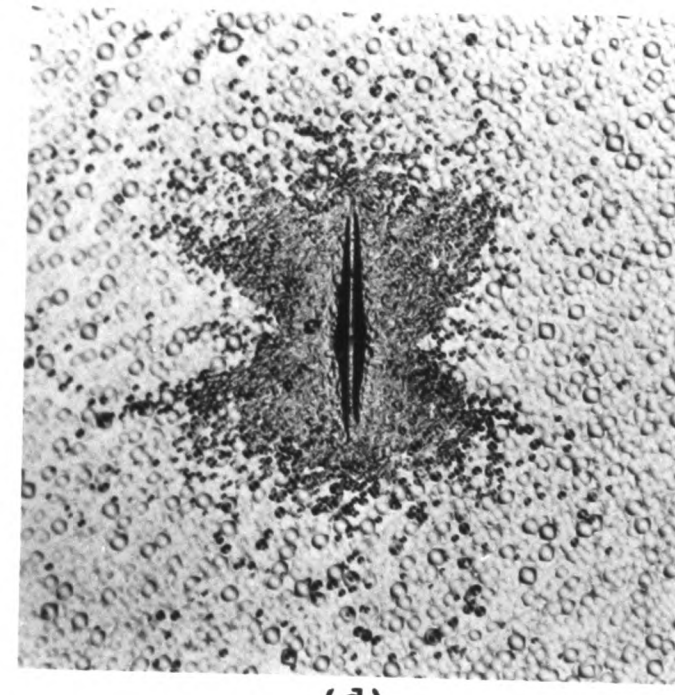
(a)



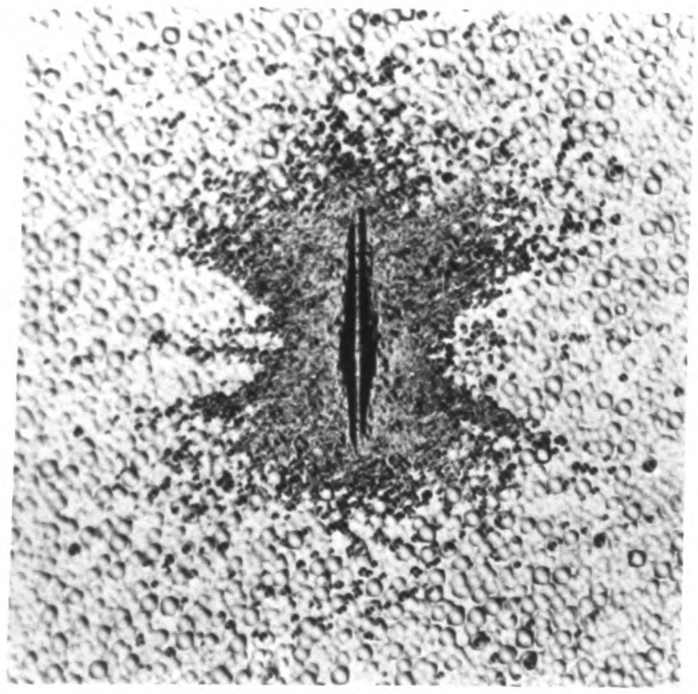
(b)



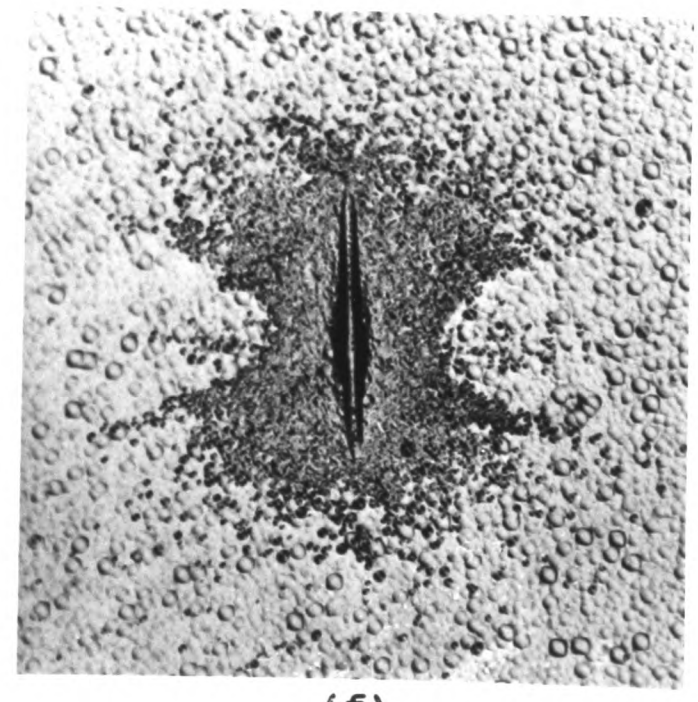
(c)



(d)



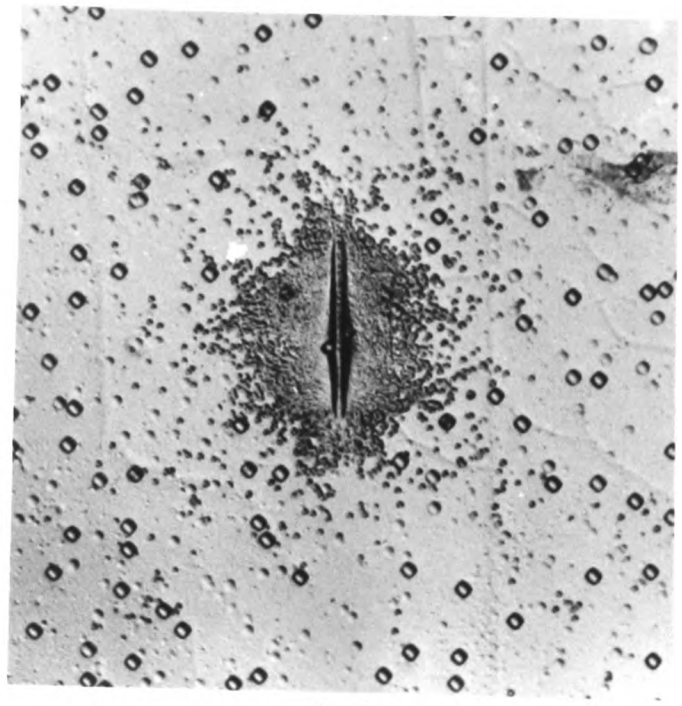
(e)



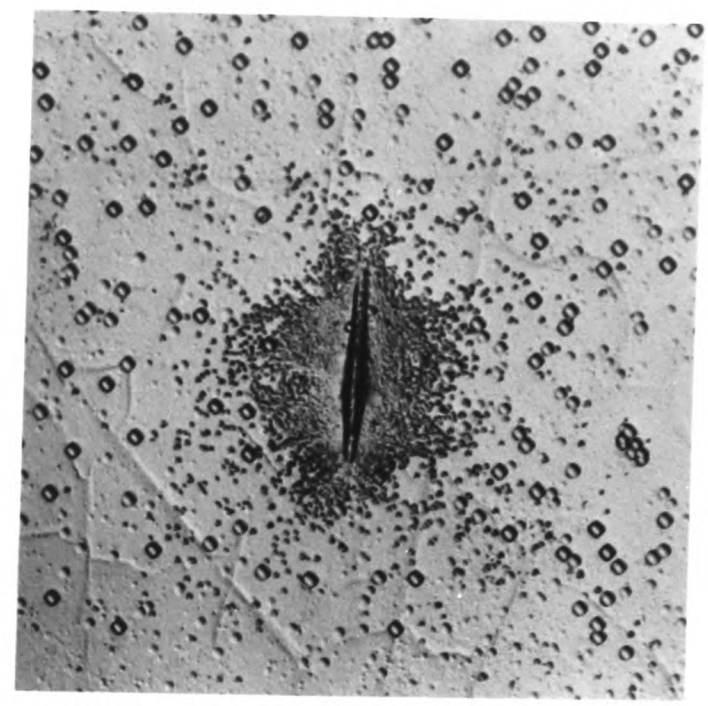
(f)

200μm

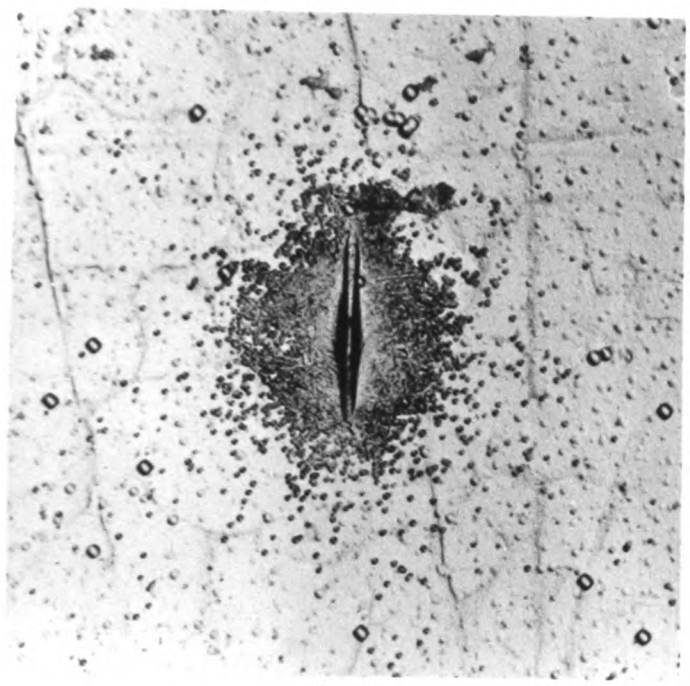
Figure 10.13 Surface dislocation arrays from 700°C <100> indentations on (001) Ge: (a) 20 second, (b) 30 second, (c) 60 second, (d) 120 second, (e) 300 second, (f) 600 second.



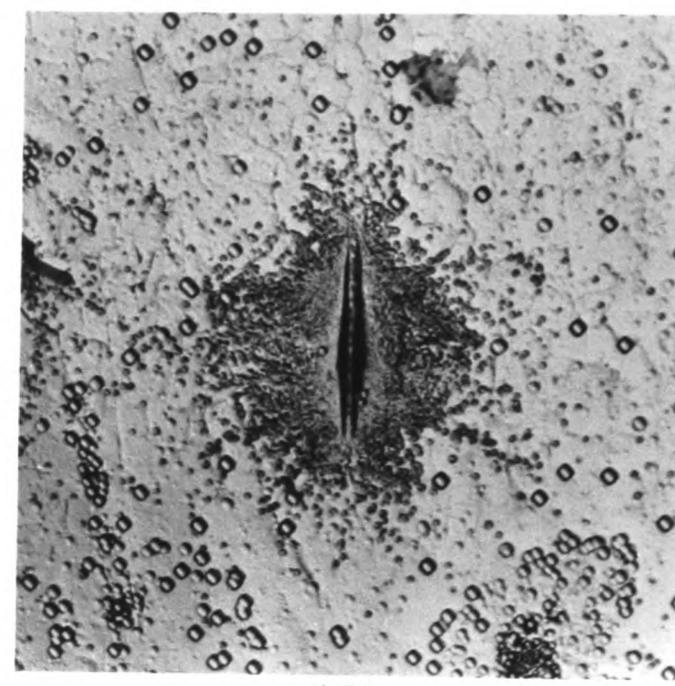
(a)



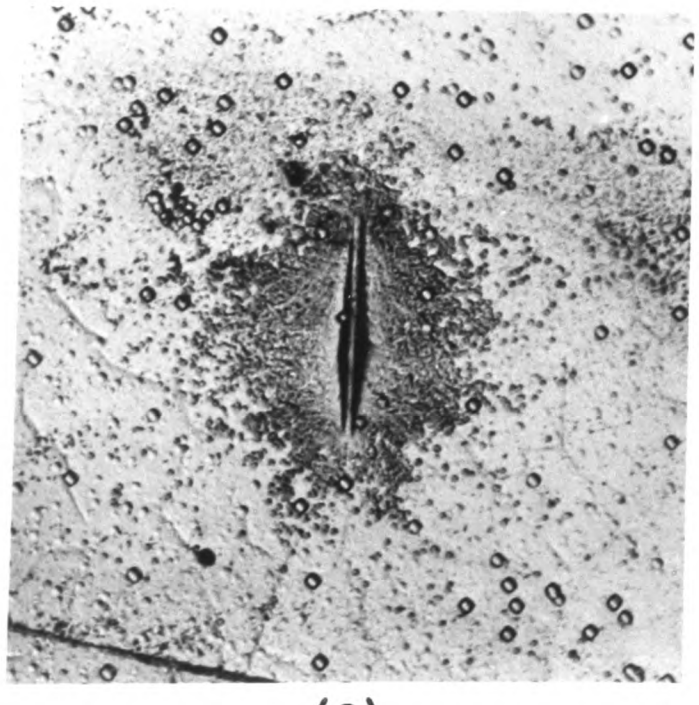
(b)



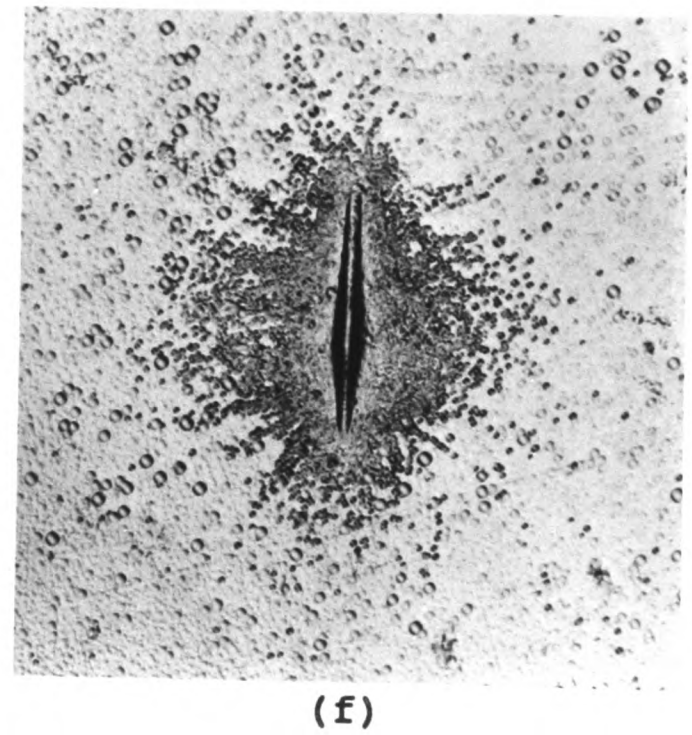
(c)



(d)



(e)



(f)

200μm

loops' long axis parallel to the surface, but the main activity is on {111} planes with loops' long axis inclined to the surface. Furthermore, planes which diverge away from the centre point of the indentation seem to be most prominent . Thus, with increased indentation time, slip takes place as existing loops are pushed further out by more dislocations generated in the high stress region surrounding the indenter. Also more slip planes (same orientation, different spatial position) are activated. The size of impression made therefore increases.

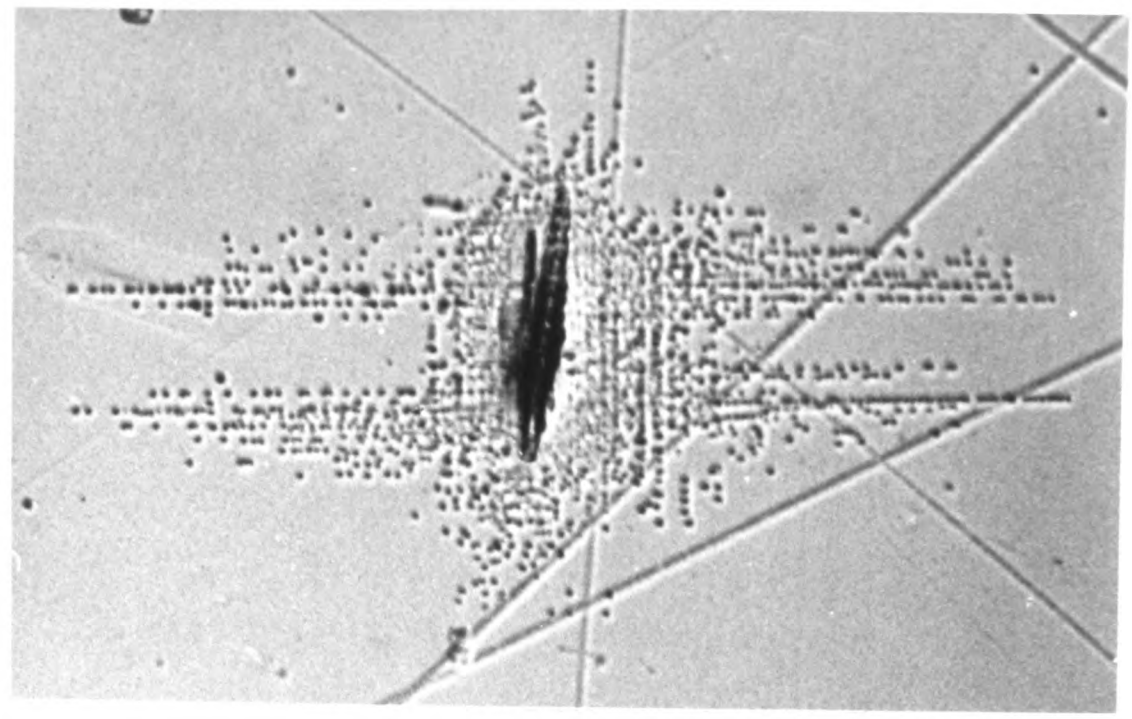
Figure 10.14(a) and (b) shows <110> indents of the same diagonal length, which were produced by the same load; but at different temperatures and with different dwell times. The longer time, 350°C, indentation shows greater dislocation activity both parallel and perpendicular to the long axis of the indenter. The long rosette arms are more widely spaced at the higher temperature. However, the width of the dense oblong area of dislocation pits around the indentation is strikingly similar; 70μm before any gaps appear, and about 90μm including the edge rows (±2 μm). The pair of <100> indents (figure 10.14 (c) and (d)) do not look so alike at first inspection, owing to the much heavier rosette type slip around the lower temperature indents, but the dense six-sided areas around the indents (as defined by the much more crowded, smaller etch pits for the 350°C indent) are of similar dimensions, about 65μm wide and 96μm length (long the indent long diagonal). These results imply that the amount of slip on planes with slip directions into the crystal is closely linked to the amount of strain (i.e. indentation size) and less influenced by the dislocation velocity and/or time of deformation. The rosette slip on the other hand is much more dependent on the dislocation velocity and dwell time.

It is difficult to identify what happens directly beneath the indenter tip because of the large amount of deformation. The etch troughs noted above suggest some particular deformation phenomena takes place in this very high stress region. It might be amorphisation (see section 8.4.6), but seems more likely to be microtwins, particularly in view of the crystallographic orientation of the etch troughs. (Microtwins have been identified under indentations in GaAs - Qin and Roberts 1989, and in sapphire - Hockey 1971).

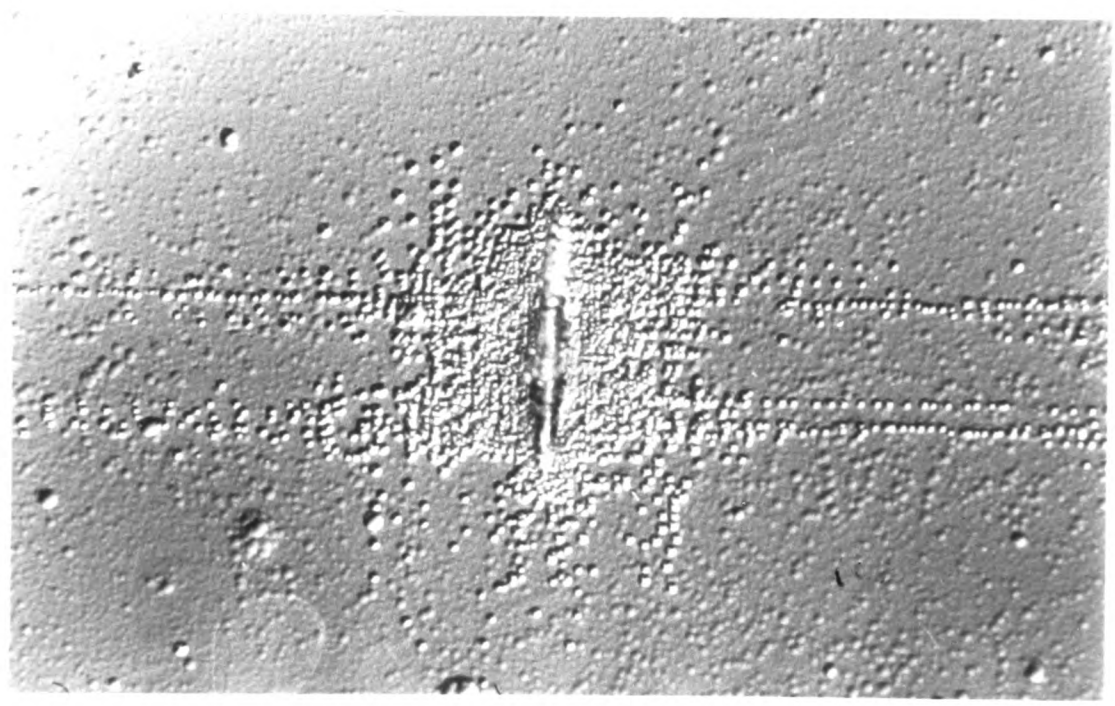
10.4.1 Slip planes

In order to analyse the creep at different indenter orientations it is necessary to consider on which planes most dislocation movement takes place. It has already been observed that the deeper sections of longer time <110> indentations showed less pits from loops moving perpendicular to the long axis of the indentation (see section 8.1.3). It might be deduced from this that the stress pushing these loops is less than for the loops on the

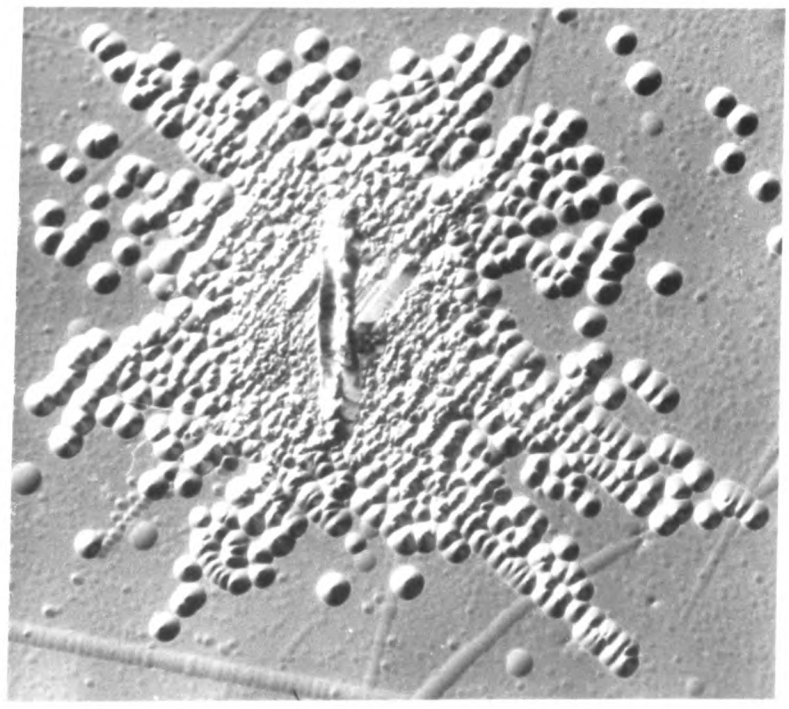
Figure 10.14 The etched dislocation patterns around two sets of same strain indentations made at differing temperatures and dwell times: (a) 600 sec <110> indent at 350°C, original diagonal 80.6μm, (b) 30 sec <110> indent at 400°C, original diagonal 80.4μm, (c) 600 sec <100> indent at 350°C, original diagonal 66.5μm, (d) 20 sec <100> indent at 400°C, original diagonal 67.7μm.



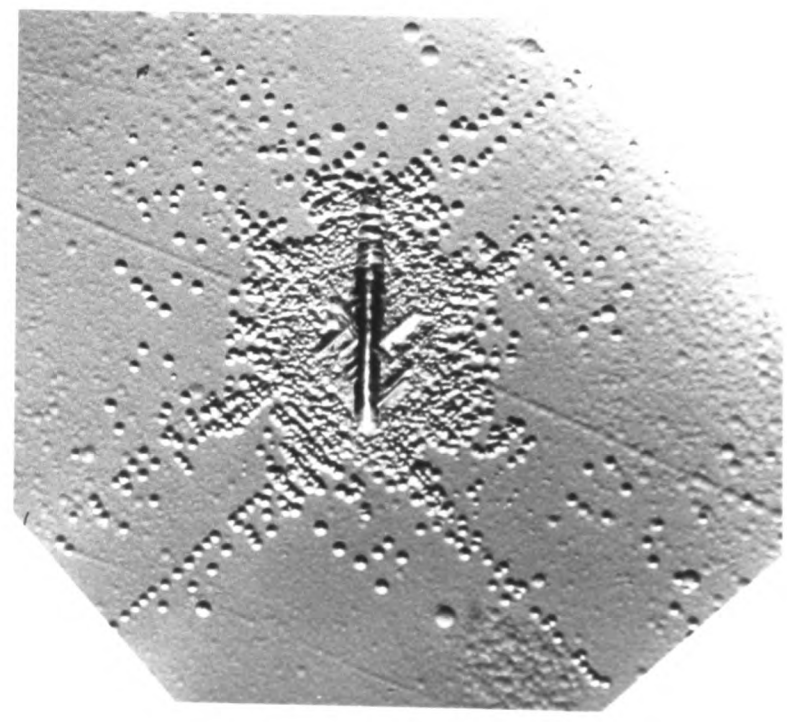
(a)



(b)



(c)



(d)

100 μm

other set of diverging planes since this would give the dislocations a lower velocity. The effect would be more pronounced at the edges of dislocation structure (i.e. at the tips of the long diagonal and the bottom of the more deeply penetrating loops), where, presumably, the total stress on each dislocation is lowest, since the dislocation velocity at lower stresses depends more strongly on stress than in the high stress regime (Patel and Freeland 1971). As creep takes place the same load is supported by a larger area of contact. Therefore the point stresses from the indenter stress field directly beneath the indenter presumably decrease, but the stress field will be further complicated by the increased number of dislocations. The sections produced by removing sample surface do indeed support the conclusion that the loops generated early on during the indentation are driven down deepest for both orientations. (The dense area of dislocation activity gradually thins out and loses the outlining dislocation rows, see surface section figures). It also seems possible that a stress envelope exists, at least for the <110> orientation. This stress envelope would be controlled by the stress field from the indenter at that particular point in space, plus the back stress from the dislocation arrays of that length.

At any one time the dislocation arrangement is a result of the strain already generated and the stress state which is operating. Presumably the dislocations arrays reach equilibrium positions at least during the "annealing" once the load is removed, if not relatively instantaneously. Hence the characteristic dislocation array length and extent seen in the etched sections. However whilst under load, loops will be generated in the higher stress regions. This in turn changes the stress experienced by the dislocations within the arrays, and forces them out along the slip planes so that the equilibrium arrays seen in etched sections of longer time indentations are longer. Such behaviour fits with the conclusions of Patel and Chaudhuri (1961)a which were outlined in section 8.2.1, namely a low dislocation generation stress, and yield behaviour controlled by the number and velocity of dislocations generated early in the deformation process.

10.4.2 Loop configuration and dislocation locks

The various loop configurations which may be present have been discussed by Roberts et al (1986). Converging {111} planes with traces in the surface both parallel and perpendicular to the indenter axis would form both Lomer-Cottrell and Hirth locks. In contrast, figure 10.15 (after Roberts et al 1986) shows loops on diverging planes, from the edge of a <110> orientated indenter for example. While interactions would still occur beween dislocations with the two possible b AE and DE forming dislocations with b AD, there are no dislocation reactions directly impeding the penetration of dislocations into the crystal. It would therefore be expected that slip on these planes would workharden less (Roberts et al 1986).

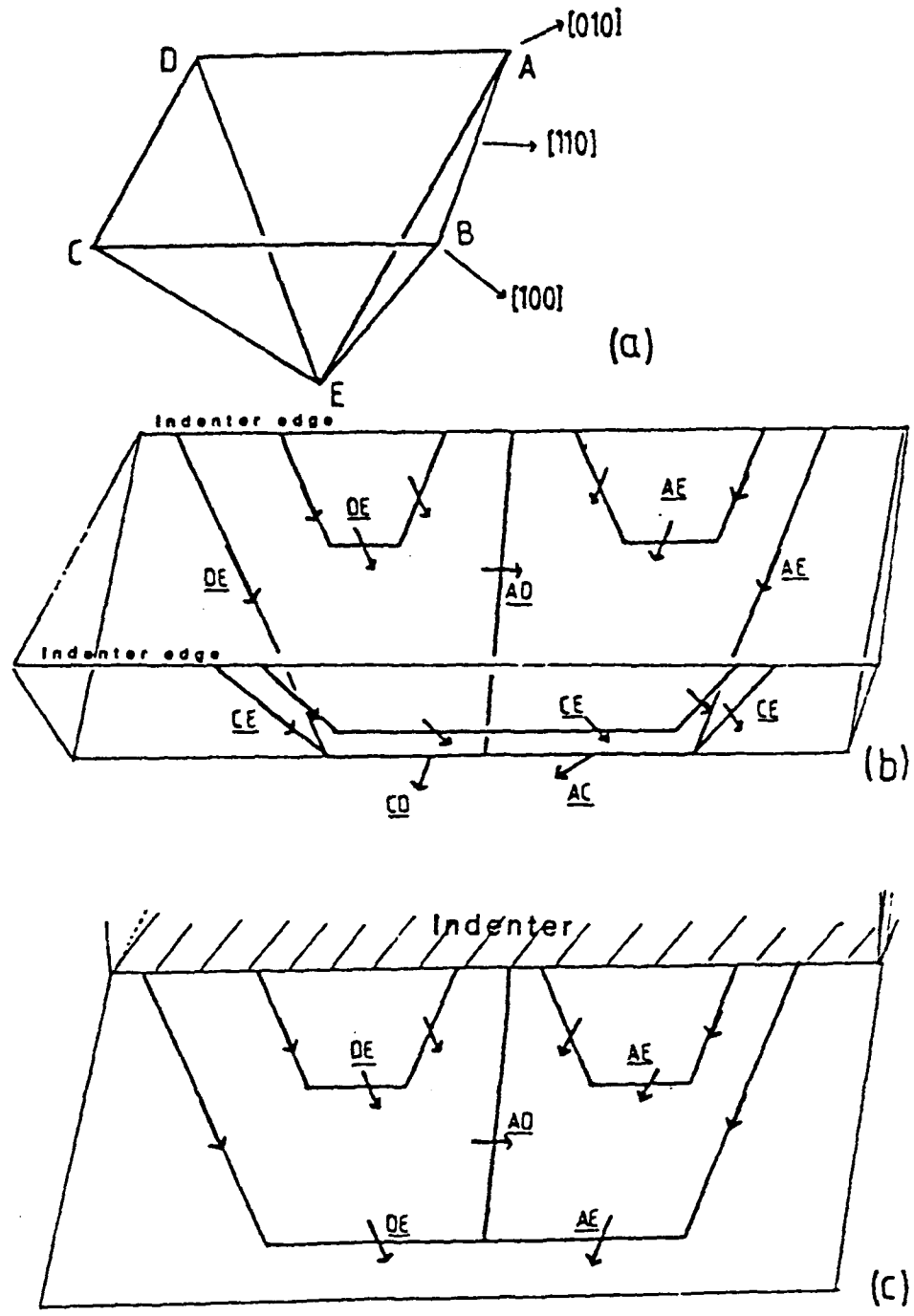


Figure 10.15 Dislocation interactions around an indenter along [110]: (a) orientation of slip planes, (b) possible reactions of dislocations on converging slip systems beneath the indenter, and (c) possible reactions of dislocations on diverging slip systems outside the indenter (Roberts, Warren and Hirsch 1986).

10.4.3 Difference in creep rate and the effect of temperature

Figure 9.1 showed the difference in creep rate between the two orientations at moderate temperatures. This can be explained by the dislocation arrangements under the indenter. The <110> orientation produces loops primarily on a set of diverging {111} planes, which intersect the sample surface parallel to the long axis of the indenter. Creep takes place by pushing loops down these planes, and increasing the number of planes on which slip is taking place. Although loops are produced on the other set of diverging planes, this deformation extends less deeply into the crystal. The high stress region directly beneath the indenter only produces microtwins parallel to the first direction mentioned, indicating much less interaction than is the case for the <100> orientation, which produces complicated interacting patterns of these features. Mutual interference produces a high strain hardening coefficient at low and moderate temperatures (Patel and Alexander 1956), so it is likely that work hardening restricts the ease of dislocation motion out of the highly deformed region. The dislocation etch patterns figures suggest a symmetrical "pyramid" of planes diverging towards a square base under the <100> indentations. (Also stress fields from dislocation arrays on systems other their own may affect the stress pushing arrays out). However at higher temperatures more thermally activated climb can take place, the strain hardening coefficient decreases, and the possible movement of dislocations out along the activated slip planes from the interacting systems beneath the <100> orientation, also becomes easier. The creep rate of the two Knoop orientations become equal, perhaps because of the change in the activated slip planes of the <110> orientation. At room temperature dislocations are produced but do not have the thermal energy to move out along the slip planes.

11. HARDNESS INTERPRETATION AND MODELS

Having obtained the "hardness" of a material under certain conditions, one is faced with the question of the meaning of that measurement in terms of physical constants, and the relationship of that result to other mechanical properties such as low and high temperature yield behaviour, tensile creep etc.. This chapter describes the main hardness models, and the way in which hardness is related to other bulk properties, before reviewing the theoretical and empirical models of the temperature and time dependence of the hardness "number", and comparing them with the results which have been outlined in previous chapters. An explanation for the observed creep and anisotropy behaviour of MgO and Ge is then presented.

The technological drive to get some realistic interpretation of indentation creep should be considerable, since it is necessary to evaluate the dimensional stability of materials during relatively high temperature applications, where creep will be appreciable. In this case the short time hardness response is probably a less applicable parameter than the hardness response under prolonged loading. Indentation creep has been investigated at higher temperatures (over $0.5T_M$), often by mutual indentation, but there are less extensive data at lower temperatures. Little work has been done on the micromechanisms involved for particular materials as indentation creep progresses.

The question as to whether or not five independent shear modes are necessary to form an arbitrary indentation is unresolved in literature. For single crystals, it may be possible to form an indentation by slip alone, with less than 5 independent slip systems, if the indent geometry is specifically aligned to the slip crystallography. For polycrystalline materials and most real single crystal situations, this would be impossible (Sargent and Page 1985). However, at loads lower than that for the onset of indentation fracture, it seems possible to make crack-free indentations in all materials. How the constraint of five independent deformation modes is satisfied in these cases is unclear, though elastic deformation, unusual deformation modes, line grain boundary movement etc. might be conceived as playing some role.

11.1 Models of Hardness

There are a number of models which seek to predict hardness values and/or relate them to the yield stress or other properties of the material under test. Yield stresses are usually measured in a uniaxial stress test that does not constrain the flow pattern. Such a test does not model the situation under an indenter, where a complex and highly

constrained flow pattern exists (Gilman 1973). However, for metals, it was observed that, when using relatively blunt indenters (such as Vickers and Knoop), the hardness was approximately equal to 3Y where Y is the uniaxial yield stress (Tabor 1970). Prandtl (1920, through Shaw 1973) first proposed a model to account for this relation, assuming rigid-plastic behaviour. (That is, the material is perfectly rigid up to a yield stress, but then deforms without work-hardening). He likened the blunt indenters to a flat punch, and calculated the mean stress on the punch for the onset of plastic flow beneath. Hill (1950) generalised this approach using slip-line field theory. The predicted relation for hardness is then H = ~2.6Y, which is raised nearer to 3 if friction is taken into account. However the basic assumptions of plastic plane strain and no elastic deformation remain. Strongly work-hardened metals approach this rigid-plastic ideal, since the flow stress is almost a constant, and Tabor(1970) found that they did indeed give the predicted 3Y hardness value. The relation can also be used for metals which strain-harden (and consequently have no definite flow stress) by taking the flow stress of the material measured at a strain representative of that caused by the indenter (Johnson 1970). The value of the representative strain is determined empirically and varies with the geometry of the indenter, e.g. 0.08 for a Vickers indenter (Atkins and Tabor 196.6). However, such empirical approaches do not help the fundamental understanding of the problem since the strain varies from a very high value to approximately zero in the defined volume.

In spite of the apparent agreement between measured values of hardness and the 3Y predicted by the slip line field theory, various investigations of flow patterns (Mulhearn 1959, Hirst and Howe 1969 and Woodward 1974) have found that these contradicted those predicted by slip-line theory. The extent of the plastic region was far deeper, and the pile-up of material around the indentation (from upward flow at the indenter/specimen interface), less than predicted. The larger the wedge angle, the greater the discrepancy between predictions and observations (Samuels 1986). Thus it may be better to regard the 3Y relation as a reasonable empirical fit rather than deriving it fromthe slip-line field analyses. A study by Westbrook (1958, through Tabor (1970), Gerk (1977) and others), found that whilst metals did have a hardness of 3Y, rocksalt structure materials could show a hardness of 35Y.

A second type of model is that based on elastic-plastic material behaviour. Contrary to the rigid-plastic models, some elastic deformation will take place for all real materials. The magnitude of the elastic strains produced will depend on the ratio of the elastic modulus to the yield stress. Elastic-plastic strains will become more important relative to plastic strains as the value of the modulus decreases in relation to the yield stress. Thus the rigid hinterland of the rigid-plastic model is replaced by an elastic hinterland (figure 11.1).

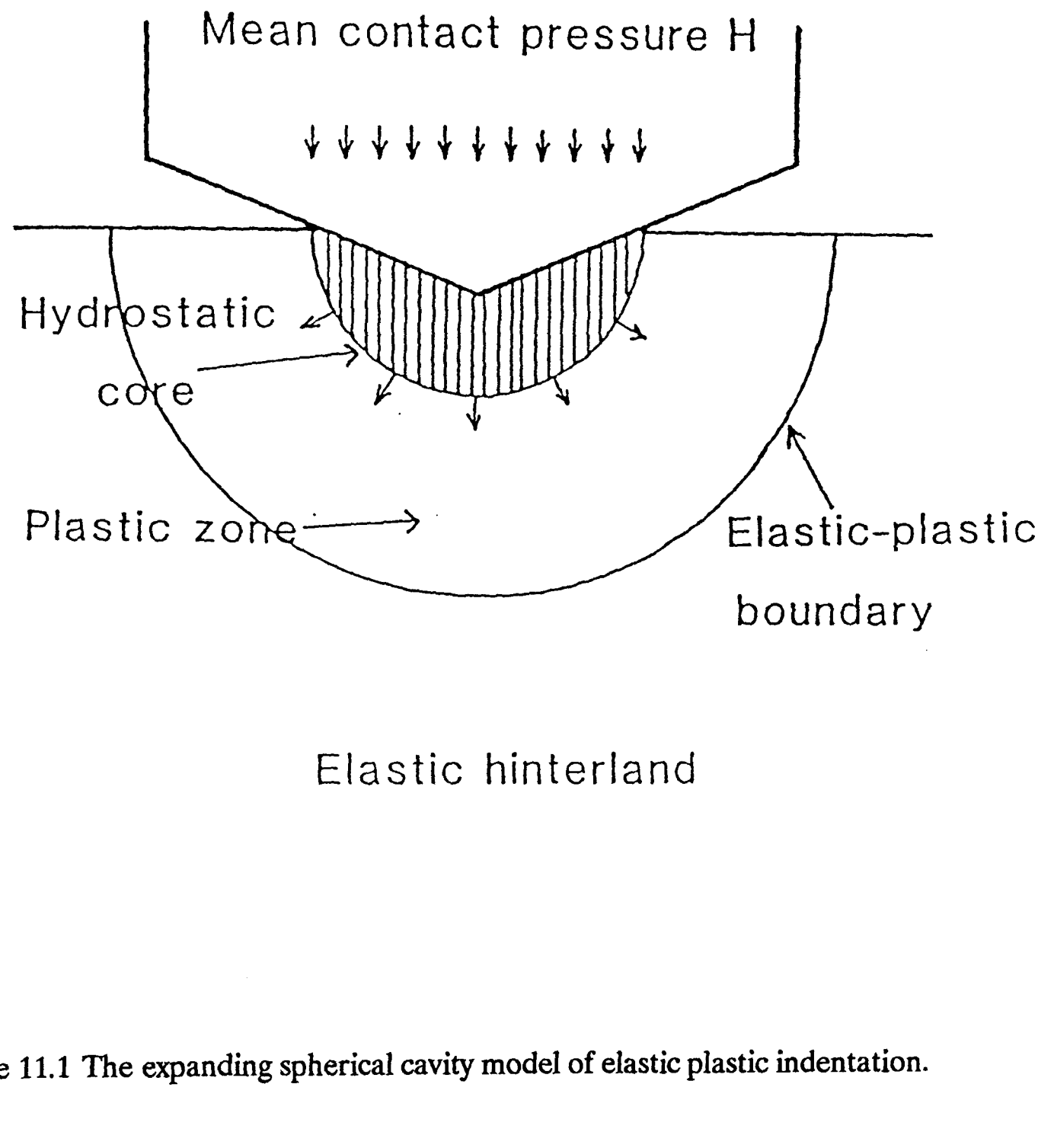


Figure 11.1 The expanding spherical cavity model of elastic plastic indentation.

The elastic-plastic models are based on an idea originally suggested by Bishop, Hill and Mott (1945), using the theoretical analysis of a cylindrical or spherical cavity expanding by an internal pressure (e.g. Hill 1950). Johnson (1970) refined the model to take account of indenter angle. He considered the indenter to be encased in a hemispherical core, as shown in figure 11.1. The core around the indenter replaced the cavity of Hill's model. The volume of the impression is accommodated by a net radial flow of the material out from the hemispherical plastic zone which is surrounded by a confining, elastically deformed, matrix. This supported the experimental observations of Mulhearn and other investigators. Further refinements have been proposed, e.g. Studman, Moore and Jones (1977) substituted values of stress which satisfied Von Mises criterion and discussed the problem of a representative yield stress. All these "radial flow" models predict the absence of pile-up around the indentation. No pile-up is observed in the harder ceramics and glasses (Tabor 1970) so these materials might be said to support the elastic-plastic analyses. Also, low magnification Nomarski often shows elastic rebound of the hinterland. As stated by Tabor (1970), it seems reasonable to consider such analyses when the elastic strains become comparable to the plastic strains, i.e. E/Y less than ~100.

For high moduli materials at lower temperatures, it may be possible to model hardness by considering only the elastic contact stress fields (although some permanent deformation obviously does take place). Solutions for the purely elastic contact of variously shaped bodies have been in existence for over one hundred years. One of the best known is that of Hertz (1895) for the stresses and strains in two spherical bodies pressed together. This solution has been used extensively to model indentation fracture beneath blunt indenters (Lawn and Wilshaw 1975). However, the Hertzian solution is analytically complex, and the Boussinesq model (1885) of a point contact pressing onto a surface is more manageable (although less relevant close to the indenter). Yoffe (1982) extended this solution to model indentation processes in brittle materials, combining it in varying proportions with the "blister" elastic stress field (Love 1929) to explain the crack patterns observed in glasses and ceramics. The modified Boussinesq stress field has also been used to model indentation fracture beneath sharp indenters (Chiang, Marshall and Evans 1982).

11.1.1 Resolved Shear Stress Models

Both the rigid-plastic and elastic-plastic models assume plastic isotropy, taking no account of the materials crystallinity and the availability of slip systems to provide flow in the directions demanded by the model. Thus they are not really applicable to the single crystal experiments described in this thesis, and indeed the indentation anisotropy exhibited by many harder materials. Many ceramics are highly anisotropic in their plastic behaviour, the limited slip around the indentation strongly influencing the nucleation and growth of

fracture. Daniels and Dunn (1949) were the first to analyse the process of indentation with a view to understanding the nature of anisotropy. They developed an explanation based upon the "effective resolved shear stress" from tensile stresses whose axes were assumed to lie parallel to the steepest slope on the indenter. An alternative model (Feng and Elbaum 1958) also used effective resolved shear stresses, but assumed the deformation to be controlled by compressive stresses with axes normal to the indenter facets. Those orientations of the indenter having the lowest effective resolve shear stress should be the hardest. Garfinkle and Garlick (1968) showed that for LiF and a number of both face-centered and body-centered cubic crystals, the hardness was dependent only on the crystallographic orientation of the long axis and not on the plane of indentation. However, the plane of indentation made a noticeable contribution to the hardness anisotropy in the case of an hexagonally close-packed crystal of titanium. They concluded that resolved shear stresses, whether based on tensile or compressive forces, did not satisfactorily explain the observed anisotropy in the hardness of crystals.

Nevertheless, Brookes, O'Neill and Redfern (1971) have produced a wide-ranging model for hardness anisotropy based on resolved shear stress analysis using tensile stresses. The resolved shear stresses in a single crystal subjected to unidirectional tension are given by the Schmid and Boas equation (1950):-

$$\tau = (F/A)\ \cos\lambda \cos\phi$$

where τ is the resolved shear stress, F the applied force, A the cross-sectional area of the specimen, λ the angle between the stress axis and slip direction and ϕ the angle between the stress axis and the normal to the slip plane. Daniels and Dunn added a rotational "constraint" factor, because the available slip planes are not free to rotate (as they would under unidirectional stress), but are influenced by the indenter orientation and the non-deforming hinterland of the material, and the adjacent deformation zone. Thus they developed an effective resolved shear stress, τ_e, of:-

$$\tau_e = (F/A) \cos\lambda \cos\phi\ \cos\psi$$

where ψ is the angle between the face of an adjacent facet and the axis of rotation for a given slip system. Brookes, O'Neill and Redfern further modified this to consider γ, the angle between the slip direction in a given plane and the adjacent facet giving:-

$$\tau_e = 1/2\ (F/A) \cos\lambda \cos\phi\ (\cos\psi + \sin\gamma)$$

From consideration of their results and those of other researchers, they concluded that hardness anisotropy is essentially determined by the crystal structure and the primary

slip systems, i.e. the variation of τ_e on the slip systems. However the model is simplified in that it ignores work-hardening effects, twinning or fracture, and assumes that the contribution of alternative and/or secondary slip is negligible. It correctly predicts the sense of hardness anisotropy in the many systems, but does not explain the difference in magnitude of anisotropy. For example, for MgO at room temperature, the <100> orientation is twice as hard as the <110> orientation, but in LiF the difference in hardness in only 20%. A direct correlation between the absolute hardness value and the above equation is not yet possible because a representative value for A cannot be defined (and the effect of work-hardening on hardness has not yet been established) (Brookes, Morris and Moxley 1971).

There is some discussion concerning the appropriate stress field that should be used to produce the resolved shear stresses. Hagan (1980) investigated surface deformation under Vickers indentation in soda-lime glass. The deformed zone was made up of a series of intersecting flow lines, which were found to be genuine shear displacements. Plastic strain concentrated on these lines while material between them is strained only elastically (Ernsberger 1979 through Hagan 1980). Roberts (1987) noted that these followed lines of maximum shear in the elastic stress field of a long flat punch (formulated by Nadai 1931). Roberts and Warren (1986) looked at the flow structures occurring under Knoop indentations of brittle single crystals, using the Nadai field to predict flow patterns around the indentations. For diamond-cubic materials, indented on {001} faces, this model predicted different flow patterns and stress variations from those of Brookes et al (1971), with the resolved shear stress on the most highly stressed systems varying little with indenter angle. Indentation of gallium arsenide appeared to confirm the Roberts and Warren model. In other cubic structures, the model's predictions of hardness anisotropy were similar to that of the Brookes et al model.

Models which try to take account of the dwell time of indentation are reviewed in the indentation creep section (11.4).

11.2 Relating Hardness to Physical Properties

The use of models such as those described above is often to relate the hardness of a material to other bulk properties, e.g. yield stress, since the processes involved in hardness deformation are the same as those which control other deformation. A number of examples are given in the 1973 ASM volume, "The Science of Hardness Testing and its Research applications", e.g. Beeuwks, Chait and Liu - flow curves of metals, Böklen - ductility from a Brinel test, Rice - machining effects on ceramics. Rice's paper relates hardness to tensile strengths, but finds even broader correlation between hardness and compressive strengths

for ceramics (or at least the upper limit for compressive strength). Gilman (1975) has related impact yield stress to hardness indentation values. Hardness anisotropy can be used to determine the operative slip systems (see section 11.5). The Vickers hardness value has, of course, long been used as a comparative tool in quality control situations.

Before such relations can be more than empirical, better understanding of the indentation processes are required. The stress pattern in the elastic plastic zone under the applied load of the indenter is quite different for the cases of a single crystal and poly-crystal sample (Raj and Ashby 1971). Even if the indentation is successfully modelled in single crystals, the challenge remains to extend this to the behaviour of polycrystalline ceramics since the deformation characteristic are more complex.

11.3 The Variation of Hardness with Temperature

The empirical effects of temperature and loading time on hardness measurements have been studied by previous workers, and some of that work was summarised by Atkins, Silverio and Tabor (1966). Variation in temperature will alter the indentation behaviour of materials. Generally the hardness decreases with increasing temperature. Many of the older models were concerned with macro-mechanisms of hardness variation (e.g.. Atkins and Tabor 1966). However, more recent analyses have been concerned with micro-mechanisms of dislocation movement etc (e.g.. Sawyer, Sargent and Page 1980) and results of this thesis obviously fall into this category. Raising the temperature alters the work-hardening behaviour of the material, especially the ease of cross-slip of screw dislocations, increases the rate of dislocation glide and climb, and may well enable secondary slip systems to be activated in single crystals (Warren 1987). As a result of these changes the yield (or flow) stress will change as the temperature increases.

Looking at metals, Westbrook (1957, through Atkins and Tabor 1966) found that there were often two regimes:

(a) Below $0.5T_M$, the hardness falls by a factor of 2 to 3 as the temperature rises to about $0.5T_M$.

(b) Above $0.5T_M$ there is usually a rapid drop in hardness.

Trefilov and Mil'man (1963) have published results showing the variation of Vickers microhardness with temperature. They found a rapid drop in hardness above 200°C ($0.39T_M$). As discussed in chapter 9, the results published in this thesis also show a rapid decrease starting at this temperature.

At low temperatures the high melting point compounds such as borides, nitrides, carbides and oxides also have limited ductility. The results for Knoop indentation on MgO which were presented in chapter 6 only covered the range up to 0.52 T_M. Within this range hardness decreased with increasing temperature, but the rate of decrease slowed in the "no indentation creep" temperature range. Only one result was obtained in the temperature region where indentation creep was again observed, so it is not really possible to comment on the likely trends in the higher temperature regime, although shorter time hardness did not give any indication of a sudden decrease in hardness.

Kohlstedt (1973) found that below $0.5T_M$, the decrease in hardness with increasing temperature for transition metal carbides, was nearly ten times more rapid than for metals and semiconductors. The hardness data, both below and above the transition temperature, fitted and Arrhenius plot and can be expressed in the form:-

$$H = K \exp. (Q/RT)$$

where K is a constant, Q is the activation energy governing plastic flow (for this particular type of deformation), T is the absolute temperature and R is the gas constant (Kohlsted 1973). The change of slope of ln H versus 1/T plots near the brittle to ductile transition suggests a corresponding change in dislocation dynamics. Naylor and Page (1979), found that the hardness of polycrystalline SiC engineering ceramics showed a virtually linear decrease in the temperature range 200 - 800°C. With sintered porous specimens, the fall in hardness is augmented by collapse of the structure by local compaction of the material around the indentation (Atkins and Tabor 1966). At higher temperatures, the behaviour of these sintered specimens became dominated by the intrinsic properties of the solid, and the hardness response closely resembled those of the fully compacted crystalline material.

Arrhenius plots of results from experiments using the Oxford machine are shown in figures 11.2 and 11.3. The higher temperature portion of each curve fits quite well to a straight line, as suggested by the equation above. (The line on the MgO data does not include the hardness values from the temperature region in which no indentation creep occurs). The "activation energies" from each straight line drawn on the Arrhenius plots are shown in table 11.1 which also lists values from other authors. The energies calculated from the Oxford data are considerably lower than the other values quoted in literature. (Note that the lower temperature range Atkins and Tabor value is the only one from data in the same temperature range as that described in this thesis). It is not clear exactly what the activation values means in a physical sense, since the stress conditions and scale of dislocation arrays are quite different for the various indentations. Perhaps the exponent is better termed a thermal softening coefficient (Brookes 1971). It is interesting to note that

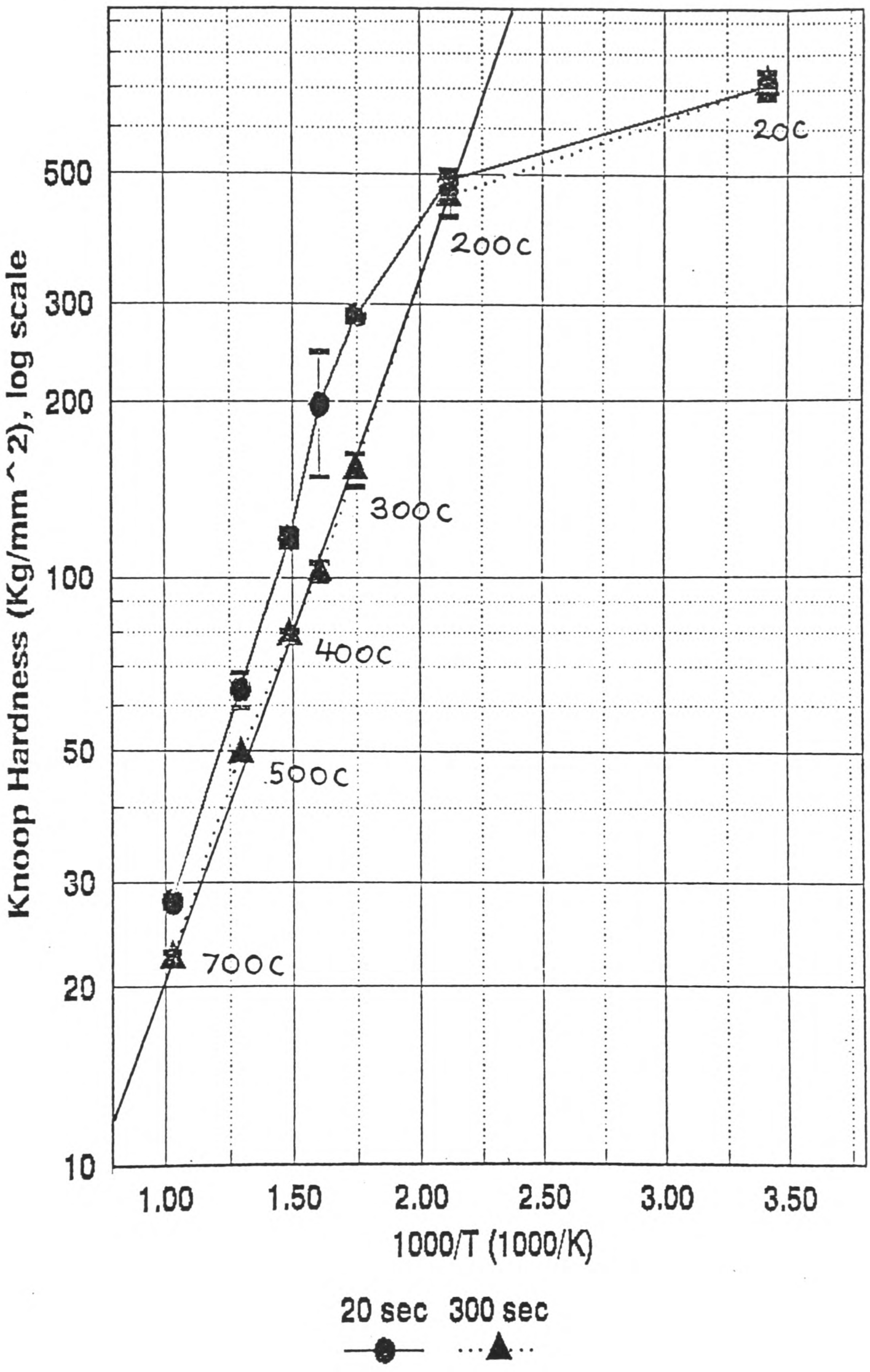


Figure 11.2(a) Arrhenius plot, log (Knoop hardness) against 1000/T, for <110> indentations on (001) Ge.

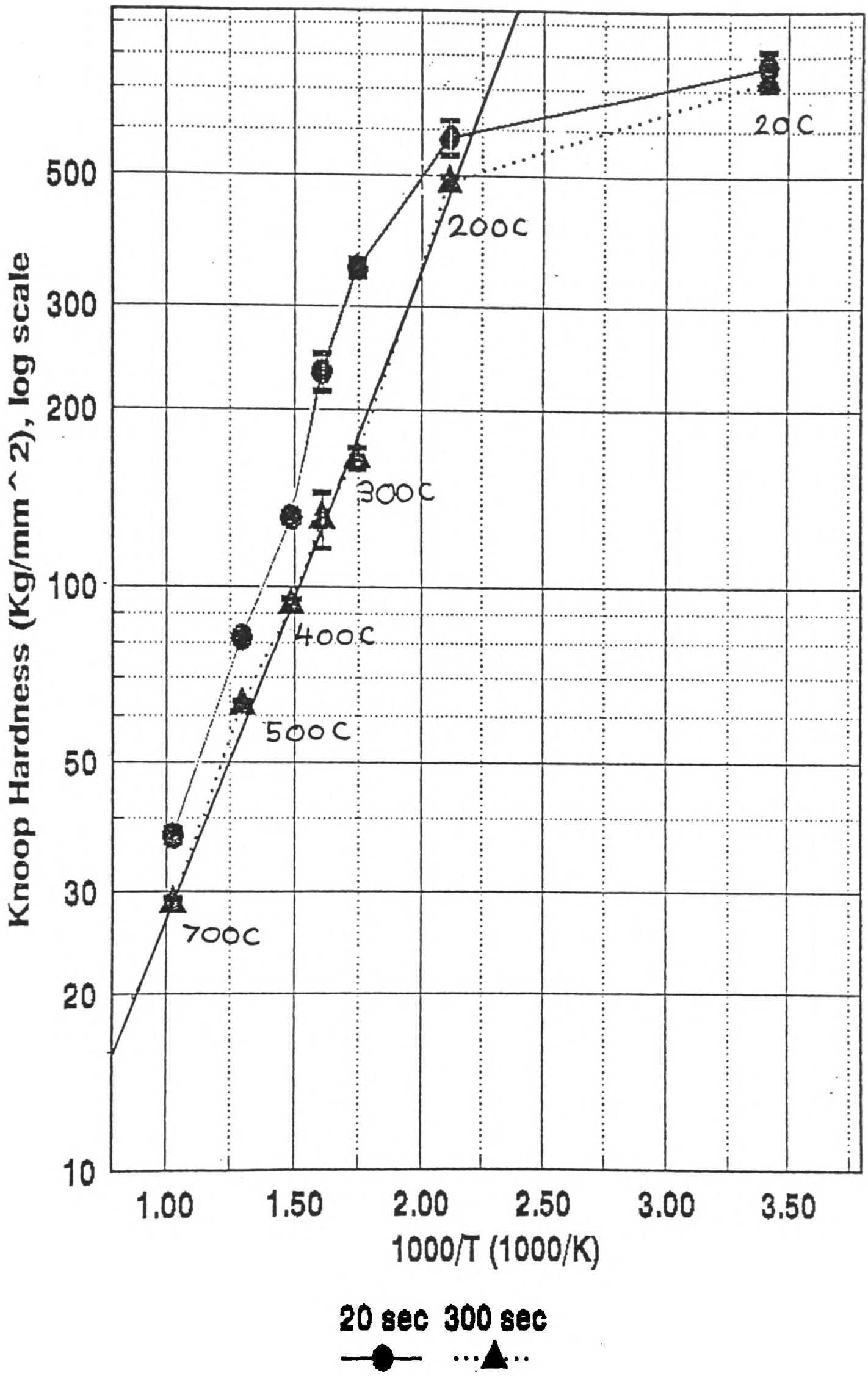


Figure 11.2(b) Arrhenius plot, log (Knoop hardness) against 1000/T, for <100> indentations on (001) Ge.

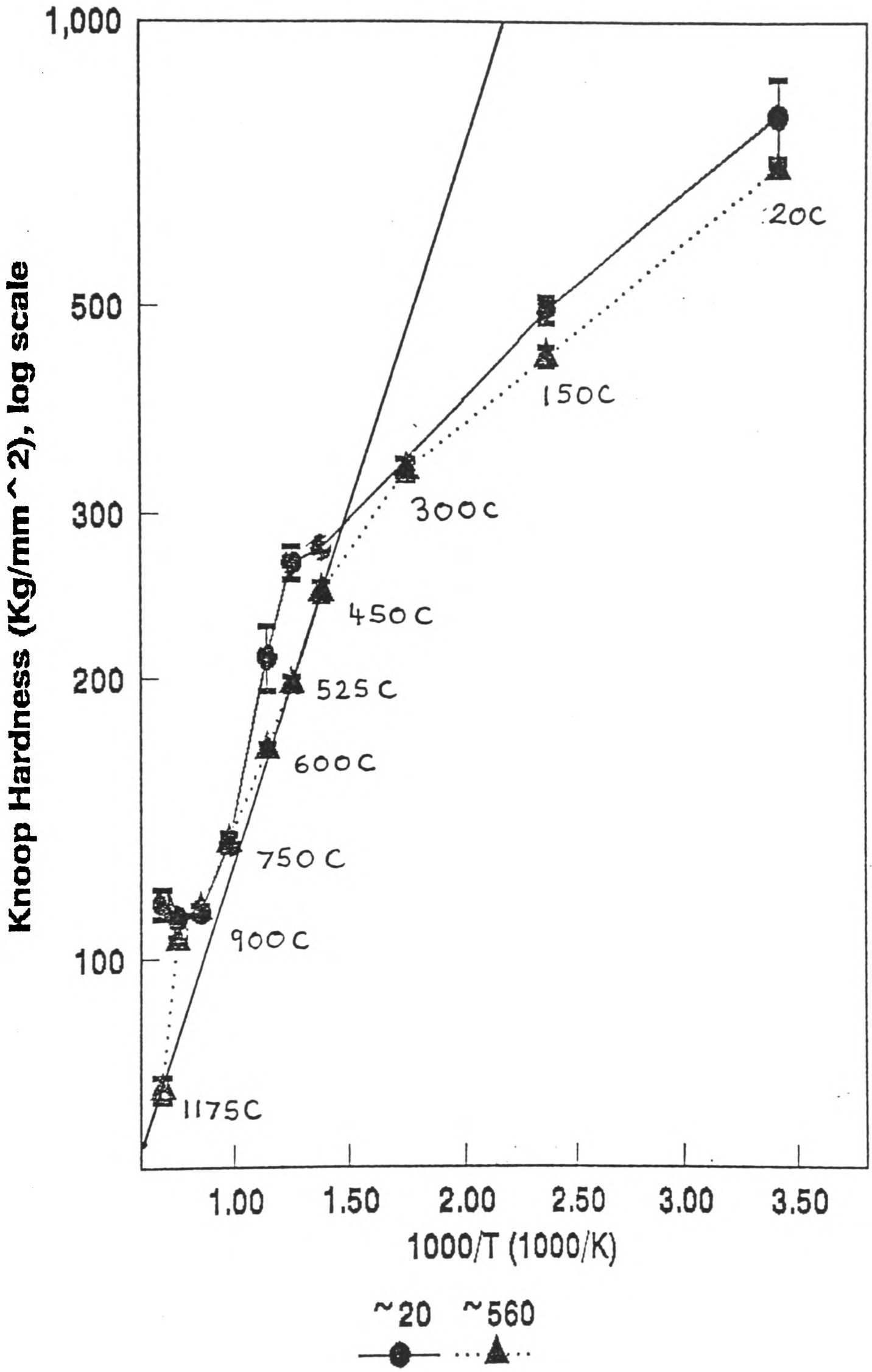


Figure 11.3(a) Arrhenius plot, log (Knoop hardness) against 1000/T, for <110> indentations on (001) MgO.

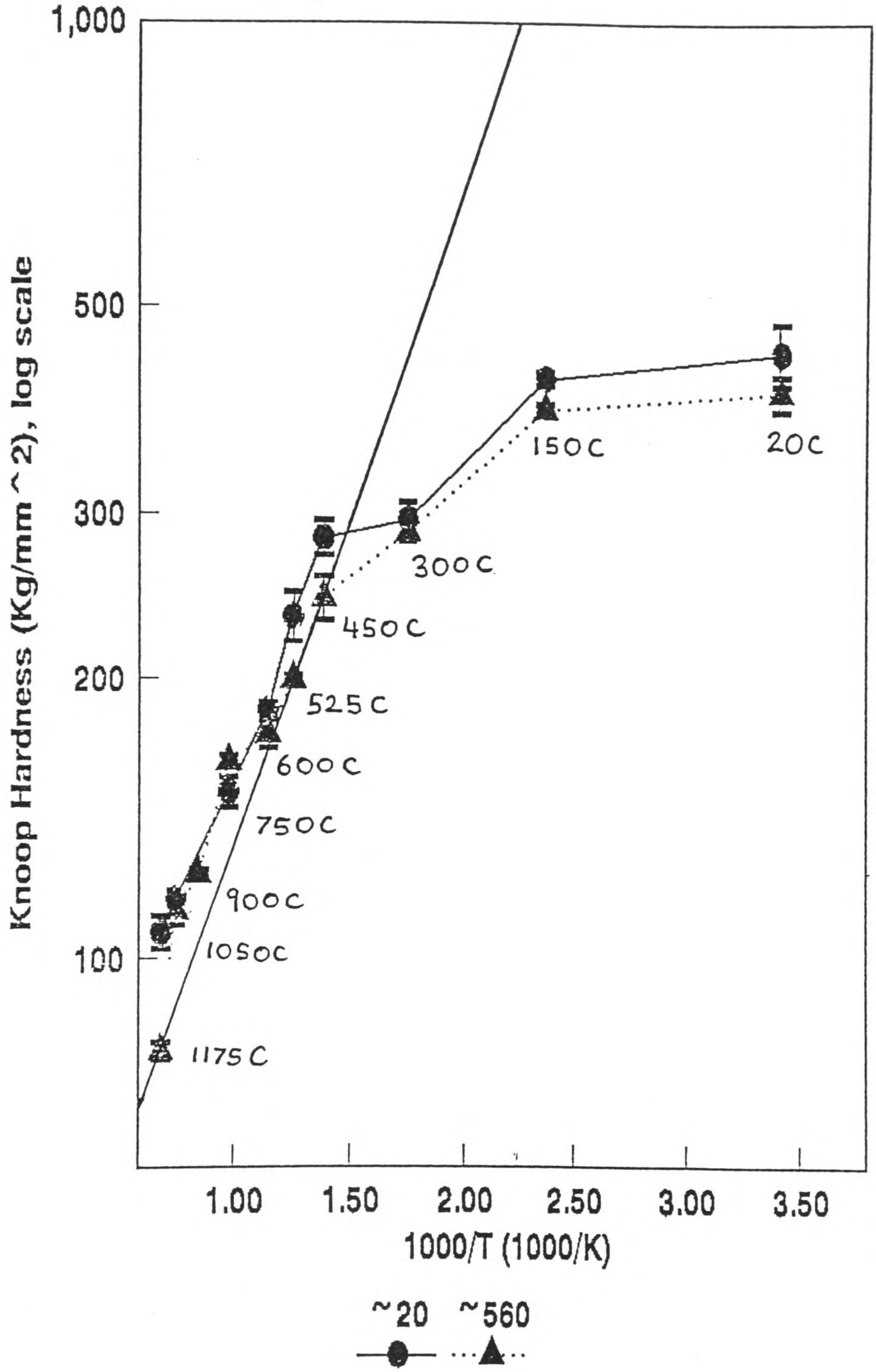


Figure 11.3(b) Arrhenius plot, log (Knoop hardness) against 1000/T, for <100> indentations on (001) MgO.

the hardness values in the "no creep" region do deviate from the straight line formed by values at temperatures above and below that range.

11.4 Time Dependent Hardness - Indentation Creep

Various workers have attempted to link the hardness behaviour of metals and alloys with their known tensile creep and creep rupture characteristics. Atkins and Tabor (1966) commented on the difficulty of performing hardness tests at higher T_M (i.e. where creep takes place) on refractory solids, and used mutual indentation of crossed cylinders or wedges. Other workers have used microhardness machines which have been specially adapted in some way (see chapter 2).

The term "creep" generally refers to the deformation of a material at constant stress. Parameters that are used to characterise a creep curve include the critical slope, the steady state creep rate, or, if no steady state creep occurs, the final total strain (Gilman 1961). Indentation creep differs from this situation (and is more difficult to analyse) because the applied stress, i.e. applied load / supporting area is not constant as the test proceeds, and the stress (and thus the flow zone) vary with the position of the indenter at any given time. However Atkins, Silverio and Tabor (1966) concluded that, at higher temperatures, the indentation hardness behaviour closely parallels the creep characteristics of the materials. Atkins (1973), working on indium polycrystalline specimens at room temperature, concluded that the rate of fall off of hardness with time, at a given temperature, was virtually independent of indenter shape providing that the indenter shape is blunt. However, this probably only applies to materials giving an isotropic plastic response. Brookes, Burnand and Morgan (1975) (working on ionic crystals) concluded that the characteristics of indentation creep were independent of normal load.

One of the few papers to attempt an overview and inclusive model of the mechanisms of creep is the recent study by Li, Henshall, Hooper and Easterling (1990). They suggest that the possible mechanisms for indentation creep are plasticity (dislocation glide), power law creep (climb plus glide), power law breakdown (glide plus climb), recovery (dislocation climb) and diffusion (volume, grain boundary or dislocation pipe). They conclude that the principal mechanism causing indentation creep is dislocation glide. In addition, indentation creep, caused by power law creep and diffusion, becomes more pronounced, though not dominant, above 0.5 T_M. The dominance of this mechanism over *whole* temperature range (i.e. room temperature and above) is due to the very high stresses involved in indentation creep. A comprehensive account is given of the relevant formula for the various forms of creep which might be affecting the hardness response. All the rate equations are derived on the assumption that steady state creep is established; this needs a

certain minimum incubation time. The period of non-steady creep is expected to be only up to a few seconds, but is difficult to treat theoretically. Thus a value for H_0, an "instantaneous hardness" is required, and can only be found by numerical treatment of experimental data. (The experimental value of initial hardness is used to set up the origin on a log(h) axis for one of the temperatures of interest.) In the light of the results previously described in this thesis, it is interesting to note that MgO is mentioned as a material which deviates from the theoretical predictions (although only above $0.5T_M$) more than most of the other materials considered! (Li et al suggested that the exponential index used might be unsuitable for the higher temperature range).

Li et al (1990) use a value for the ratio of the extent of the elastic-plastic radius, c, to that of the hydrostatic core, a, (see figure 11.1). This is assumed to be a material constant during the indentation process (Johnson 1970). It is not clear how this is estimated. Brookes, Shaw and Tanner (1987) proposed that c was related to be the radius of a hemisphere containing all the dislocations produced in the indented surface and in the bulk, whilst a is the radius of a much smaller hemispherical shell of highly dislocated material immediatley around and beneath the indentation itself. The results from this thesis certainly suggest that the rosette length around an indent is not a useful indicator of the extent of dislocated material.

Plots of log (Knoop hardness) against log dwell time for Ge and MgO are shown in figures 11.4 and 11.5. In agreement with the plots shown in the paper by Li et al (1990), the Ge data for each temperature is quite a good fit to a straight line, with a tendency towards increasing gradient at longer dwell times. The temperature showing the greatest decrease in hardness(i.e. the steepest gradient) from the 20 second value to the 600 second value, is 300°C. The MgO data does not fit to a straight line analysis such as this.

It is possible to link the gradient of such plots, (normalised by shear modulus) to power law creep (e.g. Sargent and Ashby 1989). However, values for n which are achieved are not directly comparable to the conventional "steady-state creep" index.

11.5 Anisotropy

Anisotropy of hardness response must clearly depend on the way in which the various slip systems in the bulk of the crystals respond to the applied load (Tabor 1970). The deformation around the indenter is very complex; there are a limited number of slip planes along which plastic flow can occur, and the material is forced to conform in certain directions by the shape of the indenter. At the simplest level, anisotropy in the intrinsic hardness of materials is to be expected because the resolved stresses on the different

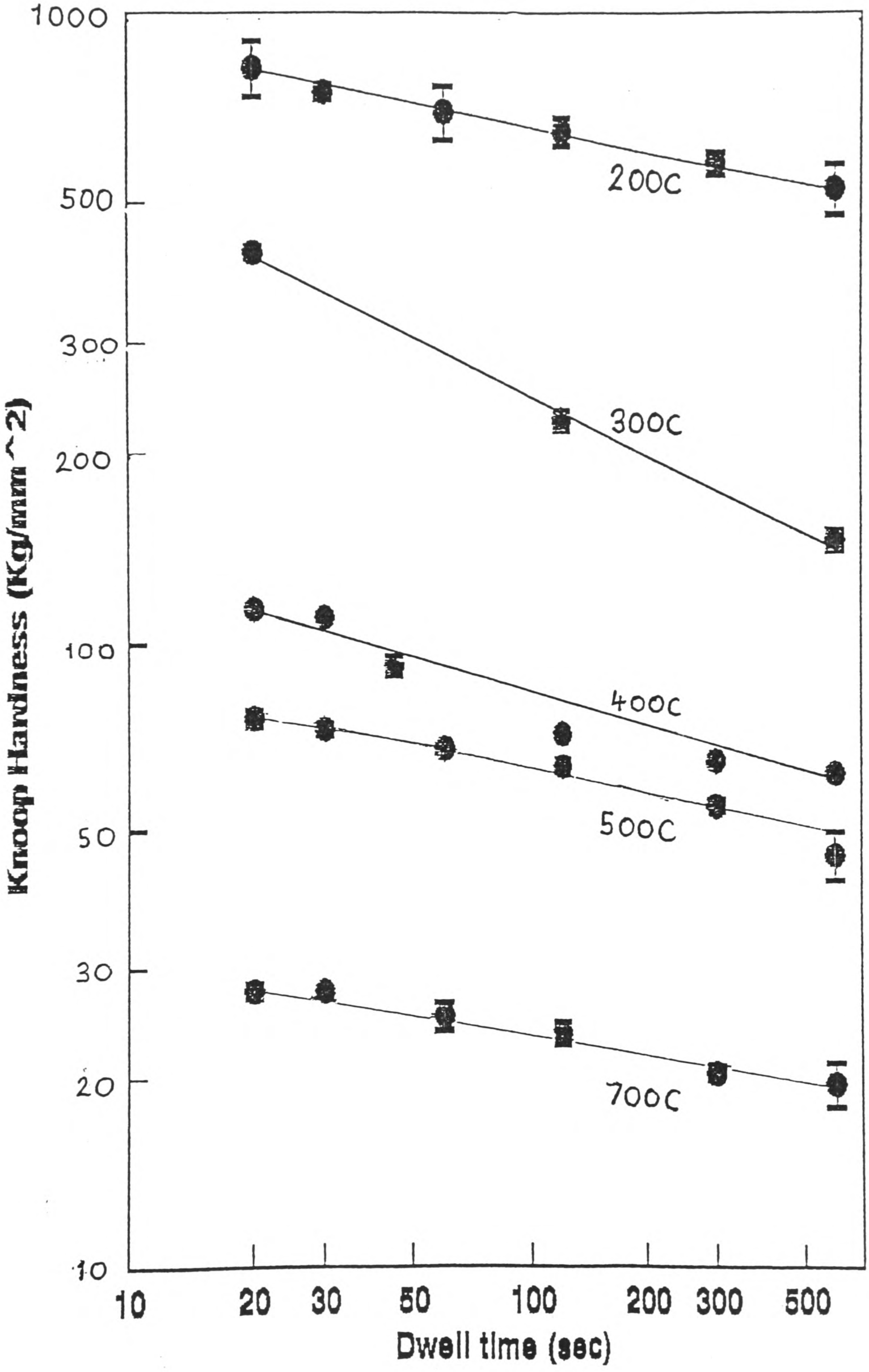


Figure 11.4(a) Variation of <110> Knoop hardness with dwell time, between room temperature and 700C, on (001) Ge.

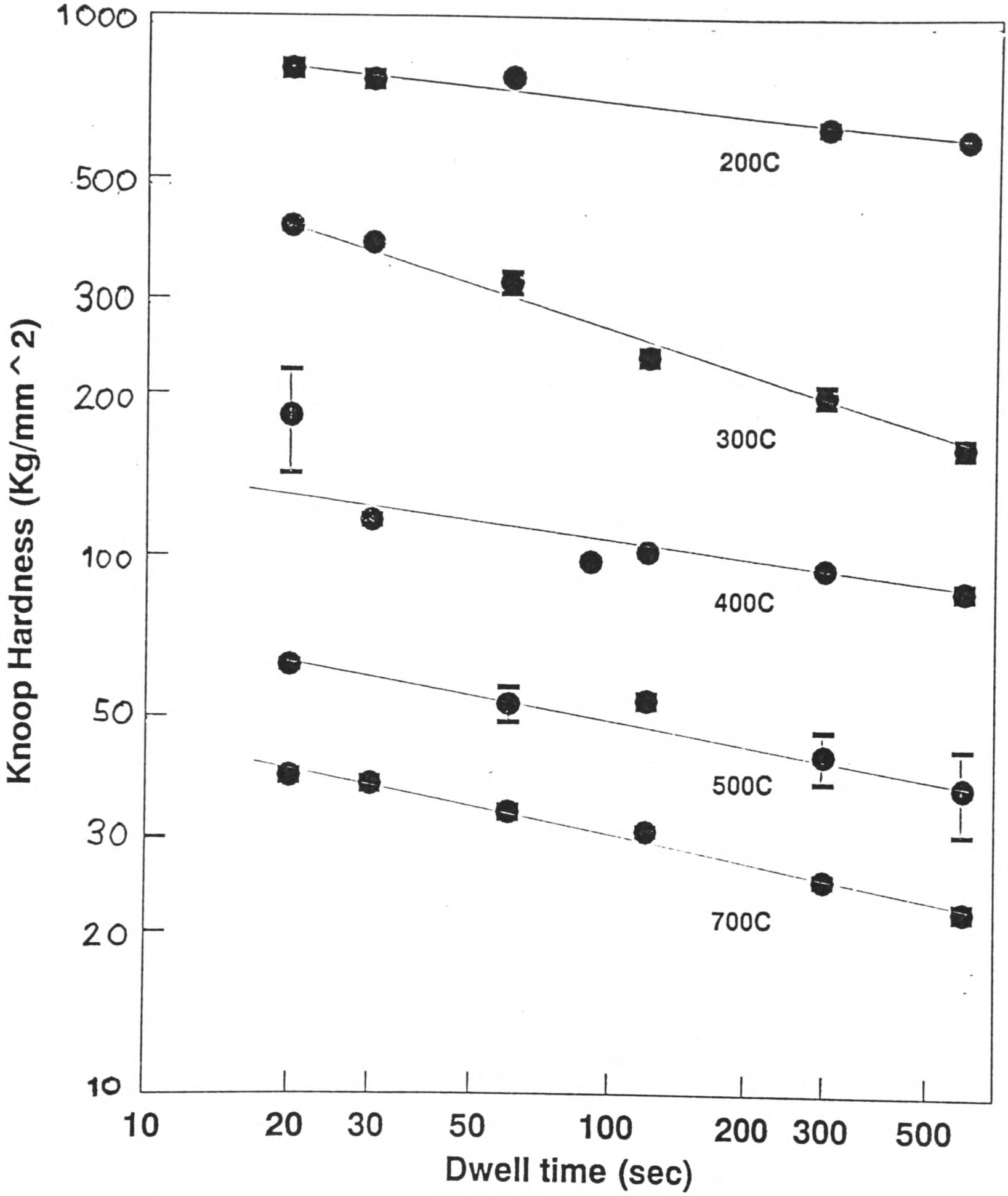


Figure 11.4(b) Variation of <100> Knoop hardness wirh dwell time, between room temperature an 700C on (001) Ge

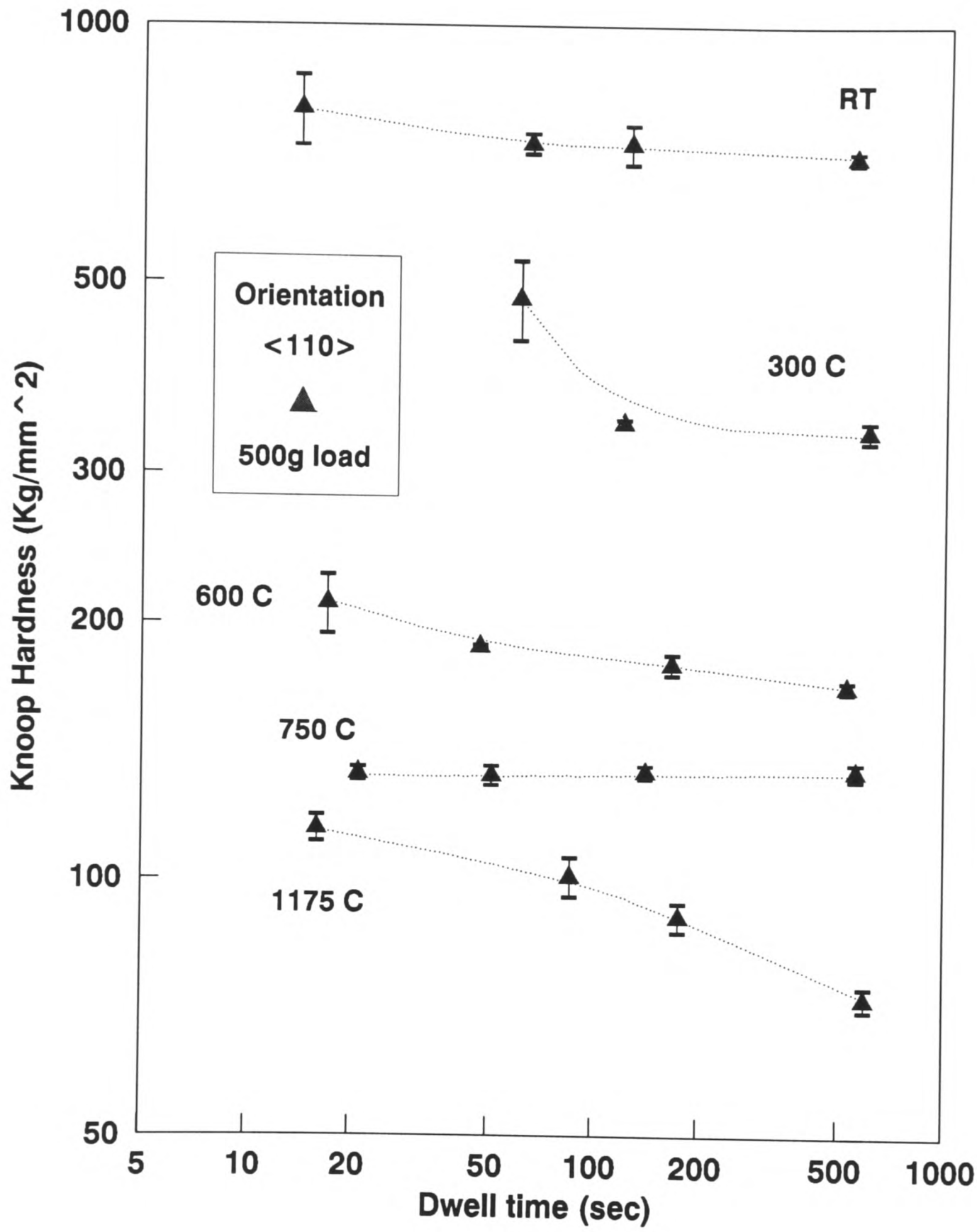


Figure 11.5(a) Variation of <110> Knoop hardness with dwell time, between room temperature and 1175C, on (001) MgO

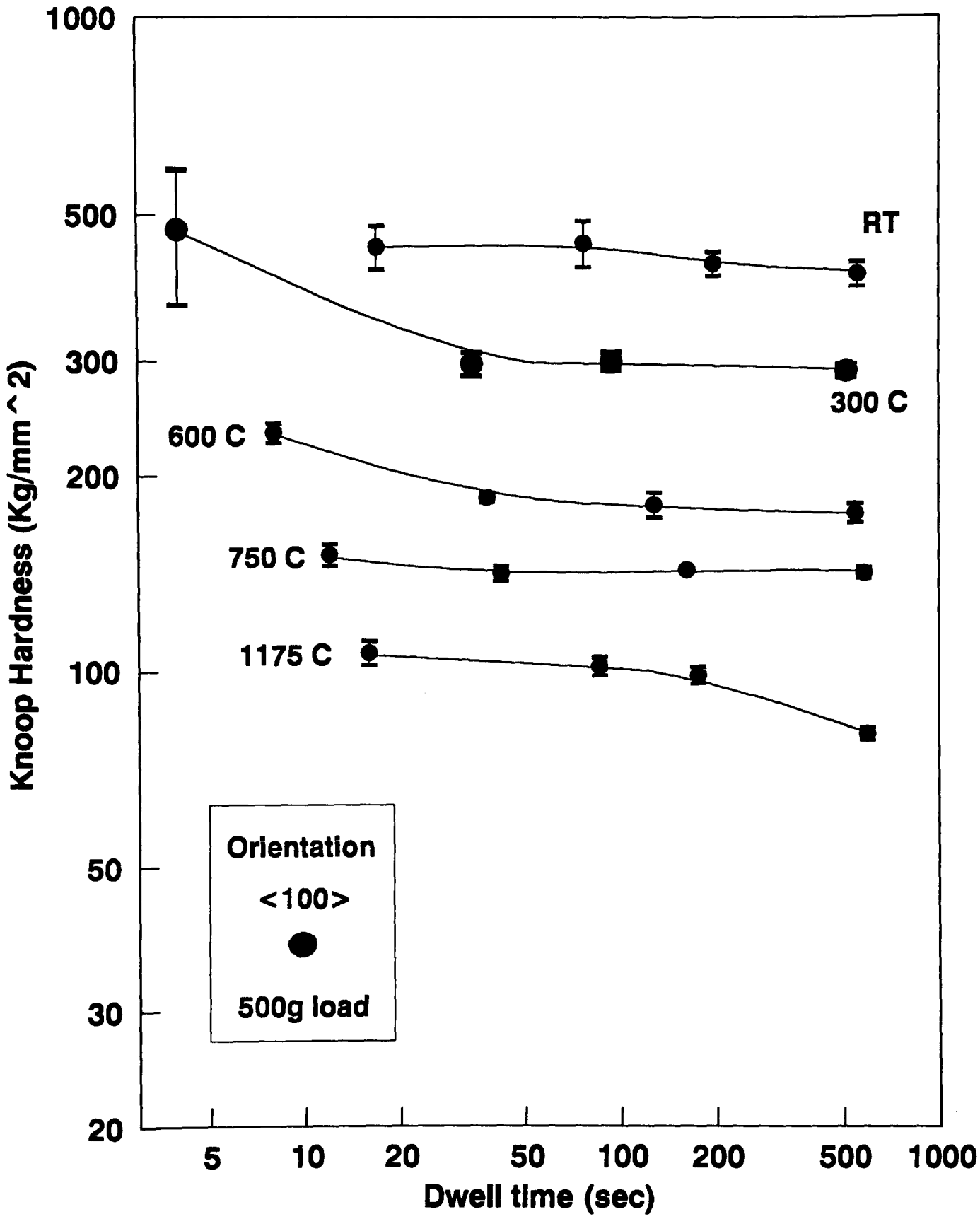


Figure 11.5(b) Variation of <100> Knoop hardness with dwell time between room temperature and 1175C on (001) MgO

Source	Temperature Range (TM)	Activation Energy KJ mol-1	eV
MgO:-			
Walker (1973)	0.5 -0.6	419	4.3
Hooper and Brookes (1984)		460	4.8
Atkins and Tabor (1966)	0.3-0.5 0.5-0.7	126 461	1.3 4.8
(Self diffusion		440	4.6)
Ge:-			
Ashby and Sargent (1985)		116-270	1.2-2.8
From Oxford Plots:-			
<110> MgO	0.3-0.5	11.1	0.12
<110> MgO	0.3-0.5	14.3	0.15
<110> Ge	0.3-0.8	20.4	0.21
<100> Ge	0.3-0.8	17.9	0.19

Table 11.1 Activation energies determined from the Arrhenius plot in figures 11.2 and 11.3, and values from literature.

deformation mechanisms will be different for different orientations of a faceted indenter. This presupposes that the plasticity of materials is crystallographically discrete and sensitive to resolved shear stress, e.g. dislocation slip and twins (Sargent and Page (1985). The effective resolved shear stress models reviewed in section 11.1.1 showed clearly that the hardness anisotropy of single crystals is determined by the crystal structure and the primary slip systems, at least at moderate temperatures. Thus the nature of anisotropy has been used to identify operative slip systems in the deformation of brittle crystals, e.g. sapphire (Hockey 1971), diamond (Brookes 1970) and transition-metal carbides (Hannink, Kohlsted and Murray, 1972). The surprising change in dislocation array around <110> Knoop indentations on (001) Ge at the highest temperature (see section 10.3.2) shows the value of such investigations since they can reveal changes in the material's response to a given stress field.

However, care is needed, since the rate of indentation creep and the temperature dependence will also be anisotropic to some degree, due to the differing degree of activation of various slip systems and their interaction. Thus, as stressed by Brookes, Burnand and Morgan (1975) in their investigation into "anomalous" anisotropy in the rocksalt type group of crystals, there is a need to control both the indentation time and the homologous temperature for accurate comparisons of hardness data in crystalline solids. However, it might be possible to utilize information from the anisotropy of creep rates to draw conclusions on the kind of deformation (in terms of which slip systems are operating, and the extent of activity on those systems) which best cause workhardening and the consequent modifications in mechanical behaviour. It is not clear if the range of no indentation creep in MgO could be extended to poly-crystal samples, or into other types of deformation.

11.6 Interpretation of the Indentation Processes - The Fundamental Factors

It must be possible to explain the different hardness response of different crystalline groups, and here specifically those of MgO and Ge, by considering the processes going on during indentation and what are the controlling factors.

Due to the very high stresses present at the tip of the indenter in the first few moment of an indent, dislocations will be nucleated, at least on the primary slip systems, for all materials. However, which of these slip systems will continue to have operative dislocation sources, will depend on the resolved shear stresses on those systems (from the particular indenter orientation / surface of indentation etc). The rate of penetration of the indenter will depend on the ease with which dislocation loops nucleate, and are able to travel away from the indenter carrying material away. Materials will give a harder response

if a higher stress is needed, because the material demands a large nucleation stress, and/or the dislocation arrays are kept short through low intrinsic velocity or low effective velocity, due to impeded movement. However the creep response will vary in these cases.

A significant rise in indentation aspect ratio occurred in MgO at the temperatures at which the creep rate was reduced to zero, and the highest value was for the orientation which crept the fastest at other temperatures. The hardness response appears to be controlled by the interaction and work-hardening which take place as planes moving material down into the crystal, meet those with a slip direction towards the surface. The velocity of dislocations in MgO is very sensitive to stress, and these dislocations are readily available. Hence the material is able to show indentation creep at homologous temperatures much lower than those for Ge, and the resolved shear stresses are such that loops travelling towards the surface are created relatively easily. For the <100> orientation at room temperature, the pile up created is very localised, and causes a low aspect ratio. At higher temperatures the pile up is more spread out, and ceases to affect the aspect ratio in the same way. The <110> orientation does not, at room temperature, activate pile up towards the surface, but as the shear stress needed to activate slip on these planes decreases with temperature, pile up begins to be seen. The rate of decrease of hardness with temperature begins to decrease above 600°C. This is associated with extensive slip close to the indenter in the first few moments of the indentation, leading to work-hardening close to the indenter. In MgO this causes significant sink-in just around the indenter, leading to the rise in aspect ratio and complete blocking of any more indentation creep.

By contrast, for Ge, enough work-hardening to achieve a significant rise in the aspect ratio is only achieved at the fastest creep rates. The highest value in aspect ratio is achieved by the orientation with the slowest creep rate of the two orientations considered. The hardness response is controlled by the effective stress very close to the indenter, because this governs the rate of nucleation of dislocation loops. The effective stress is, in turn, influenced by work-hardening of systems, as material is transported away form the indent by the dislocation loops.

For covalently bonded materials like Ge, a relatively high stress is needed to get dislocation loops moving away from the indentation at any speed. (There may be a nucleation stress connected with impurity pinning, but it is small (~1 MPa) even in the worst cases). The dislocations are fairly immobile at low temperatures and thus here is no creep or anisotropy at room temperature. However, as the temperature is raised, the stress needed to get dislocation loops travelling away from the indent becomes less, so more slip

takes place. Once the dislocations are moving, the dislocations in an array will exert a significant back-stress on the dislocation source, so they must move a certain distance away before another loop can be nucleated. Thus it might be possible to model the indentation hardness with arrays of single dislocations moving out from the indent, allowing another dislocation to form only at the time when the resolved shear stress from the indent can manage to sufficiently overcome the backstress from the array. The <110> Knoop orientation creeps faster than the <100>, because, in the latter case, more of the deeply penetrating planes with many slip intersections are activated, producing local interference and work-hardening. The presence of work-hardening is indicated by the rise in aspect ratio for <100> indentations at the temperatures where the creep rate (and the relative rate of decrease in hardness with temperature) is fastest. The rise in aspect ratio for the <110> orientation is not nearly as marked, although by 700°C it is significantly above the ideal of 7.11, supporting the conclusion that, at higher stresses, the slip begins to take place on all of the deeply penetrating planes (and cause work-hardening) in a similar way to the <100> orientation. (Hence the change in surface dislocation arrays. The rate of decrease of hardness with temperature slows above ~400°C, because, although the dislocations can travel some distance away from the indent, carrying material out into the body of the crystal, the stresses on the dislocations on the deeply penetrating planes are such that the velocity of the leading dislocations is once more reduced.

Thus the hardness response of Ge is mainly controlled by the high stress (and time) needed to move dislocations sufficiently far away from the indentation for more loops to be nucleated, and facilitate movement of material away from the site of the indentation. The stress field below an indenter is highly complex, but it might be possible to model this situation with dislocation arrays. The hardness response of MgO is dominated by the interaction and workhardening, which occurs both in close proximity to the indenter and farther away in the bulk of the material, at least at temperatures up to $0.47T_M$. This would be very difficult to model in a mechanistic way.

12. SUMMARY AND CONCLUSIONS

This chapter summarises the main experimental findings and conclusions of the thesis and looks ahead to the future work which might stem from it.

12.1 Summary of the Magnesium Oxide Results

Indentation was carried out on the (001) surface of magnsesium oxide. At room temperature the <110> Knoop hardness is considerably higher than that of the <100> orientation. However the tendency for the <110> orientation to creep faster than the <100> orientation results in a decrease of anisotropy as the temperature is raised, so that there is no significant difference in the hardness of the two orientations by about 525°C. At 750°C the anisotropy has reversed (compared to room temperature) and <100> is now the harder orientation. Between 750°C and 1050°C the material showed no indentation creep for either Knoop orientation or for Vickers indentation at various loads. This is in contrast to previously published results, and the discrepancy is attributed to improved experimental conditions of the hardness tests at Oxford, which allowed independent heating of the indenter. By 1175°C ($0.52T_M$) indentation creep was again demonstrated, <110> again creeping slightly faster than the other orientation.

The slip system of MgO is on {101} planes in the <110> directions. Dislocation etching of sample sections showed that, whilst dislocation loops were produced on all the {101} planes, the most penetrating activity took place on the planes at an angle of 45° to the sample surface. Exactly which planes contained the most loops depended on the orientation of the indenter and the temperature of indentation. Observations using interferometry to examine the surface topography around the indents showed that pile up is significant, and explained the variation in the aspect ratio of the Knoop indentations. For the <110> no pile up could be distinguished at room temperature, and the high aspect ratio was attributed to elastic recovery leading to a decreased short diagonal. As the temperature was raised pile up began to appear, and the amount of elastic recovery decreased leading to an aspect ratio nearer to the ideal 7.11. At temperatures 150°C to about 600°C the pile up consisted of two rounded hills either side of the indentation (whose extent stayed roughly constant in proportion to the length of the long diagonal); but did not cause a very steep height variation immediately adjacent to the indenter sides, thus affecting the aspect ratio relatively little. However in the no creep region, closely spaced interference fringes indicated that a steep, roughly elliptical, valley was present around the indenter causing a higher than ideal aspect ratio to be recorded. The highest temperature indentations, 1175°C, indicate that the aspect ratio began to decrease as indentation creep again became

possible. Not only was the average aspect ratio lower than that for 1050°C indentations, but it significantly decreased with increasing dwell time, suggesting that the initial workhardened shell is overcome. It seems likely that this change in behaviour is facilitated by dislocation climb and the increased favourability of the secondary slip system ({100} <110>. At room temperature the low aspect ratio of <100> orientations was caused by pile up very close to the sides of the indenter on planes which intersected the surface in the <100> direction parallel to the long diagonal. Thus the measured short diagonal was larger than it would have been on a flat surface, but the long diagonal was not affected. As the temperature was increased the pile up was still concentrated in two ridges running parallel to the long diagonal of the Knoop indentations, but spread over a larger area not so close to the short diagonal tips. The aspect ratio therefore tended more towards the ideal. In the no creep temperature range it began to rise for the same reasons as described above, although the extent of pile up around the <100> indents (and the aspect ratio) was always less than for the <110> orientation.

The differences in creep rate between the two orientations were also explained by considering the interaction between plastic flow down away from the indentation, and flow towards the surface during indentation. At room temperature the planes activated by <110> orientation carried material away from the indentation into the body of the sample, but did not actviate a significant number of planes which brought material back up to the surface. Hence there was little or no pile up and creep could take place, although slowly, since the mobility of the dislocations is slow at this temperature ($0.1T_M$). However for <100> indentations at this temperature the stresses on planes, which intersected the (001) surface parallel to the long diagonal, were such that loops travelling towards the surface were activated, causing the observed pile up. Increasing temperature increased the mobility of the dislocations, and led to a decrease in hardness with temperature; but the increasing amount of upward slip, associated with indentations of both orientations, made slip with time increasingly difficult, until no indentation creep could be observed even for indentations of 20 minutes. The relative decrease in hardness with time decreased in the region 600°C to 1050°C, which was also attributed to the increased resistance of the material to penetration of the indenter.

The existance of the "no creep" regime for indentation is exciting since it would obviously be advantageous if it could be reproduced under other conditions. It has not been reported in single crystal compression or tensile tests, so it might be concluded that a vey high dislocation density on interacting slip systems is needed, i.e. no indentation creep takes place because a large, localised strain has already taken place. Future indentation experiments on polycrystalline MgO would provide interesting information to see if enough

strain concentration could be induced to produce the same result as on single crystal. In a practical situation the difficulty would lie in producing the strain without cracking.

12.2 Summary of the Germanium Results

Indentation was carried out on the (001) surface. At room temperature the <110> and <100> Knoop hardnesses were indistinguishable, but indentation anisotropy developed as the temperature was raised and indentation creep was demonstrated, due to a faster creep rate for the <110> orientation. By 400°C the two orientations were not distinguishable at all but very short dwell times, <110> being the softer. Knoop hardness decreased slowly with temperature between room temperature and about 200°C. In the temperature range 200°C to 350°C or 400°C, the rate of decrease in hardness with temperature speeded up for both Knoop orientations, but the <110> hardness decreased most. Above this temperature the rate of change slackened, the <110> orientation more than the<100>, so that the degree of anisotropy certainly did not increase, and perhaps decreased. 30 minute indentations on p-doped Ge did not show any detectable anisotropy. Lower to medium temperature 20 second Vickers indentations showed the same temperature variation as the Knoop indentations.

The germanium slip system is on {111} planes and in the [110] directions. The analysis of dislocation arrays identified two different kinds of slip. One type,"rosette slip", gave rise to characteristic lines of dislocation etch pits along the <110> directions in the (001) surface. These pits were shown to belong to loops which were concentrated relatively close to the sample surface. The arrays increased in length as the dwell time increased (at a particular temperature), and also became longer, but less dense as the temperature was raised. Above 500°C they disappeared altogther. The more important type of slip (as far as the hardness value is concerned) is that with deeply penetrating dislocation loops with their long axes inclined down into the crystal. The favoured planes were those which diverged away from underneath the indenter, and the exact location of the activated planes with respect to each other was postulated as the primary cause of the creep anisotropy. The dislocation arrays from <100> indentations at all temperatures indicated that time-dependent slip occurred by loops moving down away from under the indenter on sets of four equivalent planes (see figure 10.10). Mutual interaction on these systems restricted dislocation motion away from the highly deformed zone beneath the indenter At low and medium temperatures the <110> orientation indents showed two major planes containing deeply penetrating loops. These planes ran parallel to the long diagonal of the indents, and diverged away from the body of the indentation. Once nucleated, loops on these planes could move away from the indenter zone relatively easily, hence the faster indentation creep rate. By 700°C the form of dislocation array has changed, probably to an array which

more closely resembles that of the <100> orientation, i.e. mutual interaction between loops on all the four planes with slip diredtion out into the main body of the crystal.

12.3 Hardness Testers

High temperature indentation testing on brittle materials has been shown to produce interesting data which can be related to the deformation produced around the indentation. However, the test is highly sensitive to the temperature of the actual indenter as the indentation begins. It is therefore important to have independent heating of the indenter if accurate data is to be produced. The modified Wilberforce design of indentation machine which has been developed at Oxford has such independent heating, and has a modified disposition of weights on the indenter beam, in order to give a load which is constant over the loading range of the indenter.

More work remains to be done in the area of monitoring indenter displacement during microhardness tests, but there are considerable experimental difficulties in the design of such a system. It must have a high displacment resolution, but be robust enough to withstand the proximity of a hot zone around the indenter. Allowance for effects caused by expansion of machine components as the machine heats up, and elimination of friction effects in the measurment chain are other problems. It would also be desirable to replace the dead weight loading system with a direct loading device. However the same experimental difficulties apply. (The Nanoindenter has, of course, got both these facitilies but only for very low loads and at room temperature).

12.4 The Indentation Response

The indentation hardness response, indentation creep rates and anisotropy are very dependent on the dislocation arrays which form in the first few moments of the indentation. Dislocation locking on interacting slip planes may dominate the indentation behaviour at all, or some, temperatures. Resolved shear stress models probably provide the best insight into the slip systems which are activated. However, quantitative models to predict the hardness of a material (or indeed the magnitude of hardness anisotropy) are still some way off. Further analysis and modelling of dislocation arrays in kink-mode crystals like Ge may provide added insight into the indentation creep models currently being suggested. TEM might be useful here.

APPENDIX A - CALIBRATION STRAIN-GAUGED BEAM

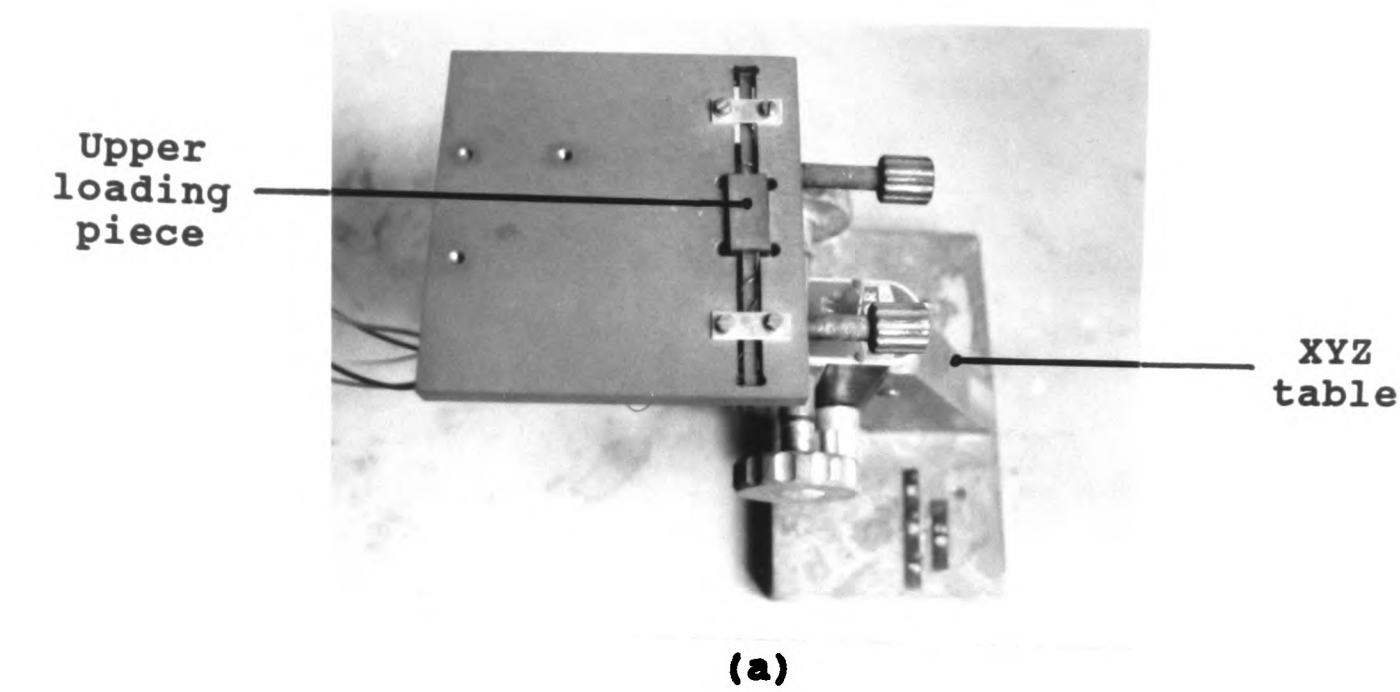
Close up views of the calibration apparatus, which was designed and built for this thesis, are shown in figure A.1. The basis of the design is four point bending of a thin beam with four gauges (two below and two above) in the middle third of the beam. The gauges are connected togethr in a Wheatstone bridge arrangement. The apparent applied load on the indenter would be measured by resting the indenter on a loading piece directly above the gauges, as shown in figure A.2. The original dimensions of apparatus were designed so that it would be possible to fit the whole system into the main body of the Oxford machine if required. This gave rise to a beam cross section of 2mm breadth and 3mm depth. The small loads (and therefore) strains which had to be measured produced quite stringent performance requirements. Although lower modulus materials were considered, tool steel was finally selected as the beam material because of manufacturing considerations. Single crystal silicon gauges were required to read the small strains. (They would take a maximum strain of 0.003, which allow to a maximum load of 7Kg and thus a satisfactory safety margin). An RSL bridge amplifying circuit was built and attached to the Wheatstone bridge formed by the gauges, and the output read on a T100B meter.

Using dead weights, the voltage output for given loads on the bridge (at a set bridge voltage), could be recorded, and a calibration chart produced. However, due to the uncertainty of producing exactly the same set up conditions at each time of calibration, a methodolgy was developed in which, after the top assembly had been removed and postioned above the beam:-

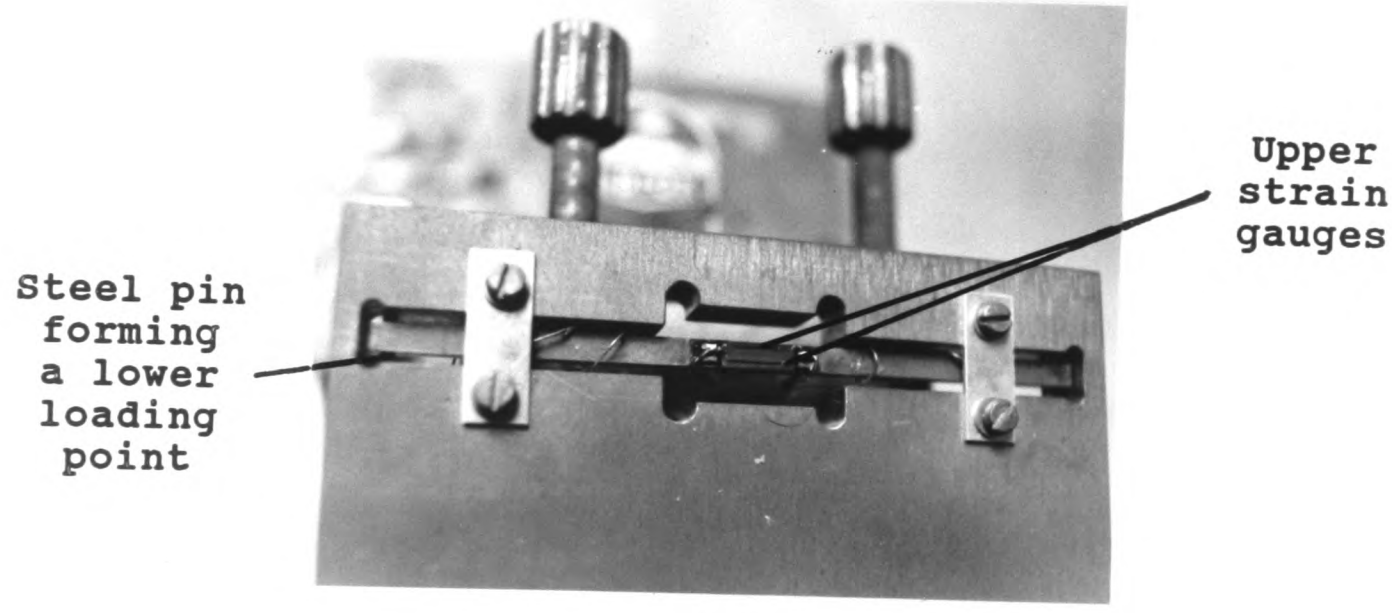
(i) The voltage readings produced by repeatedly resting a 100g weight on the loading piece were recorded, and the mean result calculated.

(ii) Sets of 10 readings were taken, and the counter weights adjusted until the same mean reading could be reproduced by the indenter loaded with the 100g weight.

This procedure was followed each time the indenter was changed, and after any machine modifications.



(a)



(b)

Figure A.1 Strain gauged beam apparatus designed and built for calibration of the Oxford indentation tester
(a) Top view, with the upper loading piece in position,
(b) Beam in position on the lower pin supports but with upper loading piece removed.

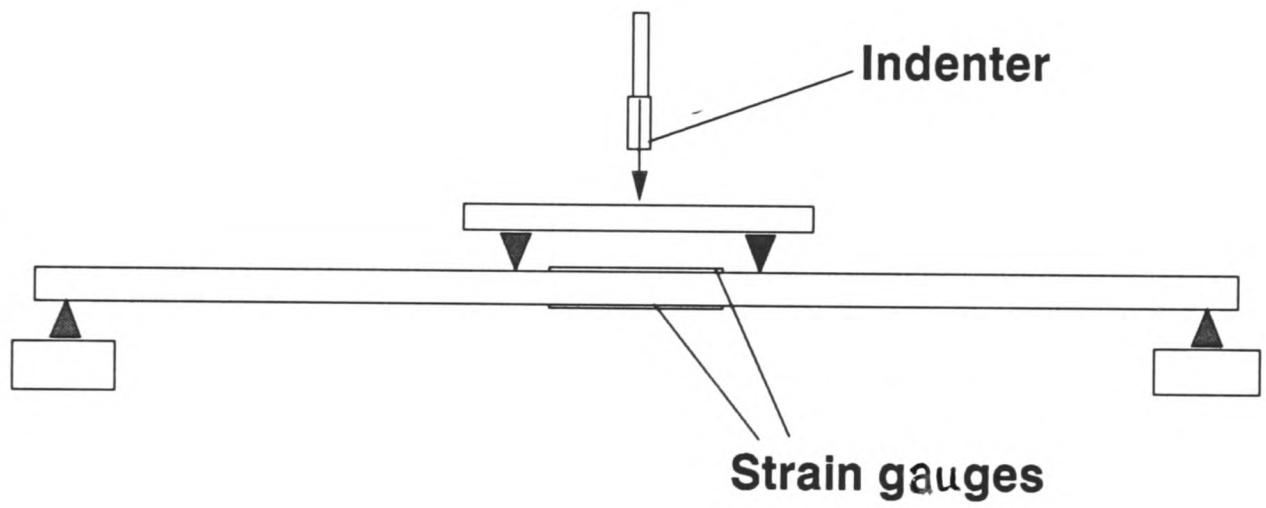


Figure A.2 Schematic view of the strain-gauged beam load calibration apparatus

LIST OF REFERENCES

Alexander, H. and Haasen, P. (1967)
Dislocation distribution in deformed Ge. *Canadian journal of Physics*, **45**, 1209-1212.

Alexander, H. and Haasen, P. (1968)
Dislocations and plastic flow in the diamond structure. *Solid state physics,* **22**, 1-531.

Amelincx, S. (1956)
The direct observation of dislocation nets in rock salt single crystals. *Phil. Mag.*, **A, 1**, 269-290.

Appel, F., Bartsch, M., Messerschmidt, U. and Nadgornyi, E.M. (1984)
Dislocation motion and plasticity in MgO single crystal. *Phys. stat. sol. (a)*, **83**, 179-194.

Armstrong, R.W. and Raghuram, A.C. (1973).
Anisotropy of microhardness in crystals. In *The Science of Hardness Testing and Its Research Applications,* edited by J.H. Westbrook and H. Conrad, American Society for Metals, Ohio, pp. 174-186.

Armstrong, R.W. and Wu, C.C. (1978)
Lattice misorientation and displaced volume for microhardness indentations in MgO crystals. *J. Am. Ceram. Soc.*, **61,** 102-106.

Atkins, A.G. (1973)
High temperature hardness and creep. In *The Science of Hardness Testing and Its Research Applications*, edited by J.H. Westbrook and H. Conrad, American Society for Metals, Ohio, pp. 223-240.

Atkins, A.G. and Tabor, D. (1966)
Hardness and deformation properites of solids at very high temperatures. *Proc. Roy. Soc,* A, **292**, 441-459.

Atkins, A.G., Silverio, A. and Tabor, D. (1966)
Indentation hardness and the creep of solids. *Journal of the Inst. of Met.* **94**,369-378.

Banerjee, R.K. and Feltham, P. (1974)
Deformation and fracture of GE single crystals. *J. Mat. Sci.*, **9**, 147-182.

Beeukwes, R., Jr., Chait, R. and Lin, H.H. (1973)
In *The Science of Hardness Testing and Its Research Applications, Westbrook*, J.H. and Conrad, H. (eds.), ASM, Ohio, 75-90.

Bishop, R.F., Hill, R. and Mott, N.F. (1945)
The theory of indentation and hardness tests. *Proc. Roy. Soc. London*, **57** (321), 147-159.

Blau, P.J. (1980)
Use of a two diagonal measurement for reducing scatter in Knoop microhardness testing. *Scripta Metall.*, **14**, 719-724.

Blau, P.J. (1983)
A comparison of four microindentation hardness test methods using copper, 521000 steel and an amorphous Pd-Cu-Si alloy. *Metallography*, **16**, 1-18.

Bohlen, R. (1973)
A simple method for obtaining ductility from a 100°-cone impression.In *The Science of Hardness Testing and Its Research Applications*, edited by J.H. Westbrook and H. Conrad, American Society for Metals, Ohio, pp.109-116.

Bondarenko, I.E, (1981)
Ph.D. Thesis, Chernoglovka, *through Nadgornyi 1988.*

Boyarskaya, Y.S., Grabko, D.Z. and Purich, E.I. (1979)
Anomalies in the knoop microhardness anisotropy of crystals. *J. Mat. Sci. Lett.*, **14**, 737-741.

Brinell, J.A.J. (1900)
2nd Cong. Int. Methods d'Essai, Paris. English account in Wahlberg 1901.

British Standard 240:1986

British Standard 427:9161

Brookes, C.A. (1971)
Indentation hardness. In *Properties of diamond,* edited J.E.Field, Academic Press, pp.381-402.

Brookes, C.A. (1990)
Personal communication, July 5th, Department of Engineering Design and Manufacture, University of Hull.

Brookes, C.A. and Green, P. (1973)
Deformation of magnesium oxide crystals by softer indenters and sliders. *Nature (Physical Sciences),* **246**, 119-121.

Brookes, C.A., Brookes, E.J., Howes, V.R., Roberts, S.G. and Waddington, C.P. (1990)
A comparison of the plastic deformation and creep of type I, type II and synthetic diamonds at 1000°C under conditions of point loading. *J. Hard Materials,* **1**, 3-24.

Brookes, C.A., Burnand, R.P. and Morgan, C.A. (1975)
Anisotropy and indentation creep in crystals with the rocksalt structure. *J. Mat. Sci.* Lett., **10**, 2171-2173.

Brookes, C.A., Hooper, R.M. and Morgan, J.E. (1987)
Some factors influencing indentation creep in crystaline solids. *European Applied Research Reports*, edited by H. Matzke, Harwood Academic Publishers, **7**, 1127-1145.

Brookes, C.A., O'Neill, J.B. and Redfern B.A. (1971)
Anisotropy in the hardness of single crystals. *Proc. Roy. Soc. Lond.,* **A322**, 73-78.

Brown, L.M. and Ineson, E. (1951)
Experimental survey of low load hardness testing instruments. *J. Iron and Steel Inst.*, 376-388, December 1951.

Bückle, H. (1959)
Progress in microindentation testing. *Metall. Rev.*, **4**, 48-49.

Bückle, H. (1973)
Use of the hardness test to determine other material properties. In *The Science of Hardness Testing and Its Research Applications*, edited by J.H. Westbrook and H. Conrad, American Society for Metals, Ohio, pp. 453-494.

Bull, S.J. and Page, T.F. (1989)
Chemomechanical effects on ion-implanted MgO. *J. Phys. D: Appl. Phys.*, **22**, 941-947.

Burnand, R.P. (1974)
Zone refining of carbides and the hardness of crystals. *Ph.D. thesis, University of Exeter.*

Burnett, P.S. and Page, T.F. (1984)
Changing the surface mechanical properties of Sialon and α-Al_2O_3 by ion implantation. *J. Mat. Sci.*, **19**, 3524-3545.

Celli, V., Kabler, M., Ninomiya, T. and Thomson, R. (1963)
Theory of dislocation mobility in semiconductors. *Phys. Rev.*, **B1**, 58-71.

Chaudhuri, A.R., Patel, J.R. and Rubin, L.G. (1962)
Velocities and densities of dislocations in Ge and other semiconductor crystals. *J. Appl. Phys.*, **33**, 2736-2746.

Chaudhuri, M.M. (1986)
The displacement of material and the formation of $\{110\}_{90}$ cracks around spherical indentations in MgO crystals. *Phil. Mag.*, **A**, 53 (4), L55-L63.

Chiang, S.S., Marshall, D.B. and Evans, A.G. (1982)
The response of solids to elastic/plastic indentation. I. Stresses and residual stresses. *J. Appl. Phys.*, **53**, 298-311.

Clarke, D.R, Kroll, M.C., Kirchner, P.D., Cook, R.F. and Hockey, B.J. (1988)
Amorphisation and conductivity of Si and Ge, induced by indentation. *Phys. Rev.*, **60**, 2156-2159.

Cook, R.F. and Pharr, G.M. (1990)
Direct observation and analysis of indentation cracking in glasses and ceramics. *J. Am. Ceram. Soc.*, **73**, 787-817.

Czernuszka, J.T. and Page, T.F. (1987)
Characterising the surface contact behaviour of ceramics, Part 1: Hardness response of glass-bonded alumina and titania. *J. Mat. Sci.*, **22**, 3907-3916.

Davidge, R.W. (1967)
The distribution of iron impurity in single crystal MgO and some effects on mechanical properties. *J. Mat. Sci.*, **2**, 339-346.

Dew-Hughes, D. (1961)
Dislocations and Plastic flow in Ge. *IBM journal of research and development*, **5**, 279-285.

Doener, M.F. and Nix, W.D. (1986)
A method for interpreting data from the depth sensing indentation instruments. *J. Mat. Res.* **1**, 601-609.

Eremenko, V.G. and Nikitenko, V.I. (1972)
Electron microscope investigation of the microplastic deformation mechanisms of Si by indentation. *Phys. Stat. Sol.*, **A14**, 317-330.

Farges, G. and Degout, D. (1989)
Interpretation of the indentation size effect in Vickers microhardness measurements - absolute hardness of materials. *Thin Solid Films*, **181**, 365-374.

Feltham, P. (1978)
Low temperature plasticity and fracture of crystals with the diamond structure. *AGh. der Akad. Win. der DDR, 66t: Math-Naturov-Techn.*

Frost, H.J. and M.F. Ashby (1982)
Deformation mechanism maps, Pergamon Press, Oxford, pp. 84-88.

Gerk A.P.(1975)
Ge microhardness and the correlation of indentation creep with dislocation velocity. *Phil. Mag.*, **32**, 355-365.

Gerk, A.P. (1977)
The effect of work-hardening upon the hardness of solid: minimum hardness. *J. Mat. Sci.*, **12**, 735-738.

Ghosh, T.K. and F.J.P. Clarke (1961)
Etching and polishing studies on MgO single crystals. *Brit. J. Appl. Phys.*, **12**, 44-50.

Gilman, J.J. (1959)
Plastic anisotropy of LiF and other rocksalt-type crystals. *Acta Met.*, **7**, 608-613.

Gilman, J.J. (1961)
Mechanical behaviour of ionic crystals. *Progress in Ceramic Science*, **1**, 146-199.

Gilman, J.J. (1973)
Hardness - A strength microprobe. In *The Science of Hardness Testing and Its Research Applications*, edited by J.H. Westbrook and H. Conrad, American Society for Metals, Ohio, pp. 51-74.

Gilman, J.J. (1973)
Hardness of pure alkali halides. *J. Appl. Phys.*, **44**, 982-984.

Gilman, J.J. (1975)
Relationship between compact yield stress and indentation hardness. *J. Appl. Phys.*, **46**, 1435-1436.

Gilman, J.J., Johnston, W.G. (1956)
Observations of dislocation glide and climb in LiF crystals. *J. Appl. Phys.*, **27**, 1018-1022.

Gilman, J.J., Johnston, W.G. and Sears, G.W. (1958)
Dislocation etch pit formation in LiF. *J. Appl. Phys.*, **29**, 747-754.

Groves, G.W. and Fine, F.E. (1964)
Solid solution and precipitation hardening in Mg-Fe-O Alloys. *J. Appl. Phys.*, **35**, 3587-3593.

Guille, G. and Matini, L. (1988)
Microindentation characteristics of silicide coatings on niobuim and titanium. *J. Mat. Sci. Lett.*, **7**, 952-954.

Haasen, P. (1966)
Dislocations in semiconductors. *J. de Physique Coll.*, **27**, C3, 30-38.

Haasen, P., Barthel, C. and Suzuki, T. (1985)
Choice of slip system and Peierls stresses in the NaCl structure. In *Dislocations in solids*, Yamada Science Foundation, University of Tokyo Press, pp. 455.

Hanneman, R.E. and Westbrook, J.H. (1968)
Effects of adsorption on the indentation deformation of non-metallic solids. *Phil. Mag.*, **18**, 73-88.

Hannink, R.J., Kohlstedt and Murray, M.J. (1972)
Slip system determination in cubic carbides by hardness anisotropy. *Proc. Roy. Soc. Lond.*, **A326**, 409-420.

Henshall, J.L., Carter, G.M. and Hooper, R.M. (1988)
Indentation creep in zirconia ceramics between 290 and 1073K. *Leciester Conference Procedings* .

Hill, R. (1950)
The Mathematical theory of Plasticity, Oxford University Press, London.

Hill, R., Storakers, B. and Zdunek, A.B. (1989)
A theoretical study of the Brinell hardness test. *Proc. Roy. Soc. Lond.*, **A423**, 301-330.

Hirai, T. and Niihara, K. (1979)
Hot hardness of SiC single crystal. *J. Mat. Sci.Lett.*, **14**, 2253-2255.

Hirao, K. and Tomozawa, M. (1987)
Microhardness of SiO_2 glass in various environments. *J. Am. Ceram. Soc.*, **70**, 497-502.

Hirsch P.B. (1981)
Plastic deformation and electronic mechanisms in semiconductors and insulators. *J. de Physique Coll.,* **42**, C3, 149.

Hirsch, P.B., Roberts. S.G. and Samuels, J. (1987)
The dynamics of dislocation generation at crack tips and the brittle ductile transition. *Scripta. Met.*, **21**, 1523-1528.

Hirst, W. and Howse, M.G.J.W. (1969)
The indentation of materials by wedges. *Proc. Roy. Soc.*, **A311**, 429-444.

Hirth, J.P. and Lothe, J. (1982)
Theory of dislocations, 2nd edition, John Wiley and Sons, New York.

Hockey, B.J. (1973)
Use of the hardness test in the study of the plastic deformation of single crystals. In *The Science of Hardness Testing and Its Research Applications*, edited by J.H. Westbrook and H. Conrad, American Society for Metals, Ohio, pp. 21-50.

Hockey, B.J.(1971)
Plastic deformation of aluminium oxide by indentation and abrasion. *J. Am. Ceram. Soc.*, **54**, 338-231.

Holmes, P.J. (1959)
The orientation dependence of etching effects on Ge crystals. *Acta. Met.*, **7**, 293-290.

Hulse, C.O. and Pask, J.A. (1960)
Mechanical properties of magnesia single crystals in compression. *J. Am. Ceram. Soc.*, **43**, 373-378.

Humble, P. and Hannink, R.H.J. (1978)
Plastic deformation of diamond at room temperature. *Nature*, **273**, 37-39.

Hutchings, I.M. (1990)
Personal communication, 28th June, Department of Materials Science and Metallurgy, Cambridge University.

Johnson, K.L. (1970)
The correlation of indentation experiments. *J. Mech. Phys. Sol.*, **18**, 115-126.

Johnson, O.W. (1965)
High stress, low temperature, dislocation kinetics of Ge. *J. Appl. Phys.*, **36**, 3247-3250.

Johnston, W.G. (1961)
Progress in ceramic science. Vol 2, pp. 1-75. Pergammon Press.

Johnston, W.G. and Gilman, J.J. (1959)
Dislocation velocities, dislocation densities and plastic flow in LiF crystals. *J. Appl. Phys.*, **30**, 129-144.

Kabler,M.N. (1963)
Dislocation mobility in Ge. *Phys. Rev.*, **131**, 54-58.

Keh, A.S. (1960)
Dislocations in indented magnesium oxide crystals. *J. Appl. Phys.*, **31**, 1538-1545.

Knoop, F., Peters, C.G. and Emerson W.B. (1939)
A sensitive pyramidal diamond tool for indentation measurements. *J. Res. Nat. Bur. Stand.*, **23**, 39 - 61, through Thibault and Nyquist (1947).

Kohlstedt, D.L. (1973)
The temperature dependence of micro-hardness of the transition metal carbides. *J. Mat. Sci.*, **8**, 777-786.

Kollenberg, W. (1988)
Plastic deformation of Al_2O_3 single crystals by indentation at temperatures up to 750°C. *J. Mat. Sci.*, **23**, 3321-3325.

Kuczynski, G.C. and Hochman, R.F. (1957)
Phys. Rev., **108**, 946, through Westwood and Macmillan (1973).

Kumashiro, Y., Nagai, Y. and Kato, H. (1982)
The Vickers microhardness of NbC, ZrC and TaC single crystals up to 1500°C. *J. Mat. Sci. Lett.*, **1**, 49-52.

Lawn, B. and Wilshaw,R. (1975)
Review: Indentation Fracture, principles and applications. *J. Mat. Sci.*, **10**, 1049-1081.

Lawn, B.R. and Marshall, D.B. (1979)
Hardness, toughness and brittleness: An indentation analysis. *J. Am. Ceram. Soc.*, **62**, 347-350.

Lawn, B.R., Hockey, B.J. and Richter, H. (1983)
Indentation analysis: applications in the strength and wear of brittle materials. *J. Microscopy*, **130**, 295-308.

Li, W.B., Henshall, J.L., Hooper, R.M. and Easterling, K.E. (1990)
The mechanisms of indentation creep. Submitted to *Acta. Met.*

Louchet, F., Cochet Muchy, D., Brechet, Y. and Pelissier, J. (1988)
Investigation of dislocation mobility in Ge in the low temperature range by *in situ* experiments. *Phil. Mag.*, A, **57**, 327-335.

Marshall, D.B., Noma, T. and Evans, A.G. (1982)
Comm. Am. Ceram. Soc., **65**, C-176, through Sargent and Page (1985).

Menoi, C.S., Hu, J.Z. and Spain, I.L. (1986)
Ge at high pressures. *Phys. Rev.*, **34**, 362-368.

Moriyoshi, Y., Kingery, W.D. and Vander Sande, J.B. (1978)
Dislocation motion in magnesium oxide. *J. Mat. Sci. Lett.*, **13**, 2507-2510.

Mulhearn, T.O. (1959)
The deformation of metals by Vickers type pyramidal indenters. *J. Mech. Phys. Sol.*, 7, 85-96.

Nadgornyi, E. (1988)
Dislocation dynamics and mechanical properties of crystals. In *Progress in Materials Science*, edited by J.W. Christian, P. Haasen and T.B. Massalski, Pergamon Press, Oxford, **31**.

Naylor, M.G.S. and Page, T.F. (1979)
The effect of temperature and load on the indentation behaviour of SiC. *Proc. of the* 5th *Int. Conf. on liquid and solid impact (ELSI V)*, Newnham College, Cambridge. Published RAE Farnborough.

Naylor, M.G.S. and Page, T.F. (1981)
Micrhardness, friction and wear of SiC and Si_3N_4 material as a function of load, temperature and environment. *Third annual technical report: DA-ERO-78-G-010*, European research office, United States Army, London.

Naylor, M.G.S. and Page, T.F. (1983)
Microstructural studies of the temperature dependence of deformation structures around hardness indentations in ceramics. *J. Microscopy*, **130**, 345-360.

Nikitenko, V.I. and Farber, B.Ya.(1989)
Experimental investigation of kink motion in a field of random forces. *Inst. of Phys. Conf. Series.*, **104**, pp. 257-280.

Nikitenko, V.I., Myshlyaev, M.M. and Eremenko, V.G. (1968)
Plastic deformation of Si in the brittle fracture region. *Soviet Physics - Solid State*, **9**, 2047-2052.

Okada, A., Yamamoto amd Yoda, R. (1987)
Hot-hardness and indentation creep characteristics of pure metals. *J. Iron and Steel Institute Japan*, **73**, 1186-1192.

Oliver, W.C., Hutchings, R. and Pethica, J.B. (1986)
Measurement of hardness at indentation depths as low as 20 nanometers. In *Microindentation Techniques in Materials Science and Engineering*, edited by P.J. Blau and B.R. Lawn, American Society for Testing and Materials, ASTM.STP **889**, pp. 99-108.

Patel, J.R. and Alexander, B.H. (1956)
Plastic deformation of Ge in compression. *Acta. Met.*, **4**, 385-395.

Patel, J.R. and Chaudhuri, A.R. (1961)a
Generation of dislocations during deformation of "dislocation-free" Ge. *Bull. Am. Phys. Soc.*, **6**, 163.

Patel, J.R. and Chaudhuri, A.R. (1961)b
Apparent delay time of plastic deformation in dislocation-free Ge. *Bull. Am. Phys. Soc.*, **6**, 163-164.

Patel, J.R. and Chaudhuri, A.R. (1963)
Macroscopic properties of dislocation free Ge and other s.c. materials. I. Yield behaviour. *J. Appl. Phys.*, **34**, 2788-2799.

Patel, J.R. and Chaudhuri, A.R. (1966)
Charged impurity effects on the deformation of dislocation-free Ge. *Phys. Rev.*, **143**, 601-608.

Patel, J.R. and Freeland, P.E. (1971)
Velocities of individual dislocations in Ge. *J. Appl. Phys.*, **42**, 3298-3303.

Penning, P. and De Wind, G. (1959)
Plastic creep of Ge single crystals in bending. *Physica*, **25**, 765-774.

Pethica, J.B. (1982)
Micro-hardness tests with penetrations less than ion implanted layer thickness. *Ion implantation into metals*, edited Ashworth and Grant. Pergammon Press, London.

Pethica, J.B., Hutchins, R. and Oliver, W.C. (1983)
Hardness measurement at penetration depths as small as 20nm. *Phil. Mag.*, **A, 48**, 593-606.

Pirouz, P., Dahmen, U., Westmacott, K.H. and Chaim, R. (1990)
The martensitic transformation in Si-III, comparison with other work. *Acta Metall. Mater.*, **38**, 329-336.

Ponton, C.B. and Rawlings, R.D. (1989)a
Vickers indentation fracture toughness test, Part 1: Review of literature and formulation of standard indentation toughness equations. *Mat. Science and Tech.*, **5**, 865-872.

Ponton, C.B. and Rawlings, R.D. (1989)b
Vickers indentation fracture toughness test, Part 2: Application and critical evaluation of standardised indentation toughness equations. *Mat. Science and Tech.*, **5**, 961-976.

Prandtl, L. (1920)
Uher die haerte plastischer koerper, nach der akad wiss, Math-Physikalische Klasse, p.74, *through Shaw 1973.*

Qin, C-D. and Roberts, S.G. (1989)
Slip patterns and slip modes under Knoop indentations on (001) GaAs. *Mat. Res. Soc. Symp. Proc.*, **138**, 491-496.

Raj, R. and Ashby, M.F. (1971)
On grain boundary sliding and diffusional creep. *Metall. Trans.* **2**,1113-1127.

Rebinder, P.A. (1928)
Proc. Sixth Phys. Conf., State press, Moscow, through Westwood et al (1981).

Rice, W.R. (1975)
Correlation of hardness with mechanical effects in ceramics. In *The Science of Hardness Testing and Its Research Applications*, edited by J.H. Westbrook and H. Conrad, American Society for Metals, Ohio, pp. 117-133.

Rickerby, D.G. (1979)
Observations on the hardness anisotropy of MgO and LiF. *J. Am. Ceram. Soc.*, **62**, 222.

Rinder, W. and Tramposch, R.E. (1965)
Plastic indentation of Ge at room temperature. *J. Appl. Phys.*, **36**, 2079.

Roberts, S.G. (1988)
Knoop hardness anisotropy and predicited and observed slip patterns in MgO. Phil. Mag., A, **58**, 347-364.

Roberts, S.G. and Pirouz, P. (1985)
Micro-indentation investigation of doping effects on the fracture behaviour of Ge. In *Microstructural Science*, **13**, (Philadelphia Conference) edited by C. Bagnall, R.E. Witkowski and G.F. Vander Voort.

Roberts, S.G. and Warren, P.D. (1986)
Flow and fracture patterns around indentations in brittle single crystals in British Ceram. Proc., **37**, 273-279.

Roberts, S.G., Pirouz, P. and Hirsch, P.B. (1985)
Doping effects on indentation plasticity and fracture of Ge. *J. Mat. Sci.*, **20**, 1739-1749.

Roberts, S.G., Warren, P.D. and Hirsch P.B. (1986)
Knoop hardness anisotropy on {001} faces of Ge and GaAs. *J. Mater. Res.*, **1**, 162-176.

Rowe, G.W., Smethurst, E. and Downing, A.H. (1982)
A reassessment of accuracy in diamond pyramid hardness testing. *J. Mat. Sci. Lett.*, **1**, 109-112.

Samuels, L.E. (1986)
Microindentations in metals. In *Microindentation Techniques in Materials Science and Engineering*, edited by P.J. Blau and B.R. Lawn, American Society for Testing and Materials, ASTM.STP **889**, pp. 5-25.

Sargent, P.M. (1979).
Factors affecting the microhardness of solids. *Ph.D. diss., University of Cambridge.*

Sargent, P.M. (1989)
Indentation size effect and strain hardening. *J. Mat. Sci. Lett.*, **8**, 1139-1140.

Sargent, P.M. and Ashby, M.F. (1989)
Indentation Creep. *Cambridge University Engineering Department report,* CUED/C-Mats./TR145.

Sargent. P.M. and Page, T.F. (1985)
Factors affecting the measurement of hardness anisotropy. *J. Mat. Sci.*, **20**, 2388-2398.

Sawyer, G.R., Sargent, P.M. and Page, T.F. (1980)
Micro-hardness anistropy of SiC. *J. Mat. Sci.*, **15**, 1001-1013.

Schaumberg, H. (1970)
Velocity measurements on screw- and 60°- dislocations in Ge. *Phys. Stat. Sol.*, **40**, K1-K4.

Seitz, F. (1952)
The plasticity of Si and Ge. *Phys. Rev.*, **88**, 722-723.

Shaw, M.C. (1973)
The fundamental basis of the hardness test. In *The Science of Hardness Testing and Its Research Applications*, edited by J.H. Westbrook and H. Conrad, American Society for Metals, Ohio, pp. 1-11.

Shaw, M.C. and De Salvo (1972)
The role of elasticity in hardness testing. *Metals Eng. Quart.*, **12**, 1-7.

Singh, R.N. and R.L. Coble (1974)a
Dynamic dislocation behaviour in "pure" magnesium oxide single crystal. *J. Appl. Phys.*, **45**, 981-989

Singh, R.N. and R.L. Coble (1974)b
Dynamic dislocation behaviour in iron-doped magnesium oxide crystal. *J. Appl. Phys.*, **45**, 990-995

Smith, R. and Sandland, G. (1925)
J. Iron and Steel Inst., **174**, p.25.

Srinivasan, M. and Stoebe, T.G. (1973)
Thermally activated flow parameters in the deformation of MgO single crystals. *J. Mat. Sci.*, **8**, 1567-1572.

Stein, D.F. and Low Jr., J.R. (1960)
Mobility of edge dislocations in silicon-iron crystals. *J. Appl. Phys.*, **31**, 362-369.

Stokes, R.J. (1965)
Thermal mechanical history and the strength of magnesium oxide single crystals: I, mechanical tests. *J. Am. Ceram. Soc.*, **48**, 60-67.

Stokes, R.J., Johnston, T.L and Li, C.H.(1959)
Further observations of strobe cracks in MgO single crystals. *Phil. Mag.*, **A, 4**,137-138.

Studmen, C.J., Moore, M.A. and Jones, S.E. (1977)
On the correlation of indentation experiments. *J. Phys. D: Appl. Phys.*, **10**, 949-956.

Sumino, K. and Hasegawa, H. (1968)
Temperature dependence of hardness and dislocation distribution formed by indentation of Ge crystals. *Trans. J.I.M.*, **9**, *supplement*, 749-755.

Tabor, D. (1970)
The hardness of solids. *Rev. of Physics in Technology*, 1, 145.

Tabor, D. (1986)
Indentation hardness and measurement. In *Microindentation Techniques in Materials Science and Engineering*, edited by P.J. Blau and B.R. Lawn, American Society for Testing and Materials, ASTM.STP **889**, pp.129-159.

Tarasov, L.P. and Thibault, N.W. (1947)
Determination of Knoop hardness numbers independent of load. *Trans. ASM*, **38**, 331-353.

Thibault, N.W. and Nyquist, H.L. (1947)
The measured Knoop hardness of hard substances and factors affecting its determination. *Trans. ASM*, **38**, 271-330.

Trefilov, V.I. and Mil'man, Y.V. (1964)
Aspects of the plastic deformation of crystals with covalent bonds. *Soviet Phys. Doklady*, **8**, 1240-1242.

Tyler, W.W. and Dash, W.C. (1957)
Dislocation arrays in Ge. *J. Appl. Phys.*, **28**, 1221-1224.

Upit, G.P. and Varchenya, S.A. (1973)
The size effect in hardness of single crystals. In *The Science of Hardness Testing and Its Research Applications*, edited by J.H. Westbrook and H. Conrad, American Society for Metals, Ohio, pp. 135-146.

Val'Kovski, S.N. and Nadgornyi E.M. (1975)
Temperature dependence of dislocation mobility. *Sov. Phys. Solid State*, **17**, 1733-1736.

VAMAS (Versailles project on advanced materials and standards) (1989)
Hardness test round robin on ceramic materials, edited by D.M. Butterfield, D.J. Clinton and R. Morrel, NPL DMA report **685**.

Vogel, F.L., Pfann, W.G., Corey,H.E. and Thomas, E.E. (1983)
Observations of dislocations in linear boundaries in Ge. *Phys. Rev.* **90**, 489-490.

Wagatsuma, Sumino, Uchida and Yamamoto (1971)
Distribution patterns of strain and dislocations around indented areas in Ge crystals as observed by X-ray topography. *J. Appl. Phys.*, **42**, 222-229.

Wahlberg, A. (1901)
Brinell's method of determining hardness and other properties of iron and steel. *J. Iron and Steel Inst.*, **59**, 243-298.

Westbrook, J.H. (1957)
Proc. Amer. Soc. Test Mat., **57**, 873, through Atkins and Tabor (1966).

Westbrook, J.H. and Jorgensen, P.J. (1965)
Indentation creep of solids. *Trans. AIME*, **233**, 425-428.

Westwood, A.R.C. and Macmillan, N.H. (1973)
Environment-sensitive hardness of nonmetals. In *The Science of Hardness Testing and Its Research Applications*, edited by J.H. Westbrook and H. Conrad, American Society for Metals, Ohio, pp. 377-418.

Westwood, A.R.C., Ahearn, J.S. and Mills, J.J. (1981)
Developments in the theory and application of chemo-mechanical effects. *Colloids and Surfaces*, **2**, 1-35.

Wolfenstine, J. and Kohlstedt, D.L. (1988).
Creep of (Mg, Fe) O single crystals. *J. Mat. Sci*, **23**, 3550-3557.

Woo, C.H. and Puls, M.P. (1977).
The Peierls mechanism in MgO. *Phil. Mag.*, **35**, 1641-1652.

Woodward, R.L. (1974).
Strain fields associated with the indentation of metals. *J. Australian Inst. Metals*, **19**, 128-135.

Wyatt, O.H. and Dew-Hughes, D. (1974)
Metals, Ceramics and Polymers, Cambridge University Press, London.